Polymeric Solar-Thermal Flat-Plate Collectors

Christoph Nikolaus Reiter

A thesis submitted in partial fulfilment

of the requirements of De Montfort University

for the degree of Doctor of Philosophy (PhD)

November 2014

Institute of Energy and Sustainable Development
De Montfort University Leicester

Institute of new Energy Systems
Technische Hochschule Ingolstadt

Declaration

I declare that the content of this submission is my own work. The contents of the work have not been submitted for any other academic or professional award. I acknowledge that this thesis is submitted according to the conditions laid down in the regulations. Furthermore, I declare that the work was carried out as part of the course for which I was registered at *De Montfort University*, United Kingdom from January 2010 until June 2014. I draw attention to any relevant considerations of rights of third parties.

Abstract

State-of-the-art solar-thermal flat-plate collectors suffer from a limited potential to decrease production costs for the necessary higher economic benefit of solar-thermal systems. Costly metallic materials and corresponding manufacturing processes prevent further cost reductions. For that issues, plastic materials can offer a promising approach.

The main hurdle for the use of cost-effective plastics lies in the high thermal loads on the collector components — absorber and insulation — which were identified in a field-testing. The necessary overheating protection approaches to lower these thermal loads were investigated in a literature review. A large number of relevant concepts was evaluated related to achievable temperature reduction, influence on solar yield, additional costs and intrinsic safety. Therefore, a mathematical model was developed to determine the solar-thermal collector´s behaviour in a solar-thermal system for hot water and space heating. This way, the most promising overheating concepts were simulated and analysed with regard to component temperatures and system performance. Omitting the selective absorber coating and reducing the backside insulation was found to be the most suitable solution for component materials with limited temperature resistance like polypropylene.

In the second part of the research, collector design concepts were developed on the basis of the characteristics of plastic material processing. The identified unit costs showed savings of more than 50 % in comparison to state-of-the-art collectors. The analysis regarding temperature loads and annual solar yield by simulation proved the performance of the concepts. The collector costs and the simulation results were used to define the total costs of the solar-thermal systems and to evaluate the economic benefits by means of the collector concepts.

The benefits were similar to state-of-the-art set-ups. Thus, further adjustments at system level are necessary to lower the total costs. Therefore, the system set-up has to be harmonised with the collector requirements and investigated in detail.

Acknowledgements

This research was carried out at the *Institute of Energy and Sustainable Development* at *De Montfort University Leicester* in cooperation with the *Institute of new Energy Systems* at *Technische Hochschule Ingolstadt*.

I want to express my gratitude to Prof Vic Hanby, Dr Simon Rees and Prof Wilfried Zörner for having initiated this research work, for their excellent support and guidance as well as for the revision of this thesis.

I also wish to thank Carina Dittenhauser for the linguistic revision of this thesis.

Moreover, I am very grateful to the colleagues who accompanied me during the years at the *Institute of new Energy Systems*, especially to Sebastian Brandmayr, Holger Müller, Tobias Bader, Hermann Riess and Dr Christoph Trinkl.

Finally, I would like to thank my mother and my grandmother for their unequivocal support and their encouragement throughout the work. I would also like to thank my deceased father for his support and guidance throughout my childhood, which was the essential basis for my future work and career.

Table of Contents

List of Figures

List of Tables

Abbreviations

CPC	compound parabolic concentrator
EPDM	ethylene propylene diene monomer
GBP	Great Britain Pound
GdMg	gadolinium magnesium
HDT	heat deflection temperature
ICS	integrated collector storage
IEA	International Energy Agency
IL	interference lithography
LC	liquid crystals
LME	London Metal Exchange
MP	mechanical processing
PA	polyamide
PC	polycarbonate
PE	polyethylene
PMMA	polymethylmethacrylate
PP	polypropylene
PPE	polyphenylene ether
PPE+PS	polyphenylene ether/polystyrene (blend)
PPS	polyphenylene sulphide
PU	polyurethane
PV	photovoltaics
PVC	polyvinyl chloride
PVD	physical vapour deposition

r.h.	relative humidity
RTD	resistance temperature detector
SHC	Solar Heating and Cooling Programme
TISS	thickness-insensitive spectrally selective
VAT	value added tax
WO_3	tungsten oxide

Symbols

A	area	[m^2]
F'	collector efficiency factor	[-]
F_R	heat removal factor	[-]
Nu	Nusselt number	[-]
G	solar irradiance	[Wm^{-2}]
I_{el}	electrical current	[A]
K	extinction coefficient	[m^{-1}]
L	characteristic length	[m]
Pr	Prandtl number	[-]
Q_{aux}	energy consumption of an auxiliary heater	[kWh]
$Q_{conventional}$	energy consumption of heater of a conventional heating system	[kWh]
Q_d	total system load of the house (for domestic hot water and space heating)	[kWh]
$\dot{Q}$	heat flow rate	[W]
Ra	Rayleigh number	[-]
Ra_β	angle adjusted Rayleigh number	[-]
R_{el}	electrical resistance	[Ω]
R_{th}	thermal resistance	[KW^{-1}]
Ra_{crit}	critical Rayleigh number	[-]
Re	Reynolds number	[-]
S	absorbed solar radiation	[W]
dT	temperature change	[K]
T	temperature	[K]
U	overall heat loss coefficient of the collector	[$Wm^{-2}K^{-1}$]

U_{el}	electrical voltage	[V]
a	linear heat loss coefficient	[$Wm^{-2}K^{-1}$]
b	quadratic heat loss coefficient	[$Wm^{-2}K^{-2}$]
c	specific heat capacity	[$kJkg^{-1}K^{-1}$]
d	diameter	[m]
dt	per time unit	[s]
f	friction factor	[-]
f_{Pr}	Prandtl number correction factor	[-]
f_{sav}	fractional energy savings	[%]
f_{β}	collector slope correction factor	[-]
g	acceleration due to gravity	[ms^{-2}]
h	heat transfer coefficient	[$Wm^{-2}K^{-1}$]
k	heat conductivity	[Wm^{-1}]
l	pipe length	[m]
m	mass	[kg]
$\dot{m}$	mass flow rate	[kgs^{-1}]
n	refraction index	[-]
r	reflection factor	[-]
s	distance	[m]
t	time	[s]
u	velocity	[ms^{-1}]
Φ	form factor	[-]
α	absorption coefficient	[-]
β	collector slope	[°]

γ	intermittency factor	[-]
ε	emission coefficient	[-]
η_0	zero loss efficiency	[-]
θ	incidence angle at collector surface (in relation to surface normal)	[°]
ν	kinematic viscosity	[m^2s^{-1}]
ρ	reflection coefficient	[-]
σ	Stefan-Boltzmann constant	[-]
τ	transmission coefficient	[-]
τ_a	transmittance without reflection	[-]

Subscripts

a	absorber
air	air
amb	ambient
c	casing
$coll$	collector
$cond$	heat conduction
$conv$	convection
dir	direct
$diff$	diffuse
$edge$	collector edge
f	fluid
$forced$	forced (convection)
$free$	free (convection)
g	glazing
in	inlet / previous node
lam	laminar flow
max	maximum value
mw	mineral wool
$mean$	average fluid temperature of the collector
n	item
$pipe$	inner surface of the riser pipe
r	reflected
rad	radiation
sky	sky / atmosphere
t	transmitted

$total$	total
$turb$	turbulent flow
$wall$	cross-section area of the pipe wall
$wind$	wind
$\perp$	vertical
$\parallel$	parallel

1 Introduction

Considering the rapidly increasing costs of aluminium and copper the solar-thermal flat-plate collector industry is showing increasing interest in polymeric materials, which have a remarkable potential for cost reduction. Apart from moderate material costs, especially for commodity plastics and an outstanding flexibility in the scope of the design regarding product development, highly efficient production processes provide an interesting application for the use of polymeric materials (Zörner 2004). Treikauskas and Zörner (2005a) have already shown this potential for collector casings made of alternative materials.

However, several technological challenges have to be met prior to the use of polymeric materials in a wide range of applications for collectors, ranging from limited mechanical and thermal properties to low UV-durability and low heat conductivity of various polymers in comparison to copper or aluminium. Therefore, both the component and the system designs need to be adapted to polymer characteristics.

1.1 Materials and Production Costs of Flat-Plate Solar-Thermal Collectors

Solar-thermal flat-plate collectors are typically used for solar domestic hot water preparation and space heating in Central European climates. Currently, the state-of-the-art flat-plate collector design contains the following major parts: absorber, glazing, thermal insulation and casing (Duffie and Beckman 2006).

The absorber is the main element of the collector and is in most cases fabricated from copper. It transmits the incoming solar radiation, consisting of a direct and a diffuse part, and converts the radiant energy into thermal energy. Most absorber types are of the fin-and-tube design. The plate with a black or a selective surface receives radiation. On the back of the plate fluid pipes dissipate the thermal energy.

The glazing above the absorber reduces the heat loss of the absorber plate by convection and radiation. The glazing is typically made of special break-proof glass with a very good light-transmitting characteristic.

An insulation typically consisting of rock wool reduces the heat losses on the backside and the edges. The insulation is between 40 and 60 mm thick on the backside and about 15 mm on the edges.

The absorber, the glazing and the insulation of the collector are embedded in a casing to protect them against environmental influences and to fix the collector to an underground. Common casings are fabricated from aluminium in riveted frame or deep-drawn casing designs (Figure 1.1).

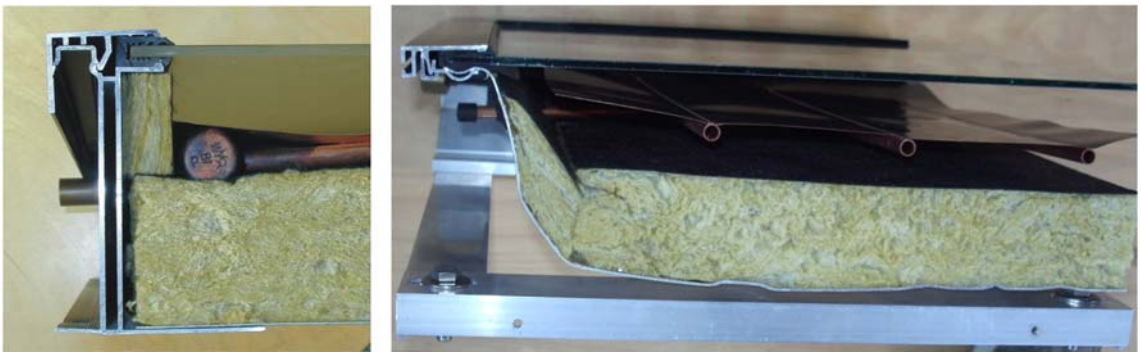

Figure 1.1: Typical frame (left) and deep-drawn casing (right) designs of a flat-plate collector

In recent years, numerous industrial development projects in the field of flat-plate collectors have focused on the enhancement of collector efficiency, for example by non-reflective glass, double-glazing or highly selective absorber coating. This led to an increase in production costs and eventually to an increase of collector prices.

Furthermore, soaring costs for the commonly used raw materials, mainly copper and aluminium, intensified this trend. Solar-thermal flat-plate collector design has a very high mass percentage of the materials copper, aluminium and glass. Figure 1.2 illustrates the materials mass percentage of a state-of-the-art collector of a German manufacturer.

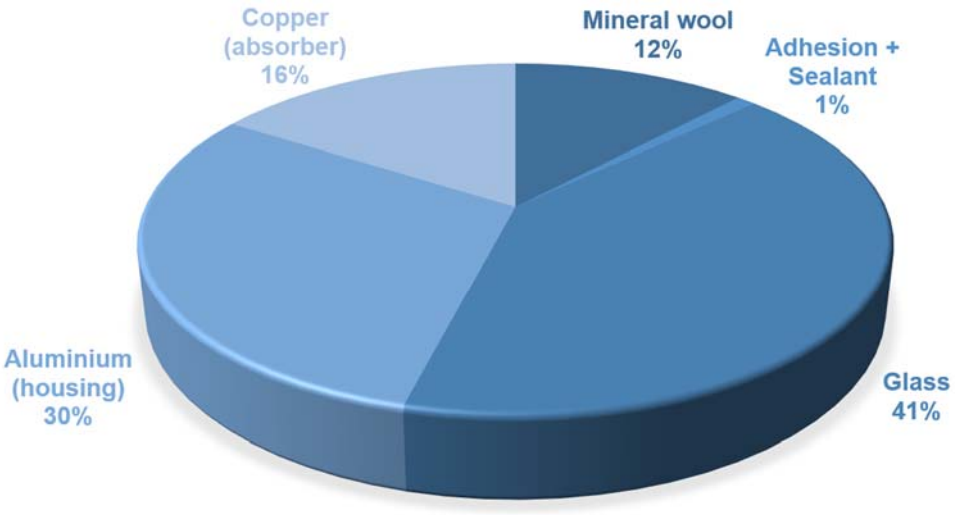

Figure 1.2: Materials mass percentage of a state-of-the-art flat-plate collector (according to Hochreiter and Trinkl 2008)

Figure 1.3 demonstrates the price development of copper between January 2002 and December 2013 with the price soaring from 1,530 US dollars to 7,060 US dollars per ton (Westmetall n.d.). The price hit a local all-time high in February 2011, surging to 10,120 US dollars per ton.

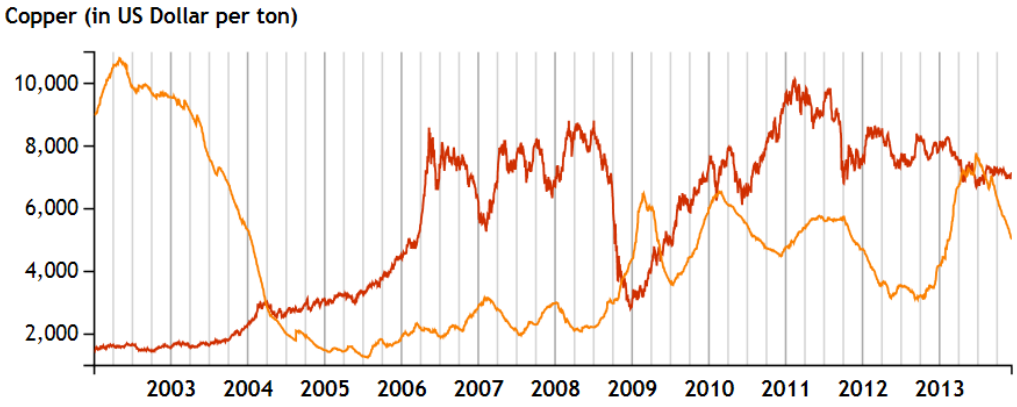

Figure 1.3: Price development of copper (red; LME copper 3-month) and copper stock (orange; LME copper stock) between 2002 and 2014 (Westmetall n.d.)

Figure 1.4 demonstrates the price development of aluminium between January 2002 and December 2013 with the price skyrocketing from 1,380 US dollars to 1,770 US dollars per ton and reaching a record high of 3,340 US dollars (Westmetall n.d.).

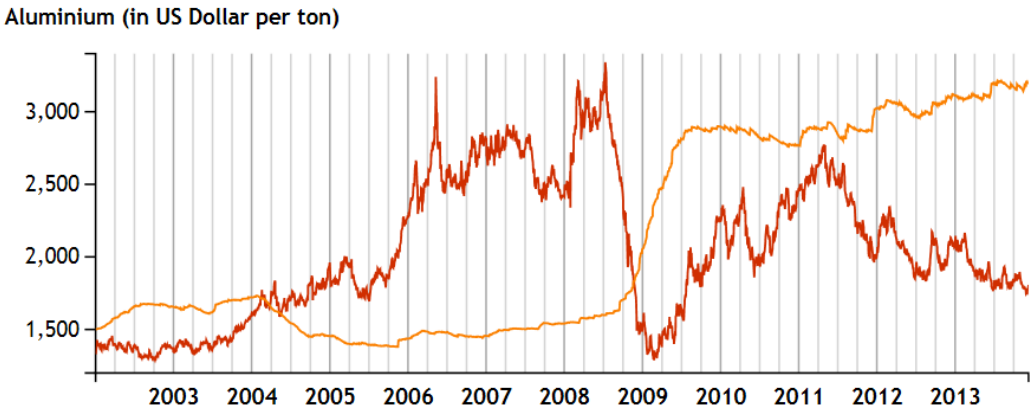

Figure 1.4: Price development of aluminium (red; LME aluminium 3-month) and aluminium stock (orange; LME aluminium stock) between 2002 and 2014 (Westmetall n.d.)

Against this background, the markets as well as the national and European policymakers are calling for a decrease of consumer prices for solar-thermal systems in order to reduce the subsidies for these systems in the future. As a consequence, the solar collector industry for example increasingly replaces copper by less cost-intensive aluminium for the absorber (Zörner 2004). As shown in Figure 1.5, the absorber, the glazing and the casing represent a considerable share of collector production cost.

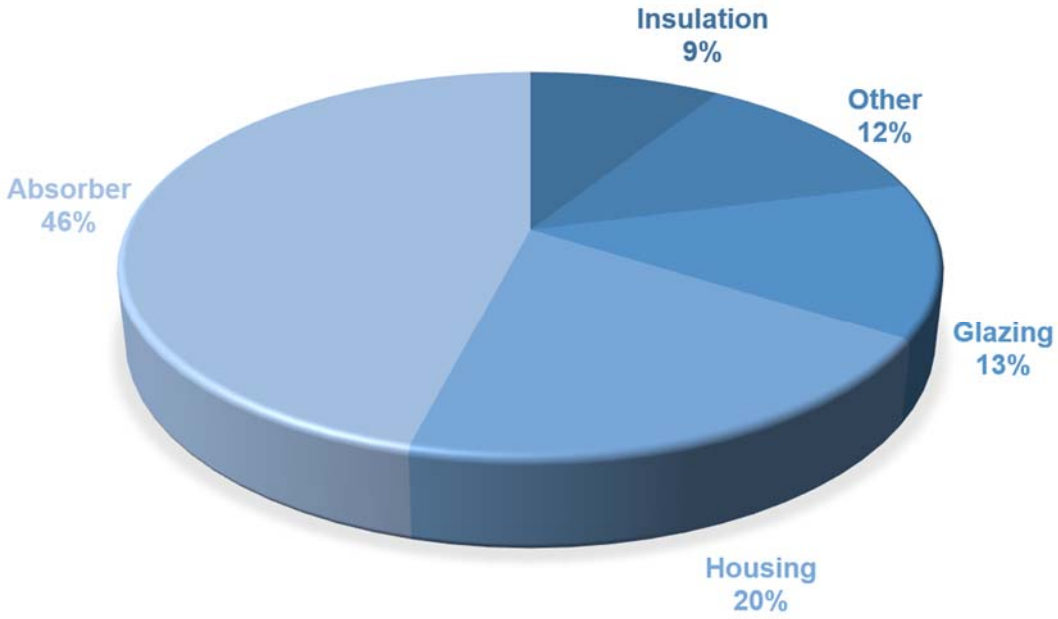

Figure 1.5: Typical breakdown of the production costs of solar-thermal flat-plate collectors (according to Hochreiter and Trinkl 2008; Treikauskas and Zörner 2005b)

The efforts of manufacturers to reduce production costs are undermined by the development of the price curves. Another reason for the high production costs of metal parts is the limited suitability for mass production of the processes involved. These processes require a large degree of assembly work as well as manual work such as mounting the aluminium frame. This is a particularly negative drawback when bearing in mind that the market for solar-thermal collectors is subject to major changes to the advantage of high volume production. The production costs of solar-thermal flat-plate collectors are much higher when producing copper and aluminium manufactured parts, i.e. with the absorber causing half of the costs and the housing a fifth respectively (Figure 1.5).

A market volume of about 8.5 million m² per year for solar-thermal collectors is expected in Europe by 2020 (Müller and Zörner 2008). The annually produced collector area in Europe was 1.7 million m² per year in 2009 and is predicted to increase within the course of the next 10 years by a factor of about 5 (Figure 1.6). This development will be a great challenge for the manufacturers to supply the market.

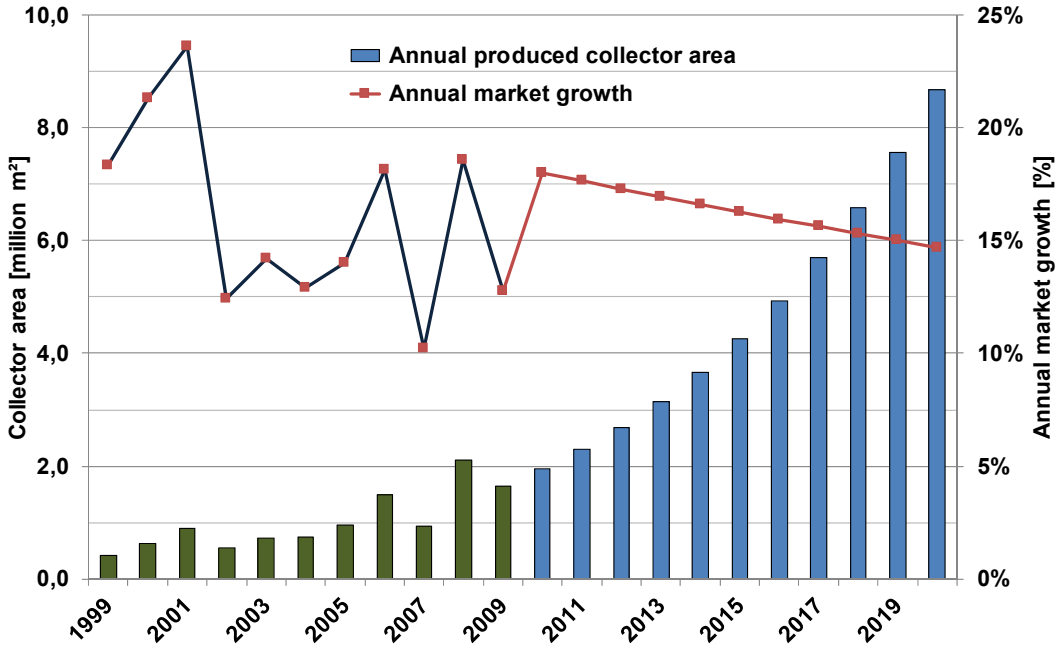

Figure 1.6: Increase of the produced collector area in Europe until 2020 (Müller and Zörner 2008)

The highly improved production processes in conventional assembly lines have no further potential of being optimised. Hence, production processes of state-of-the-art collectors lead to limited cost advantages by economies of scale. On the contrary, production techniques for polymeric parts have a great potential for mass production. These machines — or to be more precise production lines — are linked to high investment costs. Additionally, a large number of units is required for an adequate depreciation. However, if large production quantities can be reached, low production costs will be achievable.

In this regard, polymeric materials show a remarkable potential for cost reduction. However, the replacement of copper and aluminium by polymers for absorber or casing is not possible within the current collector design. Polymers can generally only be a cost-effective alternative if the product design is adapted to both the characteristics of the polymeric material and the polymer production processes. The sole replacement of materials in a metallic material optimised design will not show satisfactory solutions, and certainly not when targeting at mass production.

1.2 Overview of Polymeric Materials in Solar-Thermal Collectors

Polymeric materials are already used in several solar-thermal applications. These are usually not fully polymeric collectors, but rather conventional materials of single parts replaced by polymers. Polymers are mainly used in unglazed absorbers such as for pool heating. There were also polymeric materials used in simple applications like thermosyphon or integrated collector storage (ICS) systems. A general overview on polymeric materials in solar-thermal applications is given by Meir (2008). More details as to when polymeric collector parts are already available on the market will be described below.

1.2.1 Absorber

Polymeric absorbers are currently used for pool heating applications by various manufacturers, since pressure and temperature are low within those systems.

These unglazed solar absorbers can supply the system with heat on a very low temperature level (30–40°C). Hence, high thermal and mechanical stability are not required for the absorbers. Additionally, pool water is pumped directly through the part and therefore a resistance against glycol is not needed. The required properties for absorber materials are ideal for the use of low-cost polymers. Mainly, low-cost polymers like polyethylene (PE), polypropylene (PP) and EPDM are used. These rather inefficient unglazed and non-insulated pool heating absorbers cannot be used for hot water preparation and space heating under Central European climates.

Two types of absorbers are available on the market, volumetric absorber structures on the one hand and absorbers with parallel channels on the other hand.

Volumetric absorbers with holohedral flow are rigid and frost-resistant. They are produced from black polyethylene (PE) by means of extrusion blow moulding (cf. e.g. Meir 2008; OKU Obermaier GmbH n.d.; Roth Werke Gmbh n.d.). Figure 1.7 shows in an exemplary way the product of *OKU Obermaier GmbH*. Both the British company *Solco Ltd.* as well as the German company *Roth Werke GmbH* offer a similar range of absorbers.

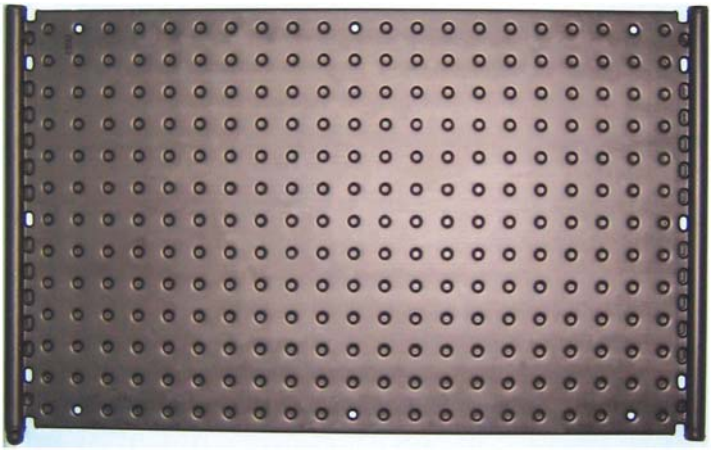

Figure 1.7: Unglazed and non-insulated absorber for pool heating (OKU Obermaier GmbH n.d.)

Another kind of the above-mentioned absorber type is made from flexible material. *Texsun AB* manufactures the unglazed absorber *El Nino* from black elastomeric flexible polyvinyl chloride (PVC) by means of welding two sheets together (TEXSUN AB n.d.), characterised to be frost-resistant.

The second type of absorbers, which are extruded as sheets with intrinsic channels or as single pipes, has straight channels. Sheets with intrinsic channels made of polypropylene (PP) are produced by the US company *FAFCO, Incorporated*. The German company *MAZDA-SOLAR* pursues a similar design and uses ethylene propylene diene monomer (EPDM), an extremely flexible material. Figure 1.8 shows the elastic, coextruded absorber with a red surface matching the colour of the roof (MAZDA-SOLAR n.d.; Meir 2008).

Figure 1.8: Flexible pool heater from MAZDA-SOLAR (MAZDA-SOLAR n.d.)

The pool heater from *Heliocol* is a bundle of single PP tubes added together. Figure 1.9 shows the pool absorber during the production process in the assembly line on the left hand and on the right it demonstrates the absorber when already mounted on a roof and connected to the system.

Figure 1.9: Pool absorber from *Heliocol* (Heliocol n.d.)

1.2.2 Housing

When considering glazed and insulated solar collectors for hot water preparation and space heating, polymers are still rarely used in collector parts. Nevertheless, polymeric housing provides a wide scope of flexibility and lightweight design of

polymeric housings due to polymer production processes, which can be attributed to the major advantages in comparison with housings made of metals.

The Austrian company *Fasalex* produces parts from composites of wood and plastic material. A frame of this composite is used for a prototype similar to the common aluminium frame construction for collector housings. The collector made by *Bosch Thermotechnik GmbH*, a German company, has a frame of glass-fibre reinforced plastics. Figure 1.10 illustrates the described collector frames.

Figure 1.10: Collector frame constructions from *Fasalex* and *Bosch Thermotechnik GmbH* (Meir 2008)

The company *Roth Werke GmbH* produces thermoformed collector casings made of black polycarbonate (PC) by means of a thermoforming process. The honeycomb structure on the bottom of the housing increases mechanical stability (Meir 2008; Roth Werke GmbH n.d.). Figure 1.11 illustrates the PC part and its honeycomb structure.

Figure 1.11: Thermoformed PC casing with honeycomb structure from *Roth Werke GmbH* (Roth Werke GmbH n.d.)

1.2.3 Glazing

Partly, transparent polymeric covers are used in collectors. Three types of polymeric glazing are available. The basic version consists of a plane sheet analogue to standard shatterproof glass. Exactly this sheet which is made from PMMA is used for the flat-plate collectors from *Stiebel Eltron GmbH & Co. KG*. When it comes to achieving higher mechanical stability, the bended plate represents another alternative to a single-sheet glazing. In particular, collectors of larger sizes benefit from the curvature. The British company *Imagination Solar Ltd.* uses exactly this type of curved PC plates for collectors. The thermosyphon collector manufactured by *Stibetherm S.A.* as well as the ICS collector produced by *Solarpower GmbH* are comprised of bended acrylic glazing. Figure 1.12 shows the glazing with dome structure.

Figure 1.12: Flat-plate collector from *Stibetherm S.A.* (*Stibetherm S.A.* n.d.) and ICS collector from *Solarpower GmbH* (Meir 2008) with dome-structured glazing

The twin-wall sheets, a tremendous choice of which is available on the market, are also used as polymeric collector glazing. Most of all, these plates can be found in carports or terrace roofs. Transparent plates are extruded from PC or PMMA combining both low weight and high stability and show, therefore, great potential for light weight construction. The correspondent product of *Solar Twin Ltd.,* a collector manufacturer, is equipped with PC twin-wall sheet amounting to 10 mm thickness (Figure 1.13).

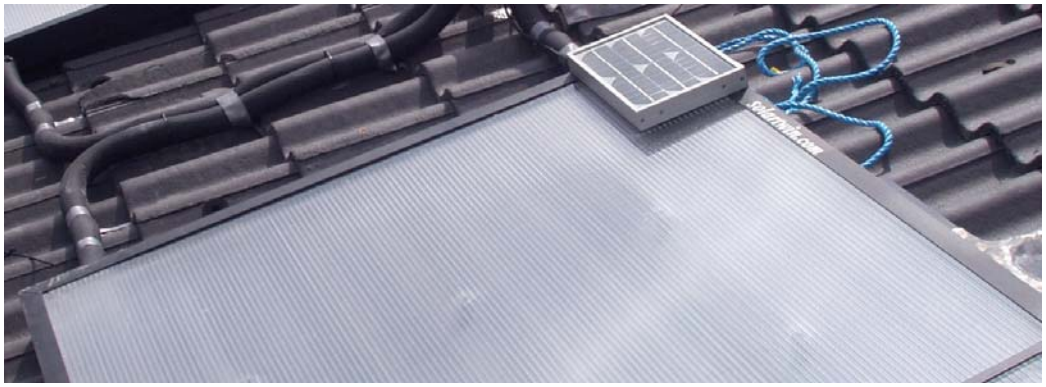

Figure 1.13: Solar collector with a polycarbonate twin-wall sheet (Solar Twin Ltd. n.d.)

1.2.4 Fully Polymeric Collector

Most previous work has been limited to single parts of the collector. A fundamental investigation of how to apply polymeric materials not only for single parts but in integrated polymeric collectors is currently not available.

The Norwegian manufacturer *Aventasolar AS* presented a collector almost fully manufactured from polymers (Figure 1.14). However, the collector was designed for a cost-effective drain-back system for domestic hot water and space heating being integrated into low-temperature heating systems. The collector's efficiency is rather low in comparison to state-of-the-art collectors in order to limit the maximum temperature of the absorber. Basically, the industrial developments remain on a low technical level and focus on the replacement of materials for single parts. The cover sheet of the collector is an extruded twin-wall sheet made of PC with an additional UV protective layer. The absorber consists of an extruded twin-wall sheet with fixed end caps made of the high-quality material polyphenylene sulphide (PPS). The extruded aluminium frame establishes stiffness and a modular application of the collectors. The collector has the following size: a width of 600 mm, a variable length of up to 6 m and a specific weight of 5 kg/m² (Aventasolar n.d.). Figure 1.14 shows a sectional view of one collector module.

Figure 1.14: Sectional view of the polymeric collector from Aventa AS (Aventasolar n.d.)

The polymeric collector from *Solar Twin Ltd.* was developed by the Edinburgh Napier University and can be integrated additionally into an existing heating system. The collector module with an aperture area of 2.8 m² is designed for small system applications (Figure 1.13). Within the heat carrier the light design of the collector has a weight of 33 kg. *Solar Twin Ltd.* offers this solar-thermal system as an installation kit containing all necessary parts for the integration to in the heating system. The solar circuit pump is driven by a small photovoltaic cell for an off-grid power supply. The cover is an extruded PC twin-wall sheet and the flexible absorber pipes are made of silicone rubber. This absorber is resistant when ranging between -60°C and 200°C. The volume expansion of the freezing fluid inside the absorber cannot break the elastic pipes. Hence, this flexible absorber system is also frost-resistant. The required stiffness of the collector is achieved by an aluminium frame (Solar Twin Ltd. n.d.).

1.3 Overview of Research Activities of Polymeric Materials in Solar-Thermal Collectors

Additionally, in the field of solar-thermal flat-plate collectors, research has been conducted. Research work about polymeric collector parts, material science and overheating protection is presented in the following paragraphs.

1.3.1 Collectors and Parts

Bartelsen et al. (1999) investigated elastomer-metal-absorbers for the use in roof and facade elements. The metal plates of these absorbers have integrated clip profiles for the application of an elastomeric tube (Figure 1.15). The main advantage of this absorber is the inherent freeze resistance making an operation possible without any antifreeze additives. Moreover, the resistance against corrosion enables the option to operate directly as a solar desalination system for sea water.

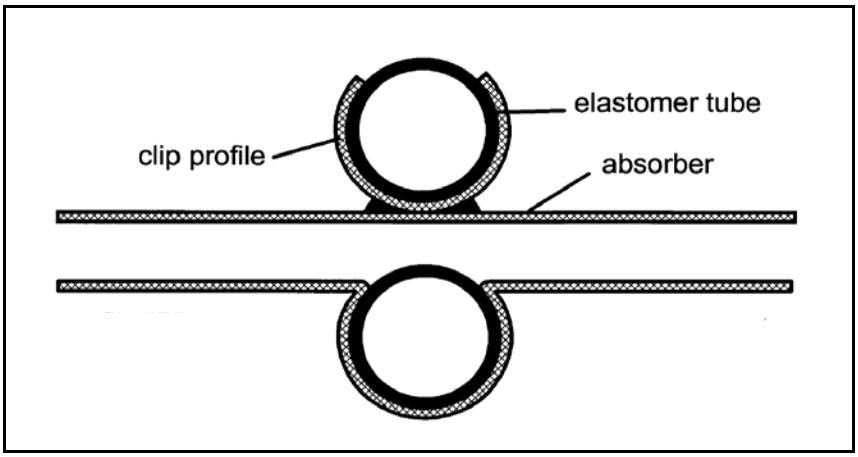

Figure 1.15: Absorber with a clamping profile (Bartelsen et al. 1999)

Concerning research work in the field of polymeric solar-thermal collectors, an investigation of selectively coated polymer absorbers was carried out by Rommel et al. (1997). They proved the capability of alternative absorber materials in combination with adequate geometries. The efficiency of the investigated absorbers reached is comparable to state-of-the-art metal fin-and-tube absorbers proved in calculations and in prototype tests.

Brunold (2010) also described an approach for a cost-effective polymer collector. This concept was adjusted to polymeric production processes and a first analysis of the manufacturing costs was conducted. The measured efficiency curve of a prototype with non-selective absorber and glass cover showed satisfactory results in comparison to a state-of-the-art collector thanks to the optical properties and the collector efficiency factor in particular. However, the estimated maximum temperatures were too high for the proposed polymeric materials. Also the tested

thermotropic absorber layer for overheating protection was not sufficient to solve the issue completely.

Simulations in order to evaluate the thermal performance of polymeric collectors and future prospects of these materials in solar collectors were also carried out by Cristofari et al. (2004) and O'Brien-Bernini and McGowan (1984). The simulation results showed that polymeric flat-plate collectors have been able to achieve comparable efficiencies like state-of-the-art metal collectors.

Kaiser et al. (2012) investigated solar-thermal systems by means of simulation in order to derive requirements for polymeric materials in collectors. In his analysis a basic polymeric collector design with twin-wall sheet glazing was implemented in the simulation tool. A thermotropic layer and a surface cooler for overheating protection were also analysed in this simulation. The results of the system simulation were compared to a conventional system to estimate the influence on the system efficiency and the part temperatures.

1.3.2 Materials

Ruesch and Brunold (2008) investigated the ageing behaviour of glazing materials, particularly transparent plastics, for solar-thermal collectors. 52 polymeric glazing types have been exposed in Switzerland over 20 years. Therefore, the conditions of solar-thermal collectors have been imitated by building small collectors with a selective steel plate inside. The PMMA sheets showed good transmission results even after 20 years of exposure. The brittleness of these PMMA types proved to be a problem, but the current materials are expected to be more resistant. The PC types of 1984 can resist high thermal loads and show favourable transmission properties. However, the low UV-resistance caused a relatively high degradation. Therefore, a UV-protection layer is required for solar-thermal collector glazing made of PC. For that kind of application the other transparent polymers tested are not suitable for application.

Kahlen and Wallner (2008) tested the ageing behaviour of different polymeric materials for the use in absorbers of solar heating systems. The material samples

of PC, polyphenylene ether/polystyrene (PPE+PS) blend, PP and polyamide 12 (PA12) were exposed to hot air (140°C) for 500 h as well as to hot water (80°C) for 16,000 h and were then analysed in regular time intervals.

Kurzböck et al. (2012) investigated black pigmented PP materials with high solar absorbance for the use in absorbers, focusing mainly on the test of the developed compounds with regard to their ageing behaviour. The requirements of the materials were improved mechanical properties at operating temperatures of up to 90°C for more than 10 years and a solar absorbance of at least 90 %.

Orel et al. (2010) investigated thickness-insensitive spectrally selective (TISS) paints for the use on metal as well as plastic absorbers. Moreover, the optical properties of the paint were analysed. The degradation of the paint under common absorber conditions was also tested. Hence, the paint is a profitable option to conventional selective absorber coatings. In particular the spraying process for the application on the surface is interesting for polymeric substrates.

An analysis of polymeric insulation materials for solar-thermal applications was carried out in Zauner et al. (2011). Rigid foam as well as flexible foam of polyurethane (PU) were tested amongst others for the use in the backside insulation of collectors. The analysis embraced the investigation of thermal properties, degradation and outgassing of the materials.

1.3.3 Overheating Protection

Some research work was done on thermotropic layers on the glazing to reduce high temperatures in flat-plate collectors for example by Resch et al. (2007). Furthermore, thermochromic films on the absorber that switch their optical characteristics depending on the temperature were investigated by Huot et al. (2008) and Marty et al. (2008). Triggered ventilation is another way of controlling critical temperatures. Most investigations concentrated on arrays with venting dampers at the ends of the collector, which allow an air exchange above or below the absorber to carry the heat away from the radiation exchanger (Meir et al. 2008;

Harrison et al. 2004; Kearney et al. 2005). Further overheating protection concepts are shown in detail in the following chapters.

1.4 Formulation of the Research Topics

Several products proved the feasibility of polymer use in collectors and showed that there is a huge technical as well as economic potential. Most concepts, however, only substituted the material of single collector parts without changing the design. Thus, the full potential of polymeric production processes could not be tapped and the unknown component temperatures were only solved by choosing more temperature resistant, hence more expensive materials. The projects in the field of polymeric materials for solar-thermal collectors focused on single concepts or topics without considering all details and options for a polymeric collector approach with regard to manufacturing cost in comparison to the system yield. Hence, the application of polymers is still not possible on an integrated level as major gaps in the knowledge exist. This thesis addresses these gaps by using experimental measurement, computer simulation and design analysis. It covers the four major topics relevant to the conceptual design of a polymeric flat-plate collector:

- *Identification of the thermal loads in solar-thermal flat-plate collectors*
- *Analysis of concepts for overheating protection in solar-thermal flat-plate collectors*
- *Development of polymeric collector design concepts with regard to manufacturing costs*
- *Analysis of polymeric collector design concepts relating thermal loads to system performance and economic potential*

2 Collector Loads

Solving the hurdles of the use of low-cost polymers with their limited thermal and mechanical stability, overheating protection measures for the solar-thermal collector are necessary. Analysing the loads occurring in a state-of-the-art solar-thermal system and adjusting this system will be the basis for the use of such polymers.

In an initial step, a modern system for domestic hot water and space heating with state-of-the-art solar-thermal flat-plate collectors was analysed in a field-testing building (Reiter et al. 2012). The measurement data were assessed including the following aspects: maximum temperatures at the collector components, dynamic behaviour of thermal loads and accumulated exposition times, i.e. thermal load profiles. By measuring the fluid pressure of the solar-thermal system the mechanical loads were also investigated. The collected data provide the fundamental basis for polymeric material selection or development, for an evaluation of material property changes over the life time as well as for an adoption of solar-thermal systems and collector designs to polymer requirements.

2.1 Field-Testing System and Measurement Instrumentation

For the field-testing building a single-family house inhabited by four persons was chosen. The house is equipped with a modern solar hot water and a space heating system with standard flat-plate collectors reaching approximately 19 m² of collector surface. Table 2.1 shows the boundary conditions of the field-testing.

Table 2.1: Description of the investigated heating system in the field-testing

Design data		
System:		
Building type	Single family house	
Location	Near Munich (Germany)	
Total system load	approx. 23,500	[kWh]
Space heating load	approx. 22,000	[kWh]
Domestic hot water load	approx. 1,500	[kWh]
Heat distribution system	Floor heating + radiators	
Auxiliary heater	Condensing oil boiler 18 kW	
Buffer storage volume (nominal)	1,000	[l]
Solar collectors:		
Aperture area	19.03	[m²]
Collector azimuth	-39 (South=0)	[°]
Collector slope β	48	[°]
Optical efficiency	0.798	[-]
Linear heat loss coefficient	3.34	[$Wm^{-2}K^{-1}$]
Quadratic heat loss coefficient	0.0075	[$Wm^{-2}K^{-2}$]
Heat capacity	9.5	[kJK^{-1}]

The living space is heated by floor heating and radiators. The section for space heating in the buffer storage has the set-point temperature of the radiators. A three-way valve mixes flow and return in the heating circuit to supply the floor heating with the required set-point temperature. Domestic hot water is provided by an external heat exchanger connected to the storage. The condensing oil boiler directly supplies the hot water section, the section for space heating and the heat distribution system. The collector array consists of 10 collectors connected in line and operates with a water-glycol mixture. The volume flow rate through the collector array amounts to 16.5 $lh^{-1}m^{-2}$. During the summer period

some radiators in the basement operate to cool down the buffer storage and to avoid stagnation in the collector array.

The installed measurement instrumentation consisted of a unit for recording weather data as well as sensors for measuring the thermal loads on the collector parts. Additionally, sensors to measure flow and return temperatures as well as volume flow rates were installed in all heating circuits of the system.

The measurement devices for recording the weather data to evaluate the ambient conditions consisted of a silicone pyranometer in the collectors' plane as well as a combined temperature and humidity sensor in a ventilated housing. Moreover, a cup anemometer was installed in the collectors' plane to measure the wind speed along the glazing. Table 2.2 lists the sensors for measuring weather data of the field-testing.

Table 2.2: Description of the sensors used in the field-testing for analysing the weather data

Measurand	**Sensor**		**Accuracy**
Solar irradiance	Silicone pyranometer	0–2.000 Wm^{-2}	±(1.0 + 0.15T) %
Relative humidity and temperature	Capacitive humidity sensor and resistance temperature detector (RTD) – Pt-100	0–100 % r.h. -30 – +70°C	±(2.0 + 0.1T) % r.h. ±(0.3 + 0.0073T) K
Wind velocity	Cup anemometer	0–50 ms^{-1}	±0.5 ms^{-1}

For the evaluation of the mechanical loads on the solar circuit and therewith on the absorber, a sensor for measuring the absolute fluid pressure was integrated in the basement. In order to be able to analyse the operation of the collector array and the volume flow rate, an electromagnetic flow meter was installed in the solar circuit. In combination with two temperature sensors (calibrated by pair) in the flow and the return of the solar circuit near the external heat exchanger at the buffer storage, the heat flow rate of the solar array was determined. Table 2.3 demonstrates the sensors and their properties.

Table 2.3: Description of the sensors used in the field-testing for analysing the solar circuit

Measurand	**Sensor**		**Accuracy**
Fluid pressure (absolute)	Piezo-resistive pressure transducer	0–10^6 Pa	+0.2 %
Volume flow rate	Electromagnetic flow meter	0.8–3.39 m^3h^{-1}	[-0.17; +0.11]
Temperature	RTD – Pt-100	-30 – +250°C	±(0.15+0.002T) K

The measured temperatures from the sensors at the parts of the collectors were the most important results from the field-testing. For the latter, a new collector equipped with measurement instrumentation was embedded in the existing solar system. Furthermore, a dry collector without any connection to the solar-thermal system and fluid was installed to refer to the maximum loads during continuous stagnation year.

The last collector in the line of the array represents at the same time the hottest collector during the system operation. Consequently, this collector was equipped with temperature sensors at each part. Figure 2.1 shows the temperature sensors at the back side and at the frame of the collector housing fixed with rivets using heat-conductive paste.

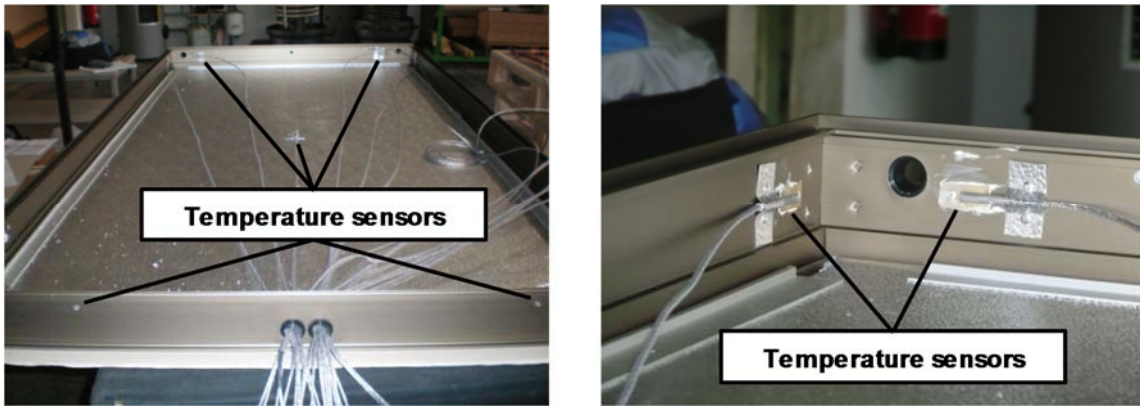

Figure 2.1: Temperature sensors at the back side (left)
and at the frame of the housing (right; Reiter et al. 2012)

The three temperature sensors at the backside were distributed over the full length of the absorber. Even two temperature sensors were fixed at the top edge

of the frame near the inlet and outlet pipe. Moreover, two sensors were installed at each side of the frame and at the bottom edge.

In total, the absorber sheet consists of nine riveted sensors. The sensors were fixed in the middle between two riser pipes. Hence, the sensors were measuring the highest temperatures at the end of the fin. Figure 2.2 shows the fixed temperature sensors at the absorber sheet in detail and in general view.

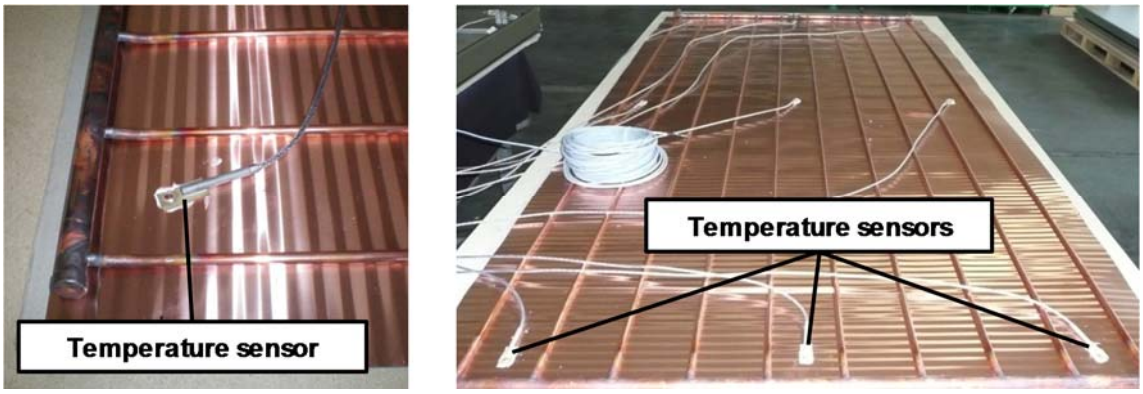

Figure 2.2: Temperature sensors at the absorber sheet

The temperatures at the glazing of the collector (top, middle and bottom) were measured inside the collector by bonded surface sensors. Aluminium foils were fixed around the sensors to shield them from incoming solar radiation. Table 2.4 shows the sensors used in the test collectors.

Table 2.4: Description of the sensors used in the field-testing for analysing the collector temperatures

Measurand	**Sensor**		**Accuracy**
Temperature	RTD – Pt-100; riveted type	-30 – +250°C	±(0.15+0.002T) K
Temperature	RTD – Pt-100; bonded foil type	-30 – +130°C	±(0.15+0.002T) K

In addition to the test collector in the system, an identical collector, which was, however, not embedded in the system had been equipped with sensors and then mounted on the roof. This collector which was permanently stagnating was used as a reference for maximal temperature loads. The collector parts were provided

with analogical temperature measurement instrumentation. Figure 2.3 shows the installed test collectors on the roof.

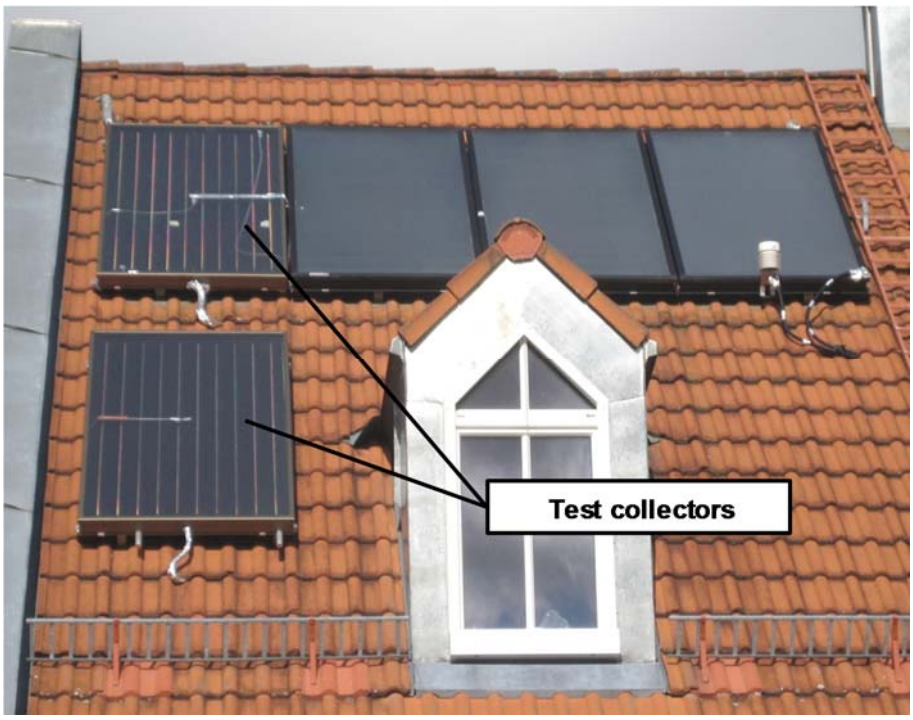

Figure 2.3: Part of the collector array with the system integrated test collector (top, left) and the test collector which is permanently stagnating (bottom, left; Reiter et al. 2012)

In addition to the solar circuit, the other heating circuits connected to the buffer storage had embedded temperature sensors in flow and return (calibrated by pair).In the return, a sensor for measuring the volume flow rate was installed to analyse the transferred heat flow rates in the system. Additionally, a temperature sensor was integrated in the buffer store at 80 % in relative height from the bottom. Table 2.5 shows the sensors used in the heating circuits.

Table 2.5: Description of the sensors used in the field-testing for analysing the heating system

Measurand	**Sensor**		**Accuracy**
Volume flow rate	Ultrasonic flow meter	0–10 m^3h^{-1}	±1.0 %
Temperature	RTD – Pt-100	0 – +100°C	±(0.15+0.002T) K

During the two and a half years testing period, the signals from the sensors were logged and saved directly in a data base at the testing object. In a further step

the results were analysed and visualised on a semi-automated way by using a programmed script. As a consequence of that, the different stages of operation or to be more precise the collector loads could be analysed. The evaluation of the thermal loads was carried out by analysing the temperature gradient at certain stages of the system. A detailed analysis on a day-to-day basis as well as annual histograms for load profiles of the collector parts provided further information.

For analysing the results the sensors at absorber, glazing, frame and backside with the most meaningful temperature data have been chosen. Figure 2.4 and Figure 2.5 display the metering points of the collector in the system and the dry collector out of operation used for the evaluation of the temperature loads on the collector parts.

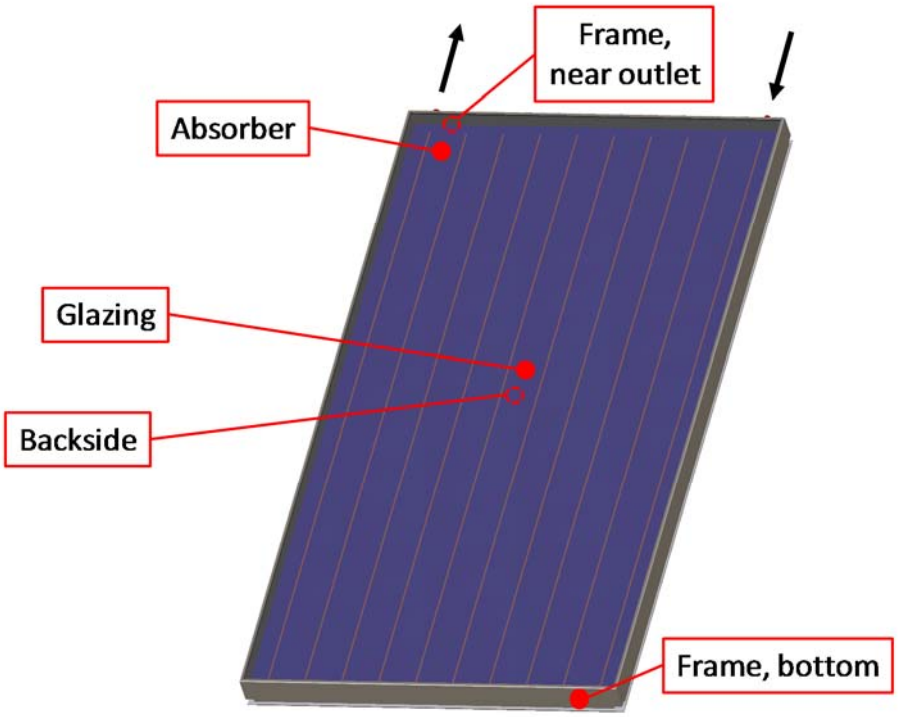

Figure 2.4: Chosen metering points at the collector in the system

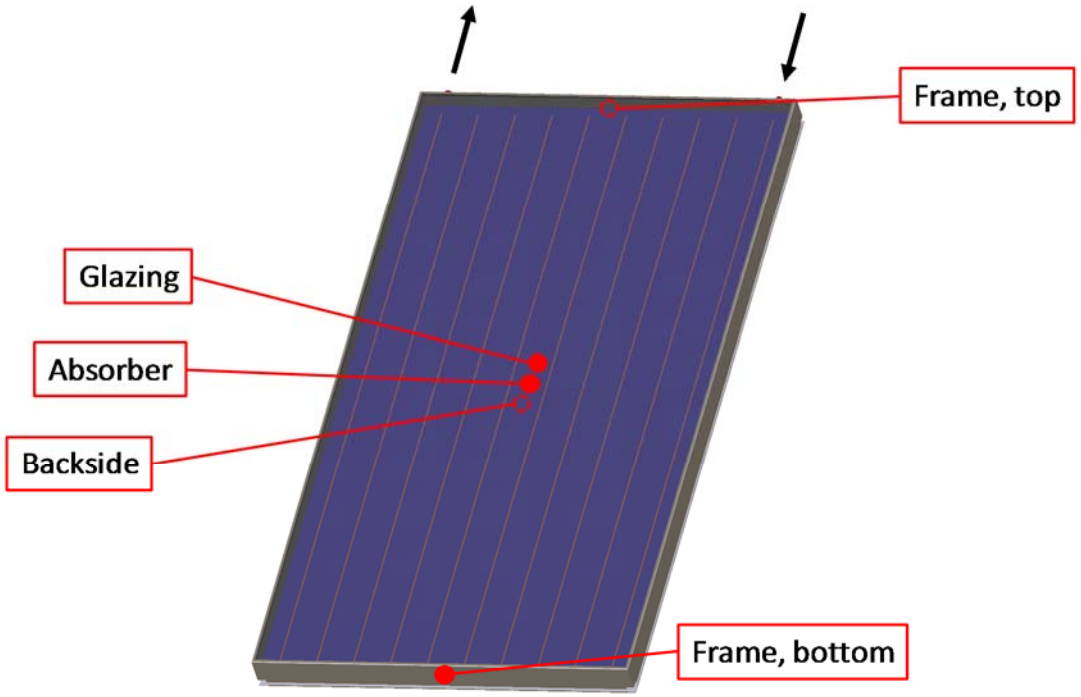

Figure 2.5: Chosen metering points at the dry collector

2.2 Thermal Collector Loads

The temperature loads of the collector parts were investigated regarding their time dependent behaviour on the one hand and their annual temperature loads on the other hand.

The time dependent temperature profiles show the maximum temperatures of the parts at different weather conditions and operating points of the system to figure out the potential points to act for overheating protection and an adoption of the solar-thermal system to polymer needs. Furthermore, the dynamic of the temperature change and temperature differences between the parts provide an overview for advices in design because of the thermal expansion for example.

The annual load profiles provide information about the duration at the various temperature levels as well as about the maximum loads. This will be the basis for the selection of materials and design details beside the development of overheating protection measures.

2.2.1 Temperature Profiles of Collector Parts

The following evaluation of the collector part temperatures in detail is visualised as a time dependent gradient.

The 16th August 2009 was chosen as an exemplary day for high temperature loads on the parts during the testing period. On that clear, hot day the global irradiance at the collector plane reached 1.000 W/m² and the ambient temperature rose to 34°C. Figure 2.6 shows the temperature profiles of the parts of the collector in the system.

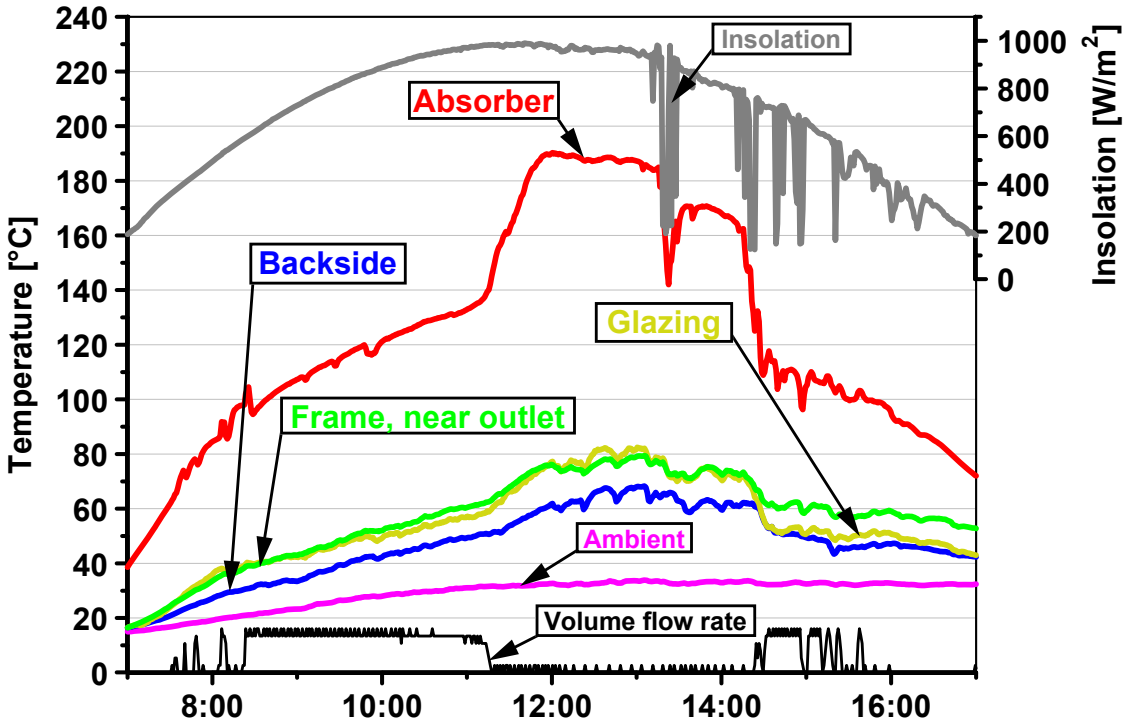

Figure 2.6: Temperature profile of the collector in the system during a summer day (16th August 2009)

As early as in the operating phase of the solar-thermal system the absorber reached final temperatures of up to 130°C. The sensors at the glazing and at the frame near the outlet measured temperatures of about 60°C. Meanwhile temperature rose to approximately 50°C at the backside. After 11 o´clock a.m. the circulation in the solar circuit stopped and the stagnating state of the system set in.

Therefore, the final temperature of the absorber soared to 190°C and even surpassed that level. During this period the temperature of the glazing rose to up to 80°C and the frame showed almost the same results. Furthermore, at the backside a peak value of 68°C was recorded. The graphic also demonstrates the dynamic movements of the temperature level of the absorber when the insolation on the collector shortly decreased.

In Figure 2.7 the temperature profiles of the dry collectors' parts on the above-mentioned day are shown. With rising intensity of the sun the temperatures of the absorber increased and reached a maximum of 195°C. The respective figure for the glazing peak on this day amounted to 85°C. While the sensor at the frame near the outlet was reaching temperature as high as approximately 70°C, the backside was heating up to 65°C.

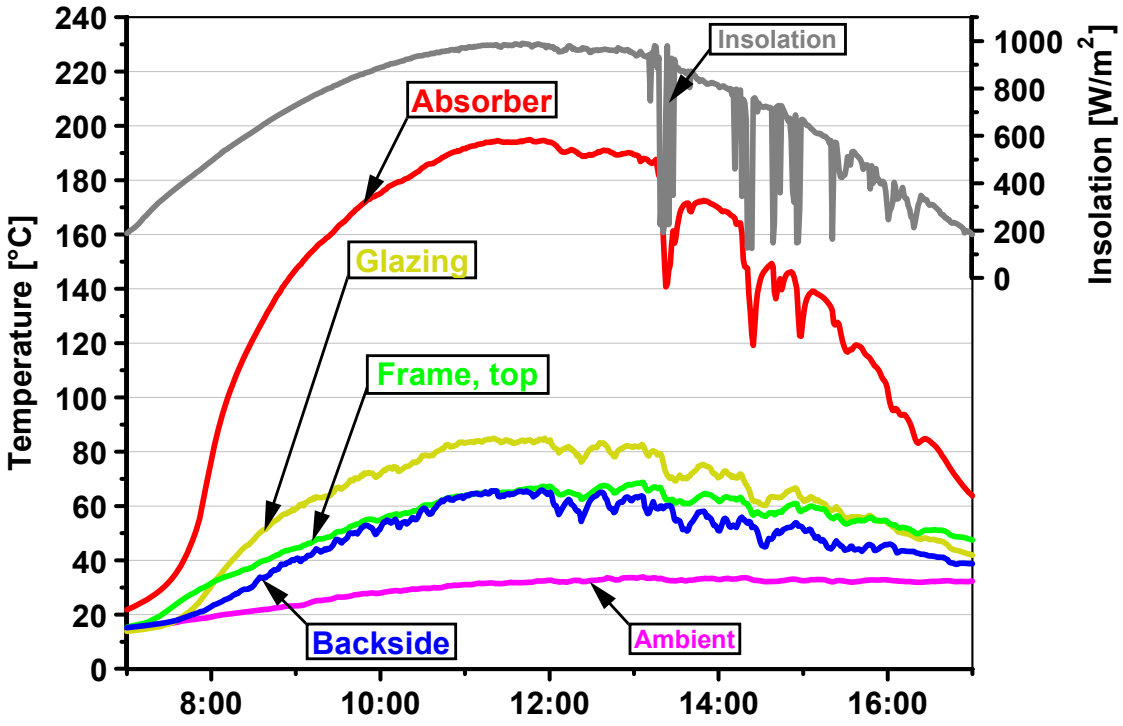

Figure 2.7: Temperature profile of the dry collector during a summer day (16th August 2009)

Figure 2.8 visualises the temperature profile of the collector in the system on 9th January 2009 while at the same time insolation was varying and low ambient temperature prevailed. This diagram is a perfect example to demonstrate the dependency on the insolation. The figures for the absorber fluctuated heavily as the

absorber was subject to solar irradiance, whereas the parts of the housing varied only marginally. The temperature of the glazing was also affected slightly by these changes. At about 1 o´clock p.m. the absorber temperature was hot enough to supply the storage and the circulation set in. The fluctuations in fluid and absorber temperature were obviously caused by a chopping of the pump in the solar system while the collector flow temperature was ranging around the set-point temperature of the controller. The absorber temperature was increasing until the collector operation started off. Afterwards, the temperature level was almost constant. The temperatures of the casing and the glazing had risen to 16°C and 19°C, before the temperature dropped due to decreasing insolation (Reiter et al. 2009a, 2009b).

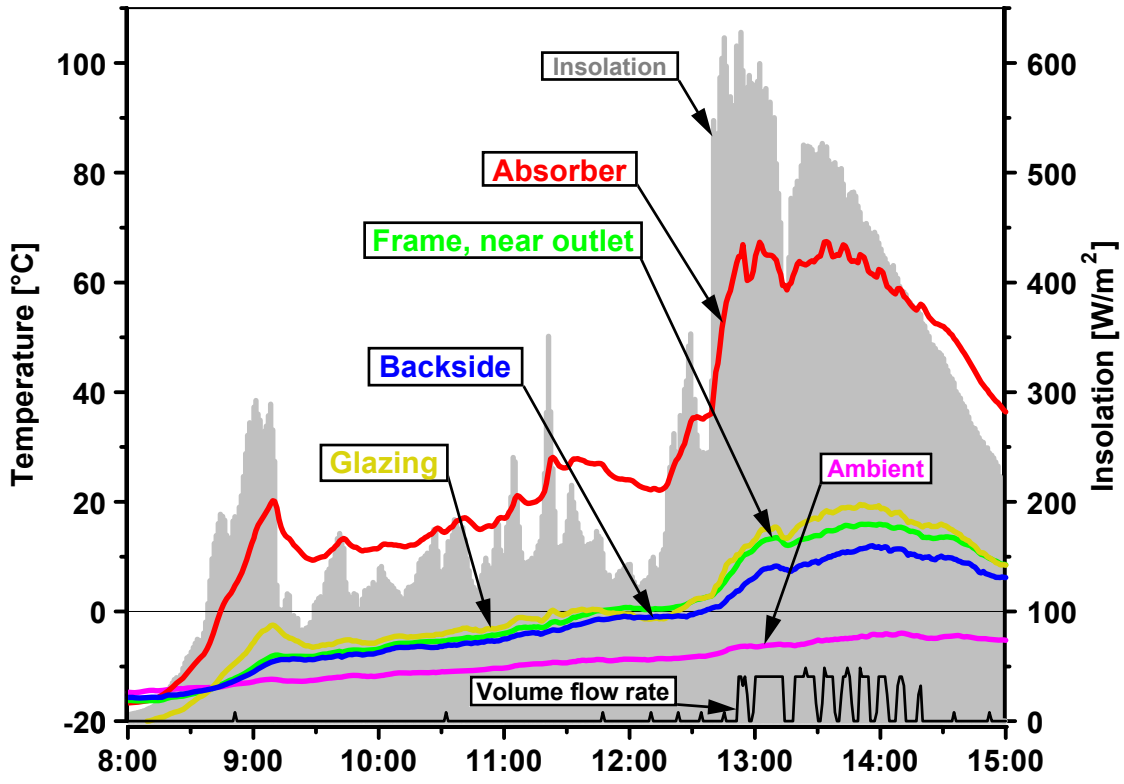

Figure 2.8: Temperature profile of the collector in the system (9th January 2009)

Figure 2.9 displays the temperature profiles of the dry collector for the same period. When having an insolation of only 600 W/m² and an ambient temperature of -5°C, frame temperatures as high as 15°C and a backside temperature of 10°C

were reached. During the peak sun-hours starting at about 12.30 o'clock the absorber temperature increased well above the level of 100°C whereas the absorber temperature of the collector in the system reached only 67°C. Under these ambient conditions the temperature differences at the housing between the dry collector and the collector in the system were only marginal. Moreover, the influence of the ambient air at these conditions was crucial for the housing parts.

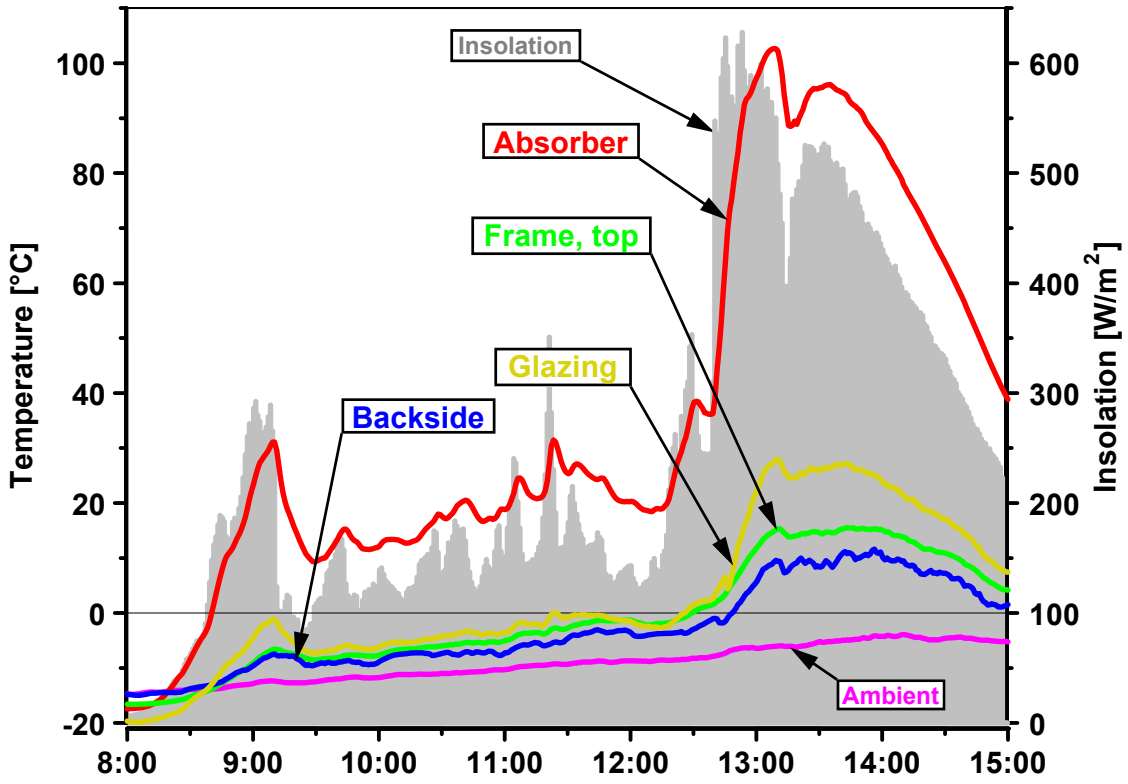

Figure 2.9: Temperature profile of the dry collector (9th January 2009)

Beside the maximum values of the temperatures at the collector, the dynamic behaviour of collector parts is of significant importance. On the one hand the quick temperature changes have to be considered in the construction of the collector because the parts have different thermal expansion properties. On the other hand time intervals for the reaction of overheating protection measures can be estimated. Figure 2.10 exemplary shows a rapid increase of the absorber temperature in the dry collector on 14th January 2008. Back then the absorber temperature rose to 140 K within 40 minutes although the ambient temperature was slightly above 0°C. In this case, the housing parts saw only a slight increase in

temperature to about 25 K. As a reason for this, housing parts can be characterised as relatively inert.

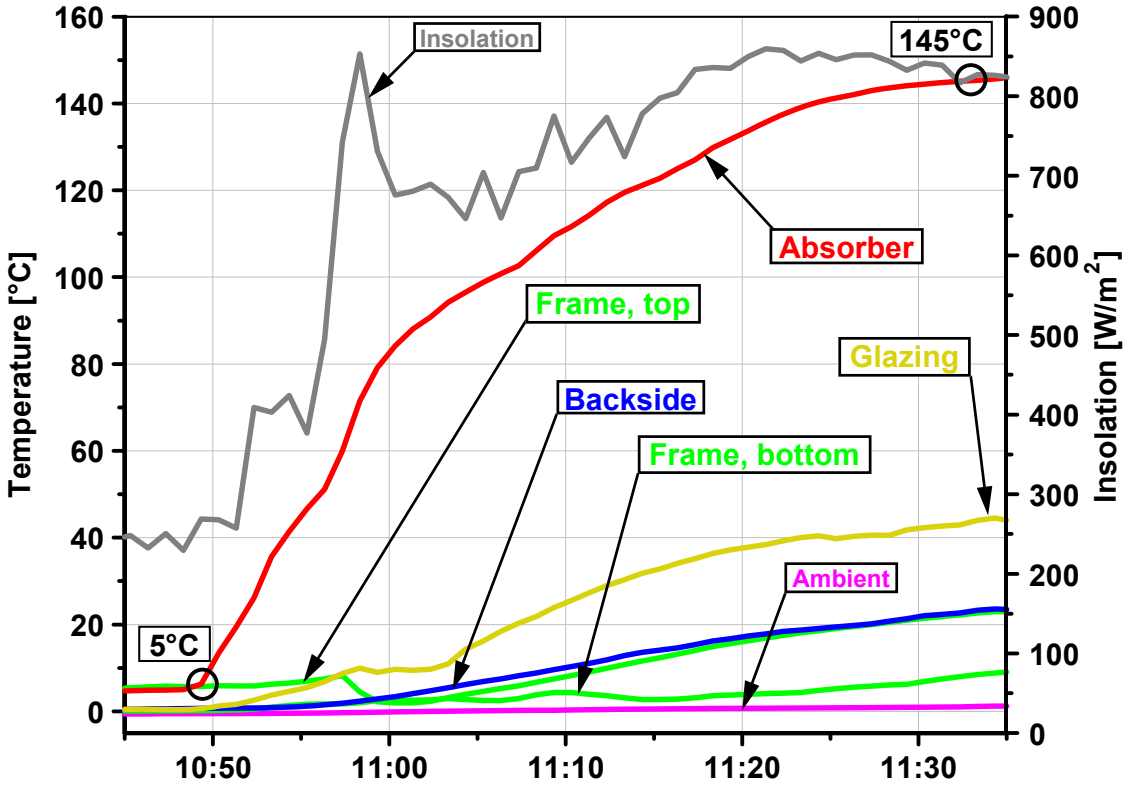

Figure 2.10: Temperature increase of the dry collector (14th December 2008; Reiter et al. 2012)

Figure 2.11 clearly shows the heavy fluctuations in the temperature of the absorber during stagnation. The chart demonstrates that the absorber reacted heavily within the given period to boundary conditions whereas the frame and backside sheet fluctuated only marginally. Within 2.5 h the temperature has risen to 125 K and again decreased to 121 K. The sequence of the cooling curve is larger than the expected cooling curve with constant cloudiness caused by short periods of high insolation. The longer-than-expected cooling curve has been caused by short periods of high insolation while the sky was largely cloudy. During this period the temperature of the housing rose from 12°C to 35°C. The temperature of the bottom edge reached its maximum level of almost 26°C. The ambient temperature varied between 9°C and 14°C (Reiter et al. 2009a, 2009b).

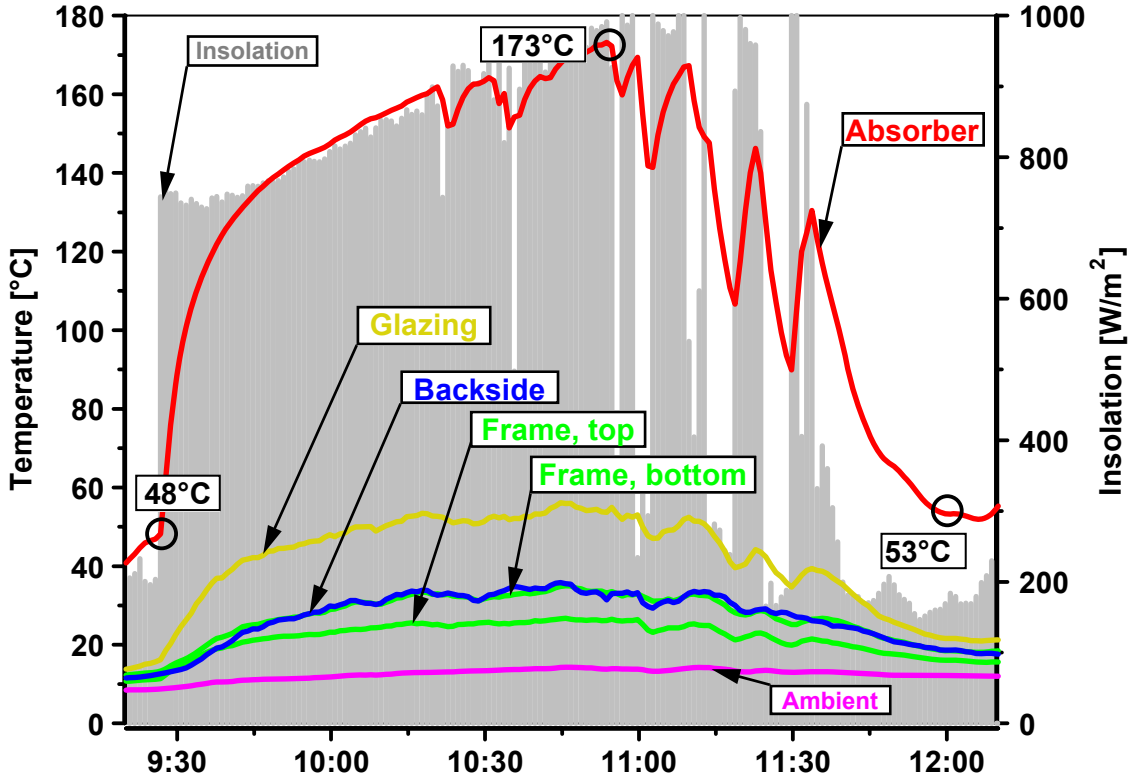

Figure 2.11: Temperature increase and decrease of the dry collector (26th September 2008; Reiter et al. 2012)

2.2.2 Annual Temperature Load Profiles

The annual occurring thermal loads were evaluated using histograms with a bin width of 10 K by applying the temperatures of the collector parts from 1st January 2009 to 31st December 2009 (Reiter et al. 2010a and 2010c). Due to problems with the data logger in March and June 30 days of the measurement period are disregarded. The coordinated systems in the diagrams are scaled to display the high temperatures. Hence, the data at low temperatures near the ambient temperature level are outside of the array and cannot be considered in detail.

The absorber in the collector in the system reached temperatures of up to 140°C during the operation of the solar circuit. On the contrary, the absorber sheet in the stage of stagnation temperatures rose to 192°C. The high temperatures were measured near the flow of the absorber in the upper part of the collector. Figure 2.12 shows the annual evaluation of this metering point. The solar-thermal

system hardly came to a halt although the collector array has large dimensions. This result was caused by the operation of the radiators in the basement. These were used as an overheating protection measure to avoid the stagnation of the system because the maximum storage temperature will not be exceeded. The general scaling of the y-axis was chosen from 0 to 500 hours to highlight the relevant temperature levels of the collector parts in the analysis. The cut-off durations at moderate temperature levels near the ambient temperature have a minor importance for the investigation of critical thermal loads for polymeric materials.

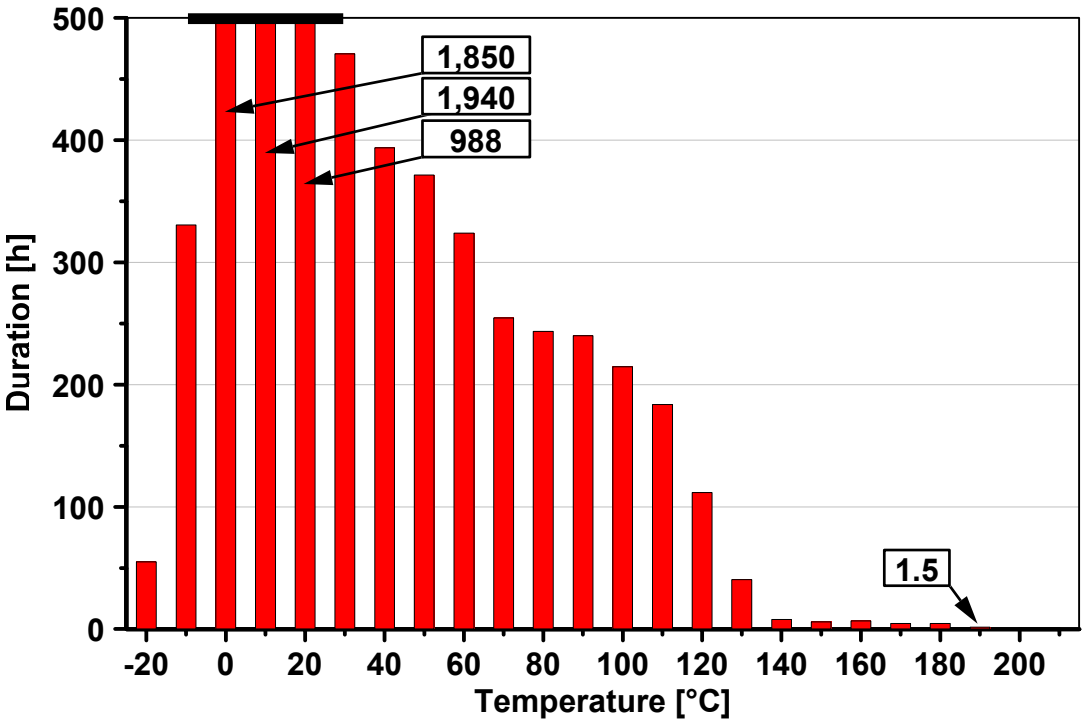

Figure 2.12: Histogram of the temperatures of the absorber sheet of the collector in the system (according to Reiter et al. 2012)

The hottest measurement point in the dry collector was situated in the middle of the sheet. The logger recorded a maximum temperature of 208°C. Figure 2.13 demonstrates that the absorber has reached high temperatures several times. For more than 1,100 h in the year the absorber was at temperature levels above 95°C.

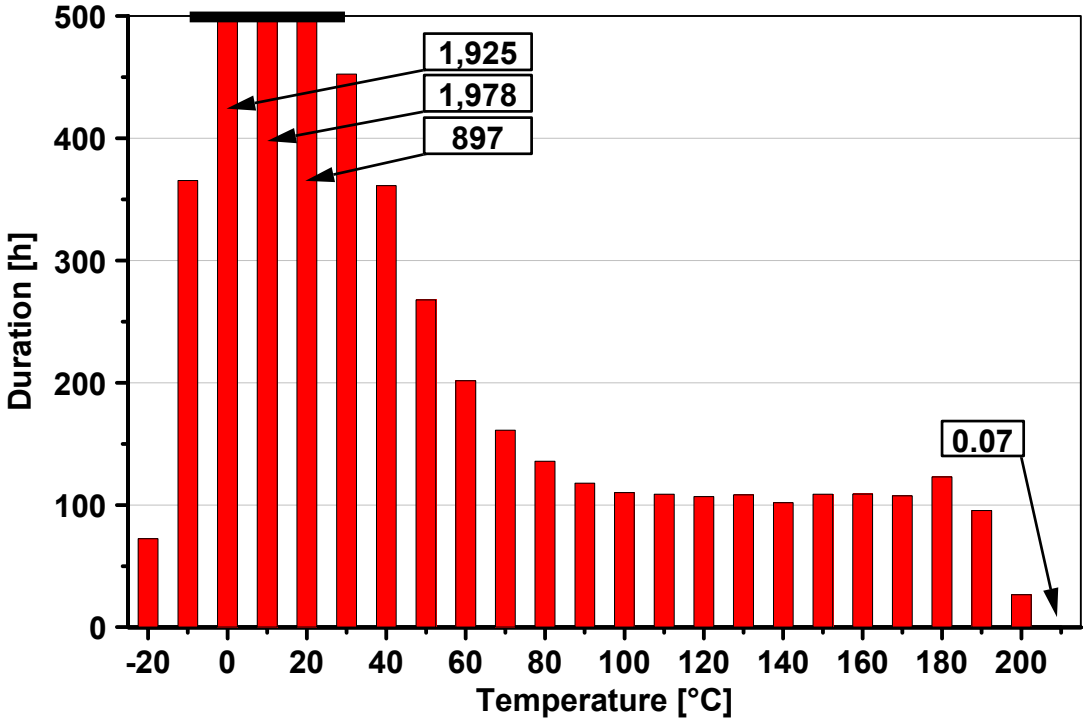

Figure 2.13: Histogram of the temperatures of the absorber sheet of the dry collector (according to Reiter et al. 2012)

The temperature of the transparent cover was measured with a bonded sensor at the inner surface installed at the centre of the sheet. Thermal load above 55°C mainly occurred during stagnation periods of the system (Figure 2.14). The highest measured temperature has been 82°C. Almost always the cover temperature for the use of transparent polymeric materials has been ranging within harmless temperature ranges.

The temperature sensor of the cover in the dry collector had the same position. The metered values were significantly higher than the values of the collector in the system (Figure 2.15). Within the stated period the cover temperature was under consideration 585 h over 55°C with the maximum temperature of 86°C.

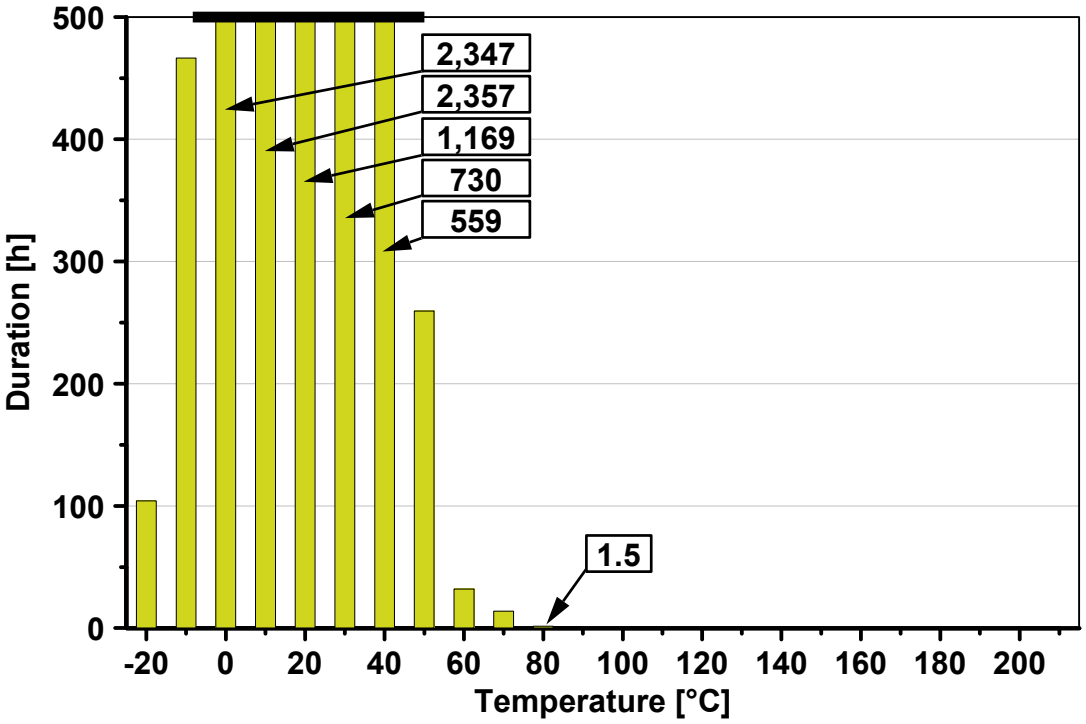

Figure 2.14: Histogram of the temperatures of the glazing of the collector in the system (according to Reiter et al. 2012)

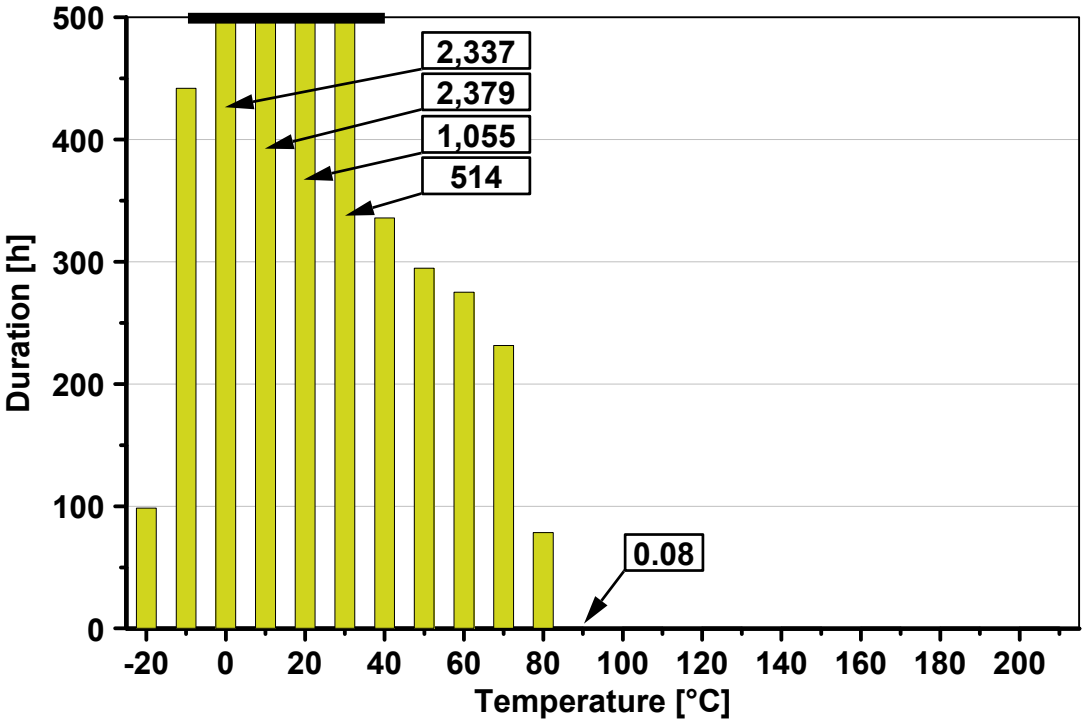

Figure 2.15: Histogram of the temperatures of the glazing of the dry collector (according to Reiter et al. 2012)

In order to identify the temperatures of the frame sensors have been riveted on the inner surface of the aluminium frame. On each edge two sensors have been fixed between the side insulation and the frame. The investigated and displayed sensor has been positioned at the top edge near the flow. Consequently, with this position it was the hottest measurement point of the frame. Figure 2.2 shows the sensor in the right picture. At this position the temperature reached a value of 79°C. The major part of the measured period, however, the frame temperature remained below 65°C due to the influence of the ambient temperature. Figure 2.16 displays the common low temperature level near the flow.

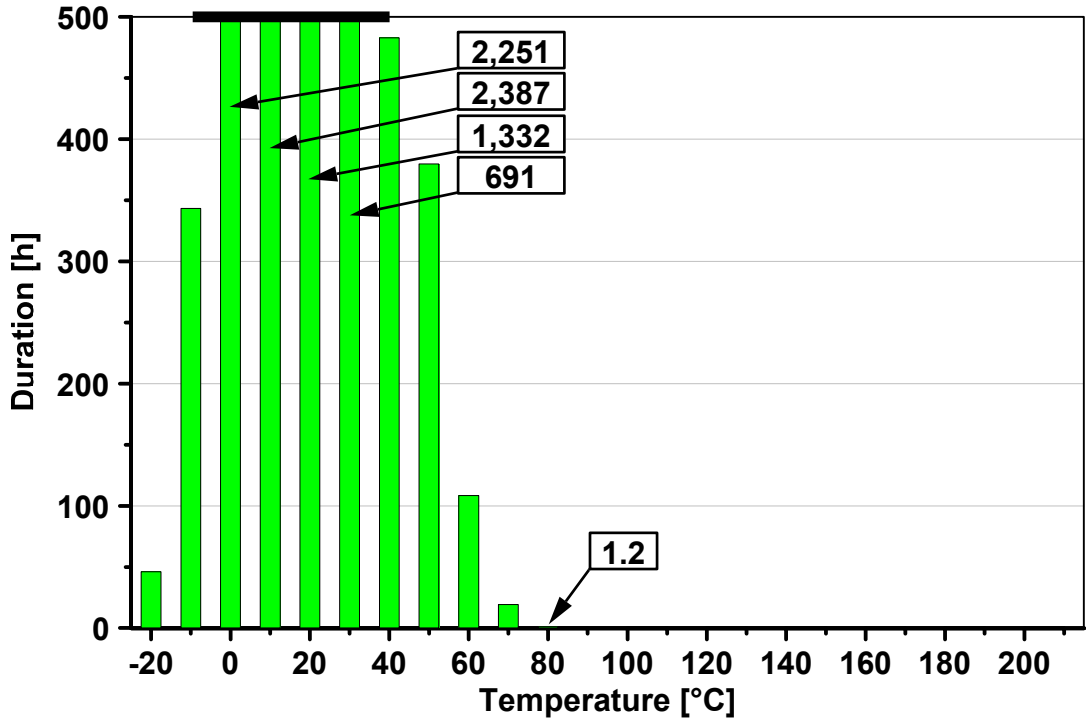

Figure 2.16: Histogram of the temperatures of the frame of the collector in the system (according to Reiter et al. 2012)

The metering point at the dry collector was positioned at the centre of the upper frame part. The temperature reached slightly lower values as the hot header pipe did not have any impact on the absorber (Figure 2.17).

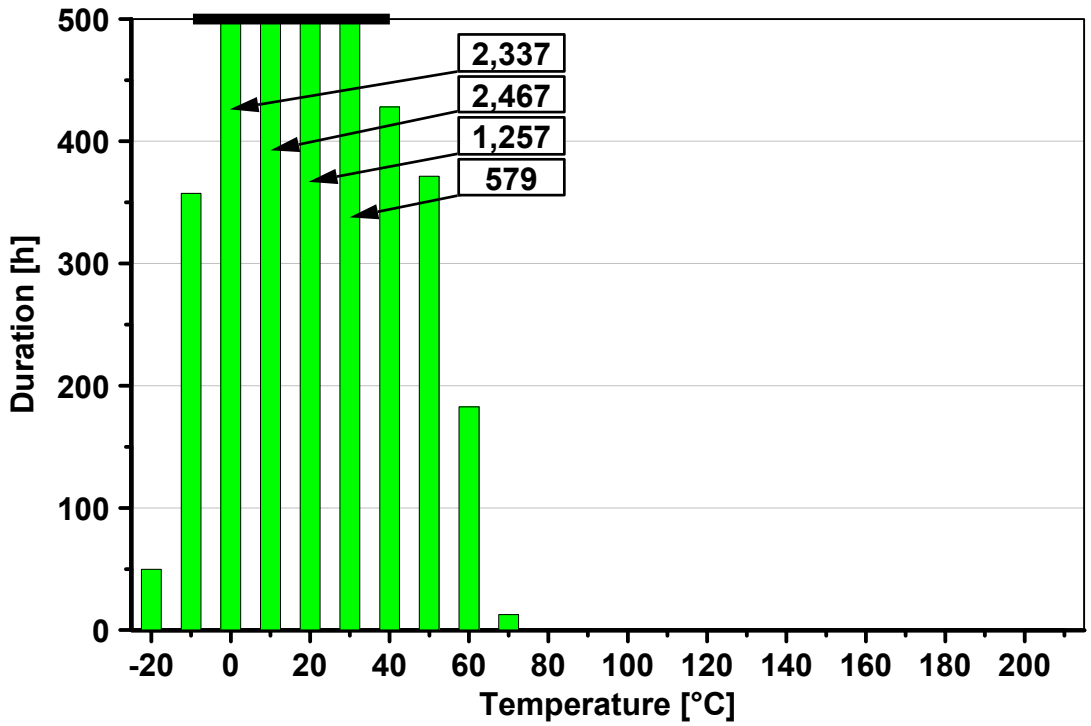

Figure 2.17: Histogram of the temperatures of the frame of the dry collector (according to Reiter et al. 2012)

The temperature of the backside plate of the collector in the system was measured in central position. Figure 2.18 shows that relatively low temperatures of this part were recorded. The temperature level of 68°C was not exceeded. Generally, this level is very low and is not considered to have negative impacts on the process of the material selection for this array.

In comparison to another metering point in the upper part of the collector in the system below the header, the dwell at temperatures with around 50°C and 60°C was significantly higher. The maximum temperature of 72°C differed only marginally. The metering point of the dry collector was also in central position of the backside sheet. The maximum temperature of the sensor in the collector which was not installed in the system was 66°C (Figure 2.19). Finally, during the whole year no harmful temperatures for low-cost polymers were recorded.

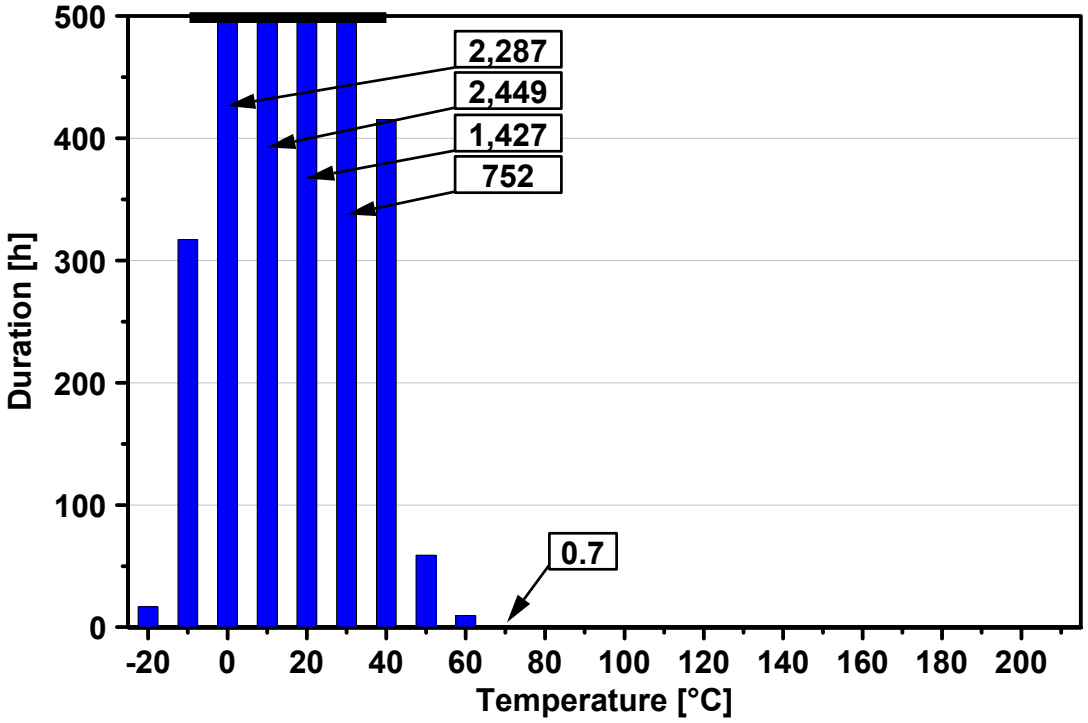

Figure 2.18: Histogram of the temperatures of the backside sheet of the collector in the system

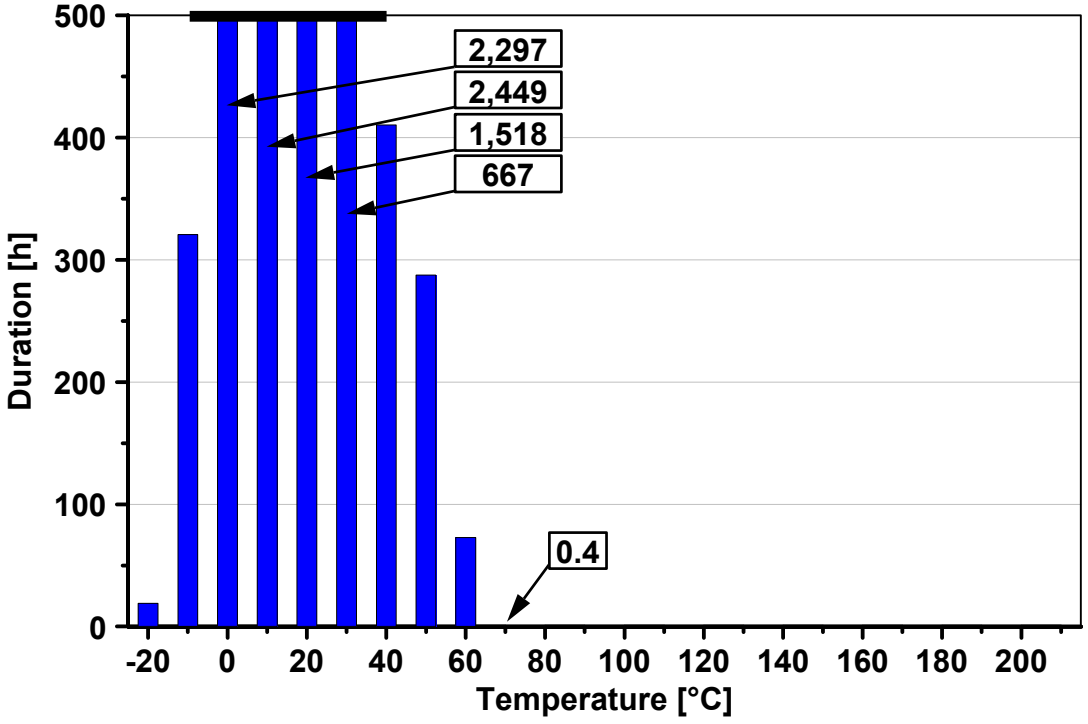

Figure 2.19: Histogram of the temperatures of the backside sheet of the dry collector

In summary, the field-testing measurement shows that the material selection depends on the specification of each part of the collector regarding to the temperature gradient. Hence, a common maximum temperature of the collector as it is currently determined in standardised measurement procedures e.g. according to DIN EN 12975-2 (2006) is not an adequate approach. As a result from field-testing the measured data clearly show that temperatures at the housing do not represent major obstacles for low-cost polymers, even in state-of-the-art collectors. The absorber as well as the arrays with contact to the absorber such as the insulation reach high temperatures and are at the same time subject to considerable temperature fluctuations.

2.3 Pressure Loads in the System

The pressure loads were measured in the solar circuit near the store in the basement. The solar circuit is equipped with a membrane expansion vessel (nominal volume 60 l) and a safety valve, which allows a maximum pressure of 600,000 Pa. The measured absolute pressure in the circuit combines the static pressure and the dynamic pressure in the system. The value of the static pressure consists of the sum of the pressure of the fluid from filling the system as well as of the weight of the hydrostatic head in the pipe up to the collector (Hadamovski and Jonas 2000).

There are three elements contributing to an increase in the system pressure, namely the dynamic pressure caused by the pump as well as by the pressure drop through friction at the walls of the pipes and the third component is the viscosity of the fluid.

The pressure mainly depends on the fluid temperature. The hot fluid has an expanded volume and fills the membrane expansion vessel while the gas buffer is compressing and the pressure is rising steadily. Under extreme weather conditions the hot fluid even evaporates and its volume rises enormously. This state

occurs during stagnation of the system and as a consequence of which the pressure reaches the peak value. Figure 2.20 shows the three described system states in the membrane expansion vessel.

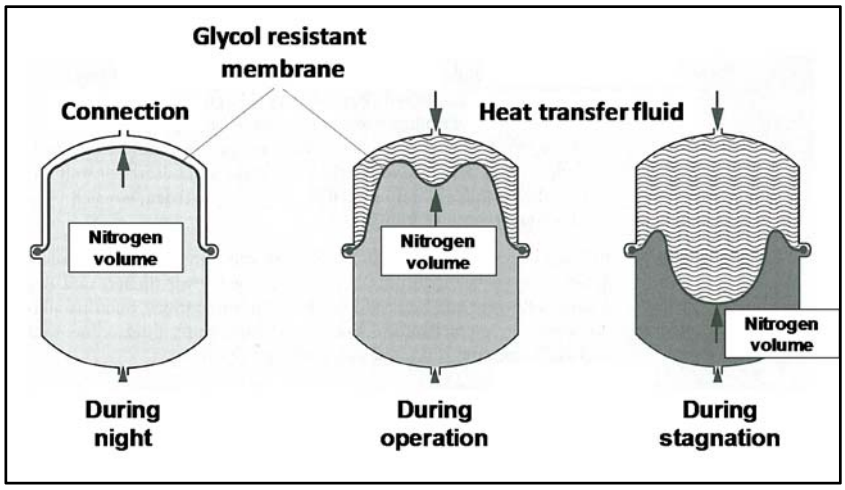

Figure 2.20: Operating conditions of the membrane expansion vessel (according to Hadamovski and Jonas 2000)

Figure 2.21 shows the gradient of the system pressure during the night, system operation and stagnation (red array).

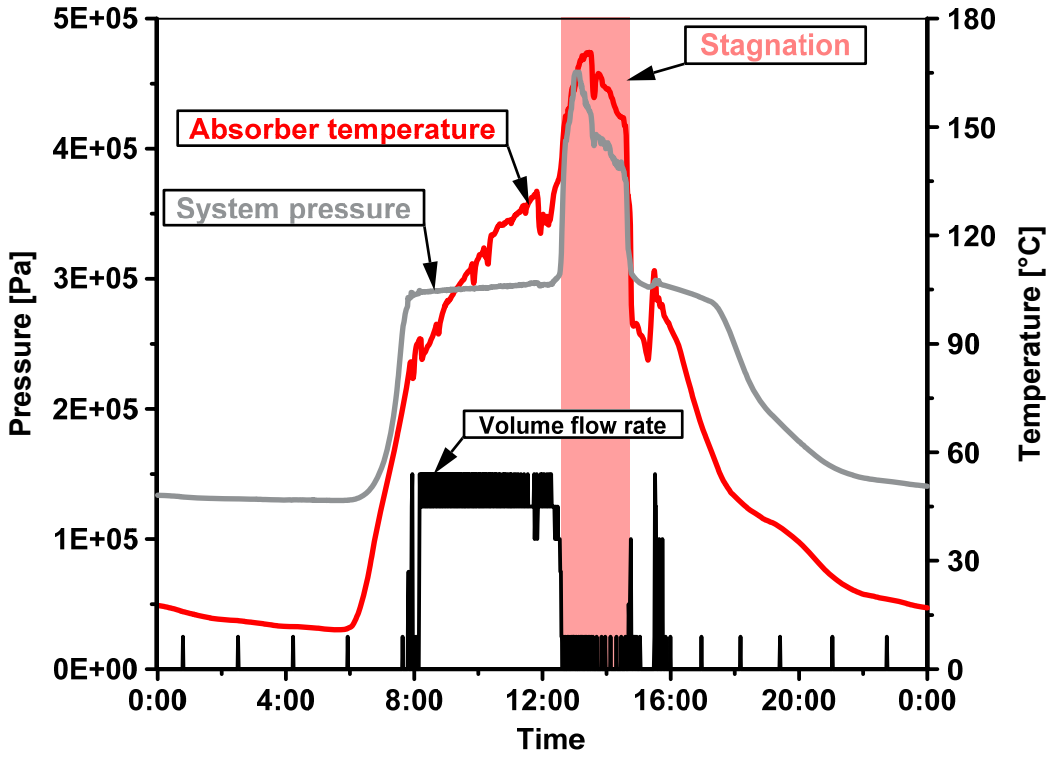

Figure 2.21: Increase and decrease of the pressure in the solar circuit during operation and stagnation (1st August 2009)

In the case of the above-mentioned field-testing the system pressure during the night was lower than the primary pressure in the membrane expansion vessel. Hence, the vessel was empty and the pressure of the fluid in the system rose along with the temperature. The system pressure was rising between 6.00 and 8.00 o'clock a.m. until the system pressure is equal to the primary pressure in the expansion vessel. Afterwards, the fluid filled the vessel and compressed the gas pocket. During this process the system pressure was relatively constant because the fluid volume changed only slightly in comparison to the gas volume of the vessel. In the interval between about 8.00 and 12.00 o'clock a.m. the solar-thermal system was in operation. After operation the fluid temperature rose abruptly and the fluid evaporated. During stagnation the volume change of the evaporated fluid was large and the gas pocket was compressed strongly. Hence, the pressure was subject to rapid changes and reached its maximum.

Figure 2.22 demonstrates that under low temperatures the static pressure was between 100,000 Pa and 150,000 Pa during the night. The pressure under the conditions during the operation of the solar-thermal system was around 290,000 Pa.

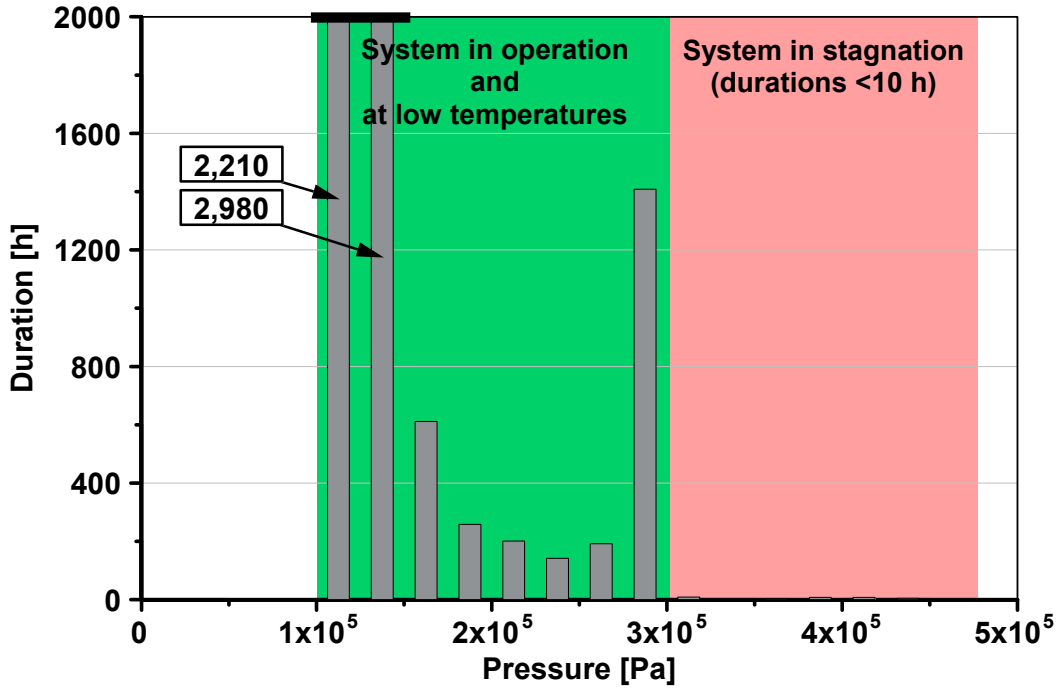

Figure 2.22: Histogram of the fluid pressure in the solar circuit

Stagnation in the system only occurred when the fluid or absorber temperatures rose above 140°C. Figure 2.23 shows the duration of the system pressure during stagnation in a detailed view. The pressure rose in a range between about 300,000 Pa and a peak value of 462,000 Pa.

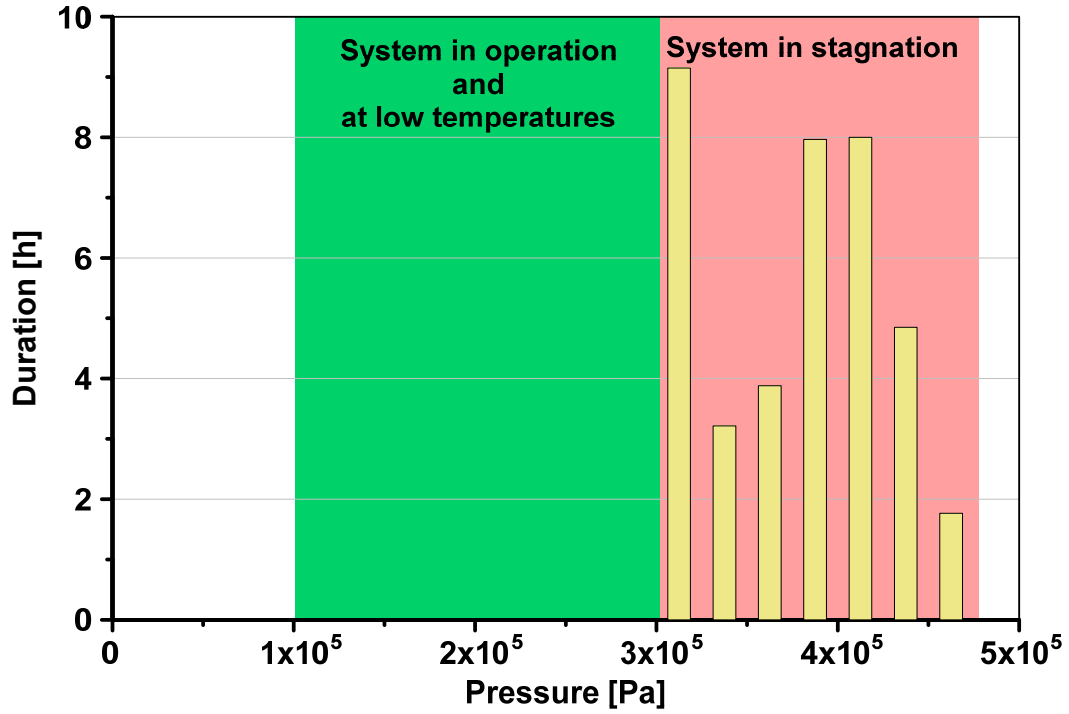

Figure 2.23: Histogram of the fluid pressure in the solar circuit during stagnation (detailed view)

As expected the system pressure rises to high values and is a main obstacle for plastics with limited mechanical strength. In particular at temperatures near the maximum temperature of the material the pressure load is at its maximum value. The mechanical strength, however, decreases with the material temperature. Moreover, most volumetric absorbers designs used for polymeric absorber constructions are even more deformable under these conditions because of their disadvantageous large channel width. Hence, a non- or extremely low-pressurised system is necessary for the use of plastics in absorber.

3 Overheating Protection

The identified critical high temperature loads — especially at the absorber — have to be avoided to realise polymeric collector designs. Therefore, potential concepts for the necessary overheating protection have to be developed and investigated according to the conceptual design process described in Pahl et al. (2007).

In a functional analysis of the collector and the solar-thermal system, the main functions and sub-functions of the components were analysed in order to identify and systematise basic operating principles which avoid critical component temperatures. Accompanied by a worldwide literature and patent research in various fields of technology, this was followed by the development and the investigation of applicable overheating protection approaches. Finally, a preselection of the most promising approaches according to their obvious properties was conducted. This selection is the basis for an extensive simulation analysis regarding thermal collector loads and solar yield.

3.1 Functional Analysis of Collector and System

For the development of overheating protection concepts, the complete system was analysed with regard to its sub-functions and was mapped onto a function structure based on thermal processes. The function structure consists of several levels, where the top level shows the overall function considering the flow of material, energy and signals. This can then be divided into main functions and sub-functions of the different parts of the collector. The advantage of this methodology is the illustration of the entire thermal processes regarding components and system in the detailed function structure, where potential possibilities for overheating protection and their operating principles can be identified systematically. The system was therefore divided into two parts, where on the one hand the collector and on the other hand the solar system without the collector were analysed.

On the top level of the function structure of the collector only the flows of material, energy and signals crossing the system boundary of the collector were considered (Figure 3.1). The overall function of the collector was defined as "conversion of radiation into heat''. The heat is removed from the collector by a cold medium flow through the collector. A part of the collector's energy is released due to losses from the collector to the ambient. A control signal is led from the collector to the solar system controller. Figure 3.1 illustrates that the collector is supplied with energy by solar radiation and dissipates the energy via losses and fluid circulation. Thus, there are two obvious principles to prevent overheating: Either the incidence respectively the conversion of solar radiation in the collector is reduced or the thermal energy in the collector is removed.

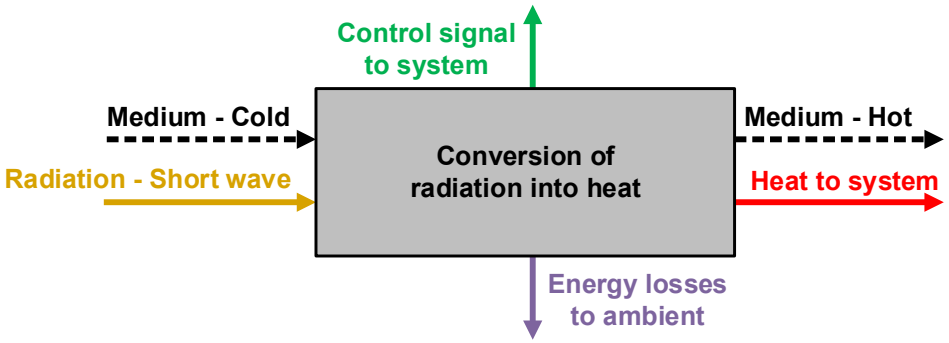

Figure 3.1: Function structure of the solar-thermal collector with overall function and flow of material, energy and signals

The main functions of the collector refer to the parts of the collector (Figure 3.2). The transparent cover has the functions to let pass the incoming short-wave radiation and to reduce the energy losses of the absorber at the front side. The functions of the cover sheet are obviously connected to energy losses. The absorber converts the solar radiation into heat, which is removed from the collector by the fluid, and as well causes energy losses. The control signal contains the temperature of the absorber. The back side insulation reduces the heat losses of the absorber.

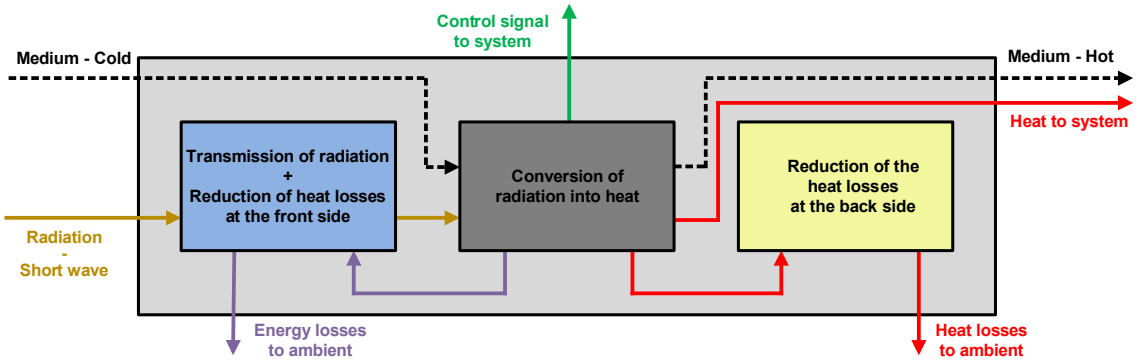

Figure 3.2: Function structure of the solar collector with main functions of transparent cover, absorber and back side insulation

Figure 3.3 shows the next deeper level of the function structure for the cover with its sub-functions.

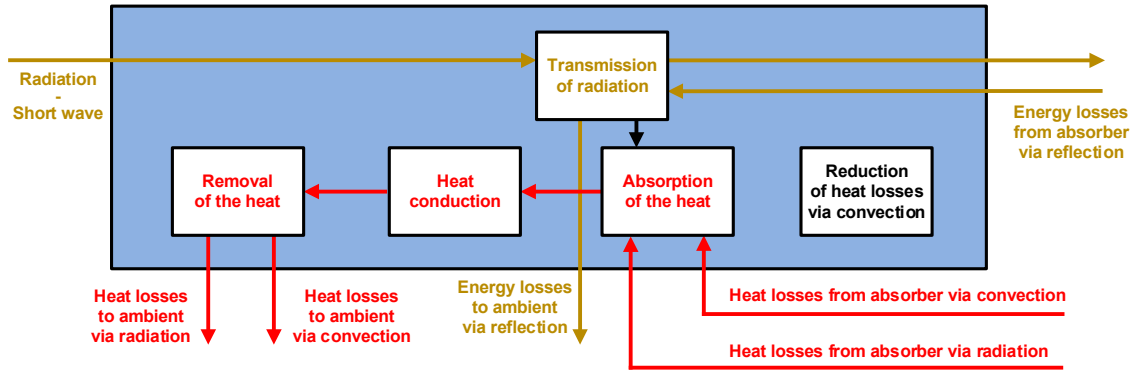

Figure 3.3: Sub-functions of the transparent cover

Possibilities for overheating protection at the transparent cover can for example be found in the functions “transmission of radiation” and “reduction of convection”. Hence, the collector could be protected by reducing the amount of radiation transmission or by increasing the convective losses at the front side.

Figure 3.4 shows the function structure of the absorber with its sub-functions. In the operating state of the solar-thermal system a cold medium flows through the absorber while the absorber converts the incident solar radiation into heat and transfers the heat to the medium. Potential overheating protection at the absorber could be the variation of the absorption characteristics for solar radiation or the variation of the emission characteristics regarding infrared radiation. Apart from that, unused heat could be transported out of the collector by the fluid loop.

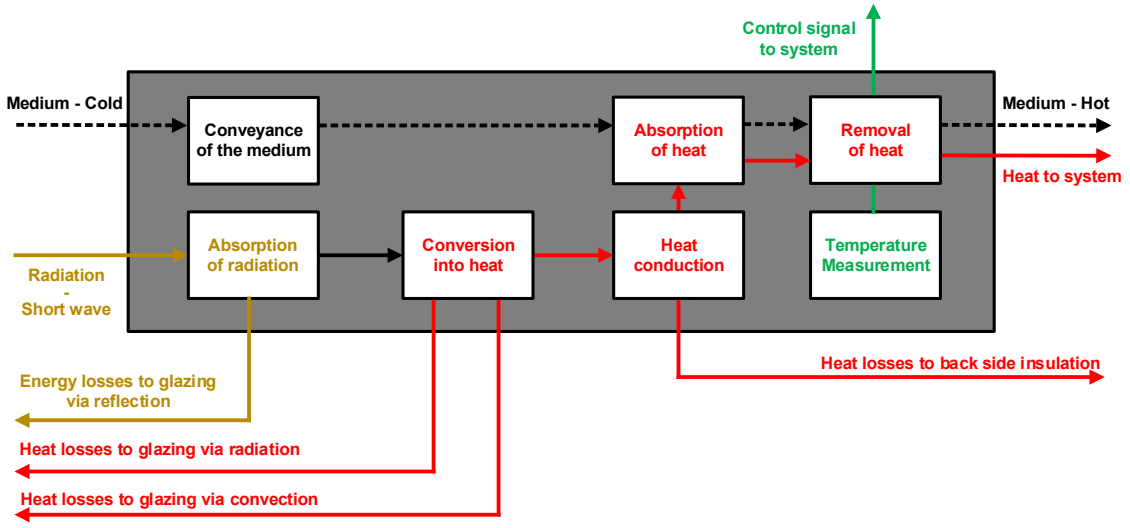

Figure 3.4: Sub-functions of the absorber

Figure 3.5 illustrates the function structure of the back side insulation with its sub-functions. At the back side insulation for example the function “reduction of heat transfer” could actively be influenced depending on the operating state.

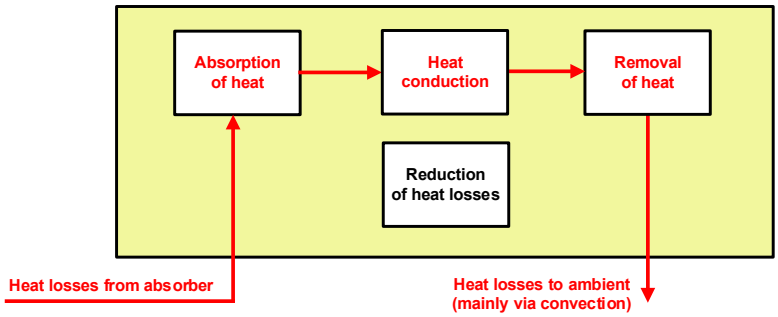

Figure 3.5: Sub-functions of the back side insulation

Apart from the collector, the solar-thermal system was analysed where the overall function is to supply the consumer with heat (Figure 3.6). A typical system has a thermal storage that absorbs and emits thermal energy through several fluid circuits to execute this overall function. The system controls the fluid circuit of the collector and extracts thermal energy from the medium. Additionally, heat is supplied by a back-up system. The control signal of the collector is transferred to the controller, which activates or deactivates the fluid circulation. Electricity is required by the system to operate the circulation pumps as well as the measurement and control equipment. Thermal energy is removed from the system by heat

supply to the consumer and by losses. Thus, the system provides two basic possibilities for the removal of thermal energy from the collector: The energy can be removed by thermal losses to the ambient or by transferring the heat to a sink.

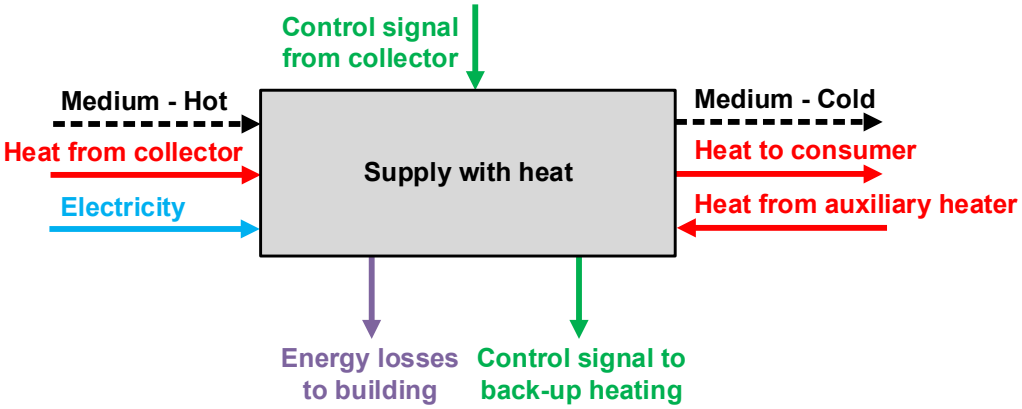

Figure 3.6: Function structure of the solar-thermal system (without collector) with overall function and flow of material, energy and signals

Figure 3.7 shows the function structure of the solar-thermal system with its main functions related to assembly groups. The first group consists of the fluid circuit connected to the collector and the controller, which activates the fluid circuit and transfers heat from the collector to the thermal storage. For managing the operation mode of the pump, the controller uses the temperature signals from the collector and the thermal storage. The second assembly group contains the thermal storage unit transferring heat to the consumer and absorbing heat from the back-up heating if required.

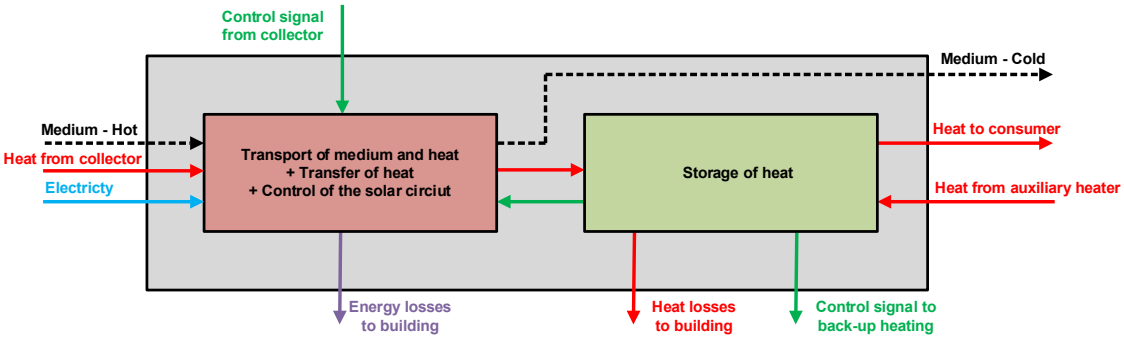

Figure 3.7: Function structure of the solar-thermal system with main functions of the assembly groups fluid circuit and thermal storage

Figure 3.8 shows the function structure of the fluid circuit with its sub-functions. The pipes of the fluid circuit convey the medium from the solar collector to the

heat exchanger in order to transfer the heat of the medium to the thermal storage. There are thermal losses in the piping through heat conduction to walls and convection at the insulation of the pipes.

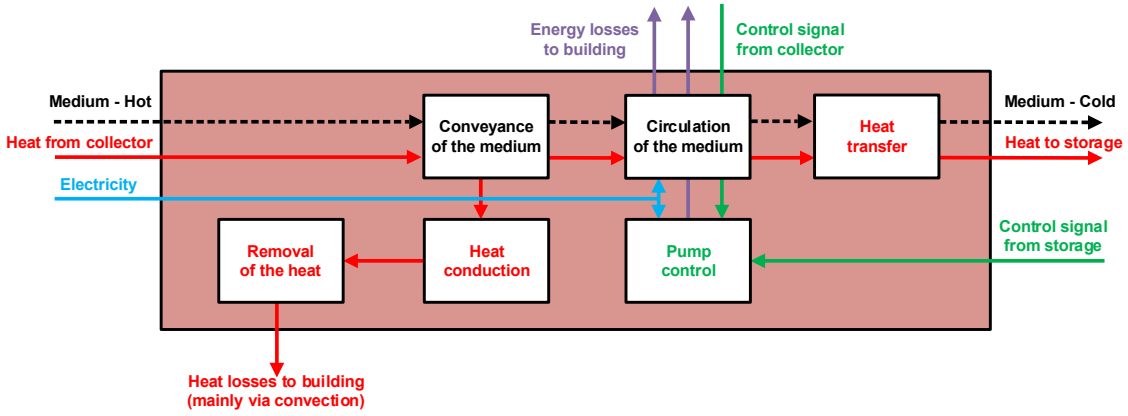

Figure 3.8: Sub-functions of the fluid circuit

The thermal storage shown in Figure 3.9 absorbs the heat from the collector and the back-up heating and emits the heat to the consumer, when it is requested. When heat is stored, there is a loss of thermal energy due to heat conduction through the storage wall and convection at the surface of the insulation. The integrated temperature measurement transmits information for the controller of the fluid circuit and the back-up heating regarding charging of the thermal storage.

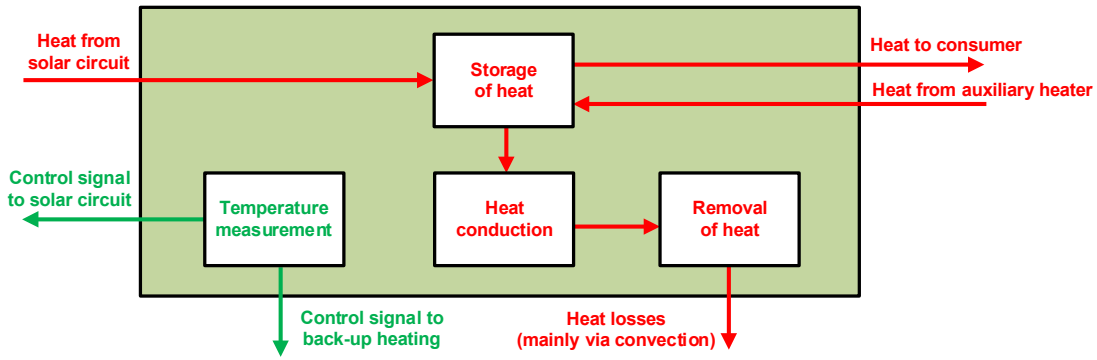

Figure 3.9: Sub-functions of the thermal storage

3.2 Overview on Approaches for Overheating Protection

Based on the derived function structure of component and system, where fundamental mechanisms regarding overheating could be identified systematically, applicable operating principles and solution approaches for overheating protection of collectors were developed (Reiter et al. 2010b; Reiter et al. 2012). Additionally,

a worldwide literature and patent research in various areas of technology was carried out. Finally, approaches were summarised and classified aiming at the creation of a systematised overview on known, studied or potential overheating protection measures for solar collectors.

For an overall systematisation of overheating protection measures, two basic principles have to be differentiated: firstly, the optical efficiency can be reduced or, secondly, the removal of excess thermal energy can be increased (Figure 3.10).

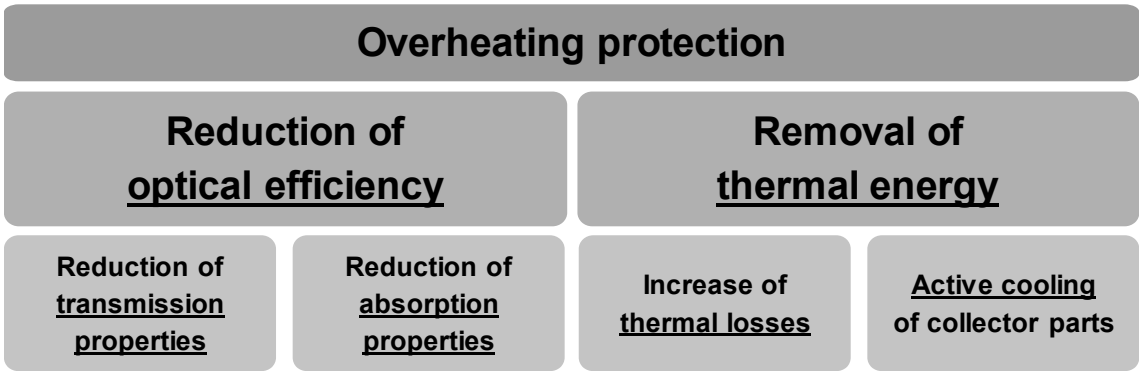

Figure 3.10: Systematisation of overheating protection measures
(according to Reiter et al. 2012)

A reduction of the optical efficiency means that either the collector front side transmits less solar radiation or alternatively the absorber surface converts less solar radiation into heat. Hence, these measures change the effective transmission-absorption product. Figure 3.11 shows the potential mechanisms that can reduce the optical efficiency of a collector.

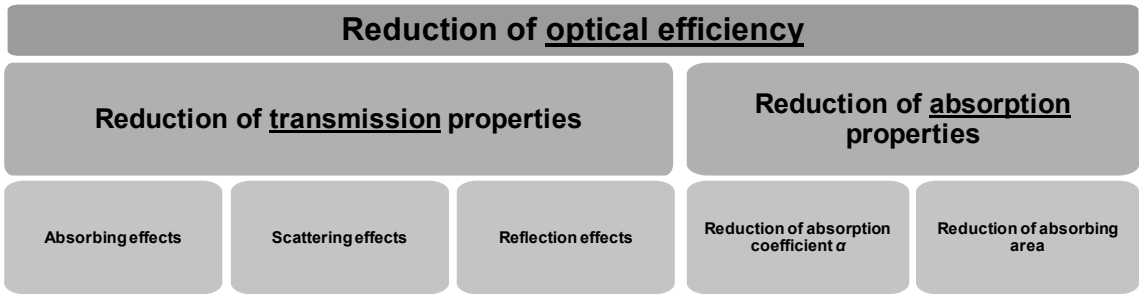

Figure 3.11: Overview on mechanisms reducing the optical efficiency
(according to Reiter et al. 2012)

In addition to reducing the optical efficiency, the removal of excess thermal energy is an option (Figure 3.10) realised either by thermal losses of the solar collector or by cooling with fluid circuits. Figure 3.12 shows the categories for the removal of thermal energy, which can be applied in the collector or in the solar-thermal system.

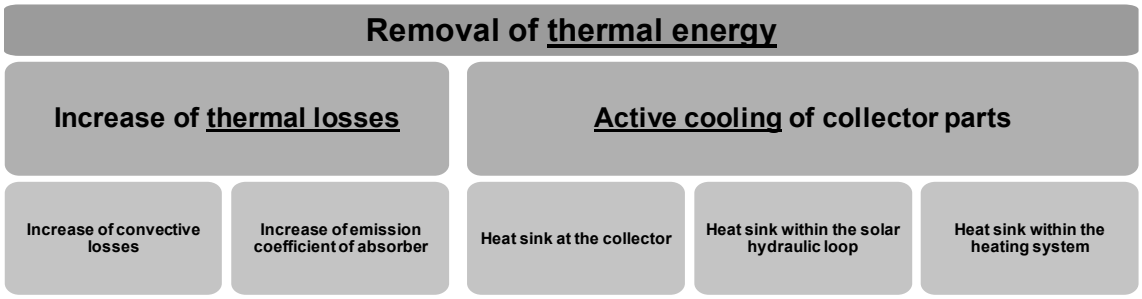

Figure 3.12: Overview on mechanisms and solutions for the removal of excess thermal energy (according to Reiter et al. 2012)

For any mechanism shown, several technical solutions are in principle available and described below.

3.3 Changing the Transmission Properties

The transmittance of a collector can be reduced by measures having absorbing, scattering or reflecting effects. These measures can be characterised into their technical solutions presented in Figure 3.13.

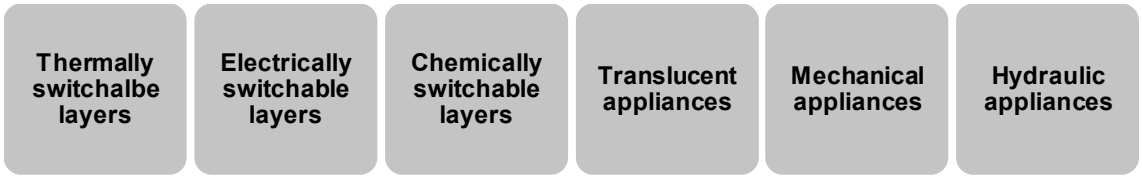

Figure 3.13: Groups of technical solutions for the reduction of the transmission properties (according to Reiter et al. 2012)

3.3.1 Thermally Switchable Layers

Thermal switchable layers for changing the transmission properties of the front side of the collector are clear for solar irradiation in the normal state and reduce their transmittance above a certain temperature range. Therefore, the material

properties become partially absorbing or scattering for sun light. Due to these effects it must be differentiated between thermochromic and thermotropic layers.

3.3.1.1 Thermochromic Layers

After having reached a certain temperature, thermochromic layers change their colour and/or its absorption or reflection behaviour. As an application to the glazing, the above-mentioned layers are able to absorb the incoming solar radiation which normally increases during periods of high temperature. Afterwards, the converted heat is transferred to the ambient air as well as to the cold sky.

Babulanam et al. (1987) investigated a layer for “smart” windows eliminating the incidence of sun light at high ambient temperatures while solar gains at low ambient temperatures are accepted. The layer mainly consists of VO_2 and rapidly changes its semiconductor state into a metallic state at 68°C. For solar irradiance, the layer is very transparent in its semiconductor state. Should the layer convert into a metallic state, the main infrared part of the insulation is reduced by reflection and absorption. For the production of the layer, physical vapour deposition (PVD) is used. In this process an evaporated coating material condenses on the substrate in an evacuated space. In this case, the coating material is evaporated by sputtering. Therefore, the target or rather the coating material is bombarded with ions to extract vaporised material. The sputter deposition is carried out at temperatures between 300°C and 500°C. Hence, this layer is not suitable for an application on polymeric parts.

3.3.1.2 Thermotropic Layers

A thermotropic layer is a thin film suitable for deposition on a glazing or an absorber being transparent up to a certain trigger temperature. Above the trigger temperature this layer changes its state into a milky white state and is scattering or rather reflecting for incoming irradiance due to the particles which have evolved

and/or released during the process, crystals or droplets having a different refraction index when compared to the remaining material of the matrix. On bounding surfaces with different refraction indexes, the incoming beam changes its direction. Hence, the layer reduces its transmission coefficient since the light is deflected in all directions at a multitude of bounding surfaces. Several approaches for layer materials are possible to get this effect. These approaches can be divided into two main groups with phase separating systems on the one hand and systems with fixed domains on the other hand (Nitz and Hartwig 2005; Nitz and Wilson 2008).

The advantage of this overheating protection measure lies in the autonomous activation caused by the actual temperature. Thus, the protection is directly connected to the temperature of the component. This factor, however, needs to be controlled. The layer works automatically and does not have to be started by any mechanism and is intrinsically safe since it also functions during blackouts of the solar-thermal system or of the grid.

The phase separating systems consist of different components decomposing their phases above a trigger, hence a demixing temperature. Therefore, the material changes into a light scattering state. The principle occurs in various systems:

- *Hydrogels* have been developed for the use in smart windows. The layers consist of an aqueous polymer gel containing another long-chained polymer. Such polymer chains fade to a light scattering state above a certain trigger temperature. The gels are produced in a sandwich construction between two transparent plates to protect them against dehydration. Therefore, high standards have to be applied for the sealing. Also, the long-term stability level is very low and the layer has to be protected against UV radiation by a protective film (Nitz and Hartwig 2005; Resch and Wallner 2009). Hydrogel layers can be adjusted for trigger temperatures between 5°C and 60°C. A maximum transmission coefficient of 82 % is possible. After the opaque state has been reached, the transmission coefficient can

be reduced by up to 77 % (Resch and Wallner 2009). The costs vary significantly depending on the use of natural or synthetic materials. For windows in the building sector, a Japanese product with such a layer available has already been launched. The high requirements for sealing and UV-protection as well as the heavy weight and the material costs for the double glazing sandwich make the application in polymeric low-cost collectors almost impossible although the switching properties (change of transmission and trigger temperature) are promising (Resch and Wallner 2009).

- *Liquid Crystals* are used for layers to reach a light scattering level above a certain trigger temperature, achieved by means of a phase change or phase separation. Until now, no appropriate product has been launched onto the market (Nitz and Hartwig 2005).
- *Polymer Blends* are layers made of two liquid components turning into a homogenous mixture below a certain temperature. In the mixture, there are no local differences of the refraction indexes, whereas the layer appears clear. Above the set temperature, the components begin to separate and local regions with different refractive indexes can occur. As a result, the incoming radiation disperses, lacking clear orientation. Only partially suitable switching properties are provided for protecting the layer against overheating. The trigger temperature varies between a level of 30°C and 130°C, whereas the transmission coefficient for solar irradiation shows a level of 85 %. Transmission coefficients in the opaque state below 38 % are possible. However, switching from the clear state to the opaque state only occurs when wide temperature ranges are involved. Furthermore, the change from an opaque to a clear state has a large hysteresis of 15 hours. The layer is also damageable by humidity, causing an opaque state. Since there is still no suitable product available on the market and based on the above-mentioned problems, the use of such a layer type for overheating protection in collector is not possible (Resch and Wallner 2009; Nitz and Hartwig 2005).

Systems with fixed domains consist of two components with one component being the polymer matrix that contains the second component. The embedded component changes its refractive index when changing from a solid to a liquid state. Both materials show the same refractive index in the solid condition. If the component in the matrix melts, the refraction index changes and the material mixture scatters light (Resch and Wallner 2009; Nitz and Hartwig 2005). Layers with a thermotropic resin system significantly change their transmission within a transition region of 15 K. The maximum transmittance of these systems lies at 84 % with a reachable change of 25 %. The trigger temperatures can be varied by additives in an array between 25°C and 100°C (Resch and Wallner 2009).

Wallner et al. (2008) investigated possible applications of thermotropic glazings in solar-thermal collectors by means of simulation. The efficiency curves of various design approaches at 0°C and 30°C ambient temperature and 1,200 Wm^{-2} were computed. The approaches of the investigation were carried out by flat-plate collectors with single glazing and black absorber, single glazing with selective absorber, double glazing with black absorber and double glazing with selective absorber. The results indicated a large influence of the ambient temperature on the performance of the collector approaches with selective absorber. The lower heat radiation from the absorber to the glazing reduced the overall heat flow rate through the collector front side. Hence, the influence of the ambient conditions on the glazing as well as the thermotropic layer temperature rose enormously. In that case, it is not possible to define a suitable trigger temperature of the layer to protect the collector parts and to reach an efficient collector operation in all situations over the year. There is also an influence of the ambient temperature on the layer performance at the set-up with black absorber and single glazing. Therefore, a collector with black absorber and a layer on the inner surface of the double glazing is regarded as most suited because of the thermal insulation by the embedded air volume.

3.3.2 Electrically Switchable Layers

Electrically switchable layers change their optical properties by means of an electric current or an electric field. These technologies have not found their way onto the market yet as they are still in the beginning stage of being established and are thus also very expensive. For blocking the transmission of solar irradiation through transparent material the following technologies are feasible.

3.3.2.1 Electrochromic Layers

Electrochromic layers are used as sun protection glazings in facades/windows in the building sector as well as in car windows (Flachglas Markenkreis; Saint-Gobain Sekurit; GESIMAT). An intended blue colouring of the layer absorbs a part of the incoming insolation which helps to decrease the transmittance. The effect can be compounded by building up a multi-layer. Two transparent conductive layers at outer surfaces include a film made of tungsten oxide (WO_3), a film containing charge carriers (mostly lithium ions) and a separating, conductive polymer film in the middle. In the transparent state tungsten oxide and lithium ions only occur in their own separated film. After having closed the electric circuit of the two outer conductive layers the lithium ions penetrate into the interlayer, enter the film with tungsten oxide and build molecules out of the tungsten oxide. These molecules cause the blue, absorbing colour in the multi-layer build-up. The intensity of the colouration can be varied by control from outside. When being in a steady state, an electrical field and/or electric supply become completely irrelevant. Electric energy is only expanded to colour and discolour (BINE Informationsdienst 2002). Switching between clear and coloured state can take up to 15 minutes. The electric current flow cannot be increased unlimitedly since high current flows cause irreversible reactions in the tungsten oxide film (Dittrich 2003).

Granquist (1992) tested a WO_3 layer with a transmittance level between 15 % and 80 %. The layer was damageable by dehydration of the liquid electrolytes and showed a strong dependency to the temperature. Thereby, the excellent switching properties could only be reached at room temperature. Moreover, it is only

possible to deposit the layer on small areas like shading rear mirrors in cars or displays. Also Mathew et al. (1997) investigated an electrochromic layer on the basis of tungsten oxide with a transmission factor of 70 % to 80 % in clear state and 5 % to 10 % in modified state. The layer was tested at temperatures of up to 85°C but showed an insufficient long-term stability in this temperature range. The shifting time was less than 5 minutes and in an endurance test 20,000 switches without any defects were conducted.

Due to the limited thermal resilience and the high costs of these layers, this approach is not capable of being integrated as overheating protection in polymeric solar-thermal collectors.

3.3.2.2 Electrotropic Layers

These electro-optical layers have been developed for screen glazing (Interpane; Saint-Gobain Glass). The layers have optical characteristics similar to thermotropic layers. The layer can switch from a transparent to a milky white state and appears light scattering. This technology is used for screens in outdoor and indoor applications of buildings and means of transport as well as for projection surfaces. Such so-called LC (liquid crystals) layers consist of a laminate of two plastic films with indium tin oxide layer and an interlayer of liquid crystals. These crystals are normally non-directional oriented and scatter the incoming light. At each film there is a pole of the power supply connected. In case of a voltage application, an electric field is generated between the layers, which aligns liquid crystals and change the layer into a transparent state. The layer is only transparent during an operation voltage supply. Hence, the system is intrinsically safe for overheating protection in case of power blackouts. However, the layers only achieve a low reduction of the solar transmission and have a low maximum operation temperature. According to these disadvantages, the application in solar-thermal collectors is not feasible.

3.3.2.3 Switchable Mirrors

Huiberts et al. (1996) report investigations with regard to hydrides of yttrium, lanthanum and trivalent rare earths changing from a clear state to a reflecting state due to the admittance of hydrogen and the triggered reaction. A thin palladium coating protects the layer from oxidation with ambient air and catalyses the hydrogen molecule adsorption and hydrogen atom absorption. A layer consisting of gadolinium magnesium alloy (GdMg) with a reflection of 70 % is considered to be an advancement. The layer is black in the transition region and absorbs light similarly to electrochromic layers. The clear state has a transmittance of more than 70 %. The hydrogen for the switching operation is extracted from a reservoir between the GdMg layer and a transparent counter electrode. The voltage from the power supply between GdMg layer and transparent counter electrode drifts the hydrogen in the GdMg layer and converts the layer into a clear state. If hydrogen is to be removed in order to get a reflective state, the voltage has to be switched. Thus, the hydrogen is pushed back to the reservoir (van der Sluis et al. 1997). Another improvement is a so-called all-solid-state layer consisting of a WO_3 layer as hydrogen reservoir, which is by far easier to produce (Griessen und van der Sluis 2001). This kind of layer is developed for architecture, displays and optical devices. However, a low-cost, marketable solution for the requirements as overheating protection in solar-thermal collectors is still not available.

3.3.3 Chemically Switchable Layers

A chemically switchable or rather gasochromic glazing consists of two glass sheets with a gap. On the inner surface, a WO_3 coating and a catalyst layer are placed. By means of a gas supply, hydrogen flows into the gap. The catalyst layer converts the hydrogen molecules into hydrogen atoms reacting with the oxide of the WO_3 layer to water. The water vapour passes from the surface and leaves oxide defects in the WO_3 coating changing the layer´s colour (Georg et al. 1998). This leads to a transmission decrease from 50 % to 15 % (BINE Informationsdienst 2002). This technology is used for controlling solar transmission of

windows in buildings and is still in an early stage of development. For that reason, the devices are very expensive and not suitable for overheating protection in collectors.

3.3.4 Translucent Appliances

Translucent appliances are devices with a partial light transmission, which cannot be directly controlled. In case of an overheating protection for collectors, translucent appliances partially block the incoming sun light. Increasing the efficiency of a collector by using insulations, covers and selective layers while permanently decreasing the efficiency by reducing the transmittance of the front side seems to be a conflict at first glance. Therefore, the translucent element is adjusted to reduce the insolation on the absorber only when heat is not required or rather when an excessive supply of solar energy is present. Most of the time such scenarios occur during summer which is characterised to have a small zenith angle of the sun. It is recommended to have translucent elements to control the solar transmission depending on adjusted angles. Hence, translucent elements are a seasonal overheating protection approach. The irradiation of the sun in autumn, winter and spring shall smoothly penetrate through the window. In summer time, however, incoming irradiance with small zenith angles is reflected, scattered or refracted to reduce the amount of solar energy on the absorber. Depending on the configuration of the solar-thermal system it may be a disadvantage to reduce the optical efficiency permanently during summer. Critical thermal operational states for polymeric parts can easily also occur in spring and autumn when this measure is not applicable. Hence, for translucent elements there is no intrinsic safety. Furthermore, the unknown influence of different collector slopes and different zenith angles of various sites on temperature reduction and system efficiency have to be considered. The fact that the operational state of the solar-thermal system does not have any influence on this kind of overheating protection turns out to be major advantage. This measure can also protect the collector during blackouts and hydraulic system failures. It is also possible to combine the

above-mentioned measure with another measure in order to reach a more effective protection. Translucent elements can be realised by two different approaches. On the one hand, the transparent cover can be structured directly by shaping. On the other hand, the surface of the transparent cover can be adjusted to translucent behaviour.

3.3.4.1 Geometrical Structuring of the Glazing

Nitz (2006) described in a patent application how a geometrical structured glazing worked for seasonal reduction of thermal loads on solar-thermal collectors. Thereby, the transmission of insolation is decreased at certain incidence angles. If a light beam through a boundary surface of transparent glazing penetrates another refractive index compared to the ambient air, the incidence angle of the beam changes. With a second boundary surface of the glazing the opposite is the case. Despite the refraction, this leads to the same beam angles before and after the glazing (Figure 3.14).

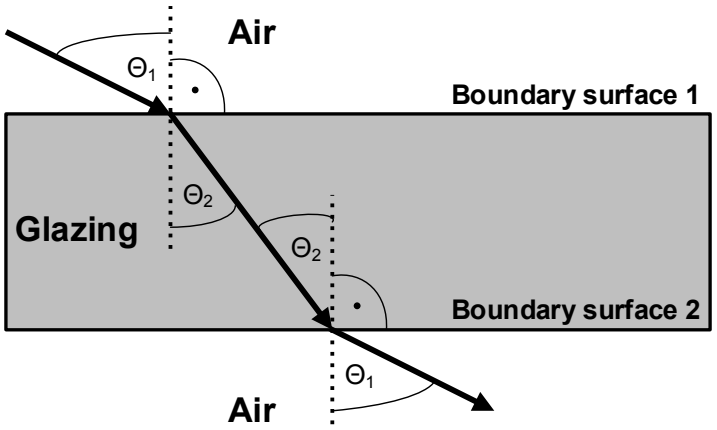

Figure 3.14: Transmission of insolation through a plane, transparent glazing

If this glazing is structured geometrically meaning that the boundary layers are no plane parallel surfaces, the incidence angle to the absorber can be changed in certain cases. As an example, the left side of Figure 3.15 shows the direction of the sunbeam under vertical or almost vertical incidence where the largest part of the light leaves the glazing under flat angles. That means that most of the sunbeams are screened off by total reflection on the second boundary surface of

the glazing. In temperate zones like in Europe, such situations will mainly occur at noon and during midsummer. This leads to a reduction of solar energy on the absorber surface and prevents the collector from overheating under these conditions. The remaining times of the days the direct radiation under flat incidence angles at the structured glazing occur where the major part of the light transmits without any losses. Figure 3.15 shows an exemplary beam transmission under the above-mentioned conditions on the right side.

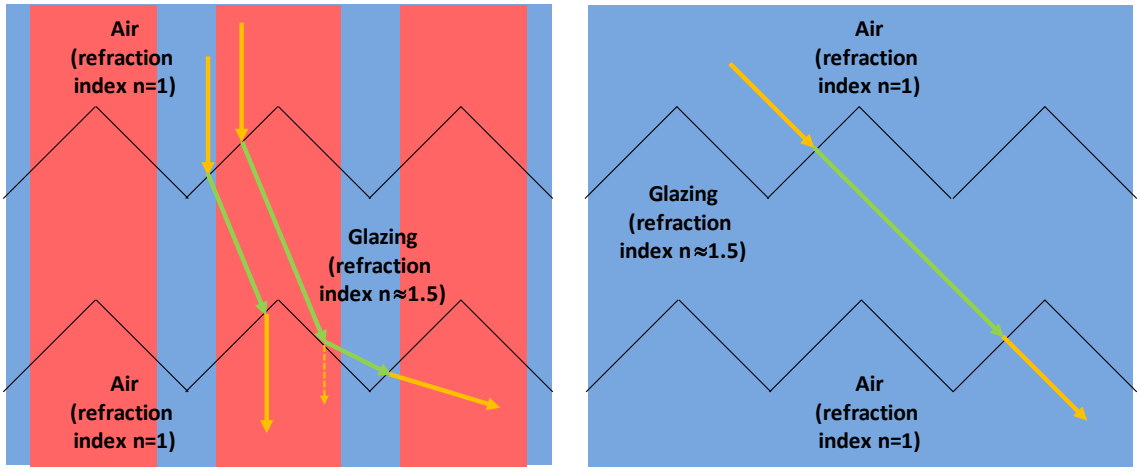

Figure 3.15: Description of the beam penetration at different incidence angles (blue region: full transmission; red region: reduced transmission)

A structured glazing provides several advantages for the use in solar-thermal collectors. The glazing lowers the reduction by reflexion under flat incidence angles during the heating period compared to planar cover sheets. The glazing reduces the irradiance on the absorber in midsummer when heat supply for domestic hot water preparation is less needed. Hence, the glazing avoids situations of possible overheating. The glazing is also cheap in manufacturing by extrusion or thermoforming. The correct operation of the measure is independent from the hydraulic circuit of the solar-thermal system and the power grid. The fact that the reaction cannot be controlled, however, constitutes the main disadvantage. Thus, critical temperatures occurring in spring and autumn cannot be prevented by a structured glazing adjusted for protection in midsummer. Another problem is the unknown effectiveness of a standard adjustment of the structure for different angles of the collectors' azimuth and slope. In principle, the approach is of interest

for the use in flat-plate collectors but there is no product available on the market. Furthermore, it has neither been investigated nor documented so far of how effective the procedure would be for overheating protection in solar-thermal collectors.

3.3.4.2 Microstructures on the Surface of the Glazing

Nitz et al. (2007) investigated micro-structured layers for controlling the solar irradiance in transparent elements for buildings. These layers are supposed to increase the available natural light in autumn, spring and winter. On the other hand, the layers will reduce overheating and glare in summer. This technology is implemented on polymer films which are spanned or fixed within insulation glass (Figure 3.16).

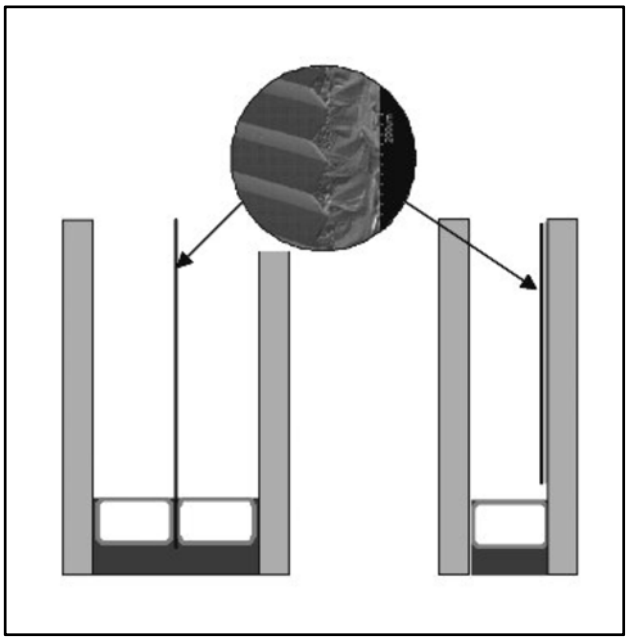

Figure 3.16: Applications of micro-structured films in solar control glazing for buildings (Nitz et al. 2008)

Figure 3.17 describes the beam penetration through vertical micro-structured layers in summer (yellow) and winter (cyan). The light beams from the sun in summer with flat incidence angles on the surface are directed by the layer to the second surface which reflects the major part backwards. The light beams from the sun in winter with steep incidence angles on the surface pass the application.

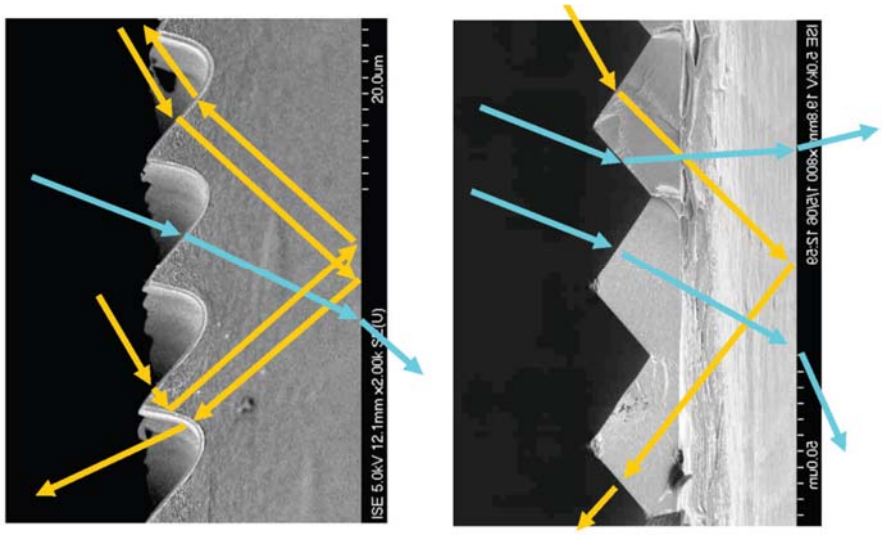

Figure 3.17: Beam penetration through micro-structured layers in summer (yellow) and winter (cyan) for vertical solar control glazing for buildings (Nitz et al. 2008)

Figure 3.18 presents the curve progressions depending on the incidence angle on the microstructures produced by interference lithography (IL) and mechanical processing (MP).

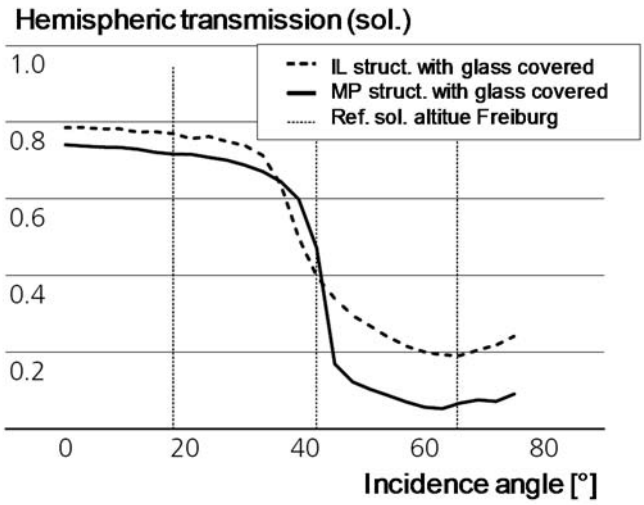

Figure 3.18: Comparison of the solar transmittances of two glazings with micro-structured layers against the incidence angle (according to Nitz et al. 2007)

Mechanical processed films are relatively cost-efficient to manufacture by roll embossing. The rolls are produced by ultra-precision machining like diamond milling or turning. However, these layers developed for vertically mounted building windows have contrariwise performance characteristics.

Nitz (2004) investigated a micro-structured layer for inclined surfaces to reflect vertical sunbeams made from PMMA. Figure 3.19 shows the structure of the so-called compound parabolic concentrators (CPC) in detail. The reflecting metallisation is deposited by a PVD process. The layer is designed for roof-lights to reflect insolation with incidence angles in the array of the perpendicular and to enable high transmission under flat incidence angles. Thus, this layer has suitable performance characteristics for overheating protection at the inner surface of the collector glazing.

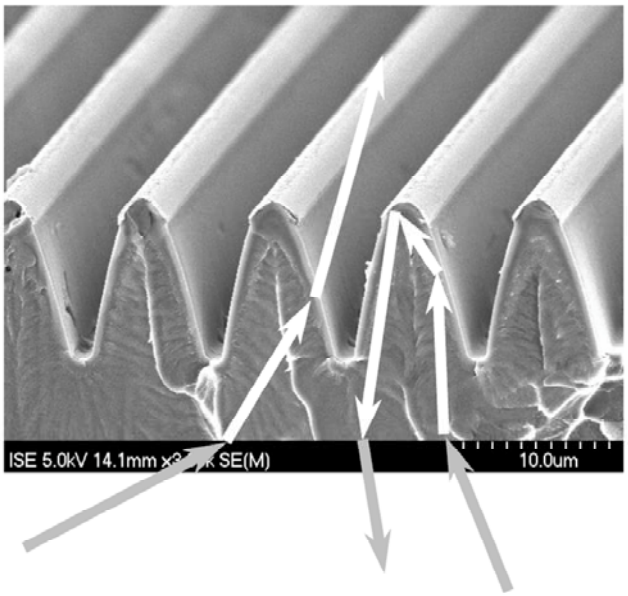

Figure 3.19: Compound parabolic concentrators with metallised ridges for the reflexion of vertical direct radiation (Nitz 2004)

3.3.5 Mechanical Appliances

The field of mechanical protection devices comprises all measures reducing or preventing transmission through the collector front by a mechanically controlled process.

3.3.5.1 Shading Elements

Shading elements are all devices reducing or disabling the transmission at the collector front by impenetrable materials. These devices are either mounted fixed or flexibly on the collector front. Such elements are already used at inclined and

vertical glazings in buildings to control light intensity and indoor climate. Rotating and contracting lamellas are an example of flexible elements. Due to rotating lamellas, there are permanently shaded areas on the absorber whose position has to be found in order to prevent a further reduction of the optical efficiency of the collector. Moreover, all kind of curtains or roller shutters being moved by a mechanical drive may be applied. The reflecting outer surface further improves the overheating protection. It can avoid absorption and residual heat inside the collector. In the majority of cases, flexible shading elements have no significant influence when it comes to the efficiency of the collector. They ensure a completely controllable thermal protection. However, the complex set-up (shading element, motor, controlling unit) is accompanied by various problems such as a reduced lifespan, moveable parts, a high collector weight and high initial costs. There is also a dependency on electrical power supply which could only be solved by additional costs for PV elements or storage batteries.

Beikircher und Schmidt (2009) developed the prototype of a high-efficiency collector by using this technology with a shading film (Figure 3.20). The collector has a transparent film for the reduction of the convective losses or a reflecting film for the prevention of solar absorption stretched in front of the absorber depending on the operation mode. The film unit is implemented into the collector by the film reel principle. Therefore, a roll with a PV-driven motor moves the film. A barrel arbor to stretch and to roll up the film complements the unit.

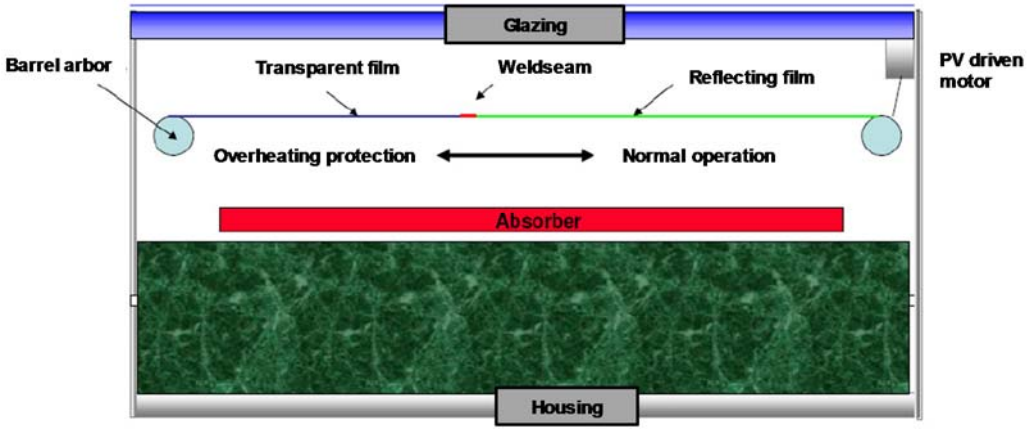

Figure 3.20: Design of a flat-plate collector for high flow temperatures with film insulation and shading element (according to Beikircher und Schmidt 2009)

Apart from automatically controlled shading elements, *Radiant Floor Company* describes a simple system regarding the overheating protection of evacuated tube collectors (Radiant Floor Company n.d.). Therefore, a knitted polymer screen, for example, can be used to cover the collectors when the weather conditions cause high absorber temperatures (Figure 3.21). The basic intention of this approach is the reduction of the solar yield during periods of high solar irradiance and low demand of heat in order to prevent stagnation of the system. The approach ensures a sufficient temperature reduction and causes low additional costs. However, a missing intrinsic safety due to the manual triggering of the measure and a difficult accessibility of the collectors on a roof are major drawbacks.

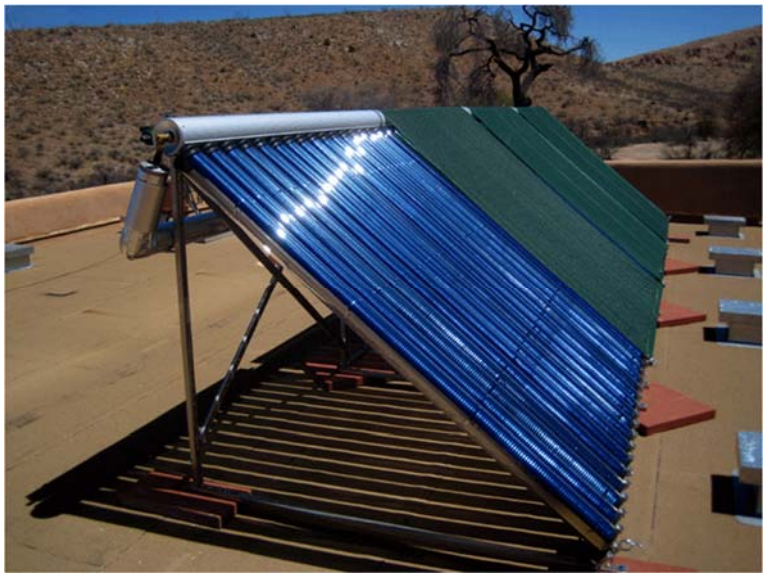

Figure 3.21: Uncovered and covered evacuated tube collectors (Radiant Floor Company n.d.)

3.3.5.2 Infilling of Shading Material (Bulk Goods)

Harrison (1975) patented a device for the transmission reduction of windows and flat-plate collectors. In this case, granulate is pushed, by means of an air blower, into the gap of a double glazing or a collector to reduce or prevent the light transmission. The main advantages are the controllability and the high temperature reduction. However, the large and complex design of the measure leads to high initial and maintenance costs. The appliance also has no intrinsic safety to protect

the collector during a power blackout. Due to the above-mentioned disadvantages, the measure is not suited as overheating protection in cost-efficient flat-plate collectors.

3.3.5.3 Rotation of the collector

The change of the incidence angle on the collector surface changes the optical efficiency. This is how the collector can be repositioned to follow the sun and absorb solar radiation reaching the vertical incidence area. This leads to low losses by reflection and the highest radiation density (Figure 3.22). In cases of potential stagnation the incidence angle can be changed until the reflexion wanes and the radiation density reaches temperatures regarded as not harmful to the collector parts.

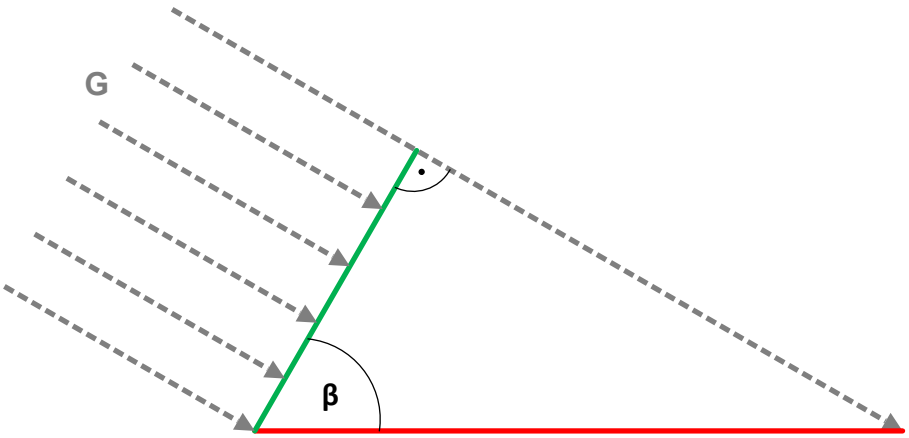

Figure 3.22: Relation of radiation density at vertical (green) and inclined (red) incidence

Such tracking devices are already used in solar-thermal power plants and PV systems. The complex construction and high initial costs, however, outweigh the advantages of making use of this method for overheating protection in flat-plate collectors.

3.3.6 Hydraulic Appliances

Hydraulic protection devices consist of a double glazing in which a fluid is pumped in order to alter the optics of this specific part. The device uses scattering and absorbing effects to control the transmittance.

3.3.6.1 Shading Fluid between a Double Glazing

In this device, a dark fluid is pumped into the gap of a double glazing to absorb the incoming solar irradiation and to convert it into heat. The thermal energy is quickly transferred to the ambient air by convection. Dockery (1972) patented a system to defrost and to vary the transmittance of a windshield for cars. In that system, a heated, coloured fluid is pumped from a reservoir into the gap of a double glazing. Taking the reservoir, the pumping, the double glazing and the control unit into consideration, the whole procedure turns out to be complex and expensive. Moreover, it is not intrinsically safe during power blackouts. In addition, the shading fluid has strong requirements to UV-resistance as well as to temperature stability. This limits the variety of suitable fluids. If the fluid is being left in an empty mode, the optical efficiency of the collector decreases. The advantages of a controllable measure with high possible temperature reduction in the switched mode cannot compensate these disadvantages.

3.3.6.2 Light Scattering Double Glazing

The patented appliance with double glazing by Stephens (1981) uses a light scattering surface inside the gap. The scattering effect is caused by unevenness of the surface and the different refractive indexes of the air and the interlayer material. As a result, the refraction of the light is non-directional regarding the whole surface. This leads to a decreased transmission. To accomplish a clear state, a transparent fluid with a refractive index comparable to the interlayer is filled inside the gap of the double glazing. Hence, there is no change of the refractive index at the rough surface and the scattering boundary layer vanishes for the light beam. Figure 3.23 shows the schematic device in scattering and transmissive state.

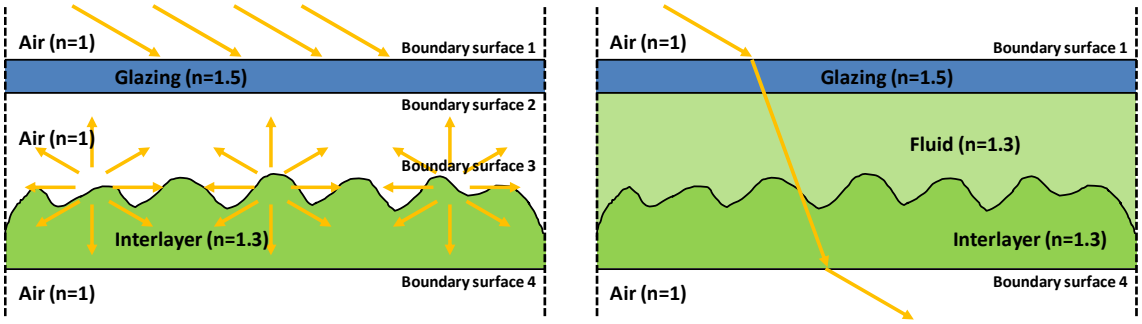

Figure 3.23: Schematic of a glazing in scattering (left) and in light-transmissive (right) state

Stephens (1981) also described a test of a conventional flat-plate collector with selective absorber coating made of black chrome. This collector was heated in a solar simulator up to a stagnation temperature of the absorber of 100°C. Afterwards, a scattering layer was implemented between absorber and glazing. This led to a temperature of 79°C under the same test conditions. In a third test phase, a fluid with a similar refractive index was filled into the gap between glazing and scattering layer to negate the scattering mode of the device. The final absorber temperature was 97°C. The test proved that the temperature can reasonably be reduced while the efficiency of the collector is only slightly influenced. The transparent fluid in this collector is adjusted to vaporise at a certain temperature, to change the refractive index and to leave the gap. As a result the transmittance of the collector front is reduced. This device is independent from the operation of the hydraulic circuit and the power grid. The measure also shows a minimal collector loss in the clear state of system operation. An elaborate installation with a scattering interlayer, a suitable fluid and a reservoir for the vapour reduces the applicability of the measure. Additionally, a temperature controlled valve between the return of the reservoir and the collector is necessary to avoid a permanent reflow and renew evaporation. Also the resistance of the fluid against UV radiation and further climatic influences like frost has to be looked at critically. Against this background an implementation in collectors seems to be unfeasible.

3.4 Changing the Absorption Properties

The absorbance of a collector can be reduced by measures having absorbing, scattering or reflecting effects. The measures are separated by their technical solutions presented in Figure 3.13. These functions control the two absorption properties with the absorption coefficient α and the absorbing area.

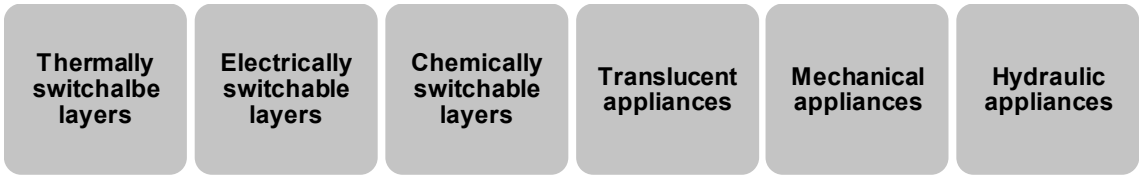

Figure 3.24: Groups of technical solutions for the reduction of the transmission properties (according to Reiter et al. 2012)

3.4.1 Changing the Absorption Coefficient

The absorption coefficient α describes the capability of a body to receive radiation and to convert it into thermal energy. For an optimal conversion of the irradiance into heat, the absorption coefficient α has to be close to 1 for the solar spectrum. Typical absorbers with selective coating reach an absorbance value of 0.95. This means that 5 % of the solar irradiance will be reflected and not be converted into heat. For overheating protection measures it is necessary to have an absorption coefficient α nearly 1 during system operation and a low absorption coefficient during stagnation. This prevents the radiation being converted into heat during system states where heat cannot be transferred by the heat transfer medium.

3.4.1.1 Thermochromic Layers with Switchable Absorption

Thermochromic colours are normally used as indicators for hot surfaces and for packaging materials. These colours fade above a certain temperature due to a change of their absorption coefficient for visible light. Thus, the capability to convert irradiance into heat decreases; this effect is caused by an organic dissolver. The dissolver is in the solid state below the trigger temperature. The pigments as well as an activator are embedded into the latter. In this state the layer is visible. When the organic dissolver melts, the layer becomes transparent and the surface

behind the colour coat visible. The primer is white for the use on an absorber to get the lowest absorbance. The transition range of such a colour is smaller than 6 K and the colour changes within seconds (Printcolor AG 2009; Gem'innov 2008). There are inks on the market with trigger temperatures of up to 80°C where a disappearance of 90 % of the colour is realised (Gem'innov 2008). Huot et al. (2008) investigated the colour gradient of two thermochromic paints (Figure 3.25). The paints showed a suboptimal colour but can be improved by another dissolver matrix.

Figure 3.25: Thermochromic colours at 25°C, 40°C and 90°C (Huot et al. 2008)

The low UV-resistance turns out to be a major disadvantage of the pigments. The admixing of metal flakes or UV-stabilisers can lower this effect. The application of a UV-protection layer is also possible (Huot et al. 2008). The potential of the layers is to be investigated further since low costs, the intrinsic safety and the switching characteristics are advantages for these layers.

3.4.1.2 Thermotropic Layers

The thermotropic layers described in Chapter 3.3.1.2 can also be applied on the absorber. The function and the effect is the same as with the glazing. The advantage of the application of such a layer on the absorber is the direct switching behaviour, since there is no influence of the ambient temperature and a short length of the control path. The application of the layer on a selective absorber is not possible because of the layers' non-selective characteristics (Wallner et al. 2008). Resch et al. (2009) described promising layers for the use of overheating protection measures on the absorber. More detailed investigations have to be carried out as to how local temperatures and the system efficiency are influenced.

3.4.1.3 Electrically Switchable Layers

In principle, the use of electrically switchable layers to control the surface properties is applicable. Therefore, an electrochromic layer on a bright or reflecting base layer is black and absorbent to change solar irradiance into heat during system operation. In case of an impending overheating, the layer rises its transmission coefficient to let the irradiance pass the reflecting base layer and to reduce the absorbance of the part. Electrotropic layers can be deposited onto the black absorber surface. They change their transparent state into a milky white state to reflect the insolation and to prevent further heat conversion before overheating of the parts. However, the previously described disadvantages of these layers described in Chapter 3.3.2 are also valid for an application on the absorber.

3.4.1.4 Chemically Switchable Layers

Chemically switchable layers, as described in Chapter 3.3.3, can also be used on an absorber layer. Since the above-mentioned disadvantages also apply for this kind of application, further investigations are not required for overheating protection in solar-thermal collectors.

3.4.1.5 Microstructures on the Surface of the Absorber

The principle of the described micro-structured layers in Chapter 3.3.4.2 can also be fixed directly at the absorber to reduce the transmission of solar radiation depending on the incidence angle. Thus, the conversion of radiation into heat by the subjacent absorber coating can be reduced or avoided. For this layer application, the temperature resistance of the layer needs to be investigated in more depth. Furthermore, a selective absorber behaviour is not possible due to the high emission coefficient of the micro-structured plastic film. Hence, the application of such a layer on the absorber has no advantages compared to the application on the glazing.

3.4.2 Changing the Absorbing Area

The reduction of the light absorbing surface of a collector decreases the transfer of irradiance into heat and lowers the maximum component temperatures. The implementation of this principle can be designed mechanically as well as hydraulically.

3.4.2.1 Mechanical Appliances

The reduction of the light absorbing surface can be realised by rotatable risers of the absorber. Also, sliding of the risers about each other can reduce the absorbing area. Another option is a grid of absorber pipes above CPC mirrors being movable to each other. During operation pipes and mirrors are positioned to concentrate the focal lines on the pipes. Thus, the whole irradiance from the mirrors is focused on the absorber pipes for a maximum energy gain. In case of overheating, the pipes or mirrors are moved one-dimensionally to differentiate the positions of pipes and focal lines. Hence, the absorbing surface of the collector is reduced. However, using mechanical appliances in collectors is not reasonable due to the high technical complexity of mechanisms for turning or moving as well as the susceptance to failure of movable parts.

3.4.2.2 Hydraulic Appliances – Black Fluid

In the 1970s and 1980s the principle of the so-called “black fluid” was investigated. In particular, in the United States approaches of solar-thermal systems with black fluid were the subject of patents. Polymeric collectors with black fluid dispose of a transparent absorber and drain-back system as solar circuit. A drain-back system has an open hydraulic circuit. Hence, during operation the fluid is pumped from the storage to the collector and backwards. If the pump stops, the fluid flows out of the collectors and is collected in the storage or an external tank. In such a system the black fluid coloured by carbon serves as the heat transfer medium as well as the absorber which converts irradiance into heat. The empty

absorber is fully transparent or has a reflecting backside plate, hence cannot convert the insolation into heat. Because of the missing absorber area of the black fluid in the empty collectors, the system has an intrinsic safety. Heat inside the collector is only generated during a fully operating solar-thermal system. The difficulty of launching coloured fluids onto the market, their absorption properties as well as their long-term stability constitute are the main drawback of this approach.

3.5 Changing the Convective Losses

Flat-plate collectors dispose of an insulation at the backside and a housing with a transparent cover to minimise the heat losses from the absorber to the ambient air. The backside insulation reduces the heat transmission with low heat conduction to the outer surface of the casing or backside sheet where the thermal energy is emitted mainly by convection. The convective heat loss on the front side is reduced by an embedded air layer between glazing and absorber. Thus, the heat flow has to be transferred by natural convection from the absorber to the glazing and from the glazing to the ambient atmosphere. If convective losses of the absorber are to be extended in order to reduce the collector temperatures, thermal resistances of the front side or the backside have to be decreased.

3.5.1 Natural Convection in the Air Gap

The fluid flow of a natural convection to transport thermal energy is driven by the density differences caused by a temperature gradient within the fluid.

An air stream from the outside of the collector through the air gap between glazing and absorber causes the rise in the loss coefficient of the front side by transporting additional thermal energy to the ambient air. Meir et al. (2008) experimentally investigated a polymeric collector with non-selective absorber and overheating protection by means of a lockable chimney in the front side of the collector. Therefore, a permanently opened ventilation slot on the bottom edge and ventilation controlled by the thermal expansion of the absorber on the top edge were installed in the collector (Figure 3.26).

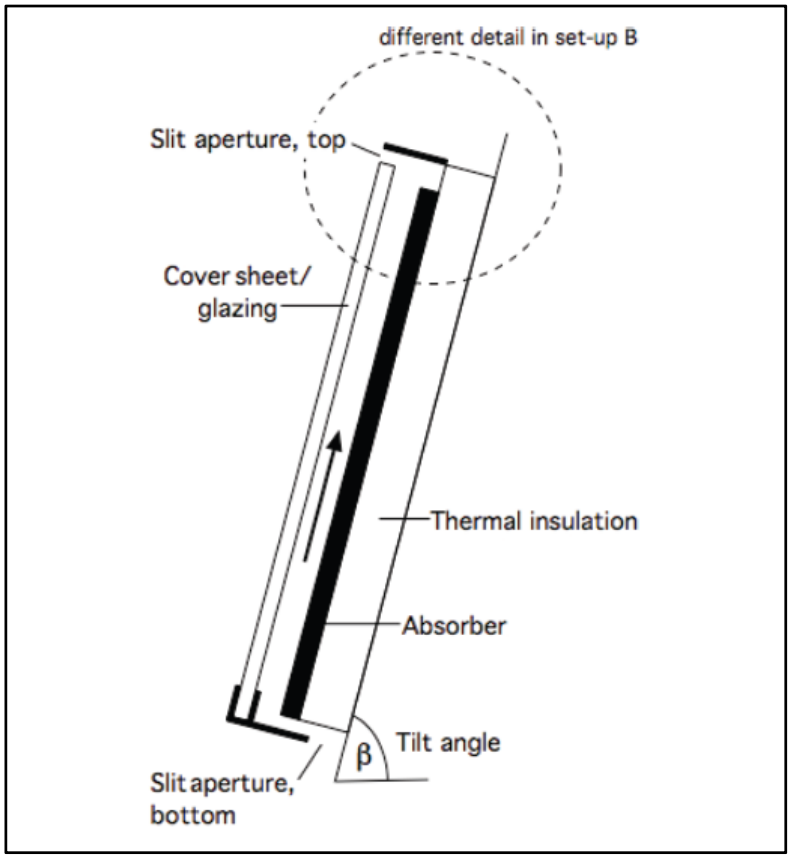

Figure 3.26: Schematic design of a polymeric collector with ventilation slots (Meir et al. 2008)

Closing the upper ventilation slot is sufficient for suitable collector efficiencies because hot air in the collector moves upwards. Thus, the natural convection of the stack-effect is blocked and the air layer shows a similar behaviour such as the air layer enclosed. The reference collector without overheating protection in the outdoor testing reached a maximum absorber temperature of 145°C in the upper part of the collector. The collector with opened ventilation dampers showed a maximum absorber temperature of about 120°C. The measurements were carried out at 30°C ambient temperature.

Harrison et al. (2004) tested a conventional flat-plate collector with selective absorber coating and ventilation dampers on bottom and top edge of the backside sheet (Figure 3.27). The air stream was controlled by the upper damper through a spring made of a shape memory alloy.

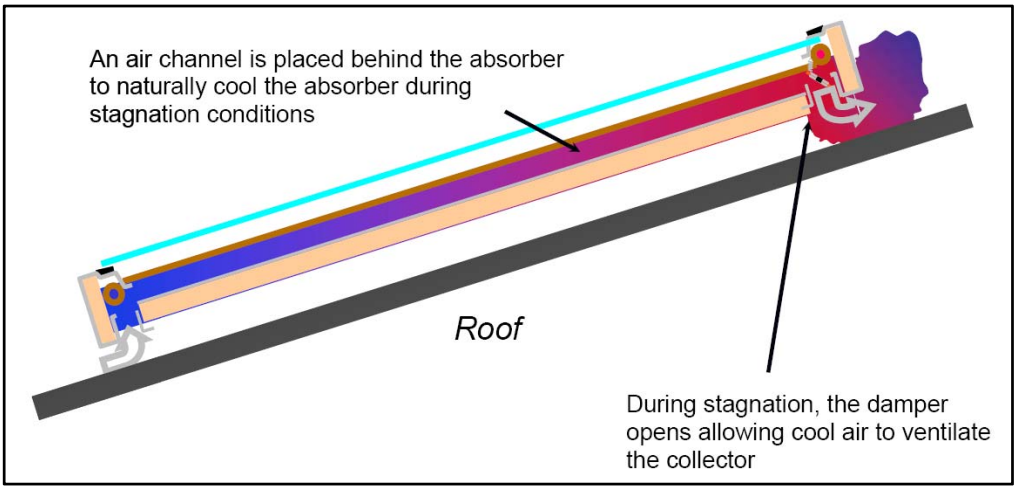

Figure 3.27: Schematic design of a polymeric collector with additional convective heat losses caused by a chimney behind the absorber (Harrison et al. 2004)

The test results of a conventional and an adjusted collector were monitored at a collector slope of 18° during dry stagnation. First tests at 1,150 Wm^{-2} irradiance and 25°C ambient temperature showed absorber temperatures of 160°C at the reference collector and 170°C at the adjusted collector with closed slots. The difference can be attributed to the fact that backside losses reduced thanks to the additional air layer of the closed chimney. Figure 3.28 shows the results of a testing day at 1,100 Wm^{-2} and 25°C ambient temperature.

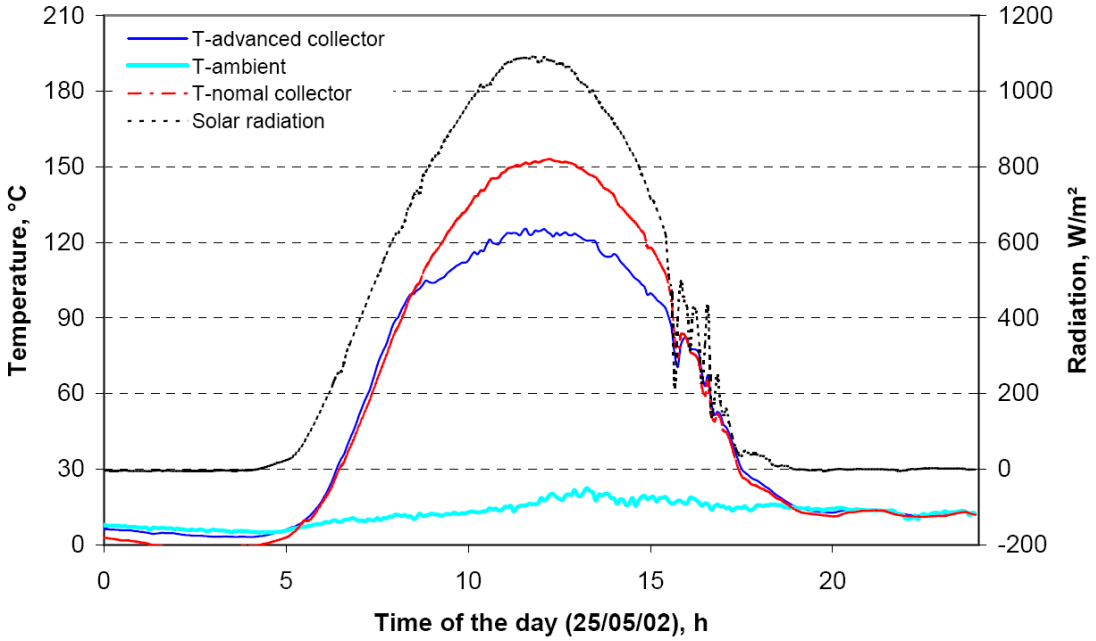

Figure 3.28: Trends of the absorber temperatures with and without ventilation by natural convection (Harrison et al. 2004)

The absorber temperatures are similar up to a value of approximately 100°C. Above this level, the dampers of the adjusted collector opened and the stagnation temperature reached only 122°C while the reference collector had a temperature of 155°C.

Kearney et al. (2005) published a survey in which he calculated the temperature reduction during stagnation for polymeric collectors with ventilation by natural convection in front as well as behind the absorber and both together. The model was simulated with an air gap and a slot of 25 mm and a collector slope of 45° under extreme weather conditions with an insolation of 1,100 Wm^{-2} and an ambient temperature of 43°C. As reference he took a conventional flat-plate collector with selective layer und single glazing. Under these conditions an absorber temperature of 205°C was reached. A second reference was a collector without selective coating representing a black polymeric absorber. In this case the maximum temperature was 149°C. The collector disposing of ventilation at the front side showed a reduced temperature of 123°C. For the ventilation at the backside part of the insulation was removed. The removed insulation also reduced the collector efficiency in the case without ventilation. The air gap behind the absorber was painted black to reach the highest distribution of thermal energy at the complete chimney surface for an effective convective heat transfer. By means of ventilation at the backside, the collector reached a temperature reduction from 144°C to 113°C under the above-mentioned conditions. Ventilation in both air gaps causes a reduction from 144°C to 102°C.

The mentioned examples show that ventilation by natural convection is only useful for collectors without selective absorber coating when commodity plastics are required.

Table 3.1 presents an overview on documented implementations of overheating protection by natural convection in solar-thermal collectors.

Venting slots can be implemented at the backside, at the frame or at the border of the glazing. The convective cooling can be switched by various elements at the slots at the top edge and possibly at the bottom edge of the collector. The

elements can be controlled by bi-metal springs, shape memory alloys, pistons, inflatable elements or linear expansion of the absorber. Except for the inflatable elements all systems are self-regulating and intrinsically safe against system failures and blackouts.

Table 3.1: Implementations of overheating protection by natural convection

Vents	**Closing Elements**	**Actuator**	**Reference**
End faces housing	Not chosen	Not chosen	Kearney et al. 2005
End faces housing	Damper, top	Linear expansion of the absorber	Meir et al. 2008
End faces housing	Damper or slide gate, bottom	Bi-metal spring	Haticon GmbH 2006
End faces housing	--	Temperature-dependent air stream	UFE SOLAR GmbH 1999
End faces housing	Dampers	Piston with phase change material (wax)	Palmer 1980
End face housing, bottom + Glazing, top	Damper, top	Bellows with phase change material (alcohol etc.)	Buckley 1979
End face housing, bottom + Glazing, top	Inflatable tubes	Pump, blower	Koenig 1983
Backside, bottom and top	Damper, top	Shape memory alloy spring	Harrison et al. 2004
Glazing, bottom and top	Gaps between glazing and housing	Bending of the glazing opens slots caused by linear expansion	Rich 1995
Glazing, bottom and top	Glazing, liftable	Linear expansion of the absorber	Scott 1977

Ventilation on the front side of the absorber can reduce the optical efficiency of the absorber by dust and insects. Therefore, a protection element like a grid has to be mounted.

Roberts et al. (2000), for example, investigated a venting measure for an ICS system with a double-walled housing being separated to the air gap of absorber and glazing by dampers. At high absorber temperatures the dampers opened and the hot air from the absorber circulated through the housing (Figure 3.29). This measure increased the surface for convective heat transfer to the outer shell and reduced the absorber temperature from 115°C to 106°C. The system was protected against pollution from outside by the closed cooling loop.

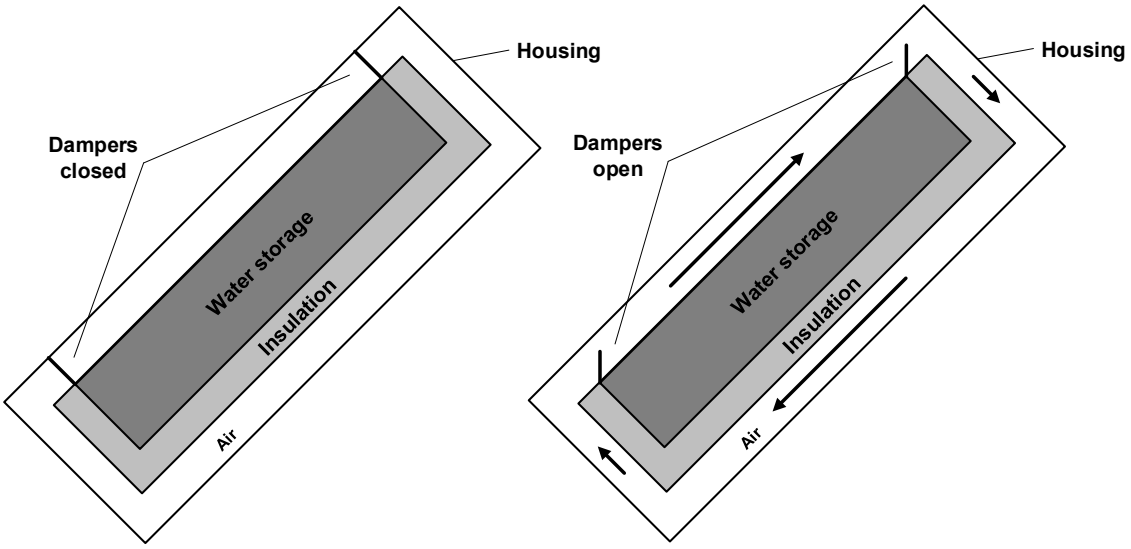

Figure 3.29: ICS system with closed cooling loop during operation (left) and during activated overheating protection (right; according to Roberts et al. 2000)

On the basis of the different approaches, two common conclusions can be made. For front ventilation, the collector design and height must not be changed because the air gap between glazing and absorber already exists. Ventilation behind the absorber requires a suitable air gap between absorber and insulation. This causes changes in collector design, height and efficiency.

The measures described for ventilation triggered by natural convection have a high intrinsic safety as well as a low efficiency decrease compared to collectors without overheating protection. The movable parts pose problems due to their

limited endurance and high production costs. Due to the fact that temperatures can only be slightly reduced, it is recommended to combine this with another method.

3.5.2 Forced Convection in the Air Gap

The use of heat transfer by forced convection means transporting of thermal energy carried by a fluid stream driven by an external force. The use of this function as overheating protection measure for collectors requires the same design as for venting by natural convection plus an additional ventilator blowing air through the collector.

Scharfman (1977), for example, patented a system with a central ventilator and collectors connected to each other by ventilation slots at the top and bottom of the backside of the casing. Air is blown through a closable damper to the front side of the absorber to cool down the surface.

Schmidt (1992) patented a collector with transparent insulation and overheating protection. Because of the high efficiency and the polymeric material of the transparent insulation, an overheating protection measure became necessary. Therefore, a temperature controlled axial fan at the end face of the casing was installed. During fan operation an air stream flowed through an air gap of 30 mm distance between absorber and transparent insulation and left the collector through opened dampers.

Intrinsic safety of such systems is only possible by means of an additional electric power supply in the form of an accumulator or a PV module. The complex design for forced ventilation with a ventilation unit, an electric energy supply and further parts in the collector housing (slots, dampers etc.) are adverse conditions for a failsafe and economic overheating protection measure.

3.5.3 Convection Combined with Evaporative Cooling

Besides cooling by natural convection, Kearney et al. (2005) also analysed the influence of natural convection in combination with evaporative cooling by means

of mathematical modelling. A standard flat-plate collector with selective coating, a standard flat-plate collector without selective coating and a non-selective flat-plate collector with controlled venting by natural convection at the backside of the absorber plus a wetted pad were simulated and compared to each other. The underlying conditions included a solar irradiance of 1,100 Wm² and an ambient temperature of 43°C. Under these conditions, the stagnation temperatures of the collectors were 205°C, 149°C and 65°C respectively.

Evaporative cooling, hence, proves to be considerably more effective than mere natural convention. Nevertheless, the complex design of the venting mechanism is exacerbated by the water pad and the temperature controlled water tap. Moreover, it is highly probable that the measure can fail due to calcification and frost damage.

3.5.4 Varying the Insulation Properties

Changing the insulation properties of the collector can also vary the heat transfer from the absorber to the ambient air. These heat losses can be controlled by modifying the geometry of the air gap in front of the absorber or the backside insulation.

Changing the insulation property of the air gap between glazing and absorber depends on the distance between the parts. Reducing the space between glazing and absorber decreases the heat transfer via convection but significantly increases the heat conduction leading to an increased heat transfer. Sharpe (1984) patented a collector concept comprising an air-tight housing blown up by an air-pump. The increased pressure inside curves the glazing whereupon the distance between glazing and absorber rises. The measure is intrinsically safe since the application of this measure only becomes necessary during the operation of the solar-thermal system. A thermally controlled valve deflates the collector at a certain trigger temperature. In consideration of coming up with cost-effective collectors, the design of an air-proof and pressure resistant housing as well as the valve, air pump and controller appear to be too sophisticated. Furthermore, the

failure probability of the parts over the life time of the collector has to be considered. Figure 3.30 shows the cross section of the collector during regular collector operation and active overheating protection.

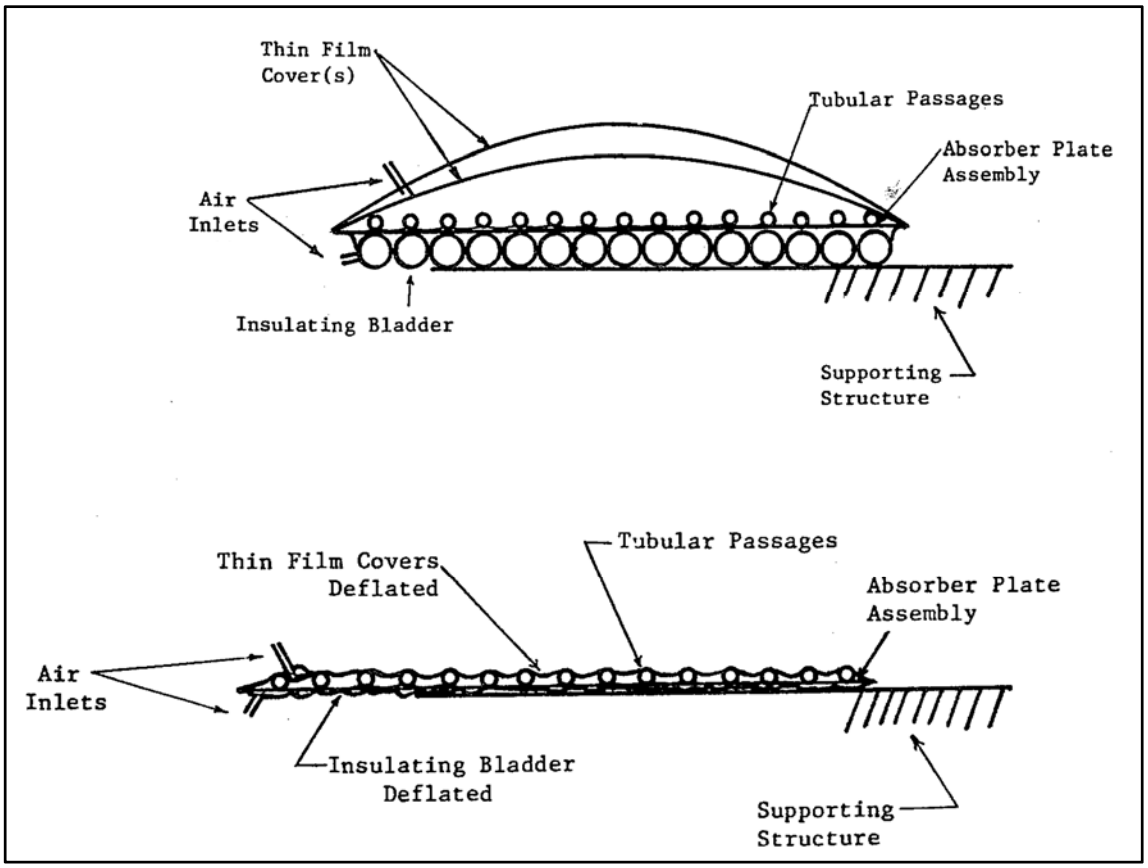

Figure 3.30: Cross section of collector with variable air gap and inflatable backside insulation during collector operation (top) and stagnation (bottom; Sharpe 1984)

The change of the heat transfer properties of the backside can also control the local temperatures of the collector. Therefore, the heat transfer coefficient of the backside insulation can be varied by using a switchable insulation. ZAE Bayern (2001) tested a prototype of a switchable insulation for building facades. The prototype consisted of an evacuated insulation panel with a glass fibre filling. A capsule with metal hydride reactor released hydrogen by means of heat which reduced the heat transfer of the panel. When the getter cooled down, the hydrogen was reversibly embedded in the getter. The heat transfer rose by a factor of 40 in the heated getter state but the panel required 5 Wm^{-2} of electricity. Hence,

the prototype panel requires an electric power supply. Due to the complex design, this measure for collectors can also be discounted for further use.

Besides the variable air gap, Sharpe (1984) also patented an inflatable backside insulation to control the absorber temperature. The collector shown in Figure 3.30 has an inflatable matting to reduce the thermal losses. An air pump and a thermally controlled valve regulate the air content of matting. The number of parts and the use of flexible materials under high temperatures and ambient conditions are two of the main drawbacks to be named for the application in collectors.

3.6 Changing the Radiation Losses

In addition to the heat losses caused by conduction and convection, also thermal radiation between absorber, glazing and the cold sky reduces the part temperatures of the collector. The change of the emission properties of the absorber can be arranged by the surface properties of the absorber and by the collector design.

3.6.1 Thermochromic Layers with Switchable Emission Coefficient

An absorber consisting of a thermochromic layer with switchable emission coefficient has selective absorption properties in the temperature array of ordinary collector operation. The surface absorbs a large part of the incoming short-wave radiation from the sun and emits only a small fraction of the converted heat to the glazing or rather to the cold sky. Above a certain absorber temperature the layer changes its emission coefficient in the long-wave region and the heat losses by means of radiation through the front side increase.

Huot et al. (2008) investigated an inorganic, thermochromic coating to protect the water-glycol mixture of a state-of-the-art flat-plate collector against overheating and resulting degradation. The ternary compound conduct changes a phase from a semiconductor state to a metallic state when a certain temperature is exceeded. In simulations a layer was identified with an emission coefficient of 5 % during operation and an emission coefficient of 40 % to keep the maximum absorber

temperature below 160°C. A similar coating with emission coefficients between 5 % and 35 % was developed. The layer had a switching temperature of about 65°C and had an absorption coefficient for solar insolation of 97.3 %. First samples of the layer were produced on laboratory scale with a PVD-sputtering process.

The application of such a coating on polymeric substrates has to be further investigated. On the one hand, the process for application has to be approved for the chosen substrate regarding its material properties such as electrical conductivity and the temperature resistance. On the other hand, the polymeric materials need a diffusion barrier protecting the layer from corrosion and flaking. The main advantage of the layer is the complete and independent intrinsic safety. For the implementation of the layer in a polymeric collector, however, the temperature reduction is too low. A further development of the switching properties or the combination with another overheating protection measure is considered to be necessary.

3.6.2 Contact between Glazing and Absorber

Moore (1983) patented a collector with either single or multiple glazing being able to be elevated by lifting elements of the absorber. In the collapsed condition when the system is not collecting solar energy, the glazing directly rests on the selective absorber. In this case, the heat from the absorber is transferred with low resistance to the glazing. The glazing emits the heat as a black body. Hence, the selective behaviour of the absorber is bypassed and the heat loss surges. Figure 3.31 shows a collector concept with an inflatable absorber as lifting element for the cover plates. During system operation the pump pressurizes the solar circuit and blows up the flexible absorber regions elevating the cover plates and creating an air gap between glazing and absorber.

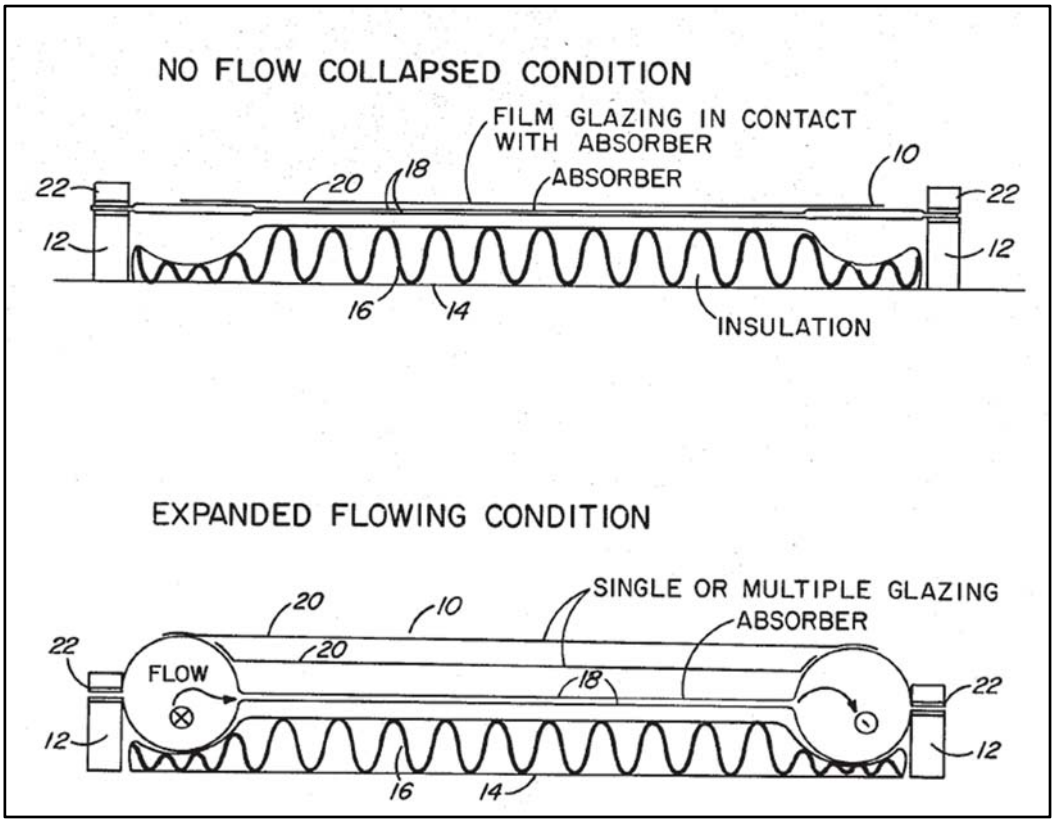

Figure 3.31: Collector with lifting elements for the glazing during stagnation (top) and during collector operation (bottom; Moore 1983)

In addition, the increased losses by radiation the thermal resistance in the air gap between glazing and absorber are also erased. Thus, the collector shows unglazed pool absorber characteristics at the front side during active overheating protection.

The intrinsic safety of the solution is provided because high temperatures occur only during measures intended to actively reduce heat losses. Apart from the fact that the measure represents a cost-effective, efficient approach to protect the collector parts from high temperatures and ensure suitable collector efficiency, all movable parts within the collector have adverse effects with regard to their purpose and their life span.

3.7 Active Cooling

For active cooling of the collector a heat carrier is used to carry away the heat from the absorber and other collector parts. Various measures with heat sinks at the collector, at the solar circuit and at the heating system are conceivable. Different kinds of measures for active cooling depending on their position are described in detail as follows.

3.7.1 Cooling Measures in the Collector

Cooling measures in the collector are measures for active temperature control directly placed in the housing of the collector. Two different systems are possible. One system has an additional emergency cooler integrated in the collector; the other system has an external open cooling circuit.

3.7.1.1 Collector Integrated Emergency Cooler

The collector integrated emergency cooler system consists of an external mounted surface radiator connected to the piping system at the absorber plate. During stagnation the heat carrier circulates between the radiator and the absorber driven by the thermosyphon effect and transports the heat from the absorber to the ambient air. Cummings (1978) patented a collector design with two heat carrier circulation systems at the absorber (Figure 3.32). One piping system is connected to the solar circuit and transports the converted heat to the buffer storage. The second circuit is connected to a fin-tube heat exchanger at the top edge outside the collector. The heat and fluid transport in the system is driven by the thermosyphon effect. A thermally switchable valve controls the heat transport and avoids the heat exchange by the overheating protection measure during temperature levels in the operational range of the solar-thermal system.

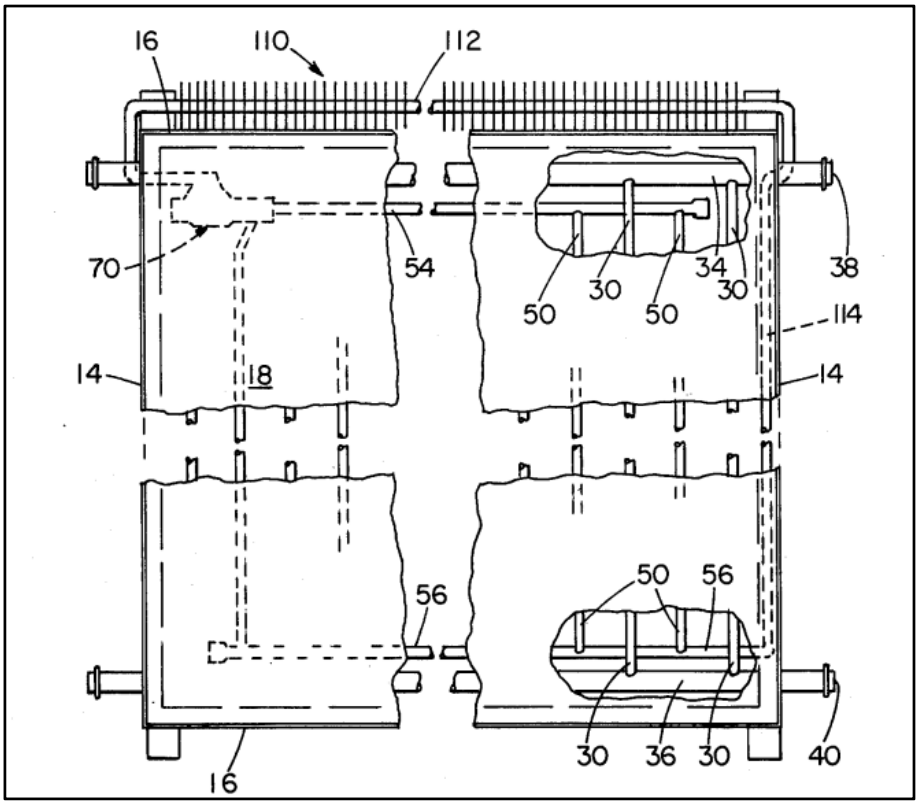

Figure 3.32: Collector with additional cooling circuit at the absorber driven by the thermosyphon effect (Cummings 1978)

The design of absorber and piping is complex and an external heat exchanger requires additional space. Furthermore, the thermosyphon circuit requires a unit to buffer the thermal expansion of the fluid to prevent damage due to extreme pressures. The measure is intrinsically safe to blackouts, but the costs and complexity for the surface radiator and the control valve remain a serious problem for the realisation.

Another design of the measure is a direct connection between the absorber and the external heat exchanger. Hence, only one piping system is implemented on the absorber and a second circuit with expansion unit is not required. Hence, the design and the production of collector are simpler, but a leakage in the solar circuit causes a breakdown of the measure. Also the behaviour of the solution during filling, draining or venting can be difficult.

3.7.1.2 Open Cooling Circuit

An open cooling circuit for overheating protection has to be placed above the absorber. This measure overflows the part with a cold fluid to transport the thermal energy away from the collector. The use of service water for being independent from blackouts and failures of the solar circuit constitutes a simple approach. A mechanical valve with a bi-metal actuator is used as a controlling unit. The hot medium draining out of the collector is collected by the roof gutter and conducted to a drain. The temperature reduction of the measure is quite large. However, the high water consumption lowers the ecological as well as the economic advantages of the solar-thermal system. The freeze resistance of the measure has to be taken into consideration as well. The calcification of the absorber surface decreases the optical efficiency of the collector. Thus, this measure cannot be implemented in modern solar-thermal collectors.

3.7.2 Cooling Measures in the Solar Circuit

Cooling measures in the solar circuit use the pipes and the collector fluid to transport the thermal energy of the collector array to its heat sink. The heat sink can be implemented as active apparatus or passive elements controlled by the pump of the solar circuit.

3.7.2.1 Additional Heat Sinks

The temperature reducing heat sinks in the solar circuit can be integrated as dissipaters or heat exchangers supplying external customers.

A dissipater or an emergency cooler in the solar circuit is an additional element in the solar-thermal system to transfer the thermal energy from the collector fluid to the ambient air. The radiator can be implemented in various designs.

A cooler driven without auxiliary energy and without pump operation in the solar circuit works in the same way as an emergency cooler being integrated in the collector. With this principle a radiator is connected to the whole collector array. The design is simpler because the collectors do not require any additional parts.

The piping and the valves are additionally clamped to the collector array. Problems arising during filling, venting and in case of leakages have to be viewed critically.

A cooler driven without auxiliary energy and with pump operation in the solar circuit is integrated parallel as surface cooler in the flow pipe of the collector field. The surface cooler can consist of a fin-tube heat exchanger, a radiator or an uninsulated pipe. A three-way valve controls the bypass of the overheating protection measure. The measure is only useful in an operational system. Hence, there is no intrinsic safety for the overload protection in the system. This measure for reducing the temperature is very efficient. However, a permanent power supply for the operation of the pump is necessary. The additional costs for the hydraulic integration and the surface cooler as well as a suitable place for the heat sink have to be taken into account.

A further enhanced version is a cooler driven without the need of any auxiliary energy and with pump operation in the solar circuit. The surface cooler with air blower has an increased cooling capacity. Hence, the size of the element can be reduced. Becker et al. (2006) analysed a solar-thermal system with 300 m² of conventional flat-plate-collectors and 27 m³ of thermal storage for Freiburg (GER) by simulation. The objective of the analysis was the prevention of high collector temperatures to protect the water-glycol mixture from degradation. In an annual system simulation the cooling unit limited the maximum collector temperature to 90°C with an operation time of about 100 hours. The required electric power supply was 1.7 kW for the air blower plus the power for pump operation during the prevented stagnation times. The cooling unit was also implemented in a bypass of the collector flow controlled by a three-way-valve. The temperature reduction reached was very high and the system´s efficiency was not impaired. However, the measure has no intrinsic safety against blackouts and failures in the hydraulic circuit. Furthermore, the investment and operational costs for a system with no intrinsic safety have to be considered.

Another measure is a heat exchanger at the flow of the collector array connected to external heat sinks. This can be the regeneration of the ground of a heat pump system, the heating of a green house or a pool as well as the exchange to the groundwater for example. However, since these measures do not provide any intrinsic safety, they do not represent a standard for implementation.

3.7.2.2 Open Cooling Circuit

Direct cooling in the solar circuit with water requires an open system. In case of overheating, an external water supply decreases the temperature in the collectors and solar circuit. The cold water can be provided in several designs and from different sources.

One possibility to cool down the collector array is the use of service water. Therefore, the system requires a discharge to drain-off the excess heat carrier. Buckley and Guldman (1983) patented solar-thermal systems with overheating protection by service water to prevent vapour formation and to use non-metallic materials in collectors. One option is a non-frost-resisting system with a closed solar circuit during operation as shown in Figure 3.33. The thermal storage is connected to the water conduit by a corrugated pipe as heat exchanger. A pressure-controlled valve fills the storage, the solar circuit and the collectors until a pre-set pressure. A temperature-controlled valve connected to the absorber regulates a discharge near the flow pipe of the collector array. At high absorber temperatures the valve opens and the water flows out of the solar-thermal system. The decreasing system pressure opens the valve at the water conduit. The cold water flows from the storage through the collectors to the discharge and reduces the collector temperature. A check valve in the collector outlet pipe ensures the correct flow direction in the system. When the absorber underruns the pre-set temperature, the valve at the discharge closes and the system pressure rises again. Afterwards, the pressure-controlled valve of the water conduit closes also and the normal operational state in the system is restored.

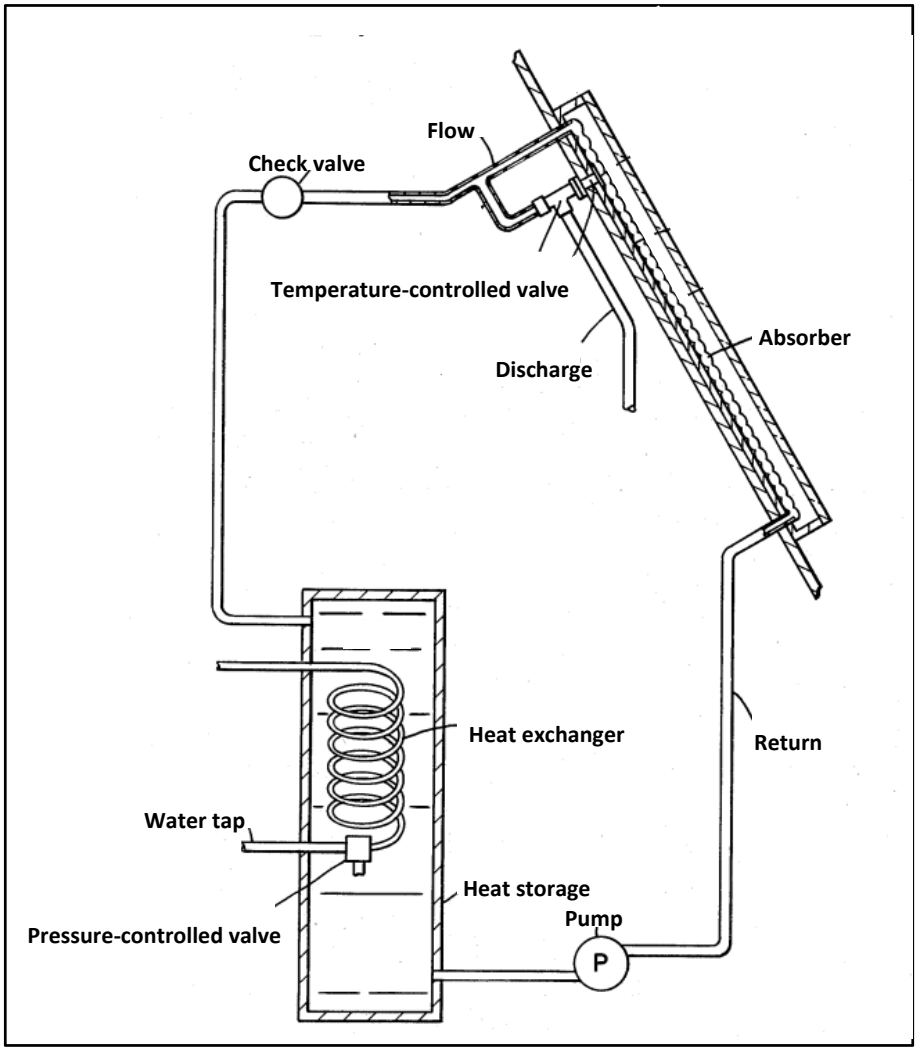

Figure 3.33: Solar-thermal system with overheating protection from service water (according to Buckley and Guldman 1983)

Laing (1985) patented an open, frost-resistant system concept with overheating protection for polymeric collector parts (Figure 3.34). The service water flows directly through the collectors and is stored in a tank for the hot water supply. The water tap is connected at the inlet of the collector array at the bottom edge and is controlled by a temperature-sensitive valve. The sensor of the valve has its position at the outlet near the absorber at the top edge gaining almost the highest collector temperatures possible. Above a pre-set temperature the valve opens and the cold service water flows through the collector array and transfers the heat to the thermal storage. Hence, the collectors cannot reach critical temperatures. The storage also has an overflow to drain-off excessive water produced during

the overheating protection. A frost sensor controls a discharge valve to drain-off the collector array for the protection against frost damage.

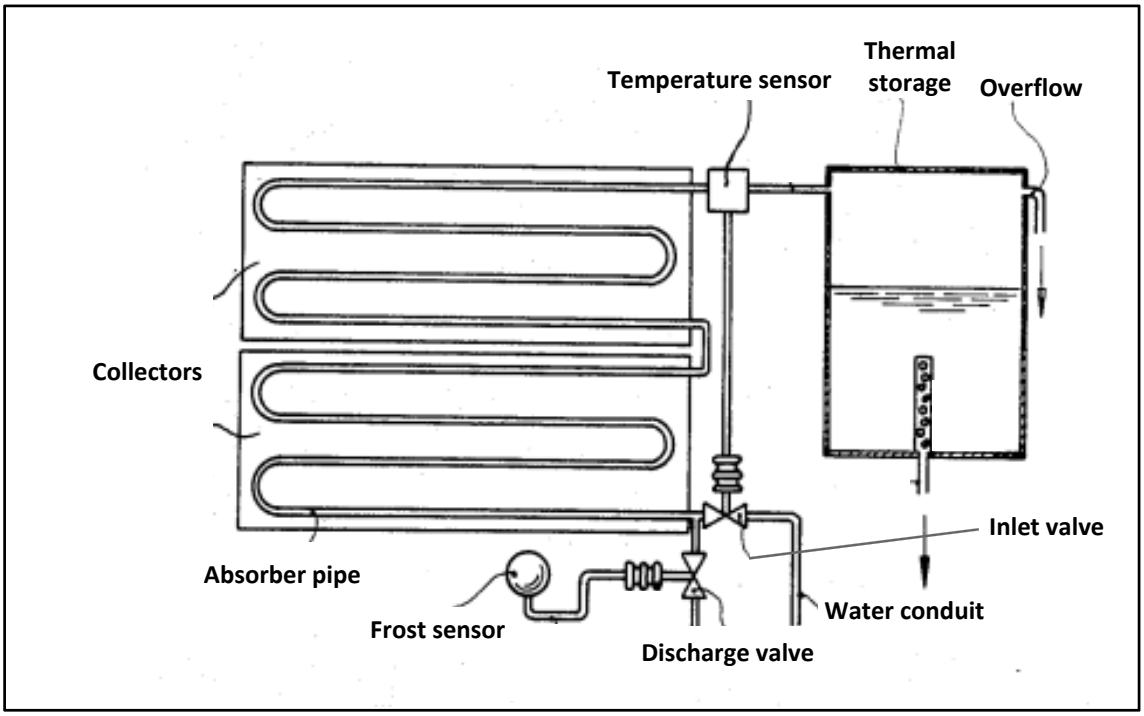

Figure 3.34: Solar-thermal system with direct flow using overheating protection with service water (according to Laing 1985)

Harrison and Harrison (1979) patented a drain-back system with service water overheating protection for polymeric collectors. During normal system operation the water is pumped from the storage to the header of the absorber at the top. The water flows from the header through a glass fibre mat behind the absorber plate. The header pipe at the bottom edge of the collector conduits the heated water back to the thermal storage. At high absorber temperatures a fluid at the absorber sensor evaporates and the actuator opens the three-way valve at the water tap. The cold service water flows also from the top edge of the collector through glass fibre mat to the thermal storage. An overflow conveys the excess water to the sewerage system or other tanks. If the absorber temperature decreases, the actuator closes the water tap. The three-way valve enables draining of the service water pipe to the collector. Thus, the measure is freeze-resisting. An additional service water pipe to the collector provides an emergency measure. The pipe with an enclosed air volume for freeze resistance is closed by a meltable

safety device. In case of complete system failures during critical absorber temperatures, the pipe opens irreversibly and supplies the collector array with cold service water. A vortex chamber acoustically signalizes the operation of the overheating protection measures and the service water consumption. The design of the system is shown in Figure 3.35. This system provides a quite high temperature reduction and is protected against blackouts and system failures. Even the system efficiency is not impaired by this measure.

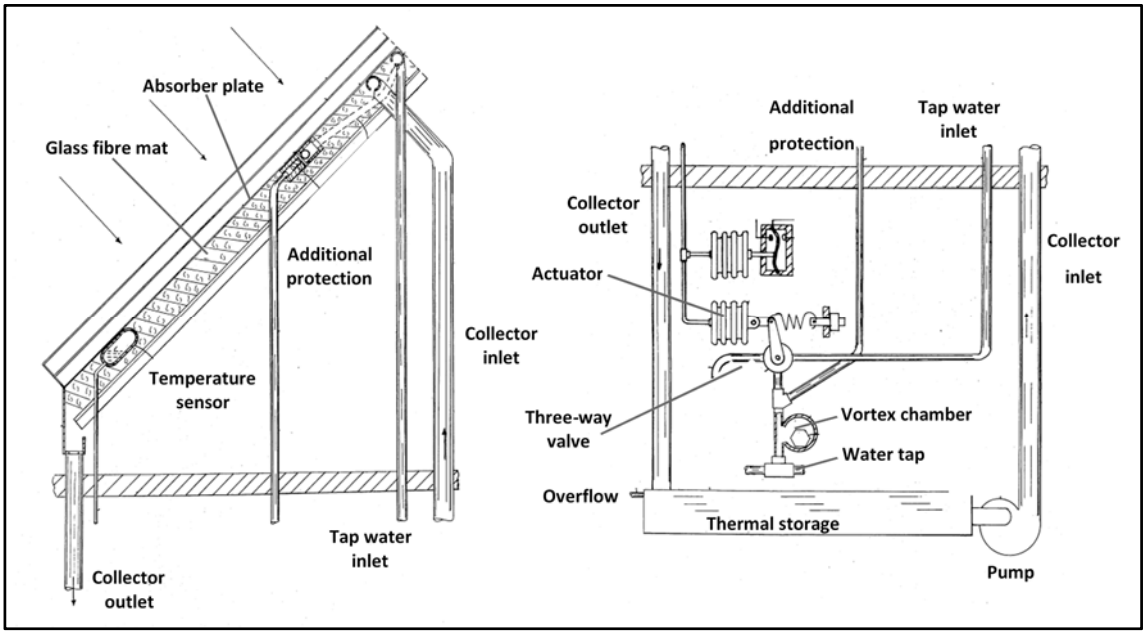

Figure 3.35: Drain-back system with service water overheating protection (according to Harrison and Harrison 1979)

However, the ecological and economic influence of the service water consumption has to be further considered. A combination with another measure to reduce the water consumption seems to be promising.

The use of groundwater is a cost-effective alternative to service water. The set-up is similar and only requires a pump for the groundwater supply. Nevertheless, the missing intrinsic safety against blackouts reduces the practicability of the approach.

3.7.2.3 Intelligent System Control

The dissipation of the thermal energy of the storage during night can prevent stagnation caused by excessive supply of solar energy. The operation of the solar circuit during night transfers the heat from the thermal storage to the collector array. The collector loses heat via convection and radiation to the ambient and cold air. Hence, the storage is prepared for a permanent operation without being overloaded the next day. This measure is quite useful for solar-thermal systems and for space heating during summer. In particular, since the solar energy available and thermal consumption will largely not be required. The measure requires a control unit to identify a potential storage overload and to start an operation of the solar circuit in order to reduce the storage temperature.

Becker et al. (2006) investigated the stagnation behaviour of a large-scale solar-thermal system (300 m² collector area, 27 m³ buffer storage volume, Freiburg - GER) with an implemented system control for collector operation during night by simulation. This measure completely avoids the storage overloading over the year and enabled a maximum absorber temperature of about 90°C. For the operation of pumps in the solar station an additional power consumption of 21 % was found to be necessary to transfer the heat from the storage to the collector array during night. The simulation showed that there was a strong dependency between the annual solar gain and the additional power consumption from the pre-set controller parameters. This included the cut-off temperature of the storage in cooling operation, the target collector temperature and the flow rate during night. Furthermore, the reverse flow direction of the solar circuit is necessary to reach a high temperature difference between heat carrier and ambient air.

This measure is independent from the set-up and the size of the solar-thermal system. Only the parameters have to be adjusted. On the basis of the documented findings, a relatively large temperature reduction of the collector parts may be possible. The additional parts and the changes in the set-up of the solar-thermal system are also relatively low. However, there is no intrinsic safety provided by this measure neither against blackouts nor system failures. The missing

overheating protection in case of an incorrect insolation prediction provides another disadvantage. Furthermore, the dissipation of thermal energy in the storage can reduce the system efficiency due to a potential mismatch of overheating protection and heat consumption. However, active overheating protection measure is only needed when an excess supply of solar-thermal energy and low heat consumption exist. Due to the increased operating costs and the absence of the intrinsic safety this measure is not deemed to be adequate as single protection element. A combination of additional measures, however, provides potential.

3.7.3 Cooling Measures in the Heating System

The cooling measures in the heating system include options to dissipate the thermal energy from the storage. Therefore, the measures or rather heat sinks are integrated in the storage or connected to the storage periphery. Such measures can only be used as additional, supporting steps because they provide no intrinsic safety for the collector array. The two possible versions of cooling measures are additional heat sinks at the thermal storage or the use of present heat sinks in the heating system by an intelligent system control.

3.7.3.1 Additional Heat Sinks

The additional heat sinks extract thermal energy from the storage to prevent thermal overloading. This measure can operate simultaneously with the solar circuit for a direct or time-delayed heat removal for a storage preparation. Therefore, heat exchangers are implemented at the thermal storage or in the heating system to transfer the thermal energy to additional consumers or to apparatuses for heat dissipation. Ground regeneration for heat pump systems, the green house, the pool, the washing machine or the dishwasher are only a few examples for additional heat sinks. The lack of standardisation of such measures is one of the main drawbacks since the implementation depends on the installation environment to a great extent. Apparatuses for heat dissipation are all kind of surface heat exchangers transferring the heat to the ambient air inside and outside the building. The additional power consumption for the operation of the solar-thermal system

and the circulation pumps as well as investment are among the major problems besides the difficulty of providing intrinsic safety.

3.7.3.2 Intelligent System Control

The discharge of the thermal storage with an intelligent system control uses the existing heat sinks in the heating system. In contrary to additional heat sinks, no retrofit or mounting of extra parts is necessary. Only the controller strategy is to be adjusted to the operation of the overheating protection measure.

Streicher (2008) suggests a flow through the inactive boiler of the burner to reduce the storage temperature. The boiler transfers the heat to the occurring air flow in the chimney. The system set-up requires a back-up heating from a burner. Hence, this measure is not independent from the installation environment. Furthermore, the performance of the overheating protection measure is too low in relation to the energy output of a collector array during stagnation.

The operation of certain radiators or heating areas in the building reduces the storage temperature and avoids stagnation in the collector array. The controller activates the pump operation of the heater circuit in the basement for example to discharge the storage parallel to the collector operation or during night for storage preparation for the next day. Such strategies are already implemented in state-of-the-art solar-thermal systems.

3.8 Adjustment of the Collector Efficiency

Beside active or passive measures controlling the performance of the collector and the part temperatures, the adjustment of the collector efficiency as well provides overheating protection. The efficiency reduction by increased losses can be divided into two effects. On the one hand, there are constant losses of the optical performance caused by the transmission properties of the glazing and the absorption properties of the absorber. On the other hand, there are temperature

dependent thermal losses caused by convection, conduction and radiation. Figure 3.36 shows the collector losses of a conventional flat-plate collector being referenced to the collector efficiency curve.

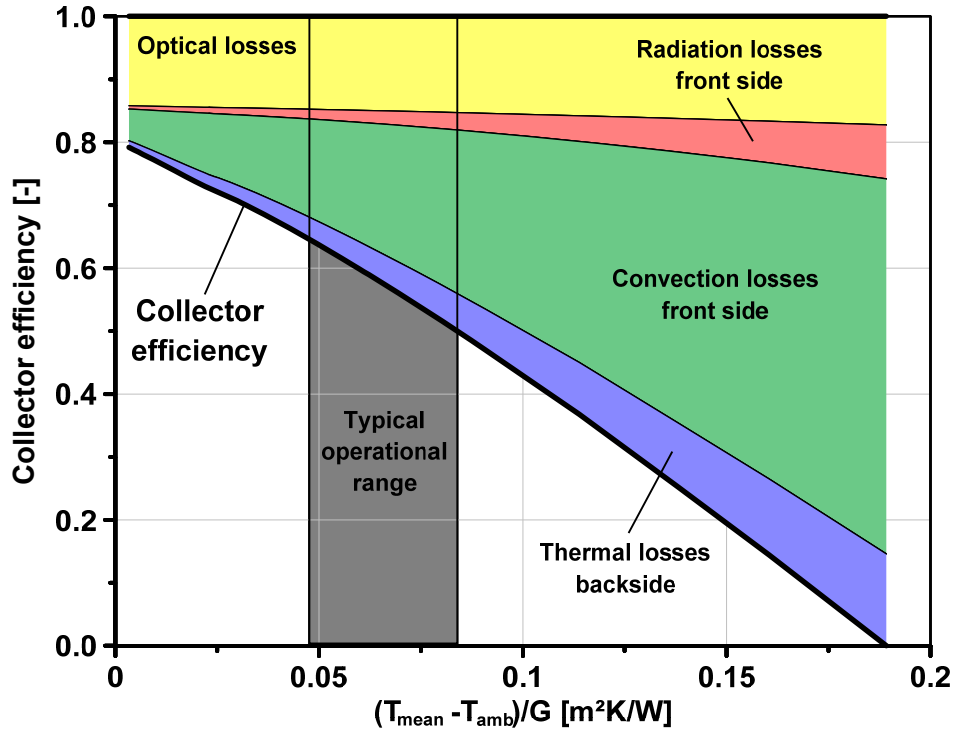

Figure 3.36: Efficiency curve and collector losses of a conventional flat-plate collector

In order to adjust the efficiency, the collector performance is to be reduced with regard to reasonable system efficiencies. During system operation, the collector efficiency of an adjusted collector must therefore be close to the efficiency of a conventional collector and should decrease at higher collector temperatures. Thus, thermal losses only should be used to reduce the collector efficiency and the temperatures since the effects increase hand in hand with the component temperatures.

As a second aspect for the efficiency adjustment, the costs for having the collectors manufactured should also be taken into consideration. Due to the lowered solar yield of the system, the collector costs are even more important to compete with state-of-the-art collectors. Thus, the approaches for cost reduction have to compensate the efficiency reduction.

By means of those requirements, efficiency reduction has to be realised by omitting manufacturing steps or material savings. There are two relevant approaches for such a performance adjustment especially with regard to polymeric collectors.

3.8.1 Increase of the Emission Coefficient of the Absorber

Performance can be adjusted by substituting or omitting the selective absorber coating. A surface with a higher emission coefficient has an increased heat transfer via radiation to the glazing and causes higher collector losses. For example, Figure 3.37 shows the collector efficiency curve and the collector losses of a collector without any selective absorber surface in comparison to the collector efficiency curve with selective coating.

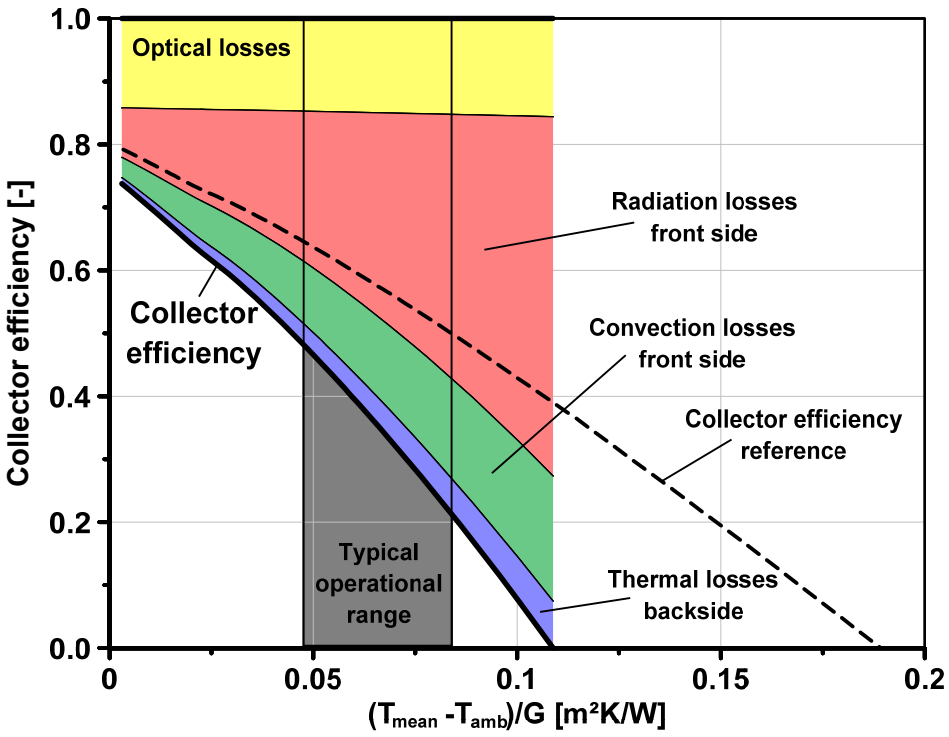

Figure 3.37: Efficiency curve and collector losses of a flat-plate collector without selective coating

The radiation losses are significantly increased and show a non-linear behaviour. This steep gradient in dependence of the reduced temperature can be used to gain a relatively high efficiency in the typical operational range of collectors for

hot water preparation and space heating and to lower the part temperatures during stagnation.

Most state-of-the-art absorber plates have coatings produced in PVD processes. The substrates for those coating processes are coils made from copper and aluminium. Polymeric absorbers produced as single pieces cannot be coated in such production lines. The polymeric material, too, is not as suitable as coating substrate. Thus, a cost-effective TISS colour (thickness-insensitive spectrally selective) with an emission coefficient ε of 0.34 (Orel et al. 2009) or only a black surface instead of state-of-the-art coatings with emission coefficients of about 0.05 are possible. In case of a black surface, a black-pigmented polymer can be used to make further treatment of the surface dispensable.

However, Figure 3.37 also shows a considerable efficiency decrease in the operational range of the collector or rather of the system. Therefore, beside the decrease in temperature, the influence on the system behaviour has to be further investigated.

3.8.2 Decrease of the Insulation Properties of the Collector Backside

Higher backside losses in combination with an advanced casing design are also a possible option to balance collector efficiency and manufacturing costs. Less insulation material or substituting the insulation by air in new casing designs are also thinkable. Figure 3.38 shows the collector efficiency curve and the collector losses of a collector with a reduced backside insulation thickness by one third in comparison to the reference collector efficiency curve. The increase of backside losses is not as drastic as the increase of the radiation losses due to the missing selective coating. In this case, the limited influence on the collector efficiency also has little influence on the maximum part temperatures. The interaction between collector efficiency, maximum temperatures and insulation properties has to be investigated by parametric analysis to identify the potential of the concept.

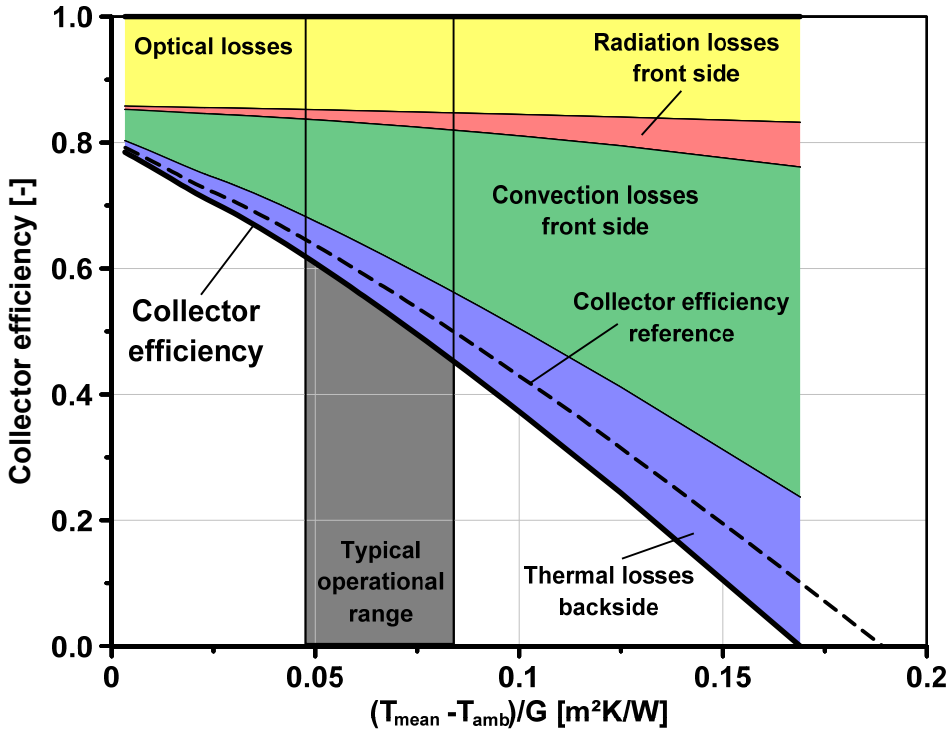

Figure 3.38: Efficiency curve and collector losses of a flat-plate collector with reduced insulation thickness

The low cost savings of mineral wool for insulation decreases the potential of the approach. However, the production of a casing with a moderate insulation in a single step represents an interesting alternative. There are two options for improved concepts ranging from casings made from rigid foam combining housing and insulation to designs with enclosed air chambers to inhibit convection losses at the backside. A further advantage of this approach is the avoidance of fogging in the collector and moisture in the mineral wool causing increased heat conductivity.

3.9 Buffering Critical Collector States

Active or passive approaches focus on keeping the part temperatures of the collector permanently on a low level. However, critical weather conditions causing high collector temperatures only occur for a certain time interval (cf. Chapter 2.2.1). Thus, the time dependent temperature rise can be delayed by increased or additional heat capacities.

3.9.1 Integrated Collector Storage

Additional heat capacities within collectors are realised in integrated collector storage solar water heaters. The storage volume is integrated in the absorber and is heated automatically by the sun. A heat exchanger removes the absorbed heat from the collector. Such systems are normally used for hot water preparation. ICS solar water heaters can be built as CPC collectors (Souliotis et al. 2013) as well as flat-plate collectors (Gertzos 2007). Figure 3.39 shows examples of CPC collectors.

Figure 3.39: Integrated collector storage solar water heaters (Souliotis et al. 2013)

The heat capacity of such collectors can be increased by using phase change materials instead of water (Chaabane et al. 2014).

Phase-change materials have their melting point at a certain temperature within the utilisation temperature range of heat storages. The absorbed thermal energy within a phase is temperature dependant and defined as sensible heat. The absorbed thermal energy during the phase change occurs at a constant temperature and is defined as latent heat (Figure 3.40). Due to the phase transition, the material is able to absorb larger amounts of heat within a limited temperature range compared to storage materials that are using sensible heat only. Commonly used materials in heat storages for solar-thermal systems have a solid-liquid phase change. Materials that show this reversible effect in heat storages are waxes or hydrated salts (Farid et al. 2004).

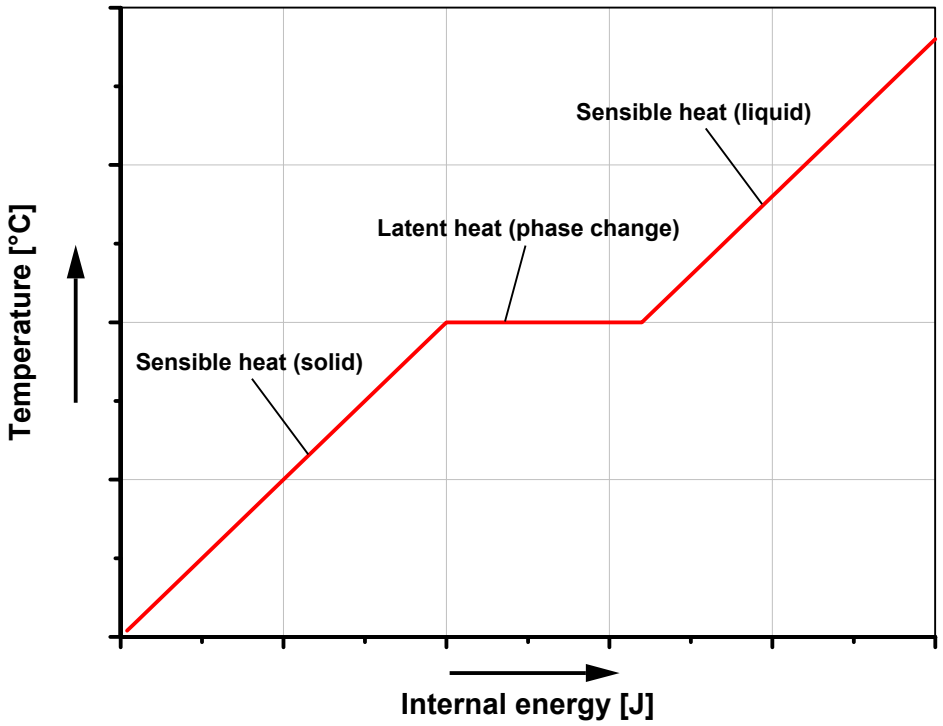

Figure 3.40: Gradient of the temperature in dependency of the absorbed thermal energy of a phase change material

The approach of ICS collectors delays the moment of reaching critical temperatures in collectors and also works during blackouts. However, there is no overheating protection in case of a full thermal storage. Therefore, the system has to be equipped with an intelligent system control, as described in Chapter 3.7.3.2, in order to keep the storage on a suitable temperature level and to ensure the highest potential of the concept. Despite the combination with a control approach, it is not possible to realise an intrinsically safe collector because of the limited heat capacity of the storage or rather the dependency on the operational state of the system. Apart from that, the cost benefit has to be regarded as critical when using expensive phase change materials.

3.9.2 Slurry Phase Change Materials as Heat Carrier

Serale et al. (2013) analysed the use of a slurry phase change material as heat carrier in flat-plat collectors. The latent heat of the phase change keeps the mean

fluid temperature on a lower level and thus causes lower heat losses of the collector. Depending on the climate efficiency increases between 5–10 % were identified.

This effect can also be used in absorbers to delay the temperature increase during stagnation. Especially, volumetric absorbers with larger fluid content have an increased effect for this reason. However, the limited heat capacity in comparison to the incoming solar irradiance during stagnation, the missing intrinsic safety and, especially, the high costs for the heat carrier are drawbacks preventing the realisation as overheating protection approach in cost-efficient collectors.

3.10 Preselection of Overheating Protection Approaches

The described overheating protection approaches were evaluated and preselected as basis for the extensive simulation analysis with respect to the reachable temperature reduction and the influence on the collector or system performance.

Therefore, the measures and approaches have to be classified regarding their intrinsic safety. Table 3.2 lists the different classes for the system.

Table 3.2: Classes of the overheating concepts regarding intrinsic safety

Class	Description
A	Measure protects the system permanently
B1	Measure protects the system during power blackouts
B2	Measure protects the system during system failures
C	Measure protects the system only in the operational state

In a second step, the concepts were evaluated regarding their pertinent properties being identified in the description in order to specify and to remove concepts in the evaluation process. Thus, the feasibility provides a first overview on approaches being suitable for polymeric collectors as well as for a further analysis.

Afterwards, the evaluation of the single approaches and the combinations for an effective protection was conducted by assessment criteria from the technical and

the economic point of view listed in Table 3.3. The evaluation by these criteria is based on the literature review and additional estimations to identify the most promising approaches for the detailed investigation.

Table 3.3: Assessment criteria for overheating protection concepts

Assessment criteria	Description
Technical criteria	
Temperature reduction	Reachable temperature reduction at the parts
Intrinsic safety	Efficiency of the measure under certain conditions
Universal applicability	Dependence of the measure from installation and system set-up
Economic criteria	
Operational costs	Additional costs for the operation of the measure
Efficiency reduction	Influence on the system efficiency
Manufacturing costs	Additional costs for the implementation of the measure

Table 3.4 and Table 3.5 show the evaluation process of the measures which change their optical efficiency. Therefore, a scale from 1 to 5 were chosen, where 1 the worst and 5 the best rating of the criteria represents. The approaches shown in red are removed because of the missing intrinsic safety or other pertinent disadvantages like e.g. ageing behaviour or reliability. Most of the approaches provide an intrinsic safety, but only several measures are suitable for a reasonable implementation in collectors.

Table 3.4: Evaluation and feasibility of the overheating approaches changing the optical efficiency — part 1: changing the transmission properties

Overheating approach (sorted by chapters)	**Intrinsic safety**	**Temperature reduction**	**Universal applicability**	**Operational costs**	**Efficiency reduction**	**Manufacturing costs**
3.3 Changing the Transmission Properties						
3.3.1.1 Thermochromic Layers	A	4	5	5	4	3
3.3.1.2 Thermotropic Layers	A	4	5	5	4	3
3.3.2.1 Electrochromic Layers	A	4	5	4	4	0
3.3.2.2 Electrotropic Layers	A	4	5	4	4	0
3.3.2.3 Switchable Mirrors	A	5	5	4	4	0
3.3.3 Chemically Switchable Layers	A	4	5	3	4	0
3.3.4.1 Geometrical Structuring of the Glazing	A	2	3	5	3	4
3.3.4.2 Microstructures on the Surface of the Glazing	A	4	3	5	3	4
3.3.5.1 Shading Elements	B2	5	5	4	5	1
3.3.5.2 Infilling of Shading Material (Bulk Goods)	B2	5	3	3	4	1
3.3.5.3 Rotation of the collector	B2	4	5	4	5	1
3.3.6.1 Shading Fluid between a Double Glazing	B2	4	4	3	3	1
3.3.6.2 Light Scattering Double Glazing	B2	3	4	3	2	1

Table 3.5: Evaluation and feasibility of the overheating approaches changing the optical efficiency — part 2: changing the absorption properties

Overheating approach (sorted by chapters)	**Intrinsic safety**	**Temperature reduction**	**Universal applicability**	**Operational costs**	**Efficiency reduction**	**Manufacturing costs**
3.4 Changing the Absorption Properties						
3.4.1.1 Thermochromic Layers with Switchable Absorption	A	4	5	5	2	3
3.4.1.2 Thermotropic Layers	A	4	5	5	2	3
3.4.1.3 Electrically Switchable Layers	A	4	5	4	3	0
3.4.1.4 Chemically Switchable Layers	A	5	5	3	3	0
3.4.1.5 Microstructures on the Surface of the Absorber	A	4	3	5	3	4
3.4.2.1 Mechanical Appliances	B2	3	5	4	5	1
3.4.2.2 Hydraulic Appliances – Black Fluid	A	5	4	4	4	4

Table 3.6 lists all measures which remove the thermal energy from the collector. The measures being implemented in the collector show a great potential. However, the most measures being integrated in the system are not intrinsically safe. Hence, they can only be used as additional, supporting approach.

Table 3.6: Evaluation and feasibility of the overheating measures removing the thermal energy

Overheating approach (sorted by chapters)	Intrinsic safety	Temperature reduction	Universal applicability	Operational costs	Efficiency reduction	Manufacturing costs
3.5 Changing the Convective Losses						
3.5.1 Natural Convection in the Air Gap	A	3	3	5	4	3
3.5.2 Forced Convection in the Air Gap	B2	5	5	3	5	2
3.5.3 Convection Combined with Evaporative Cooling	A	4	3	4	3	1
3.5.4 Varying the Insulation Properties	B2	3	4	4	4	3
3.6 Changing the Radiation Losses						
3.6.1 Thermochromic Layers with Switchable Emission Coefficient	A	3	5	5	4	4
3.6.2 Contact between Glazing and Absorber	A	4	5	4	5	3
3.7 Active Cooling						
3.7.1.1 Collector Integrated Emergency Cooler	C	5	5	5	4	2
3.7.1.2 Open Cooling Circuit	A	5	4	1	2	3
3.7.2.1 Additional Heat Sinks	C	5	4	3	5	2
3.7.2.2 Open Cooling Circuit	B1	5	5	1	5	3
3.7.2.3 Intelligent System Control	C	3	4	2	4	5
3.7.3.1 Additional Heat Sinks	C	5	3	3	5	4
3.7.3.2 Intelligent System Control	C	3	4	2	4	5

Table 3.7 shows the evaluation of the approaches applicable for the adjustment of the collector efficiency.

Table 3.7: Evaluation and feasibility of the overheating approaches by adjusting the collector efficiency

Overheating approach (sorted by chapters)	**Intrinsic safety**	**Temperature reduction**	**Universal applicability**	**Operational costs**	**Efficiency reduction**	**Manufacturing costs**
3.8.1 Increase of the Emission Coefficient of the Absorber	A	4	5	5	3	5
3.8.2 Decrease of the Insulation Properties of the Collector Backside	A	3	5	5	4	5

Table 3.8 shows the evaluation of the approaches for buffering critical collector states.

Table 3.8: Evaluation and feasibility of the overheating approaches by buffering critical collector states

Overheating approach (sorted by chapters)	**Intrinsic safety**	**Temperature reduction**	**Universal applicability**	**Operational costs**	**Efficiency reduction**	**Manufacturing costs**
3.9.1 Integrated Collector Storage	B1	3	5	5	5	1
3.9.2 Slurry Phase Change Materials as Heat Carrier	B1	2	5	5	5	1

Depending on the class of intrinsic safety, different concepts can be combined to fulfil the overheating protection in operational state as well as during failures. On the basis of this evaluation, the concepts of Table 3.9 were chosen for the more detailed investigation. This preselection will be used for the final qualitative evaluation based on the results from the simulation analysis.

Table 3.9: Chosen overheating protection concepts for simulation

Concept
Thermotropic Layers
Thermochromic Layers with Switchable Emission Coefficient
Thermochromic Layers with Switchable Emission Coefficient + Service Water Cooling
Microstructures on the Surface of the Glazing
Microstructures on the Surface of the Glazing + Service Water Cooling
Increase of the Emission Coefficient of the Absorber
Decrease of the Insulation Properties of the Collector Backside

4 Collector and System Modelling

The detailed analysis and evaluation of the approaches for overheating protection regarding their temperature reduction as well as their influence on the system efficiency require an extensive simulation model. On the one hand, a mathematical model of the collector being able to calculate the temperatures of the components is needed. The model has to be able to implement the properties of the components as well as the overheating protection measures. On the other hand, a solar-thermal system for space heating and domestic hot water preparation similar to the field-testing system has to be implemented into a simulation.

The simulation tool *Matlab/Simulink* (MathWorks n.d.) was used for the implementation of the collector and system models. *Simulink* is a simulation tool on the basis of *Matlab* being able to build mathematical systems from single blocks by connecting each other and using “drag and drop”. The block libraries embrace blocks of basic maths and common functions, interfaces for input and output as well as a multitude of build-ups of various systems. Furthermore, *Simulink* is able to embed programmes written in a lower-level programming language like *C*, for example. Thus, complex systems can be programmed and integrated easily into the system environment of the blocks.

Hafner et al. (1999) developed the *CARNOT* toolbox containing blocks for the build-up of heating systems. This library provides models for the simulation of various heat sources, heat consumers, storages, controllers, pipes and pumps. Furthermore, models for providing weather data, fluid properties and user functions are available. Also user-defined interfaces for the output of the relevant simulation data are programmed.

The detailed build-up of the collector models and the predefined heating systems as well as the test stand are described as follows.

4.1 State-of-the-Art Flat-Plate Collector Modelling

Commonly used parametric models in simulation tools are based on collector test results from the solar simulator or outdoor testing. The function of the collector efficiency curve from the test results is derived by quadratic regression (ASHRAE 2003, Cooper and Dunkle 1981). Equation (4.1) describes the simple parameter model.

$$\dot{Q}_f = A\left[G_{sun}F'(\tau\alpha) - a\left(T_f - T_{amb}\right) - b\left(T_f - T_{amb}\right)^2\right] \tag{4.1}$$

The linear heat loss coefficient a and the quadratic heat loss coefficient b characterise the thermal collector´s behaviour depending on the temperature difference between fluid and ambient air. The fraction of the converted solar energy by the absorber is limited by the so-called optical efficiency of the collector. When the mean fluid temperature is equal to the ambient temperature, almost no heat losses occur at the collector. Thus, the thermal output of the collector can only be reduced by the optical characteristics of the glazing and the absorber $(\tau\alpha)$ as well as by the collector efficiency factor F' caused by a temperature gradient in the fins, which results in heat losses.

This one-dimensional approach can be used as a multimode model to reproduce the temperature gradient of the fluid along the absorber pipe between inlet and outlet. Hafner et al. (1999) enhanced the basic equation of the parameter model by considering the heat capacity of the collector, heat losses dependent on the wind speed as well as additional radiative heat losses. However, these models are not suitable for the investigation of new collector designs. On the one hand, the parameters describe a certain measured collector but are not able to represent adjustments to the collector build or the implementation of overheating protection measures. On the other hand, the model only provides a fluid temperature. However, the thermal investigation of collectors requires a broad output of the component temperatures with respect to polymeric materials.

The steady-state model by Hottel and Whillier (1958) only provides information on the collector performance by means of the fluid inlet temperature $T_{f,in}$. Equation (4.2) describes the collector model.

$$\dot{Q}_f = F_R A\left[G_{sun}(\tau\alpha) - U_{coll}\left(T_{f,in} - T_{amb}\right)\right] \tag{4.2}$$

The optical characteristics $(\tau\alpha)$, the heat removal factor F_R and the overall heat loss coefficient of the collector U_{coll} describe the performance of the collector. These characteristics are based on the physics of the collector considering dimensions, shapes and materials. The temperature dependent heat transfer coefficients of the overall heat loss coefficient U_{coll} vary subject to the conditions. Therefore, the component temperatures and the heat transfer coefficients have to be calculated by iteration. The reproduced physics of the model enable a change into various designs or build-ups. Also, all the described overheating protection measures can be implemented into this model. Klein et al. (1974) investigated the transient behaviour of collectors or rather systems and identified significant differences to steady-state model approaches under certain conditions. During daily morning heating and rapidly changing ambient conditions like shading by clouds, neglecting the thermal capacity of the components led to different results. Therefore, a model on the basis of equation (4.2) was extended with two heat capacities. Fluid, absorber and half of the insulation show almost the same temperature and represented the first heat capacity. The second heat capacity was the glazing. Klein et al. (1974) and also Wijeysundera (1978) found that the difference between one-node models, two-node models and experimental data for normal collector build-ups and systems according to the yield became less. However, taking into consideration that overheating protection measures can most probably be influenced by quick reaction times, there are significant differences between steady-state and transient models, in particular with regard to component temperatures. The main disadvantage of the model is the consideration of average component temperatures for the entire collector. Hence, the increase in temperature along the risers during operation causing maximum and minimum temperatures is not taken into account. The collector properties, too,

are considered as homogenous for the entire model. This makes the approach incapable of considering fractional changes (e.g. at the upper half) of the properties or of the design in the collector model.

Thus, a dynamic, numerical model of a state-of-the-art flat-plate collector was developed under consideration of the relevant capacities deriving information on individual component temperatures, heat fluxes and collector performance. Moreover, the model can be adjusted to new collector parameters or designs and enables an implementation of overheating protection measures. By implementing the multi-node collector model, the capacity of absorber, fluid, glazing and casing was taken into account. The network connecting the nodes as well as the ambient are physical functions depending on geometry, size, materials and operating conditions.

4.1.1 Description of the Collector

The field-test collector was chosen for the performance simulation of state-of-the-art types. This type represents typical flat-plate collectors for solar-thermal systems for space heating and domestic hot water preparation in Central Europe. The cross section of the collector in frame design is shown in Figure 4.1.

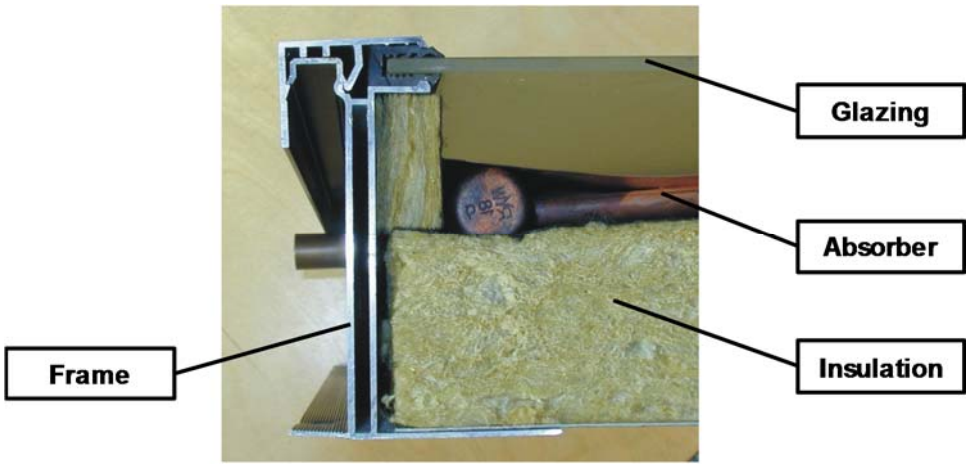

Figure 4.1: Cross section of a state-of-the-art collector with aluminium frame

The basic design data of the collector is listed in Table 4.1. The dimensions are comparable to most collectors for heat supply in the sector for residual buildings.

Table 4.1: Basic design data of the state-of-the-art collector

Gross length	1.987	[m]
Gross width	1.046	[m]
Gross area	2.078	[m²]
Aperture area	1.903	[m²]
Absorber area	1.903	[m²]
Weight (empty)	39	[kg]
Liquid content	1.12	[l]

The sheet-pipe absorber has a double harp design as shown in Figure 4.2. This design provides an improved flow distribution in the riser pipes in contrast to the conventional harp design. The following factors such as the reduced ratio between the total flow area of the riser pipes and the flow area of the header as well as the increased pressure drop in the riser pipes which is caused by the doubling of the length and the velocity of the stream, have a positive effect on the flow through the absorber (Bassiouny und Martin 1984a and 1984b).

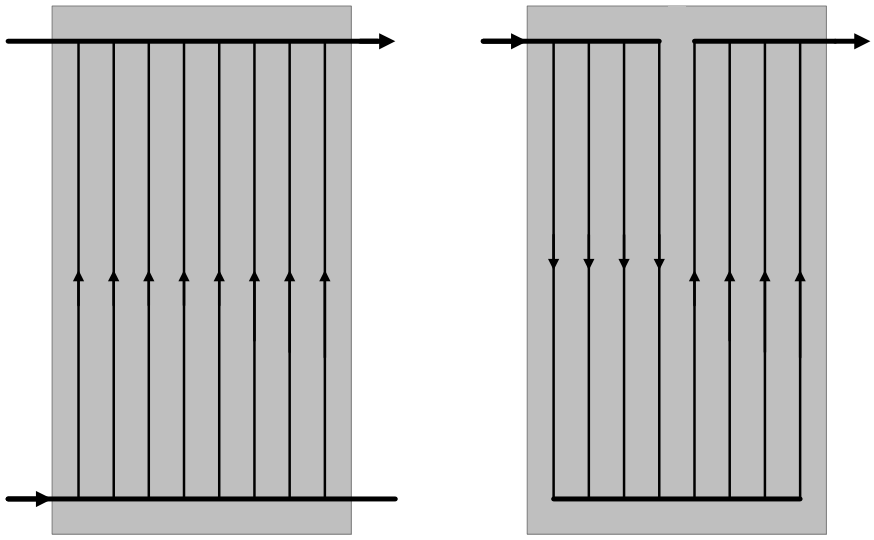

Figure 4.2: Design types of harp absorbers
(left: harp design; right: double harp design)

The ultrasonic welded absorber is made from copper. The plate is only welded to the riser pipes. The design data of the absorber is listed in Table 4.2.

Table 4.2: Design data of the absorber

Plate:		
Thickness	0.0002	[m]
Headers:		
Length (pipe)	0.926	[m]
Length (plate)	0.985	[m]
Width (plate)	0.034	[m]
Inner pipe diameter	0.016	[m]
Wall thickness	0.001	[m]
Risers:		
Number	10	[-]
Length	1.857	[m]
Width (plate)	0.0985	[m]
Inner pipe diameter	0.007	[m]
Wall thickness	0.0005	[m]

The casing consists of an aluminium frame and mineral wool insulation (Figure 4.1). The extruded frame profile is plugged together with an aluminium backside sheet. The mineral wool insulation is placed at the backside as well as at the frame. The design data is shown in Table 4.3.

Table 4.3: Design data of the insulation and casing

Casing:		
Frame height	0.093	[m]
Backside sheet thickness	0.001	[m]
Backside insulation:		
Thickness	0.045	[m]
Side insulation:		
Thickness	0.013	[m]

The collector is also equipped with a structured low-iron solar glazing and a selective absorber coating. The optical properties are shown in Table 4.4.

Table 4.4: Optical properties of the collector

Glazing:		
Thickness	0.0032	[m]
Transmission coefficient τ	0.918	[-]
Absorber:		
Absorption coefficient	0.95	[-]
Emission coefficient	0.04	[-]

The collector was tested by the Institut für Solartechnik SPF (2005), a Swiss research institute of solar energy technology. The conditions and the results of the outdoor collector performance test are listed in Table 4.5.

Table 4.5: Test conditions and efficiency curve of the collector derived from testing

Testing conditions:		
Water-glycol mixture	33.3	[%]
Volume flow rate	280	[l/h^{-1}]
Irradiance	800	[Wm^{-2}]
Efficiency curve (referenced to absorber area):		
η_0	0.798	[-]
a	3.34	[$Wm^{-2}K^{-1}$]
b	0.0075	[$Wm^{-2}K^{-2}$]
C (heat capacity)	9.5	[kJK^{-1}]

4.1.2 Simplifying Assumptions

Modelling technical components or products requires a number of simplifying assumptions to limit the complexity of the model. Various small effects in components or products are very difficult to implement into the model and can be neglected due to their limited influence on the entire system. Thus, the following assumptions described for collector modelling were made. These assumptions, however, do not alter the basic physical situation of the collector.

1. Heat transfer below and above the absorber is one-dimensional in z-direction (Figure 4.3).

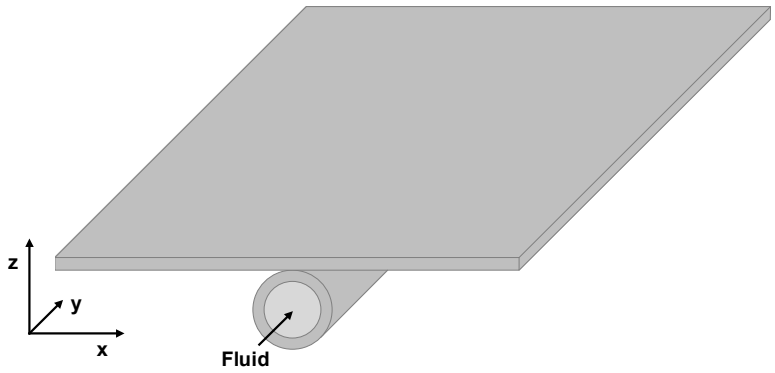

Figure 4.3: Schematic build-up of an absorber stripe

2. Headers and their plates make up only a small area of the collector and can be neglected.
3. There is no difference in the fluid flow rates in the riser pipes.
4. The temperature gradient of the absorber plate (x-direction) caused by the fin efficiency of the plate-pipe design cannot be described by any transient model with a limited number of nodes. Moreover, a one-node model with an average temperature is not sufficient since the effects of the heat losses via convection and radiation are non-linear. This is why the absorber plate has to be reproduced by a multi-mode model enabling a non-linear temperature progression. The corresponding schematic temperature gradients are shown in Figure 4.4.

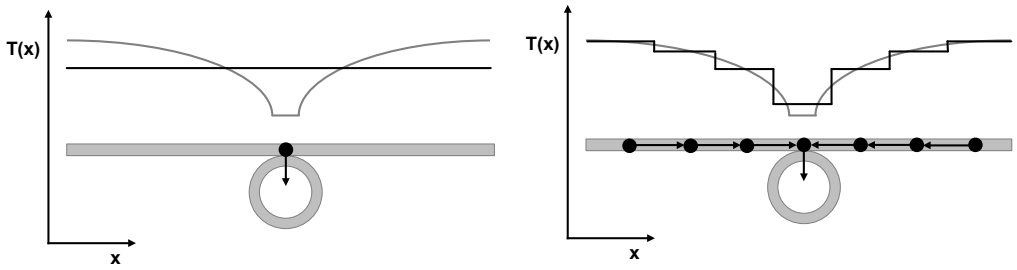

Figure 4.4: Schematic temperature distribution at the cross section of an absorber in a one-node (left) and a seven-node (right) absorber model in comparison to the analytical temperature gradient

5. Around the riser pipes no temperature gradients occur.

6. The temperature gradient of the absorber along the riser pipes (y-direction) is non-linear and cannot be described by any transient model with a limited number of nodes. A one-node model with an average temperature is not sufficient since the maximum temperatures are lowered and the effects of the heat losses via convection and radiation are non-linear. This has an impact on the other temperature nodes of the absorber as well. Therefore, a multi-node model along the fluid flow is necessary. The corresponding schematic temperature gradients are shown in Figure 4.5.

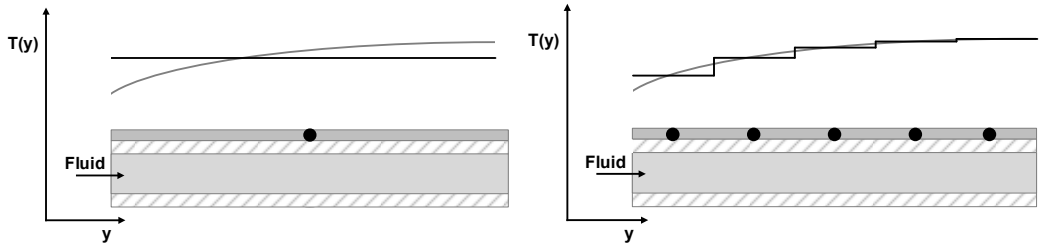

Figure 4.5: Schematic temperature distribution at the cross section of an absorber along the pipe in a one-node (left) and a five-node (right) absorber model in comparison to the analytical temperature gradient

7. The riser pipe is only connected to the fluid and the absorber nodes. The heat transfer to the air gap can be neglected since the pipe surface is relatively low. Furthermore, the temperature gradient between pipe and air is relatively low.
8. The two harps of the absorber do not influence each other thermally. Hence, there is no heat transfer between neighbouring risers of the first and second harp, neither is there any convection between the two arrays with different temperature.
9. Unsteady heat conduction in the insulation can be neglected. The analytical temperature distribution in a solid material during time-dependent temperature changes is influenced by the heat capacity of the system. Thus, a multi-node model can represent this effect. However, the required number of nodes of the model would be significantly increased. Therefore, the heat capacity of the insulation is represented by a single

node. In a second step, the linear temperature gradient through the insulation is calculated under steady-state conditions. Figure 4.6 shows the described approaches.

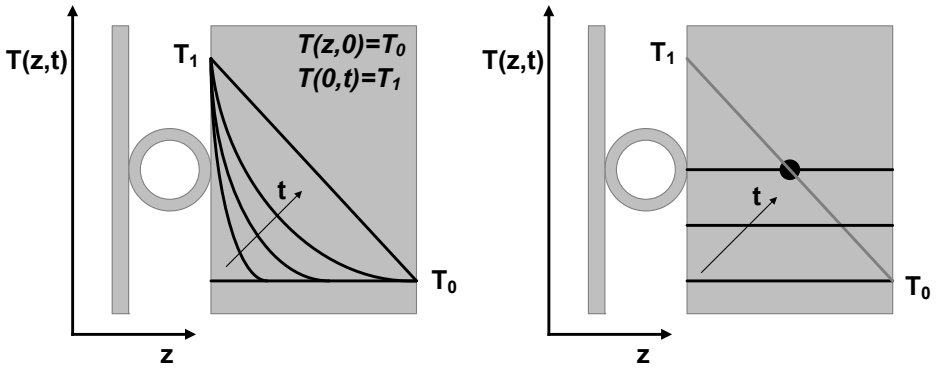

Figure 4.6: Schematic temperature distribution at the cross section of the casing or insulation during unsteady heat conduction in an analytical model (left) and a one-node model with additional steady-state calculation of the temperature gradient

10. The heat capacity of the backside sheet of the casing can be neglected due to the low mass of the component as well as the low temperature changes near the ambient air.
11. The frame of the collector is neglected. Due to the one-dimensional heat transfer through the collector, the effects in the frame cannot be taken into consideration. Furthermore, the effect of the heat capacity has only a slight influence since the temperature changes outside the collector insulation are low.
12. The temperature gradient in the glazing is neglected. The low thickness and the moderate heat conductivity of the glazing limit the influence of any heat conduction to a minimum.
13. The glazing is non-transparent for the wavelength of infrared radiation. Thus, heat radiation is completely absorbed by the glazing material. This assumption is valid for solar glass. The implementation of polymeric materials being partly transparent for infrared radiation requires an adjustment of the heat transfer network.
14. Since the impacts of the structured surface of the glazing are only marginal compared to the plain surfaces, the latter was not taken into consideration.

15. The sky is a black body for infrared radiation.
16. The ambient temperature around the collector is homogeneous.
17. The effect of wind is considered homogenously over the glazing in x-direction.
18. Wind at the backside is neglected because of the small distance between backside insulation and roof as well as the small temperature difference between outer surface and ambient air.
19. Shading from the frame at the absorber is not taken into consideration.
20. Neither are effects from operation considered (dust, dirt, degradation, moisture…) influencing the optical and thermal performance of the collector.

4.1.3 Model Build-up and Energy Balance

The developed numerical model of the collector is limited to the area of the risers. Using the symmetry of the collector, the model can be described by only one riser. This model of a riser is used for both halves of the double harp absorber. Figure 4.7 shows the cross section of the riser or rather the collector model with its capacities and its connecting energy fluxes. The ten-node model can be reduced by using the symmetry of the absorber plate to a seven-node model.

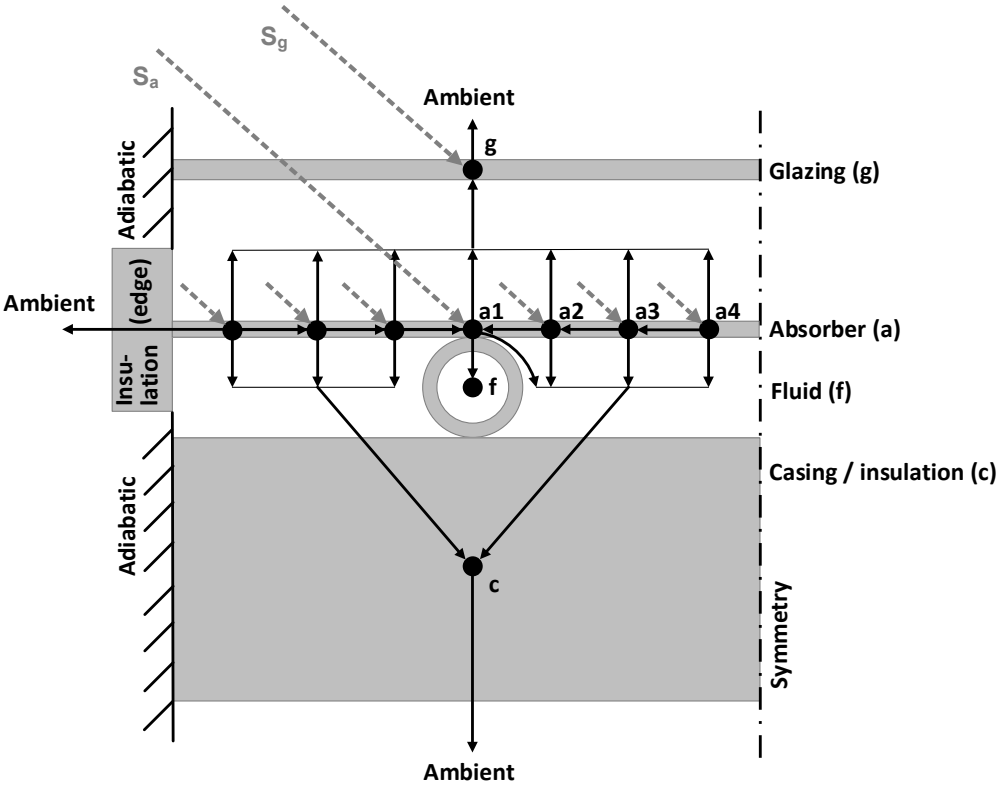

Figure 4.7: Cross section of the state-of-the-art collector model with nodes and energy fluxes

The equations (4.3) to (4.9) give an overview of the energy balance drawn in the collector model describing the capacities of each node as well as the energy fluxes between the nodes.

Glazing (g):
$$m_g c_g \frac{dT_g}{dt} = S_g + \dot{Q}_{a1-g} + 2\sum_{a=2}^{4} \dot{Q}_{a-g} - \dot{Q}_{g-amb} \tag{4.3}$$

Absorber 1 (a1):
$$m_{a1} c_{a1} \frac{dT_{a1}}{dt} = S_{a1} + 2\dot{Q}_{a2-a1} - \dot{Q}_{a1-f} - \dot{Q}_{a1-g} - \dot{Q}_{a-edge} \tag{4.4}$$

Absorber 2 (a2):
$$m_{a2} c_{a2} \frac{dT_{a2}}{dt} = S_{a2} + \dot{Q}_{a3-a2} - \dot{Q}_{a2-a1} - \dot{Q}_{a2-g} - \dot{Q}_{a2-c} - \dot{Q}_{a-edge} \tag{4.5}$$

Absorber 3 (a3):
$$m_{a3} c_{a3} \frac{dT_{a3}}{dt} = S_{a3} + \dot{Q}_{a4-a3} - \dot{Q}_{a3-a2} - \dot{Q}_{a3-g} - \dot{Q}_{a3-c} - \dot{Q}_{a-edge} \tag{4.6}$$

Absorber 4 (a4):
$$m_{a4}c_{a4}\frac{dT_{a4}}{dt} = S_{a4} - \dot{Q}_{a4-a3} - \dot{Q}_{a4-g} - \dot{Q}_{a4-c} - \dot{Q}_{a-edge} \quad (4.7)$$

Fluid (f):
$$m_f c_f \frac{dT_f}{dt} = \dot{m}_f c_f * \left(T_{in} - T_f\right) + \dot{Q}_{a1-f} \quad (4.8)$$

Casing (c):
$$m_c c_c \frac{dT_c}{dt} = \dot{Q}_{a1-c} + 2\dot{Q}_{a2-c} + 2\dot{Q}_{a3-c} + 2\dot{Q}_{a4-c} - \dot{Q}_{c-amb} \quad (4.9)$$

The node a1 is the base of the fin and includes the riser pipe. The listed energy fluxes connecting the nodes to each other are described in the following in detail.

4.1.4 Optical Properties

The optical properties of the collector comprise the behaviour of the absorber as well as the glazing under irradiance. The occurring optical effects determining the collector performance are reflection, absorption and transmission (Figure 4.8). The effects depend on the irradiance and the incidence angle as well as on the thickness, the refractive index and the extinction coefficient of the materials. The refractive index n and the extinction coefficient K of the glazing material depend on the wavelength of the incoming radiation. In the simulation model these properties are assumed to be constant for the irradiance. Duffie and Beckman (2006) considered this assumption to be ideally suited for covers made of glass.

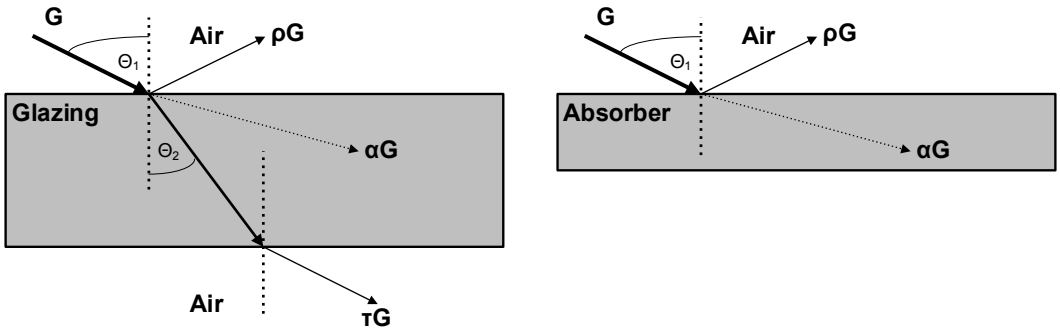

Figure 4.8: Basic optical effects at glazing (left) and absorber (right)

4.1.4.1 Refraction Factor of the Glazing

The incident unpolarised solar radiation is polarised at the boundary surface between air and glazing. The radiation is divided into a parallel and a vertical component with regard to the plane of incidence (Figure 4.9). The definition of the polarised light is necessary for the calculation of the associated reflection factor r (Eicker 2003).

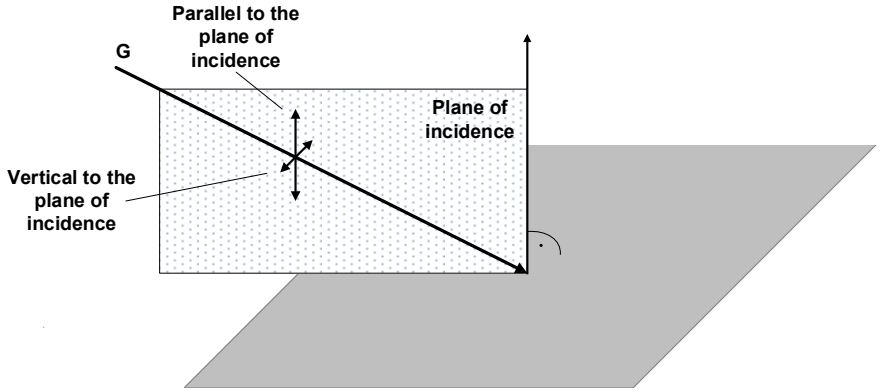

Figure 4.9: Polarisation directions parallel and vertical to the plane of incidence (according to Eicker 2003)

The reflection factor of the boundary surface of the glazing is defined as the ratio between the reflected radiation G_r and the incident radiation G. This ratio results from the average reflection factor from the perpendicular and the parallel part (equation (4.10)) (Duffie and Beckman 2006).

$$r = \frac{G_r}{G} = \frac{r_\perp + r_\parallel}{2} \tag{4.10}$$

The Fresnel formulae for smooth boundary surfaces between transparent materials with the refractive indices n_1 and n_2 are calculated according to the incidence angle θ_1 and the refraction angle θ_2 as shown in Figure 4.10.

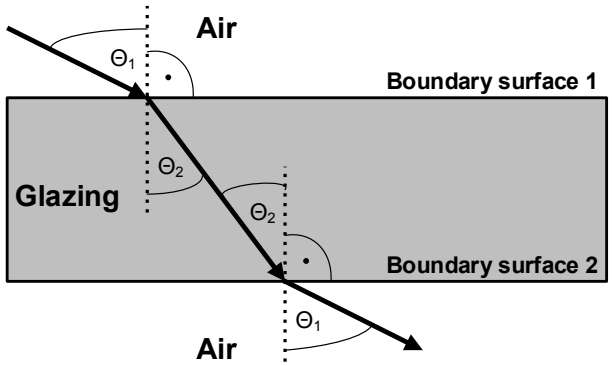

Figure 4.10: Relations between beam angle and refractive indices (according to Eicker 2003; Duffie and Beckman 2006)

The reflection factors for vertical and parallel polarised radiation are shown in equations (4.11) and (4.12).

$$r_{\perp} = \frac{\sin^2(\theta_2 - \theta_1)}{\sin^2(\theta_2 + \theta_1)} \tag{4.11}$$

$$r_{\parallel} = \frac{\tan^2(\theta_2 - \theta_1)}{\tan^2(\theta_2 + \theta_1)} \tag{4.12}$$

The refraction angle θ_2 changes with the incidence angle θ_1 depending on the two refraction indices n_1 and n_2. The relation is described by Snell's law in equation (4.13).

$$n_1 \sin\theta_1 = n_2 \sin\theta_2 \tag{4.13}$$

Vertical incidence at the boundary surface is a special case. Both angles θ_1 and θ_2 are zero. Also, the vertical and parallel refraction factors are equal. Hence, the refraction factor can be derived from equation (4.14).

$$r(0°) = \frac{G_r}{G} = \left(\frac{n_1 - n_2}{n_1 + n_2}\right)^2 \tag{4.14}$$

4.1.4.2 Absorption in the Glazing

The absorption of the radiation in the glazing caused by a partly transparent material is described by Bouguer's law. The underlying, basic assumption is that the

absorbed radiation dG is proportional to the incoming radiation G and the extinction coefficient K of the material. This relation is shown in equation (4.15) (Duffie and Beckman 2006).

$$dG = -GK\,dx \tag{4.15}$$

The transmittance without reflection τ_a is described by means of the factor of radiation passing the material. This factor is the ratio between transmitted radiation G_t and incoming radiation G. This ratio is described by equation (4.16) depending on the extinction coefficient K of the material and the path length of the radiation.

$$\tau_a = \frac{G_t}{G} = exp\left(-K\frac{d_g}{\cos\theta_2}\right) \tag{4.16}$$

4.1.4.3 Transmission and Absorption Coefficient of the Glazing

Considering both reflection and absorption in a glazing, the transmission as well as the absorption coefficient of the component can be derived. The boundary surfaces of the glazing transmit and reflect the incoming beam. Thus, there is an infinite number of transmissions, reflections and absorptions in the glazing (Duffie and Beckman 2006). Figure 4.11 shows this effect in the glazing.

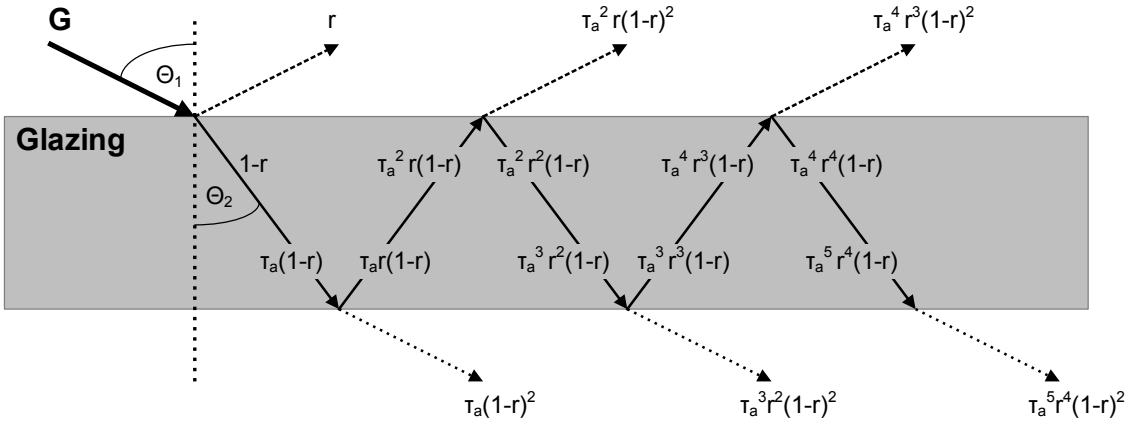

Figure 4.11: Transmission, reflection and absorption of a single glazing (according to Duffie and Beckman 2006)

The transmission coefficient τ of the glazing is the average of the transmission coefficients for both polarised directions (equation (4.17)). The infinite series of beams caused by multiple reflections can be determined via ray tracing described in equation (4.18) and (4.19).

$$\tau = \frac{\tau_\perp + \tau_\parallel}{2} \tag{4.17}$$

$$\tau_\perp = (1 - r_\perp)^2 \tau_a \sum_{n=0}^{\infty} r_\perp^{2n} \tau_a^{2n} = \frac{\tau_a (1 - r_\perp)^2}{1 - (r_\perp \tau_a)^2} \tag{4.18}$$

$$\tau_\parallel = \frac{\tau_a (1 - r_\parallel)^2}{1 - (r_\parallel \tau_a)^2} \tag{4.19}$$

The absorption coefficient α of the glazing is also calculated for both polarised directions by an infinite series described in the equations (4.20) to (4.22).

$$\alpha = \frac{\alpha_\perp + \alpha_\parallel}{2} \tag{4.20}$$

$$\alpha_\perp = (1 - r_\perp) \tau_a \sum_{n=0}^{\infty} (1 + r_\perp^n \tau_a^n) = (1 - \tau_a) \left(\frac{1 - r_\perp}{1 - r_\perp \tau_a} \right) \tag{4.21}$$

$$\alpha_\parallel = (1 - \tau_a) \left(\frac{1 - r_\parallel}{1 - r_\parallel \tau_a} \right) \tag{4.22}$$

4.1.4.4 Solar Energy Conversion in the Collector

Equation (4.23) describes the energy input at the absorber reduced by the effective transmission absorption product $(\tau\alpha)_{eff}$ of glazing and absorber (Duffie and Beckman 2006).

$$S_{a1} = (\tau\alpha)_{eff} A G \tag{4.23}$$

Simple approaches of $(\tau\alpha)$ only consider the light transmission through the glazing and the absorption of the absorber surface. In this model, however, a more

detailed approach is applied as described by equation (4.24) (Duffie and Beckman 2006).

$$(\tau\alpha)_{eff} = \frac{\tau\alpha}{(1-(1-\alpha)\rho)} \tag{4.24}$$

The multiple reflections between absorber and glazing are considered with the non-ideal absorption coefficient *α* of the absorber and the reflection coefficient *ρ* of the inner glazing surface. Figure 4.12 shows this effect in the schematic collector build-up.

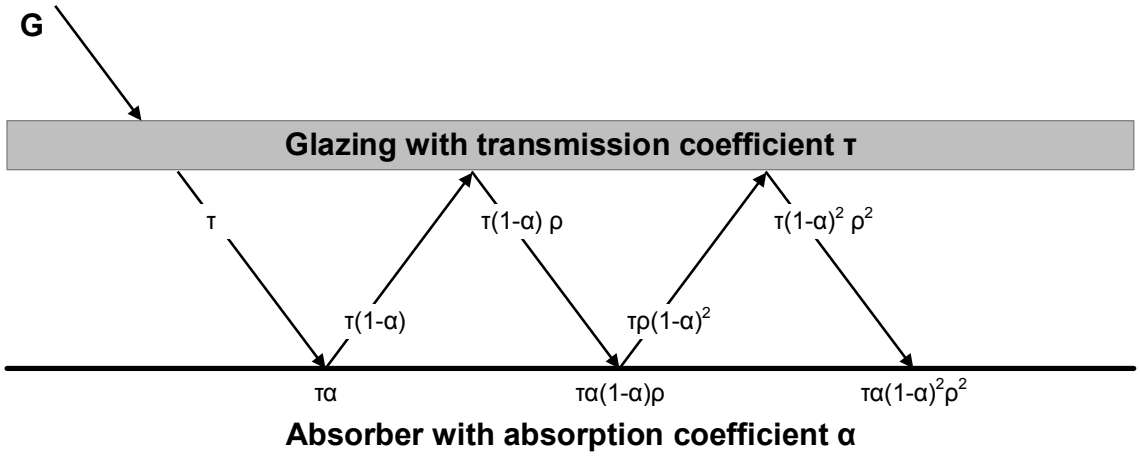

Figure 4.12: Effective transmission absorption product $(\tau\alpha)_{eff}$ of a single glazed collector (according to Duffie and Beckman 2006)

The additional solar energy input in the glazing depending on absorption of the glazing changes the temperature of this node and influences the collectors' heat losses (Duffie and Beckman 2006). The solar energy input in the glazing S_g is shown in equation (4.25).

$$S_g = (1-\tau_a)AG \tag{4.25}$$

The optical effects for solar energy conversion in absorber and glazing depend on the angle. Hence, these effects have to be considered for direct as well as for diffuse irradiance (equation (4.26)).

$$S = S_{dir} + S_{diff} \tag{4.26}$$

For the calculation of the optical properties for direct irradiance, the beam angle at the inclined collector surface is used. The diffuse irradiance from the sky is assumed to be isotropic. Depending on the collector slope β, a certain fraction of the sky appears for the glazing as well as for the absorber. Brandemuehl and Beckman (1980) investigated the relation between the sky and the inclined glazing systems for diffuse irradiation. As a result, an approach for the calculation of an equivalent angle depending on the collector slope was derived.

Equation (4.27) shows the equivalent angle of incidence for diffuse irradiance for single-glazed collectors.

$$\theta_{diff} = 59.7° - 0.1388\beta + 0.001497\beta^2 \tag{4.27}$$

4.1.5 Convection

Heat transfer by convection occurs at several layers in the collector. There is forced convection in the absorber pipes caused by the pumped heat transfer fluid and at the surface of the glazing caused by wind. Free convection occurs in the air gaps in front of the absorber and behind the absorber as well as at the glazing and at the backside of the collector. These heat transfer mechanisms are represented by equation (4.28) containing the convective heat transfer coefficient from equation (4.29), that depends on the Nusselt number Nu and the characteristic length L of the component as well as on the heat conductivity k of the fluid (Stephan 2010).

$$\dot{Q} = h_{conv} A (T_1 - T_2) \tag{4.28}$$

$$h_{conv} = \frac{Nu\ k}{L} \tag{4.29}$$

The convective heat transfer of solid bodies cannot be defined by physical equations, because of its strong dependency on fluid properties, shape, dimension and temperature difference. Therefore, the heat transfer was investigated in experiments. Empirical correlations were derived from the measurement results and

were described by the dimensionless heat transfer coefficient Nu. This approach defines the average convective heat transfer of the investigated set-up and is valid for a certain range of fluid properties and dimensions. The average heat transfer coefficient is usually referred to a uniform temperature of the body surface. Thus, average surface temperatures and average fluid properties are assumed in the constant temperature case. The constant heat flux case considering a non-uniform surface temperature is not considered due to the very small error in convective heat transfer of approximately ~0.1 % (Stephan 2010).

4.1.5.1 Forced Convection in the Fluid Channels

The forced convection in the absorber pipes is calculated according to the approach recommended by Gnielinski (1995). The characteristic length L is the pipe diameter d in this case. The flow in the pipes was assumed to be constant along the entire length without entrance effects. The temperature dependent properties of the fluid were referenced to the fluid node in the centre of the pipe.

The hydrodynamically developed laminar flow for Reynolds numbers Re below 2,300 and for a constant axial wall temperature is defined with a constant Nusselt number of 3.657 (Mills 1999).

In the transition region between laminar and fully developed turbulent flow with Reynolds numbers in the range of 2,300 and 10,000, the Nusselt number is calculated by the equations (4.30) to (4.35) for a constant axial wall temperature.

$$Nu_f = (1-\gamma)Nu_{lam,2300} + \gamma Nu_{turb,10^4} \tag{4.30}$$

$$\gamma = \frac{Re - 2{,}300}{10^4 - 2{,}300} \qquad \text{for} \qquad 0 \le \gamma \le 1 \tag{4.31}$$

$$Nu_{lam,2300} = \sqrt[3]{49.371 + \left(Nu_{lam,2,2300} - 0.7\right)^3 + Nu_{lam,3,2300}^3} \tag{4.32}$$

$$Nu_{lam,2,2300} = \sqrt[3]{1.615\left(2{,}300Pr\frac{d}{l}\right)} \tag{4.33}$$

$$Nu_{lam,3,2300} = \sqrt[6]{\frac{2}{1+22Pr}}\sqrt{2{,}300Pr\frac{d}{l}} \tag{4.34}$$

$$Nu_{turb,10^4} = \frac{\frac{0.0308}{8}10^4 Pr}{1+12.7\sqrt{\frac{0.0308}{8}}\left(Pr^{\frac{2}{3}}-1\right)}\left(1+\left(\frac{d}{l}\right)^{\frac{2}{3}}\right) \tag{4.35}$$

The Nusselt number for fully developed turbulent flow by Gnielinski (1974) for Reynolds numbers larger than 10,000 is described by equation (4.36). The friction factor f can be determined by equation (4.37).

$$Nu_f = \frac{\frac{f}{8}RePr}{1+12.7\sqrt{\frac{f}{8}}\left(Pr^{\frac{2}{3}}-1\right)}\left(1+\left(\frac{d}{l}\right)^{\frac{2}{3}}\right) \tag{4.36}$$

$$f = \left(1.8log_{10^{Re}} - 1.5\right)^{-2} \tag{4.37}$$

These approaches are valid for a ratio between the pipe diameter d and the pipe length l less than or equal to unity as well as for Prandtl numbers Pr between 0.6 and 1,000.

4.1.5.2 Convection at the Glazing

The convection on the outer surface of the glazing is a combination of free and forced convection. Based on experiments, Churchill (1977) developed an approach for an overlay of both convections as shown in equation (4.38).

$$Nu_{g-amb} = \sqrt[3]{Nu_{free,g-amb}^3 + Nu_{forced,g-amb}^3} \tag{4.38}$$

The Nusselt number for forced convection with turbulent boundary layer is considered according to the equation (4.39) by Schlichting (1958).

$$Nu_{forced,g-amb} = \frac{0.037Re^{0.8}Pr}{1 + 2.443Re^{-0.1}\left(Pr^{\frac{2}{3}} - 1\right)} \tag{4.39}$$

Therefore, the air flow caused by the wind is assumed to occur along the collector width of the glazing according to Figure 4.13.

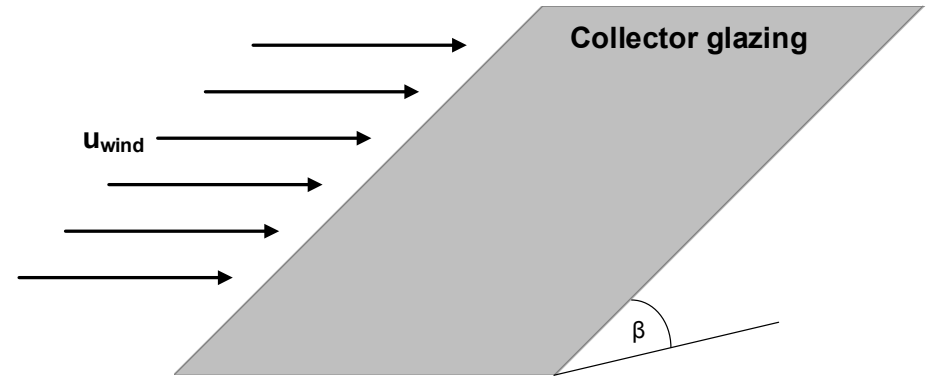

Figure 4.13: Wind at the inclined collector glazing

The average Reynolds number in equation (4.40) is calculated by the wind velocity u_{wind}, the characteristic length of the glazing L_{g-amb} and the kinematic viscosity v_{air}. The equation is valid for Reynolds numbers between 5 x 10^5 and 1 x 10^7 as well as for Prandtl numbers between 0.6 and 2,000. Even during low temperatures and wind velocities, the Reynolds numbers are in the range of the validity. Hence, laminar flow for forced convection is neglected.

$$Re = \frac{u_{wind} * L_{g-amb}}{v_{air}} \tag{4.40}$$

For free laminar convection at the glazing two cases are defined by Fujii and Imura (1972). The most important case for thermal collector simulation is the heat transfer upwards at the inclined glazing. During collector operation, the glazing

temperature turns out to be larger than the ambient temperature. Hence, the collector's heat losses are driven by the upward flowing air. The second case with lower glazing temperatures is only relevant for system simulations with fluid temperatures below the ambient air temperatures. Figure 4.14 shows these two cases for the glazing.

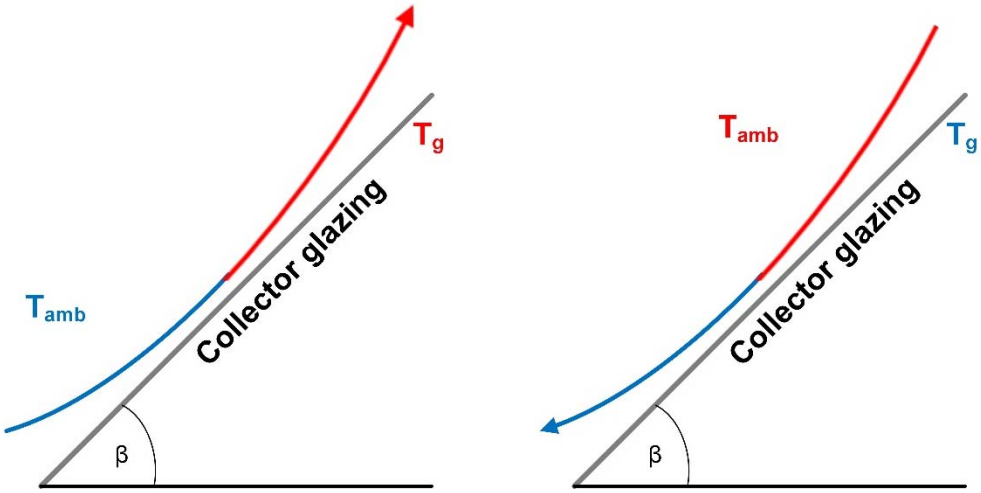

Figure 4.14: Free convection at the glazing with heat transfer upwards (left) and downwards (right)

The Nusselt number for free laminar convection at the glazing with heat transfer upwards or downwards at vertical planes is described in equation (4.41) from Churchill and Chu (1975) and is also valid for Rayleigh numbers between 1 x 10^{-1} and 1 x 10^{12}. Using the correction factor f_{Pr} in equation (4.42) by Churchill and Chu (1972) allows Prandtl numbers in the range between 0.001 and non-finite. This correlation for the Nusselt numbers is also valid for inclined surfaces by substituting the Rayleigh number Ra for the adjusted Rayleigh number Ra_β according to equation (4.43) (Fujii and Imura 1972). This adjustment considers the reduced component of gravity at the inclined plane instead of the acceleration due to gravity g. In this case the characteristic length L_{g-amb} is the length of the glazing.

$$Nu_{free,g-amb} = \left(0.825 + 0.387\sqrt[6]{Raf_{Pr}}\right)^2 \quad \text{for} \quad Ra < Ra_{crit} \qquad (4.41)$$

$$f_{Pr} = \left(1 + \left(\frac{0.492}{Pr}\right)^{\frac{9}{16}}\right)^{-\frac{16}{9}} \quad \text{for} \quad 0.001 < Pr < \infty \tag{4.42}$$

$$Ra_{\beta} = Ra \sin \beta \tag{4.43}$$

Boundary layer separation may occur for free convection at the glazing with heat transfer upwards. Hence, there is a change from laminar to turbulent flow. The laminar flow occurs for Rayleigh numbers below the critical Rayleigh number Ra_{crit} depending on the collector slope β from equation (4.44). Figure 4.15 shows the gradient of the upper limit of the critical Rayleigh number for the described laminar convection.

$$Ra_{crit} = 10^{\left(8.9 - 0.00178 * (90° - \beta)^{1.82}\right)} \tag{4.44}$$

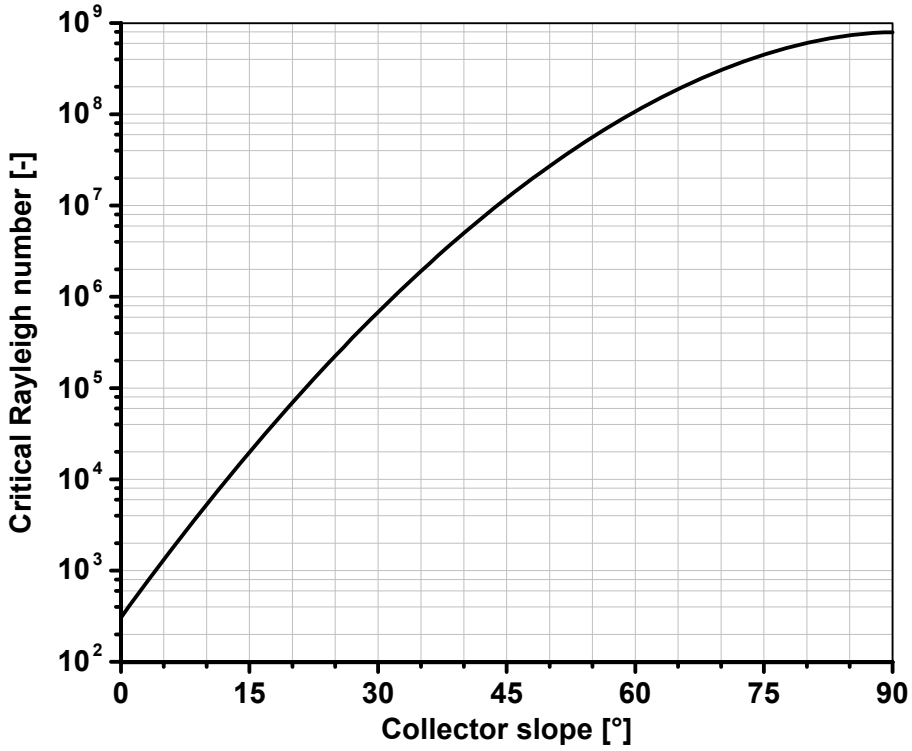

Figure 4.15: Upper limit of the critical Rayleigh number depending on the collector slope

Above the critical Rayleigh number, free turbulent convection at the glazing occurs. Fujii and Imura (1972) defined equation (4.45) accordingly.

$$Nu_{turb,g-amb} = 0.56 * (Ra_{crit} * \cos(90° - \beta))^{0.25} + 0.13 * \left(\sqrt[3]{Ra} - \sqrt[3]{Ra_{crit}}\right) \quad (4.45)$$

4.1.5.3 Convection at the Casing

Duffie and Beckmann (2006) regarded the heat transfer from the casing to the ambient by radiation and convection as negligible because of the significant impact on the backside insulation and the resulting low temperature. In this model the heat transfer coefficients from the backside to the ambient are calculated for a hypothetical windless region between collector and roof by natural convection and radiation. The effect of a chimney was also neglected. The heat transfer via convection was assumed as free convection at an inclined plane. Figure 4.16 describes the two occurring cases for solar collectors.

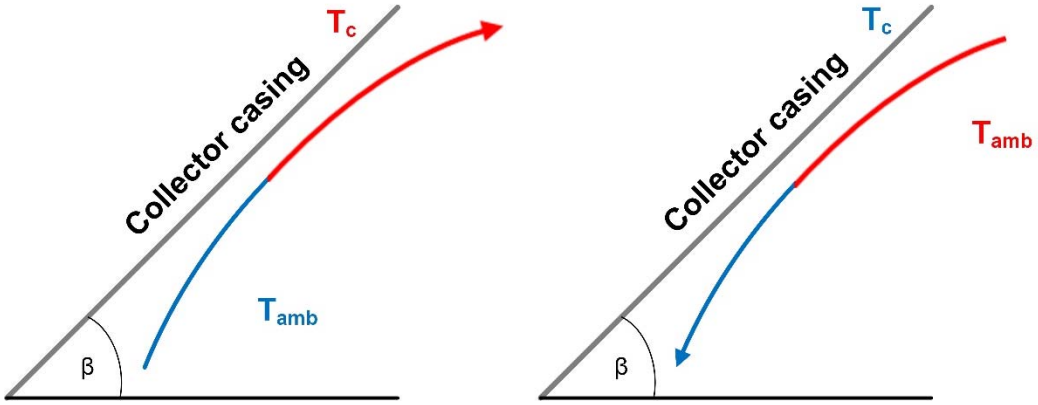

Figure 4.16: Free convection at the casing with heat transfer downwards (left) and upwards (right)

The most common case for the backside sheet is a heated plate transmitting heat downwards without any separation of the boundary layer. Thus, the Nusselt number for laminar flow from the equations (4.41) to (4.43) serves as an exploration for the free convection behind the collector. In this case, $L_{c\text{-}amb}$ is the characteristic length of the casing.

The special case of a cooled surface absorbing heat from the ambient air from below is described by the equations (4.41) to (4.43) for laminar flow. Above the critical Rayleigh number the separation of the boundary layer is expressed by

means of equation (4.44). Furthermore, the approach for turbulent flow from equation (4.45) has to be used.

4.1.5.4 Convection Between Absorber and Glazing

Heat transfer in an enclosed air gap is driven by heat conduction as well as by free convection of the circulating gas layer. This free convection between glazing and absorber with the two possible directions of heat transfer is shown in Figure 4.17.

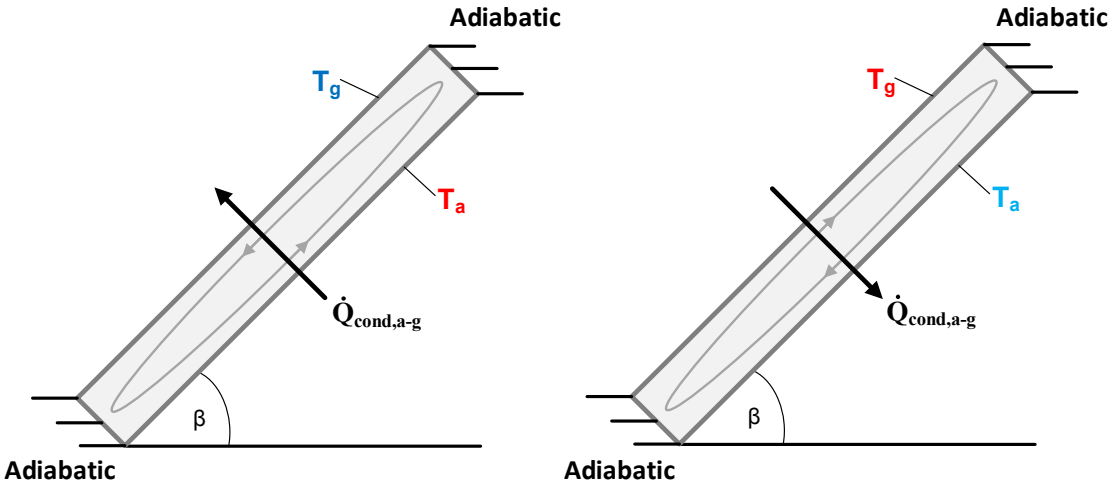

Figure 4.17: Free convection in the enclosed gas layer between absorber and glazing with heat transfer upwards (left) and downwards (right)

Upwards heat transfer usually appears in collectors between absorber and glazing. Therefore, Matuska and Zmrhal (2009) derived a Nusselt correlation from several correlations similar to Hollands et al. (1976) to verify the Nusselt number approach for an increased range of collector slopes. Equation (4.46) describes the Nusselt number for the air gap valid for slopes β from 0° to 90°. The characteristic length L_{a-g} in that system is the distance between absorber and glazing. The value of f_β in equation (4.47) constitutes an angle factor for the Nusselt number, that depends on the collector slope which was obtained as quadratic function in the derived correlation. The approach is valid for $1 \times 10^4 < Ra < 2 \times 10^6$ covering the necessary operational range of solar-thermal collectors. The correlation, too, showed good results independent of the aspect ratio between air gap length and

air gap distance. Several approaches, however, are limited with regard to the collector geometry.

$$Nu_{a-g} = f_\beta Ra^{0.29} \tag{4.46}$$

$$f_\beta = 0.1464 - 2.602e^{-4}\beta - 2.046e^{-6}\beta^2 \tag{4.47}$$

The approach for the Nusselt number with heat transfer downwards is derived from Arnold et al. (1976). Therefore, equation (4.48) is used on the basis of the calculated Nusselt number for heat transfer in vertical air layers (β=90°) derived from equation (4.46) and (4.47). The validity of this approach is similar to the approach of equation (4.46). However, the aspect ratio between air gap length and air gap distance has to be larger than 20.

$$Nu_{a-g} = 1 + \left(Nu_{a-g}(\beta = 90°) - 1\right)\sin(180° - \beta) \tag{4.48}$$

4.1.5.5 Convection Between Absorber and Casing

The heat transfer in the enclosed air layer between absorber plate and casing is equal to the Nusselt correlation for convection between absorber and glazing in Chapter 4.1.5.4. The usual approach for the region behind the absorber is free convection with heat transfer downwards expressed by equation (4.48).

4.1.6 Radiation

Heat transfer caused by radiation is based on the Stefan-Boltzmann law of a black body radiator. The energy transfer is described with an emission coefficient $\varepsilon_1 = 1$ by Eicker (2003) by equation (4.49). The Stefan-Boltzmann constant σ is shown in equation (4.50).

$$\dot{Q}_1 = \sigma A_1 T_1^4 \tag{4.49}$$

$$\sigma = 5.67e^{-8} Wm^{-2}K^{-4} \tag{4.50}$$

Bodies above a temperature of 0 K emit radiating power. Radiating power from other bodies placed in a room is also absorbed. The position of the bodies also has great influence on the behaviour as described by their form factors Φ. The form factor is the ratio between the radiation receiving surface and the entire hemisphere. Figure 4.18 shows the heat exchange of the two surfaces.

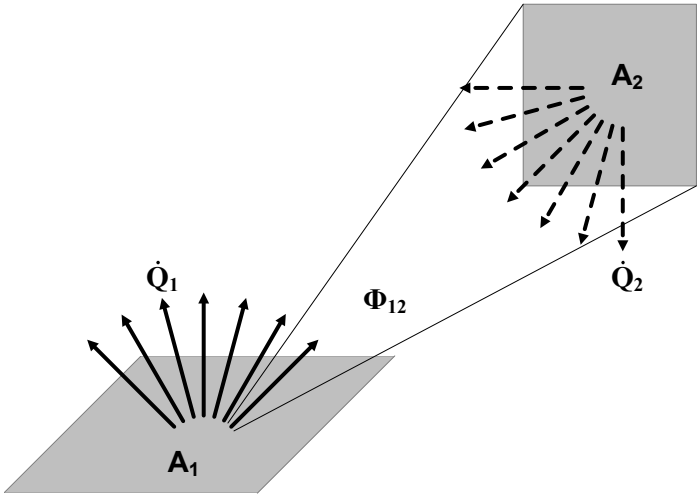

Figure 4.18: Heat fluxes via radiation between two elements (according to Eicker 2003)

The net radiation exchange $\dot{Q}_{rad}$ between two bodies takes the properties of the bodies into account and defines the heat transfer. Therefore, the difference between the radiating powers reaching the other body is taken from equation (4.51).

$$\dot{Q}_{rad} = \dot{Q}_{rad,1\rightarrow 2} - \dot{Q}_{rad,2\rightarrow 1} = \Phi_{12}\sigma A_1 T_1^4 - \Phi_{21}\sigma A_2 T_2^4 \qquad (4.51)$$

The definition of the net radiation exchange between two bodies with an emission coefficient ε smaller than unity is a more complex approach. Therefore, a multiple of reflections have to be considered.

The radiation exchange in solar-thermal flat-plate collectors embraces only two special cases. There is radiation exchange between two parallel plates e.g. between absorber and glazing on the one hand. On the other hand, radiation occurs from a limited surface to the infinite sky hemisphere.

The heat transfer by radiation has to be determined according to equation (4.52). Therefore, the heat transfer coefficients for radiation of the collector have to be defined.

$$\dot{Q}_{rad} = h_{rad} A (T_1 - T_2) \tag{4.52}$$

4.1.6.1 Radiation Between Two Parallel Plates

Due to the fact that the heat emitted is completely absorbed by the opposed area, the form factors of the two surfaces are equal ($\Phi_{12} = \Phi_{21} = 1$). It is assumed that the effects of infinitely expanded parallel surfaces apply for heat transfer in solar collectors. Multiple reflections have to be considered for grey emitters as well by introducing their emission coefficients ε into the approach. The heat transfer coefficient for radiation between two parallel plates is given in equation (4.53).

$$h_{rad} = \frac{\sigma}{\left(\frac{1}{\varepsilon_1} + \frac{1}{\varepsilon_2} - 1\right)} (T_1^2 + T_2^2)(T_1 + T_2) \tag{4.53}$$

This radiation exchange is necessary for the set-up of glazing and absorber, absorber and casing as well as casing and roof.

4.1.6.2 Radiation Between Glazing and Sky

The radiation between glazing and cold sky is a special phenomenon of heat transfer (Eicker 2003). The surface of glazing A_g is much smaller than the total sky hemisphere A_{sky}. Hence, radiation from the glazing is completely emitted to the sky. Thus, the form factor of the glazing Φ_{g-sky} is 1. In contrary to that, the form factor from the sky Φ_{sky-g} is almost zero since the proportion of the glazing surface being seen from the sky hemisphere is very small. Therefore, the emitted heat from the sky is neglected because of the infinite area of the sky's half-space. The heat transfer coefficient is shown in equation (4.54). The temperatures have to be inserted in Kelvin because radiation refers to the absolute temperature of the body or rather surface.

$$h_{rad,g-sky} = \sigma \varepsilon_g \left(T_g^2 + T_{sky}^2\right)\left(T_g + T_{sky}\right) \tag{4.54}$$

The temperature of the sky differs from the ambient air temperature (Duffie and Beckman 2006). Approaches for the definition of the sky temperature are related to the air temperature (Swinbank 1963), to the water vapour pressure (Brunt 1932) or to the dew point temperature (Bliss 1961), for example.

4.1.7 Heat Conduction

Heat conduction is prevalent at glazing, absorber and casing. Equations (4.55) and (4.56) describe the heat transfer that depends on the heat conductivity *k* and the thickness or rather distance *s* of the component (Stephan 2010).

$$\dot{Q}_{cond} = h_{cond} A (T_1 - T_2) \tag{4.55}$$

$$h_{cond} = \frac{k}{s} \tag{4.56}$$

Vertical heat transfer through thin plates in the thermal network like glazing or absorber can be neglected. In the model, the heat conduction is connecting the heat transfer from convection and radiation to the nodes of the solid materials. Hence, there are little influences on the overall heat transfer coefficients.

Relevant heat conduction occurs between the nodes of the absorber. The small area of the heat transfer area and the distance between the nodes (Figure 4.19) cause heat transfer behaviour with major influence on the collector performance.

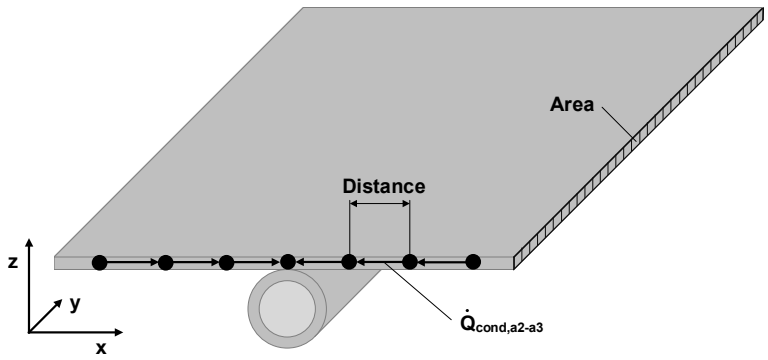

Figure 4.19: Heat conduction between the absorber nodes

The second relevant heat conduction is seen in the collector insulation. These heat losses occur at the side and backside insulation. In contrary to the massive

solid materials such as metals, the heat conductivity cannot be regarded as constant. The cavernous structure of the material also enables heat transfer effects of the enclosed air and radiation. Thus, the heat conductivity increases according to the material temperature. For dry mineral wool Ochs et al. (2004) derived a linear approach for the temperature depending calculation of the heat conductivity k_{mw} according to equation (4.57). The influence on the heat conductivity of the unknown humidity in the mineral wool is neglected. Moist mineral wool usually has highly increased heat conductivity.

$$k_{mw} = 0.035 W m^{-1} K^{-1} + 2.0 e^{-4} T_{mw} \tag{4.57}$$

4.1.8 Edge Losses

The edge losses, which comprise the heat losses through the collector frame or rather side, cannot be mathematically calculated in detail. Tabor (1958) describes an approach considering the losses only connected to the absorber node. The other nodes have an adiabatic behaviour against the edge. Equation (4.58) and (4.59) show the heat transfer between absorber and ambient air as well as the heat transfer coefficient considering only the heat conduction through the side insulation.

$$\dot{Q}_{a-edge} = h_{edge} A_{edge} (T_a - T_{amb}) \tag{4.58}$$

$$h_{edge} = \frac{k_c}{s_{edge}} \tag{4.59}$$

4.1.9 Overall Heat Transfer Coefficients Between the Nodes

The heat transfer coefficients h of the collector connect the nodes and the ambient. Most of them are embedded in a network of the thermal resistances to calculate a heat flow rate $\dot{Q}$. The electrical analogy is used to generate the overall heat transfer coefficients between the nodes based on the single thermal effects.

Equations (4.60) to (4.62) demonstrate the analogy between electrical and thermal circuits (Mills 1999, Stephan 2010).

$$Transport\ stream = \frac{Potential\ difference}{Resistance} \tag{4.60}$$

$$I_{el} = \frac{U_{el}}{R_{el}} \tag{4.61}$$

$$\dot{Q} = \frac{T_1 - T_2}{R_{th}} \tag{4.62}$$

Hence, the thermal resistance is defined according to equation (4.63). This definition suggests expressing the heat transfer rate according to equation (4.64).

$$R_{th,1-2} = \frac{T_1 - T_2}{\dot{Q}} = \frac{T_1 - T_2}{h_{1-2}A(T_1 - T_2)} = \frac{1}{h_{1-2}A} \tag{4.63}$$

$$\dot{Q}_{1-2} = \frac{1}{R_{th,1-2}}(T_1 - T_2) = \left(\frac{1}{h_{1-2}A}\right)^{-1}(T_1 - T_2) \tag{4.64}$$

On that basis the thermal and the electrical circuit have the same build-up. Thus, the build-up of series and parallel connections in circuits can be used to define the heat transfer (Figure 4.20).

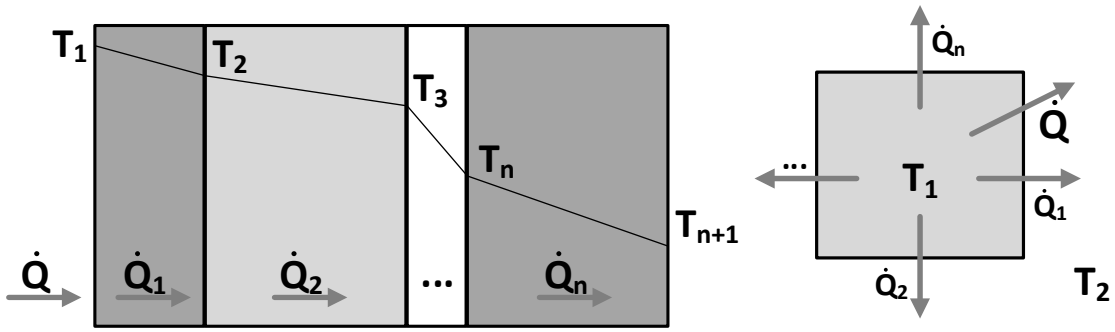

Figure 4.20: Schemes of serial (left) and parallel (right) heat transfer

Resistances connected in series have the same heat flux through every resistance in the circuit (Figure 4.21). The resistances of the circuits can be added to the total resistance.

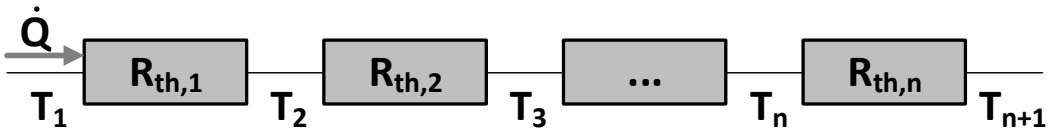

Figure 4.21: Thermal circuit of a serial connected system

Equations (4.65) to (4.67) describe the total thermal resistance of a series connection.

$$\dot{Q} = \dot{Q}_1 = \dot{Q}_2 = \cdots = \dot{Q}_n \tag{4.65}$$

$$\frac{T_1 - T_{n+1}}{R_{th,total}} = \frac{T_1 - T_2}{R_{th,1}} = \frac{T_2 - T_3}{R_{th,2}} = \cdots = \frac{T_n - T_{n+1}}{R_{th,n}} \tag{4.66}$$

$$R_{th,total} = \sum_{i=1}^{n} R_{th,i} = R_{th,1} + R_{th,2} + \cdots + R_{th,n} \tag{4.67}$$

A parallel connection of resistances is defined by the equal applied temperature difference and the splitting of the total heat flux. (Figure 4.22).

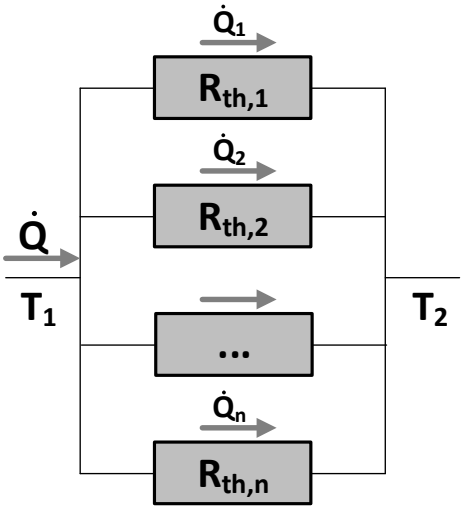

Figure 4.22: Thermal circuit of a parallel connected system

Equations (4.68) to (4.70) show the total thermal resistance of a parallel connection.

$$\dot{Q} = \dot{Q}_1 + \dot{Q}_2 + \cdots + \dot{Q}_n \tag{4.68}$$

$$\frac{T_1 - T_2}{R_{th,total}} = \frac{T_1 - T_2}{R_{th,1}} + \frac{T_1 - T_2}{R_{th,2}} + \cdots + \frac{T_1 - T_2}{R_{th,n}} \tag{4.69}$$

$$\frac{1}{R_{th,total}} = \sum_{i=1}^{n} \frac{1}{R_{th,i}} = \frac{1}{R_{th,1}} + \frac{1}{R_{th,2}} + \cdots + \frac{1}{R_{th,n}} \tag{4.70}$$

These schemes are used to generate overall resistances by combining single resistances of serial and parallel connections according to Figure 4.7. The required overall heat transfer coefficients (related to the area) of the energy fluxes from equations (4.3) to (4.9) are shown in the equations (4.71) to (4.75).

$$\frac{1}{R_{th,g-amb}} = h_{cond,g}A + \left(\frac{1}{h_{rad,g-sky}A} + \frac{1}{h_{conv,g-amb}A}\right)^{-1} \tag{4.71}$$

$$\frac{1}{R_{th,a-g}} = \left(\frac{1}{h_{rad,a-g}A_a} + \frac{1}{h_{conv,a-g}A_a}\right)^{-1} + h_{cond,g}A_a \tag{4.72}$$

$$\frac{1}{R_{th,a1-f}} = h_{cond,a1}2A_{wall} + h_{conv,a1-f}A_{pipe} \tag{4.73}$$

$$\frac{1}{R_{th,a-c}} = \left(\frac{1}{h_{rad,a-c}A_a} + \frac{1}{h_{conv,a-c}A_a}\right)^{-1} + h_{cond,c}A_a \tag{4.74}$$

$$\frac{1}{R_{th,c-amb}} = h_{cond,c}A + \left(\frac{1}{h_{rad,c-amb}A} + \frac{1}{h_{conv,c-amb}A}\right)^{-1} \tag{4.75}$$

4.1.10 Implementation in the Simulation Tool

The collector physics is implemented in the simulation tool *Matlab/Simulink* by means of a so-called “S-function (level 2)”. The S-function is a compiled source code written in *C*. The S-function is equipped with connexions for data input from fluid, weather and collector orientation. The relevant output data of the fluid at the

collector outlet as well as the part temperatures are provided at the output of the S-function. Figure 4.23 shows the Simulink block with embedded S-function (grey block) in the simulation environment. The blue blocks write the simulation data in the workspace of *Matlab*.

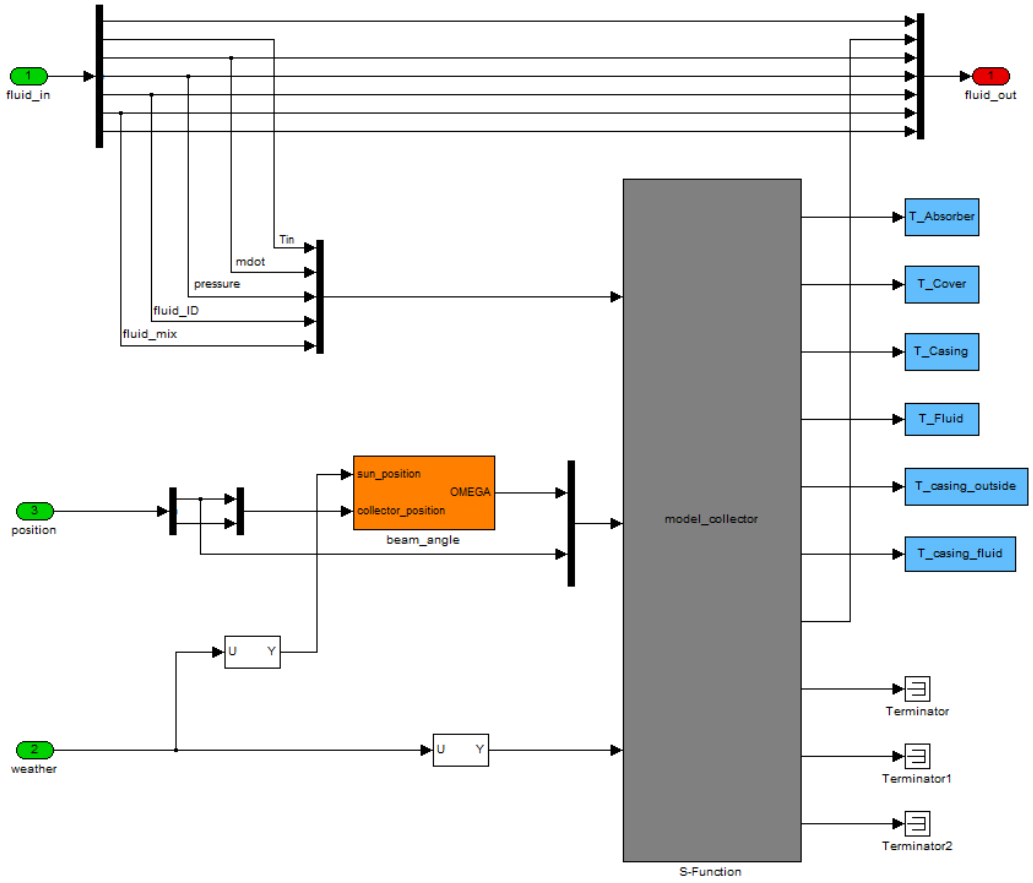

Figure 4.23: Build-up of the collector block with embedded S-function (grey) in *Simulink*

With regard to an improved clearness, the S-function block and the other relevant blocks are put into a subsystem of the *Simulink* environment. Figure 4.24 displays the masked subsystem of the embedded collector S-function. The connexions of the block are the above mentioned inputs and the output of the fluid.

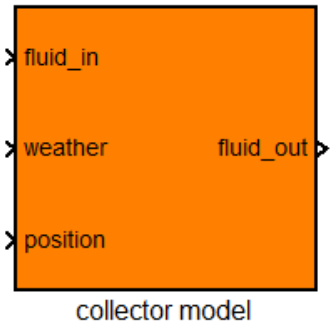

Figure 4.24: Mask of the collector block with embedded S-function of the collector in *Simulink*

The necessary data of the heat carrier and the air in the gaps to calculate the heat transfers is obtained by a link to the *Carlib Library* within the source code. The *Carlib Library* of the *CARNOT* toolbox contains the functions for the relevant material properties — like heat conductivity k and kinematic viscosity ν.

4.1.11 Validation

The model was validated using the parameter set of a tested conventional flat-plate collector. The validation of this model and physical effects is also adequate for models with implemented overheating protection measures or adjusted build-up since the defined physical effects are varied and not exchanged.

The model was tested in various settings to investigate the accuracy of the results. According to the above-mentioned simplifying assumptions in the model, there are, of course, imperfections in the build-up of the tested collectors. Hence, the differences in the results have to be identified, justified and evaluated.

4.1.11.1 Comparison with an Existing Validated Model

In a first validation step, the developed dynamic multi-node model was compared to the results of a one-dimensional multi-node model approach by Hafner et al. (1999) based on the approach of equation (4.1). Therefore, the parameters derived from collector testing identified by Institut für Solartechnik SPF (2005) and listed in Table 4.5 were implemented into the model. This validation test is only able to compare the results of the collector efficiency of an already

validated parameter model approach with exact coverage. Therefore, two test simulations were set up.

The first test comprised the simulation of the collector efficiency curve like the practical test modus in a solar simulator according to DIN EN 12975-2 (2006). Under constant ambient conditions ($G = 885\,Wm^{-2}$, $T_{amb} = 27°C$, $u_{wind} = 2\,ms^{-1}$), a single collector was tested. The heat carrier, a water-glycol mixture (33.3 %), has a flow rate of $\dot{m} = 0.08\,kgs^{-1}$ and variable temperatures through the collector.

The percentage difference of the collector efficiency describes the accuracy of the model approach according to equation (4.76).

$$Percentage\ difference = \left(\frac{\eta_{dynamic\ model}}{\eta_{paramter\ model}} - 1\right) 100\,\% \tag{4.76}$$

The values range between -1.0 % and +3.3 % for flow temperatures from 25°C to 90°C (Figure 4.25).

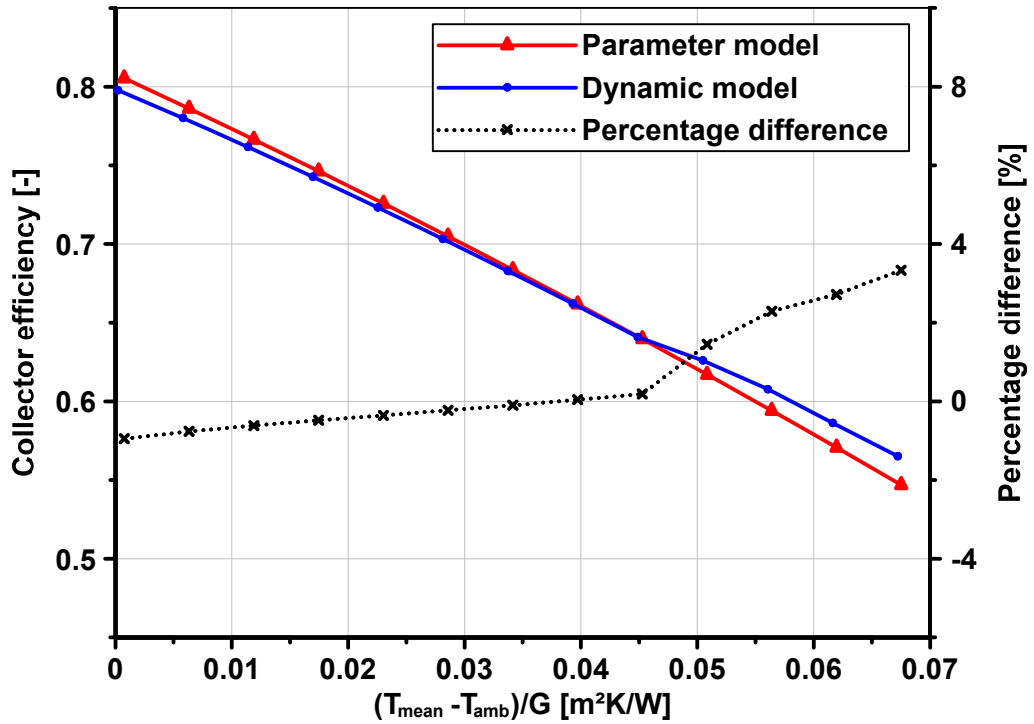

Figure 4.25: Comparison of the simulated efficiency curves of the parameter model and the developed dynamic collector model

The differences are relatively low according to the assumptions in the model. Also, the simulated temperature range in the test covers a large operational range of the collector to prove the use of the model.

The deviation is assumed to originate from the discretisation in the model. The major influence in the test is the transition from laminar to turbulent flow at higher values of the reduced temperature. The change in the model curve is remarkable because of an averaged calculation of fully-developed flow conditions for the entire riser pipe. In contrast to that, the real collector shows a continuous development of flow conditions along the pipe length. There are also neglected entrance effects increased by the vertical connection between header and riser.

Next to the analysis of efficiency, the models are compared to each other in an annual simulation of a solar-thermal heating system for domestic hot water and space heating. The build-up is equal to the system of the simulation analysis described in the following chapter. The collector surface of the parameter model was adjusted due to the reduced absorber surface of the collector model because of the missing header regions. The deviation of the solar yield is found to be +2.9 %, similar to the results found in the comparison of efficiency. The deviation originates from the fact that the major operational range of the collectors is at high reduced temperatures. This is caused by both high flow and ambient air temperatures for hot water preparation in summer as well as moderate flow and low ambient air temperatures in the heating period for space heating.

4.1.11.2 Comparison with Measurements

In a second step, the simulation results were compared to measurement data from analysing the exposed field-testing collector. The test collector was already equipped with sensors to measure the component temperatures. However, degradation of the absorber coating and humidity in the mineral wool can be named as some of the reasons, resulting in the effect that the efficiency of the collector is reduced in comparison to results from previous efficiency curves of a new collector in Chapter 4.1.11.1. Therefore, the emission coefficient of the absorber

coating and the heat conductivity of the mineral wool are adjusted to represent the degradation of the components.

The first test is the comparison of the efficiency curves. Therefore, the conditions of the test stand are reproduced ($G = 890\ Wm^{-2}$, $T_{amb} = 31°C$, $u_{wind} = 1\ ms^{-1}$). The heat carrier is water ($\dot{m} = 0.038\ kgs^{-1}$). Figure 4.26 shows the good coverage between measurement and simulation. According to equation (4.77), the percentage difference is only in the range between +0.4 % and +3.1 %.

$$Percentage\ difference = \left(\frac{\eta_{dynamic\ model}}{\eta_{measurement}} - 1\right) 100\,\% \tag{4.77}$$

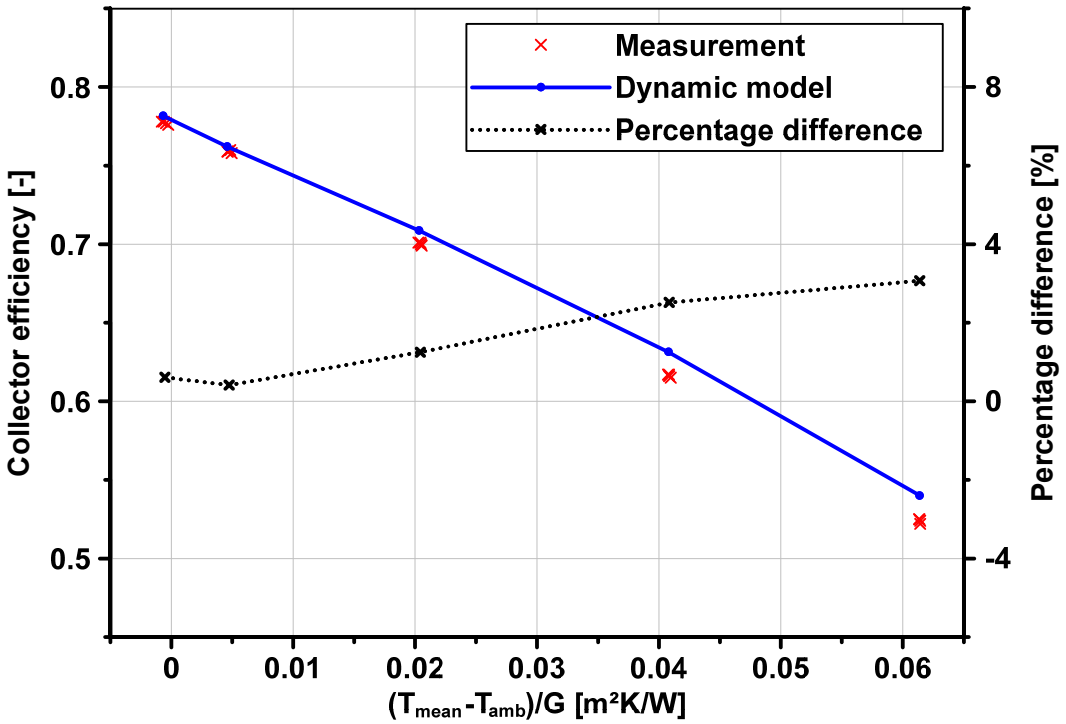

Figure 4.26: Comparison of the measured and simulated efficiency of the collector

The second test also showed satisfying conformity in particular with regard to individual component temperatures. During stagnation at insolation of 895 Wm^{-2} and an ambient air temperature of 33°C, the absorber temperature of model and test (average of 9 measurement points) differ only by +1 K. Also the average

temperatures (average of 3 measurement points) at glazing and backside vary below +1 K (Table 4.6).

Table 4.6: Collector component temperatures during stagnation of a conventional flat-plate collector in testing and simulation

	Testing	Model	Difference
Glazing	71°C	71°C	± 0 K
Absorber	174°C	175°C	+ 1 K
Backside (outside)	54°C	55°C	+ 1 K

4.1.11.3 Evaluation of the Test Results

All in all, the model proves to be valid according to the test collector. Slight differences are identified as within the theoretical limits of the model. Thanks to the assumptions that have been made, the model generates reliable results for flat-plate collectors in due consideration of the limits of the model. Comparable model approaches of state-of-the-art collectors show similar low uncertainties in simulation of efficiency or rather solar yield. The model from Koo (1999) showed percentage differences between -2 % and +3 % in comparison to experimental data of the collector efficiency curve. Matuska and Zmrhal (2009) described a percentage difference of about 3–4 % in the model validation. Furthermore, Cadafalch (2009) identified differences below 2 %. Thus, there is confidence that the model can be used for the investigation of entire systems to identify the solar yield as well as for the analysis of the component temperatures in the collector.

4.2 System and Test Stand Modelling

For the investigation of the thermal loads on the collectors as well as of the system efficiencies two simulation cases are considered. A usual solar-thermal system represents the build-up to analyse the moderate thermal loads under operating conditions and the system efficiency over the year. A test stand for dry collectors without heat removal represents the maximum thermal collector loads as a worst case scenario.

4.2.1 System

The solar-thermal heating system in the simulation is typical for a single family house in Central Europe and is described in Table 4.7.

Table 4.7: Description of the simulated solar-thermal heating system

Design data		
System:		
Building type	Single family house	
Location	Würzburg (Germany)	
Total system load	19,200	[kWh]
Space heating load	16,660	[kWh]
Domestic hot water load	2,540	[kWh]
Heat distribution system	Floor heating	
Auxiliary heating	Oil heating boiler 15 kW	
Buffer storage volume	897	[l]
Solar collectors:		
Aperture area	14.6 (8 Collectors)	[m^2]
Collector azimuth	0 (South)	[°]
Collector slope	45	[°]
Optical efficiency	0.798	[-]
Linear heat loss coefficient	3.34	[$Wm^{-2}K^{-1}$]
Quadratic heat loss coefficient	0.0075	[$Wm^{-2}K^{-2}$]
Heat capacity	9.5	[kJK^{-1}]
Heat carrier	Water	
Specific volume flow	40	[$lm^{-2}h^{-1}$]

The house requires 16,660 kWh per year for space heating and is equipped with floor heating. Additional heating energy of 2,540 kWh per year is demanded for hot water supply. The thermal energy is provided by an oil burner besides the

solar-thermal energy supply. The solar-thermal system is a pressurized state-of-the-art type. The eight collectors of the developed model are connected to buffer storage with 897 l.

4.2.2 Test Stand

The test stand for collectors is similar to the collector exposition in the system simulation. However, the collector is dry and not connected to a pressurized system. This represents the highest temperature loads on the collector components over the test year as maximum reference.

Figure 4.27 (left) shows the build-up of the test stand in *Simulink*. The input blocks feed the collector model with data from the fluid, the weather and the orientation or rather the position of the collector.

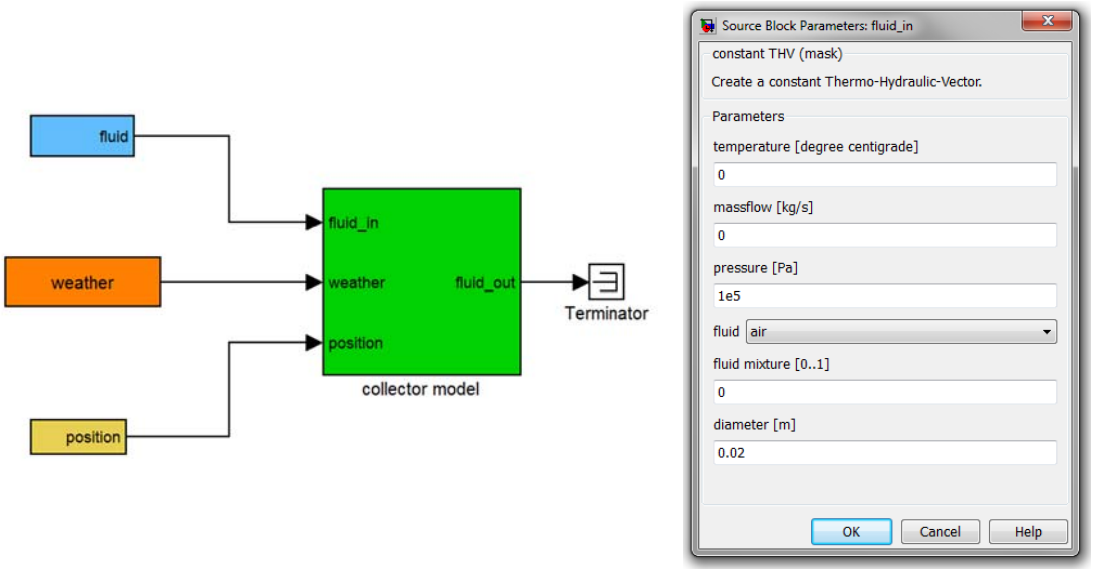

Figure 4.27: Build-up of the test stand in *Matlab/Simulink* (left) and parameter mask of the fluid block (right)

The fluid data for the model is provided by the block for constant fluid conditions from the *CARNOT* library. Figure 4.27 (right) shows the mask for the definition of the fluid at the collector inlet. The fluid data for the simulation of stagnation is set to air at ambient pressure without any mass flow. The weather dataset of the test

reference year of Würzburg is used for both, system simulation and test stand. Also the orientation is similar to the system simulation.

5 Thermal Collector Analysis by Simulation

The selected, promising overheating protection measures from Chapter 0 have to be analysed in greater depth regarding their influence on system efficiency and component temperatures. Therefore, the developed simulation model was used to derive the necessary results by implementing the measures in collectors. The approaches were investigated in annual simulations. On the basis of chosen temperature limits and a reference system the simulation results will be investigated and compared.

5.1 Evaluation Basis

For comparison and evaluation of the simulation results two cases are of major importance regarding polymeric collectors. On the one hand, reachable temperature reduction or rather limited maximum temperatures of the collector components have to be considered to allow cost-effective materials. On the other hand, the system yield of the annual simulations is necessary in order to be able to derive expectations about the heat generation costs of the systems.

5.1.1 Temperatures

Regarding thermal loads on components, two cases are of importance for the polymeric material selection. Firstly, the maximum temperature has to be identified to consider the stability of the component as well as the degradation of the material. This temperature has to be avoided or limited to short durations for components without mechanical loads. Secondly, the thermal loads over the defined life time of the component are relevant to estimate degradation as well. Above this temperature, depolymerisation and oxidation in the material occur or rather occur at an advanced rate (Biron 2013). As a result, the material has decreased mechanical properties like the impact strength. Therefore, three temperatures from material tests are used for the thermal requirements of the components:

The heat deflection temperature (HDT) according to the standard DIN EN ISO 75-1 (2013) describes a defined bend of a test specimen under a test load. Hence, this temperature is connected to the stability and defines the maximum temperature of components under mechanical loads. The HDT can be derived from stagnation tests and from peak temperatures of annual simulations. However, the focus of thermal investigation is on the durability of the materials due to degradation caused by thermal loads. The stability has to be considered in the developmental stage of the collector component design.

The short-term service temperature is defined as a temperature limit without appreciable damage of the material (Domininghaus et al. 2012; Biron 2013). Therefore, degradation and deformation is taken into account. The duration is usually set ranging between a few minutes and several hours. This temperature will be derived from annual simulations.

The long-term service temperature according to ISO 175 (2010) defines the temperature of a material specimen being resistant for 20,000 h of exposure in hot air or 10,000 h of exposure in hot oil without losing more than 50 % of its mechanical properties like the tensile strength in comparison to the reference value measured at 23°C. Therefore, the annual simulations will be used to investigate preselected material requirements according to the long-term stability.

For the evaluation of the simulation results, the temperature boundaries of basic polymeric material classes were chosen. The lowest material costs were achieved by commodity plastics like polypropylene (PP). However, the temperature limits for their use are also low. Thus, this material represents the highest requirements for temperature reduction. More durable materials are engineering plastics. A relevant and cost-efficient example is polyamide 66 (PA 66). This example considers especially the use in absorbers. Therefore, the materials are characterised for their durability against hot water. Table 5.1 shows the temperature limits of the materials being suitable for absorber, insulation and casing.

Table 5.1: Temperature limits of opaque materials for absorber, insulation and casing regarding defined tests (Domininghaus et al. 2012)

Materials	Short-term service temperature [°C]	Long-term service temperature [°C]
Commodity plastics:		
PP	140	100
Engineering plastics:		
PA 66	~185 (170–200)	~100 (80–120)

5.1.2 Solar Yield

The yield of the solar-thermal system and the influence of the overheating protection measures have to be identified by comparison of the annual simulations. The fractional energy savings f_{sav} according to the standard DIN EN 12977-2 (2012) are used to define the system efficiencies. Therefore, the energy consumption of the heater of a conventional heating system $Q_{conventional}$ and the energy consumption of the auxiliary heater of the solar-thermal heating system Q_{aux} were taken into account whereas both heating systems have to supply the annual total system load of the house Q_d (Figure 5.1).

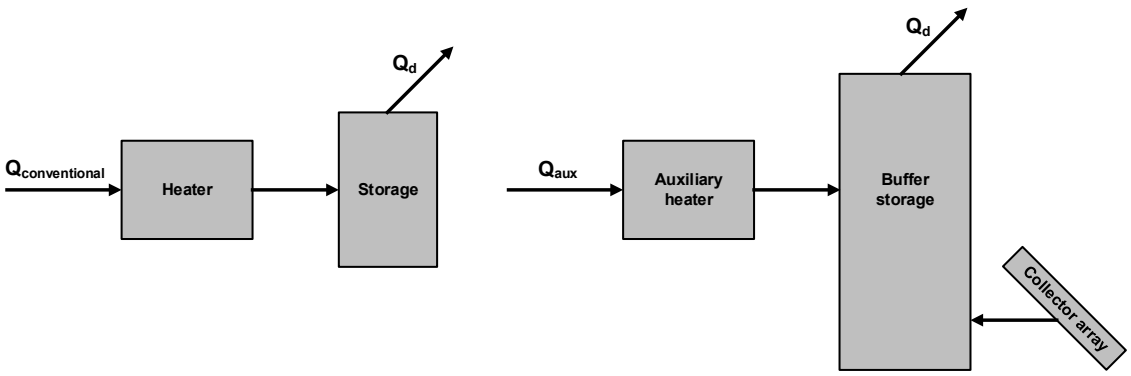

Figure 5.1: Basic energy flow of a conventional heating system (left) and a solar-thermal heating system (right)

The value of the fractional energy savings is the percentage of the energy being saved by the solar-thermal system instead of using a conventional heating system being represented in equation (5.1).

$$f_{sav} = \frac{Q_{conventional} - Q_{aux}}{Q_{conventional}} 100\,\% \tag{5.1}$$

The advantage of f_{sav} is the consideration of the additional thermal losses of the solar-thermal heating system mainly caused by the buffer storage.

Table 5.2 shows the description of the defined conventional heating systems as a basis.

Table 5.2: Description of the simulated reference heating system

Design data		
Building type	Single family house	
Location	Würzburg (Germany)	
Total system load	19,130	[kWh]
Space heating load	16,590	[kWh]
Domestic hot water load	2,540	[kWh]
Heat distribution system	Floor heating	
Heater	Oil heating boiler 15 kW	
Domestic hot water storage volume	130	[l]
Energy consumption of the heater	20,120	[kWh]

5.2 Reference Results

As a reference, the system described above was simulated with conventional flat-plate collectors. Two scenarios were taken into account — conventional flat-plate collectors with and without selective absorber coating. The scenario without selective absorber coating is used as a reference result for overheating protection measures having a non-selective behaviour as well as a distinct concept to decrease component temperatures.

The system with highly-selective coated absorbers (optical characteristics: $\alpha = 0.95$ and $\varepsilon = 0.04$) reaches fractional energy savings f_{sav} of 20.0 %. In the

same system with a non-selective absorber coating ($\alpha = 0.95$; $\varepsilon = 0.90$), the fractional energy savings decrease to 15.7 %. The higher radiation losses of the absorber cause a relative decrease of the solar yield by 21.5 % (Table 5.3).

Table 5.3: Fractional energy savings and relative decrease of the reference systems in annual simulations

System	f_{sav} [%]	Relative decrease [%]
Reference system, selective	20.0	--
Reference system, non-selective	15.7	-21.5

However, the component temperatures, too, decrease as a result of the lowered efficiency. The maximum absorber temperature declined from 223°C to 139°C. The temperatures of the selective absorber exceed the limits of both material classes whereas the non-selective absorber ranges between the short-term services temperatures of PP and PA66.

Figure 5.2 shows the histograms of the absorber temperatures of the two reference systems during operation and permanent stagnation over the period of one year. The temperature levels from 100°C to 180°C represent the short-term temperature arrays for commodity as well as engineering plastics for orientation.

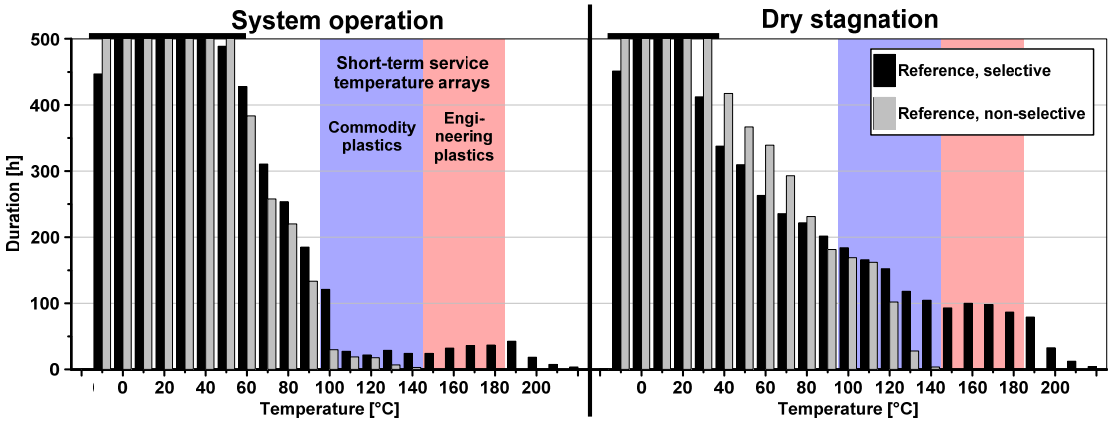

Figure 5.2: Histograms of the absorber temperatures with (black) and without (grey) selective absorber coating over one year

Beside the temperature peak, also the duration of plate temperatures above 95°C decreases considerably from 425 to 76 h for the collector being integrated into

the system. Especially the thermal loads of the dry collector were drastically lowered from 1,230 to 465 h.

5.3 Thermotropic Layers

Thermotropic layers at the collector front are able to lower the occurring temperatures of the collector components. In Resch et al. (2009) a number of layers with fixed domains of thermoplastics were investigated in detail. Two layers with the most promising properties were analysed in the system simulation to estimate their potential for solar-thermal applications. The layer C-4-5 has a relatively high hemispherical solar transmittance of about 87 % in the clear state. However, the decrease to 75 % in the scattered state is low. In contrary to that, the second layer disposes of lower hemispherical solar transmittance of about 78 % in the clear state. With a decrease to 62 %, it has, however, a better switching performance. Figure 5.3 shows the switching performance of the layers depending on the temperature.

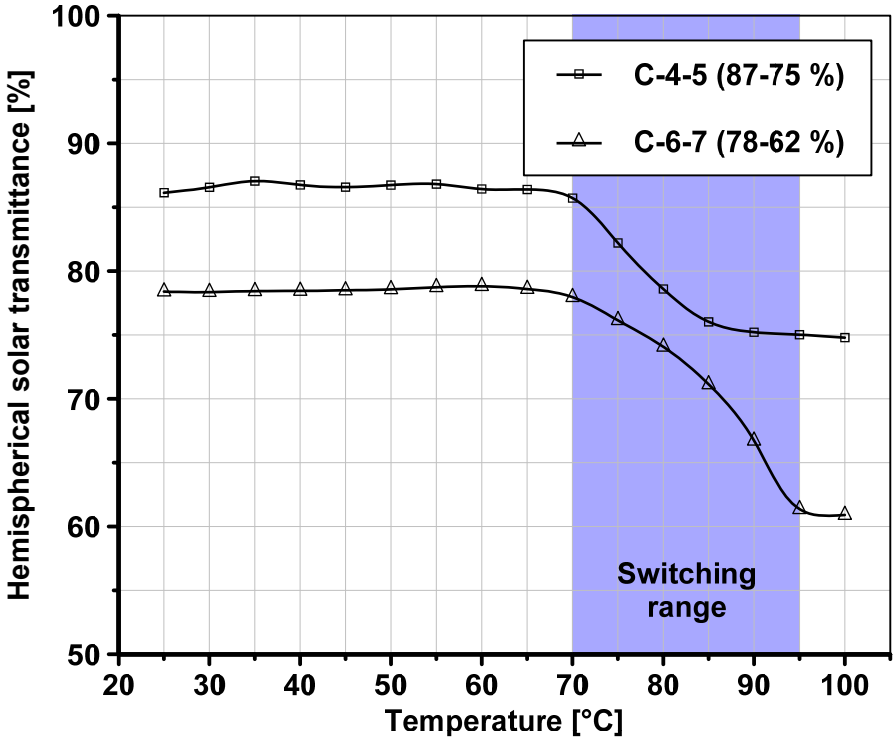

Figure 5.3: Temperature-dependent gradient of the transmittance of two thermotropic layers for simulation (according to Resch et al. 2009)

5.3.1 Application at the Absorber Surface

Switching of the layers occur in the range between 70°C and 95°C. Thus, the layer has the best switching performance being placed at the absorber surface. The influence of the ambient temperature and the high trigger temperature are disadvantageous for an application on the single glazing. Thus, the absorber temperature would exceed the proposed limits of the polymeric materials in this case. The layer application on the absorbing surface inhibits selective absorber properties.

The collector systems being equipped with the thermotropic layers show a drastic efficiency reduction in the annual simulations. The relative decrease of the fractional energy savings or rather the solar yield is between -35.0 % (C-4-5 / transmission: 87–75 %) and -42.0 % (C-6-7 / transmission: 78–62 %) compared to the selective reference system, which is shown in Table 5.4. The additional reduction of the transmittance of the collector front in clear state and the missing selective absorber behaviour are the major reasons for that loss. But also the early switch of the layer at temperature levels being relevant for the solar yield of the system is disadvantageous. The reference systems are still operating with a maximum efficiency at absorber temperatures between 80°C and 120°C whereas the protected systems decrease their efficiency due to the active overheating protection.

Table 5.4: Fractional energy savings and relative decrease of the reference systems as well as of the systems with thermotropic absorber layers in annual simulations

System	f_{sav} [%]	Relative decrease [%]
Reference system, selective	20.0	--
Reference system, non-selective	15.7	-21.5
System with thermotropic layer C-4-5	13.0	-35.0
System with thermotropic layer C-6-7	11.6	-42.0

The higher transmittance of layer C-4-5 increases the system performance, but also causes higher component temperatures due to the higher transmittance in

the scattered state. Thus, the absorber in the system is less than 3 h at temperature levels above 100°C and with a maximum value of 109°C. The absorber of the dry stagnating collector is 139 h above this temperature level and reaches a maximum temperature of 117°C. Figure 5.4 represents the durations of the absorbers at the occurring temperatures over one year.

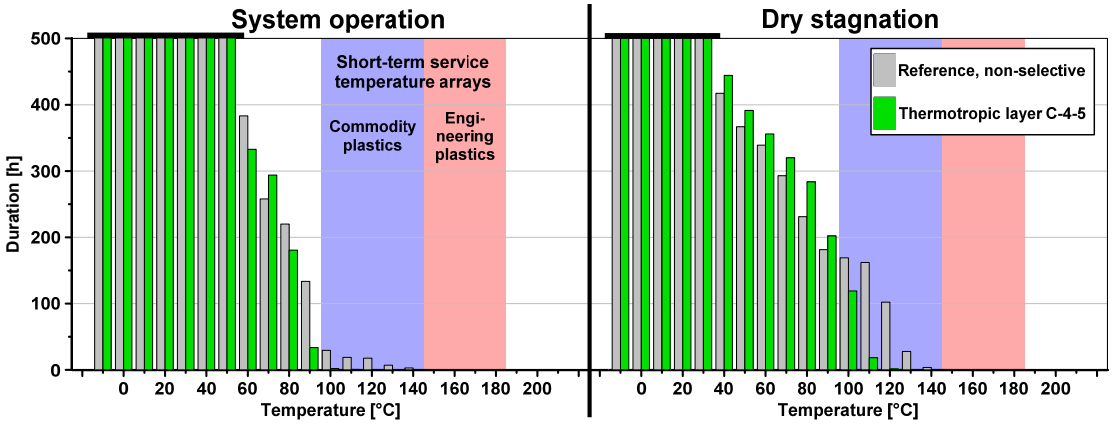

Figure 5.4: Histograms of the absorber temperatures without selective coating (grey) and with thermotropic absorber layer C-4-5 (green) over one year

The layer C-6-7 has a lower transmittance in the clear state and a large switch to the scattered state (Figure 5.5). This leads to a maximum temperature of only 90°C in the system integrated collector and 104°C in the dry collector.

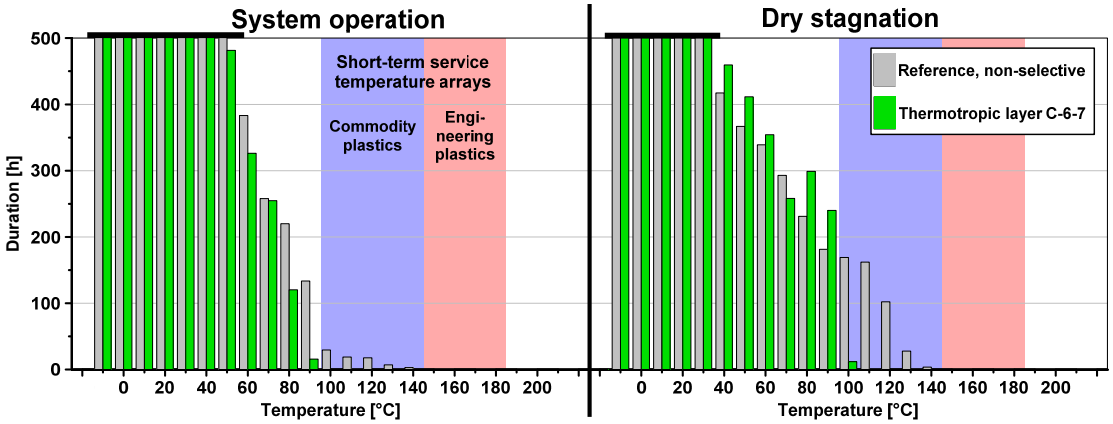

Figure 5.5: Histograms of the absorber temperatures without selective coating (grey) and with thermotropic absorber layer C-6-7 (green) over one year

5.3.2 Application at the Glazing

For comparison, the layers were also placed at the glazing. The application at the glazing causes an activation of the measure at higher absorber temperatures due to the temperature gradient between plate and cover. The switch of the layer also depends on the ambient air temperature near the glazing. Thus, the activation of the measure is not connected strongly to the absorber temperature.

The collector systems being equipped with non-selective absorber and thermotropic layers at the glazing also show a drastic efficiency reduction in the annual simulations. The relative decrease of f_{sav} is between -35.0 % (C-4-5) and -42.0 % (C-6-7) compared to the selective reference system (Table 5.5). The performance of the system is equal to the approach with the layer application at the absorber. Thus, the system efficiency is only limited by the disadvantageous optical properties of the application. The switching characteristics depending on the deposition do not have any influence on the system operation. Also the low maximum glazing temperatures of 74°C or rather 72°C cause almost no change to the optical characteristics of the layer.

Table 5.5: Fractional energy savings and relative decrease of the reference systems as well as of the systems with non-selective absorber and thermotropic layers on the glazing in annual simulations

System	f_{sav} [%]	Relative decrease [%]
Reference system, selective	20.0	--
Reference system, non-selective	15.7	-21.5
System with thermotropic layer C-4-5	13.0	-35.0
System with thermotropic layer C-6-7	11.6	-42.0

At the absorber being connected to the solar-thermal system maximum temperatures of 121°C (C-4-5) or rather 108°C (C-6-7) occur. At the absorber in the dry collector 124°C (C-4-5) or rather 119°C (C-6- 7) were reached.

In contrary to that, a set-up with selective absorber and thermotropic layer at the glazing leads to the fact that the system efficiency can be improved. The reduced

radiation from the absorber causes less thermal losses and a steeper temperature gradient between absorber and glazing. The low maximum glazing temperatures of 69°C or rather 66°C are also too low for an activation of the measure. This leads to increased system efficiencies because the operational range of the system and the switch of the layers do not overlap. The systems have a relative decrease of -10.5 % (C-4-5) and -17.5 % (C-6-7) according to the reference with selective absorber coating (Table 5.6).

Table 5.6: Fractional energy savings and relative decrease of the reference systems as well as of the systems with selective absorber and thermotropic layers on the glazing in annual simulations

System	f_{sav} [%]	Relative decrease [%]
Reference system, selective	20.0	--
Reference system, non-selective	15.7	-21.5
System with thermotropic layer C-4-5	17.9	-10.5
System with thermotropic layer C-6-7	16.5	-17.5

For both, system operation and dry stagnation, the maximum absorber temperatures of 200°C (C-4-5) and 188°C (C-6-7) are extremely high.

5.3.3 Summary

The system performance of collectors with non-selective absorber properties and thermotropic layers is independent from the place of application of the measure. The lower component temperatures of the collector with thermotropic absorber favour this set-up.

The collector with selective absorber and thermotropic glazing shows a good system performance. However, the reduced heat transfer leads to glazing temperatures below the trigger point of the layer. Hence, the layer will not be activated even at absorber temperatures of 200°C. Therefore, the expensive combination of selective coating and thermotropic layer is not useful.

Higher transmittance of layer C-4-5 leads to a better system performance whereas absorber temperatures also stay below critical levels. Thus, layer C-4-5 provides preferable collector characteristics. However, the major temperature reduction is caused by the low optical efficiencies of the approaches.

5.4 Micro-structured Layer

For the investigation of micro-structured layers for overheating protection, the tested and simulated layers from Walze (2005) were implemented. The metalized asymmetric CPC structure according to Figure 5.6 was placed at the glazing of the collector model. This structure deflects a major part of the solar radiation at low zenith angles occurring particularly during summer (incidence angle at the collector ranging between -60° and 0°). Thus, the hemispheric transmission is reduced at these conditions. For simulation, the behaviour of the tested asymmetric CPC from Figure 5.6 (right) was used in combination with a selective absorber.

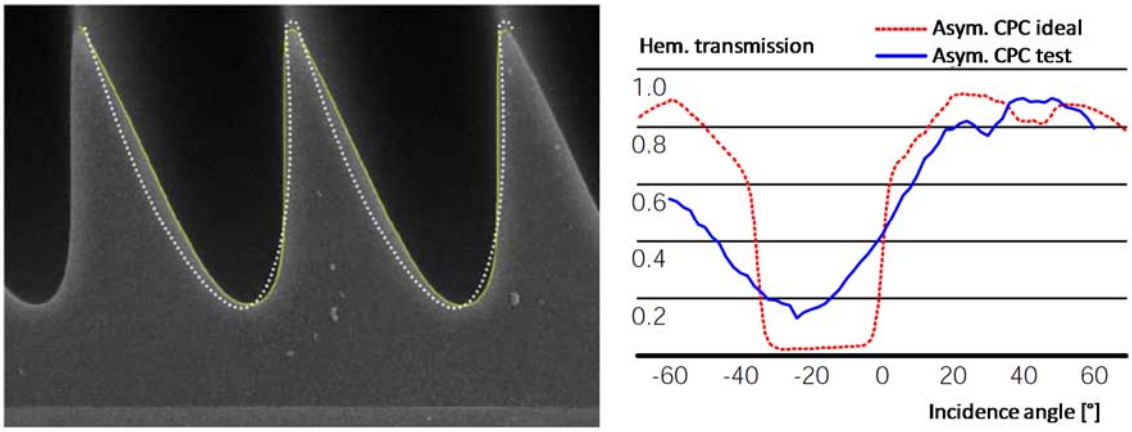

Figure 5.6: Moulding of a negative asymmetric CPC structure (left) and simulation of the transmission of metalized asymmetric CPC structures depending on the incidence angle (right; according to Walze 2005)

5.4.1 Standard Configuration

The annual simulation showed that the measure is only marginally influencing the system operation. The relative decrease according to the reference system is only -15.0 % (Table 5.7).

Table 5.7: Fractional energy savings and relative decrease of the reference systems as well as of the system with micro-structured layer on the glazing in annual simulations

System	f_{sav} [%]	Relative decrease [%]
Reference system, selective	20.0	--
Reference system, non-selective	15.7	-21.5
System with micro-structured layer	17.0	-15.0

The temperature loads on the absorbers were considerably reduced by the CPCs (Figure 5.7). Duration at temperatures above 95°C was reduced from 425 h to 9 h in the system operation test and from 1,230 h to 500 h in the stagnation test. Maximum temperatures were decreased to 133°C / 164°C for system operation / dry stagnation.

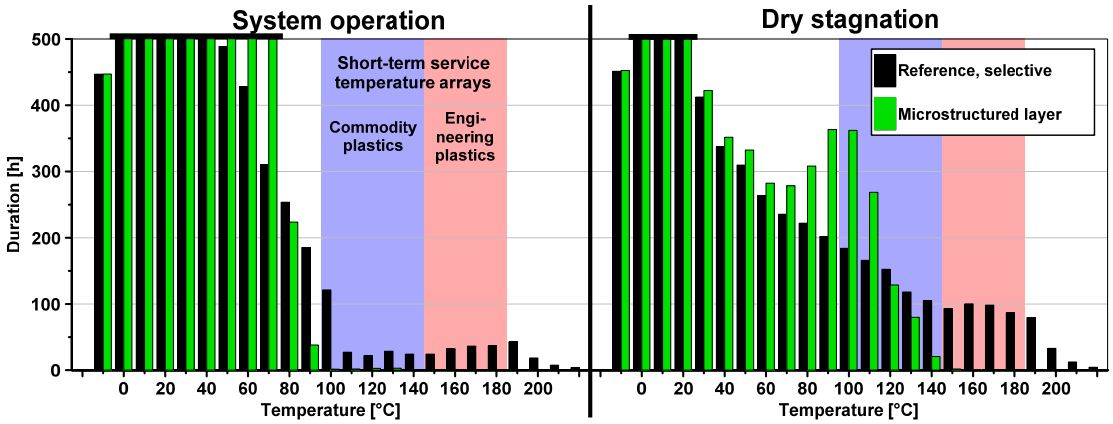

Figure 5.7: Histograms of the absorber temperatures with selective coating (black) and with micro-structured layer (green) over one year

5.4.2 Combination with Service Water Cooling

The remaining critical thermal loads at the absorber being protected by the CPC can be erased by implementing a service water cooling unit into the solar-thermal system. This measure combination was already investigated in Reiter et al. (2011) with the same simulation system, same overheating protection measure and a similar collector model. The water tap was connected to the return of the collector array. A sensor at the collector flow provides the signal for the controller for the valve of the water tap. The control strategy was set to stay below a flow temperature of 90°C. The water consumption of the annual simulation in

the system was quite low with 2.5 m³. However, the collector array in permanent stagnation required about 58 m³ to keep the flow temperature below 90°C.

5.4.3 Variation of the Collector Position

The dependency on the solar incidence requires a further investigation of various collector positions to evaluate a variable installation. Therefore, the collector slope β was changed to 30° as well as 60° and the collector azimuth was changed towards South-East (-45°) and South-West (45°) direction.

Table 5.8 shows the major influence of the position on the collector behaviour. The fractional energy savings of the system with micro-structured layer are between 11.6 % and 17.9 %, whereas the corresponding reference results are between 17.1 % and 20.0 %. Beside the rather varying fractional energy savings, especially, the maximum absorber temperatures occur in a wide range between 126°C and 184°C. Thus, the overheating protection function cannot ensure a reliable temperature decrease in dependency on the collector orientation.

Table 5.8: Fractional energy savings and maximum absorber temperature of the system with micro-structured layer on the glazing in annual simulations depending on the collector position

System with micro-structured layer			
Collector slope β	Collector azimuth	f_{sav} [%]	$T_{max,a}$ [°C]
30°	South-East	15.7	178
30°	South	17.9	184
30°	South-West	17.3	183
45°	South-East	14.5	158
45°	South	17.0	164
45°	South-West	16.5	170
60°	South-East	11.6	126
60°	South	14.1	132
60°	South-West	13.8	149

5.4.4 Summary

The micro-structured layer shows a great reduction of the thermal loads whereas the decrease of the system efficiency is relatively low. However, this measure cannot prevent high peak temperatures during stagnation. On the one hand, an additional service water cooling can reduce the temperatures. On the other hand, the economic and ecological disadvantages outweigh the advantages when taking the water consumption into consideration. Another disadvantage is of major importance towards which direction the collector is oriented. As opposed to this, the results of this measure depend to a great amount on the location with regard to the altitudes of the sun. This is why the development of further layers covering the conditions of the possible collector positions and the sales areas is required. The disadvantageous complexity of product and installation has to be considered for the evaluation regarding production as well as error rates in installation.

5.5 Thermochromic Layer with Switchable Emission Coefficient

For the analysis of thermochromic layers the investigated sample from Huot et al. (2008) was chosen. The described absorber layer has an emission coefficient ε ranging from 0.05 to 0.35 and a high absorption coefficient α of 0.973. The switch of the layer occurs in the range between 60°C and 68°C. Additionally, there is a switching hysteresis from 57°C to 52°C to the original state.

The fractional energy savings of the equipped system were sensitive to the solar yield (Table 5.9). The triggered overheating protection has less influence on the system although the switch is within a range of potential collector operation.

Table 5.9: Fractional energy savings and relative decrease of the reference systems as well as of the system with thermochromic absorber layer in annual simulations

System	f_{sav} [%]	Relative decrease [%]
Reference system, selective	20.0	--
Reference system, non-selective	15.7	-21.5
System with thermochromic layer	19.9	-0.5

The overheating protection function is limited. As expected, the absorber temperature is 172°C between the selective and the non-selective reference results because of the relatively low range of the emission coefficient ε. Figure 5.8 represents the thermal absorber loads. The total duration when the temperature levels were 100°C and more, is 280 h for the absorber in the system. With 840 h, the dry absorber increases threefold.

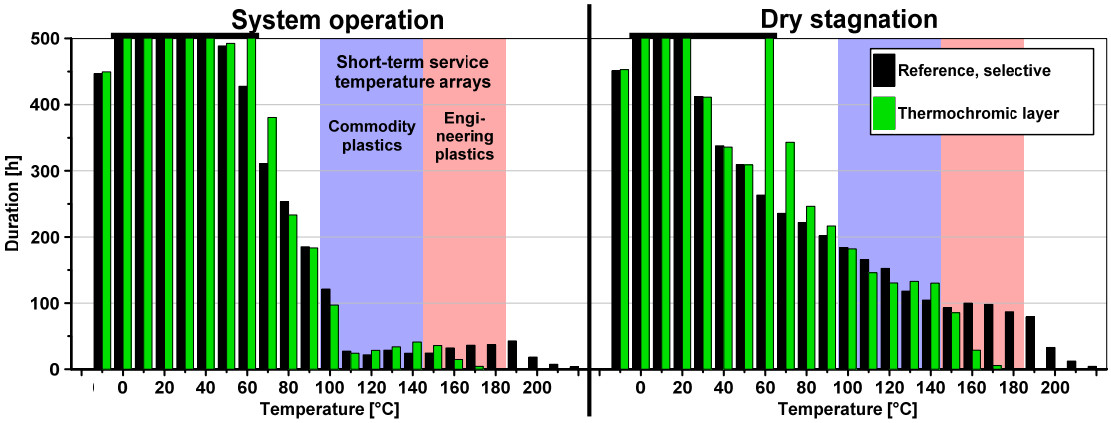

Figure 5.8: Histograms of the absorber temperatures with selective coating (black) and with thermochromic absorber layer (green) over one year

An additional service water cooling in the solar-thermal system with thermochromic absorber layer according to Chapter 5.4.2 was also simulated in Reiter et al. (2011). The water consumption was quite high. The operating system needed about 23 m³ to keep the absorber temperatures below 90°C. The system in permanent stagnation wasted about 84 m³ of service water.

5.6 Adjustment of the Collector Efficiency

Beside active measures, the adjustment of the collector efficiency was also tested in order to figure out the influence of reduced expenditure on manufacturing and simple collector designs. Therefore, the thermal behaviour of the absorber and backside was varied and analysed.

5.6.1 Reduction of the Absorber Emissivity

The first approach with an increased absorber emissivity is the reference collector with non-selective absorber coating being already investigated in Chapter 5.2.

The TISS paint investigated in Orel et al. 2009 was simulated as a compromise between the two extremes. In the simulation model the absorption coefficient α and the emission coefficient ε of the absorber surface were set to 0.91 and 0.34 (Color n.d.).

According to the surface properties of the absorber, the fractional energy savings of this system are between the selective and non-selective reference values (Table 5.10).

Table 5.10: Fractional energy savings and relative decrease of the reference systems as well as of the system with reduced emission coefficients in annual simulations

System	f_{sav} [%]	Relative decrease [%]
Reference, selective $(\varepsilon = 0.05)$	20.0	--
Variation, TISS paint $(\varepsilon = 0.34)$	17.7	-11.5
Variation, non-selective $(\varepsilon = 0.90)$	15.7	-21.5

The maximum absorber temperature of the annual simulations is 167°C. Beside the relatively high temperatures, long durations above 95°C with 210 h (operation) and 770 h (stagnation) can be achieved (Figure 5.9).

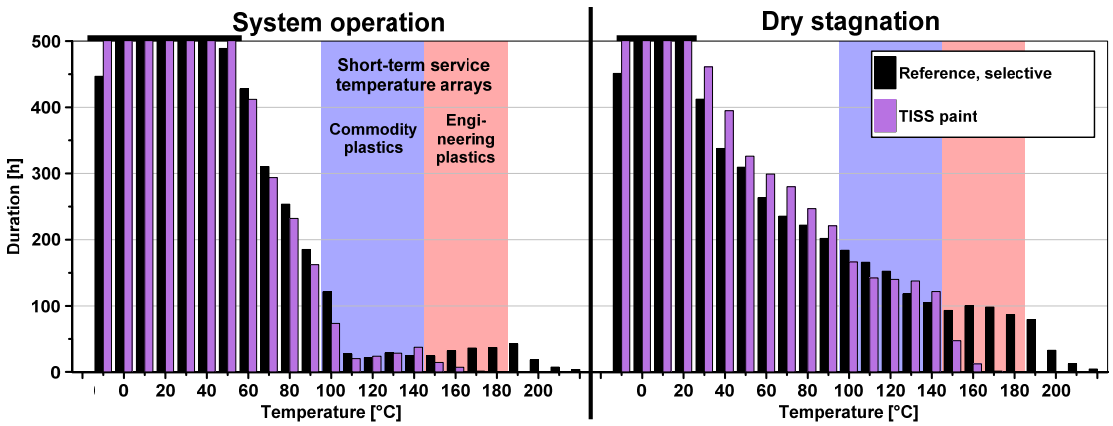

Figure 5.9: Histograms of the absorber temperatures with selective coating (black) and with TISS paint coating (purple) over one year

5.6.2 Reduction of the Backside Insulation

The reduced backside insulation was simulated by implementing less or rather no mineral wool whereas the distances inside the collector remained constant. This leads to comparable convective heat transfer conditions and decreased heights of the collector. The backside insulation of the reference collector with 45 mm was reduced step by step by 15 mm. A collector without any insulation was one extreme within the parameter variation. The two extremes of the variation was collector without any insulation. Only a thin plate was implemented as a barrier for convection as well as radiation losses. The objective of this variation is the identification of the optimal insulation thickness with respect to efficiency as well as thermal loads.

The comparison of the fractional energy savings of the different collectors showed less reaction on changing the insulation thickness (Table 5.11).

The good insulation properties of the mineral wool considerably reduced the heat transfer through the component. As a result, the inner surface temperature of the insulation is close to the absorber temperature. The small temperature gradient keeps the heat transfer of the absorber on a similar level and fewer differences between collector variations occur. Only the collector without any backside insulation shows extremely increased heat losses due to its high temperature gradient between non-insulated backside sheet and ambient air.

Table 5.11: Fractional energy savings and relative decrease of the reference systems as well as of the system with reduced backside insulation thicknesses in annual simulations

System	f_{sav} [%]	Relative decrease [%]
Reference system, selective	20.0	--
Variation 30 mm, selective	19.7	-1.5
Variation 15 mm, selective	19.2	-4.0
Variation 0 mm, selective	13.4	-34.5

The collector with 30 mm backside insulation continues to run almost 400 h at temperature levels below 100°C. Thermal loads in the dry collector occur even

for 1,170 h. The maximum absorber temperature is 215°C in both simulations. The collector has almost the same thermal loads like the selective reference (Figure 5.10).

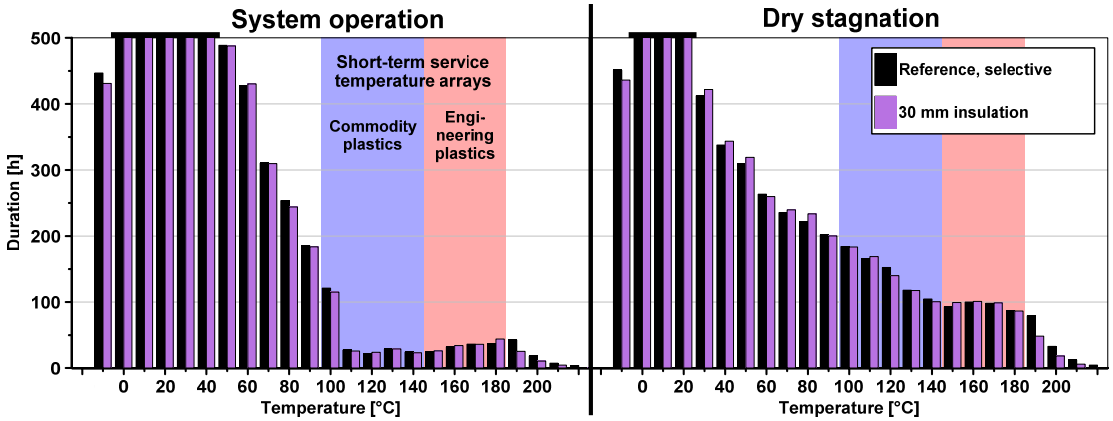

Figure 5.10: Histograms of the absorber temperatures with selective coating (black) and with 30 mm backside insulation (purple) over one year

Also histograms of the annual simulations with 15 mm backside insulation in Figure 5.11 show similar durations at these levels (350 h / 1,050 h) and a maximum temperature of 202°C. Thus, there is still almost no difference to the reference results.

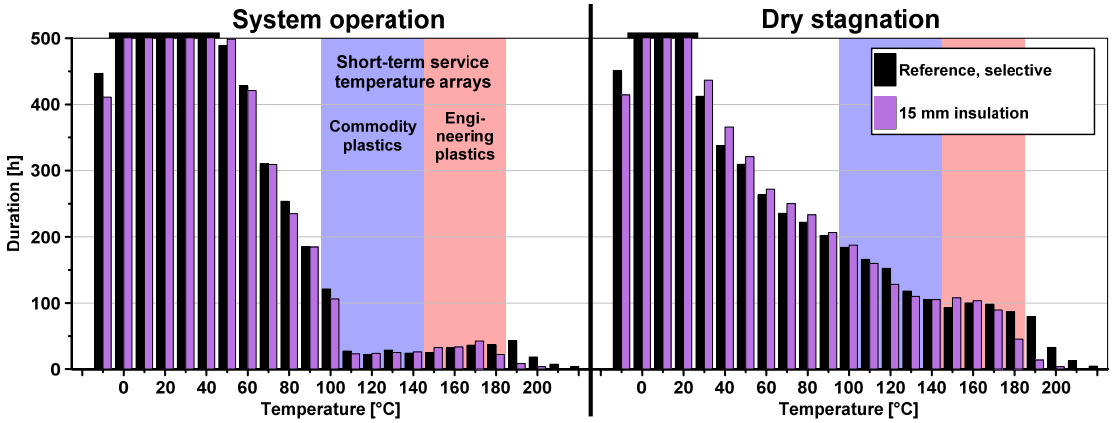

Figure 5.11: Histograms of the absorber temperatures with selective coating (black) and with 15 mm backside insulation (purple) over one year

Moderate thermal loads with 28 h appear at collectors without mineral wool alone in the range of the short-term service temperature of commodity plastics and a peak value of 122°C (Figure 5.12). In contrary to that, at temperatures between 95°C and 127°C, the dry collector continues to run for 250 h.

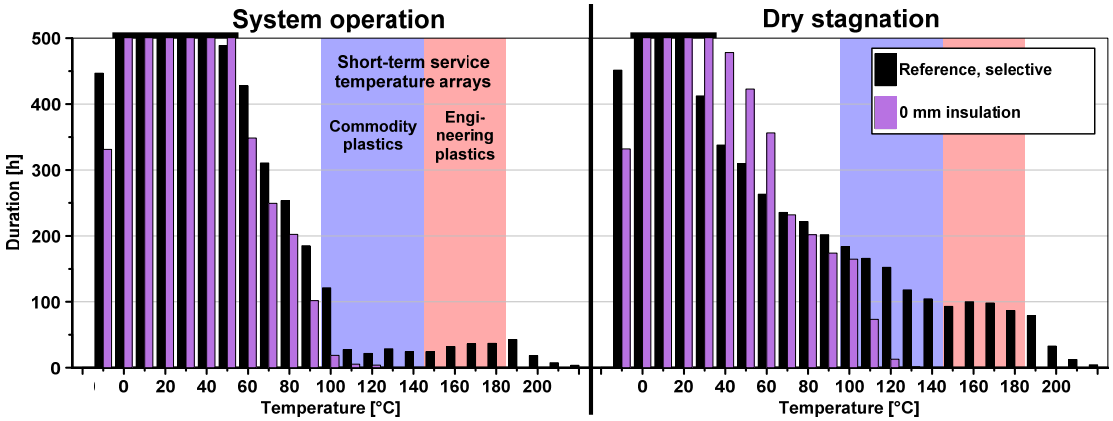

Figure 5.12: Histograms of the absorber temperatures with selective coating (black) and without backside insulation (purple) over one year

5.7 Evaluation of the Approaches

For the evaluation of the annual simulation results the fractional energy savings f_{sav} were confronted to the thermal loads. This proceeding combines the two major thermal properties for polymeric collectors to determine an overall rating. The evaluation was conducted with an adjusted rating or rather strength diagram according to guideline VDI 2225 (1998). In this case, the possible reduction of thermal loads is the technical rating and the influence on the fractional energy savings is the economic rating.

Therefore, the thermal loads were derived from the histograms of the absorber temperatures. The histogram classes (temperature levels) above 100°C were multiplied with the corresponding durations. The sum of these values represents the thermal loads of the absorber. The thermal loads were normalised to the value of the selective reference collector in dry stagnation. As this case poses the worst technical solution, the technical rating is set to 0. The approach of the system with thermotropic layer C-6-7 is the best technical solution due to the lowest thermal loads. Thus, this approach represents the highest possible technical rating (rating value: 1).

The fractional energy savings were normalised to the highest reachable solar yield which is referred to the system with selective reference collectors (economic

rating value: 1). The lowest economic rating value is defined by the result of the system with thermotropic layer C-6-7 and is set to 0.

Figure 5.13 shows the normalised results of all simulated overheating approaches in a rating diagram. System operation and dry stagnation spans a range of possible absorber loads depending on the system function. The ideal case of an approach would be located in the upper right corner of the rating diagram.

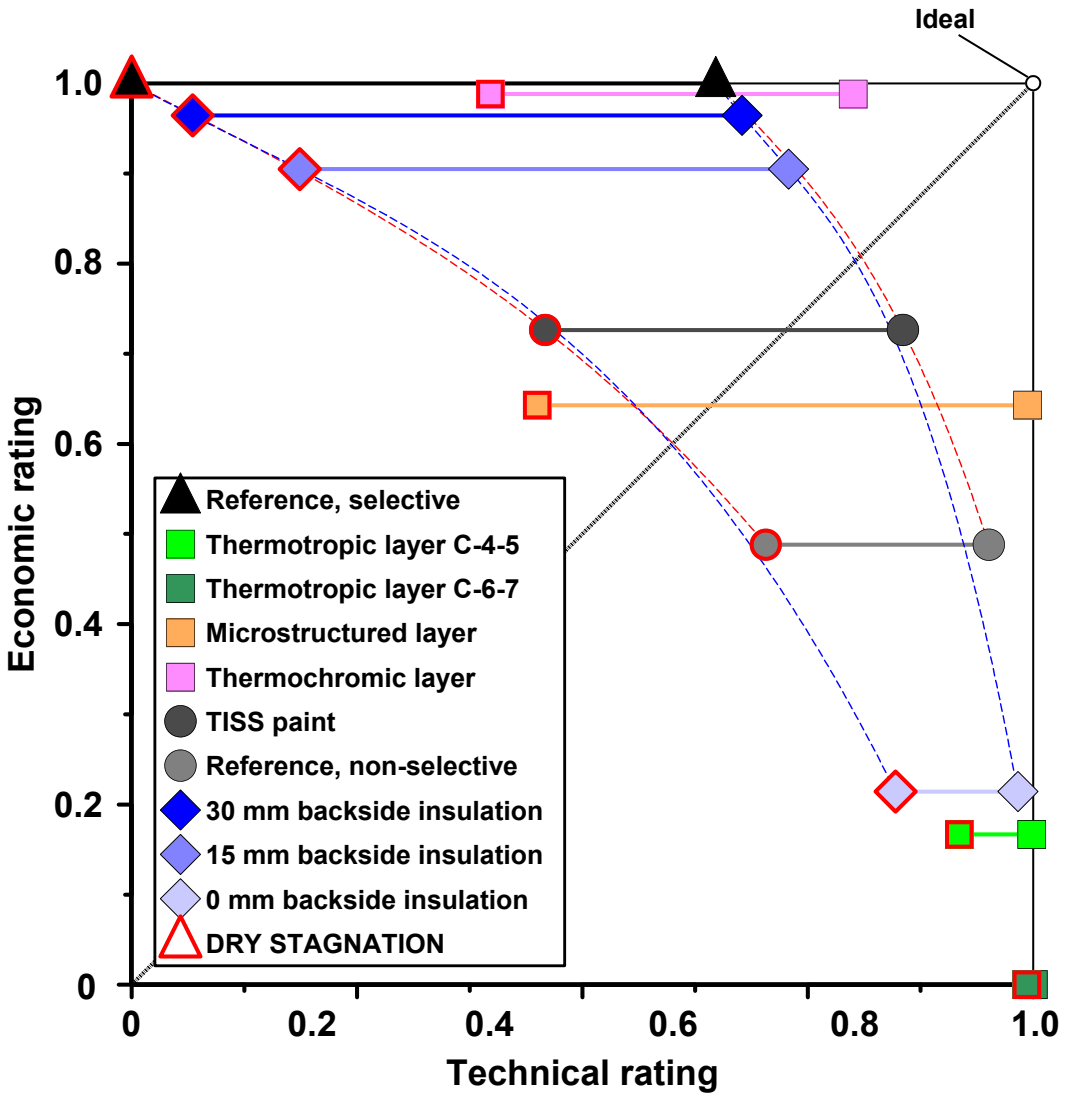

Figure 5.13: Rating diagram of the overheating protection measures

The maximum temperature is also important information to identify the most suitable solution. Table 5.12 lists overheating protection approaches by their highest absorber being reached in the annual simulations.

Table 5.12: Sorted list of maximum absorber temperatures occurring in the annual simulations

	Overheating protection approach	T_a [°C]
1.	Thermotropic layer C-6-7	104
2.	Thermotropic layer C-4-5	117
3.	0 mm backside insulation	127
4.	Reference, non-selective	139
5.	Micro-structured layer	164
6.	TISS paint	167
7.	Thermochromic layer	172
8.	15 mm backside insulation	202
9.	30 mm backside insulation	215
10.	Reference, selective	223

These two data pools are sufficient to figure out the most promising approaches for the implementation in polymeric collectors. The overheating protection measures in combination with service water cooling would be the best solution regarding thermal loads and peak temperatures. The system with thermochromic absorber layer and service water cooling represents the most efficient system variation, but the enormous water consumption of these approaches prevents the solar-thermal heating systems of being put into practise.

The two versions of thermotropic absorber layers show excellent overheating protection for polymeric materials even during dry stagnation. However, in large part, this reduction is caused by the missing selective surface behaviour and the reduced transmission of the collector front. Thus, these disadvantages are non-justifiable for any extra costs of this measure such as layer material and application.

The micro-structured layer has a great potential in a functioning solar-thermal system. The missing thermal intrinsic safety and the major dependency on collector position and location eliminate the use of this layer for polymeric collectors.

The thermochromic absorber layer enables an ideal solar yield of the system. The disadvantage of the layer is the limited overheating protection, especially for the requirements of polymers. Thus, the layers being already developed or rather investigated show an insufficient potential for cost-effective collectors. Beside the thermal behaviour, the application on polymeric components represents another hurdle for a cost-effective solution.

The absorbers with permanently reduced selective surface properties show a great reduction of thermal loads as well as peak temperatures. The reduction of the solar yield is viable only if the cost savings by omitting an absorber layer or using a paint coating are considered.

The comparison shows good results regarding efficiency for selective absorbers with reduced backside insulation. However, the thermal loads are too high for a cost-effective material choice. Only the simulation without any insulation shows enough reduced thermal loads, but also a low system efficiency.

Taking the results for the simulations as well as the identified properties of the measures into account, the two approaches for efficiency reduction by omitting production steps have the best potential for realising a fail-safe overheating protection approach without any hurdles in production as well as in durability or degradation. The combination of both approaches will balance the conflict between temperature and efficiency by means of low collector manufacturing costs. Therefore, the design approaches of polymeric collectors have to be analysed in simulations to derive the optimum collector properties.

6 Development and Analysis of Polymeric Collector Designs

Next to the overheating protection investigation, the polymeric collector design concepts has to be developed on the basis of the acquired knowledge from literature review, theoretical framework and simulation.

By means of the boundaries of suitable polymeric production processes and suitable materials, collector concepts have to be derived. An adjusted simulation model is necessary to predict component temperatures and solar yield to define the optimal parameters of the geometries. This is also the relevant data for a final economic evaluation polymeric collectors against state-of-the-art collectors on system level.

For development of polymeric collector concepts the focus is on thermoplastics and the associated manufacturing processes. This combination greatly fulfils the required low component costs and high output rates. In contrary, thermosets have a limited potential due to their higher material costs as well as their manufacturing processes mostly being suited for small and medium output (Biron 2013). They are also not suitable for further manufacturing steps like thermoforming or welding because of their special molecular structure being resistant against melting. Additionally, this structure is also the reason that thermosets are not reusable as virgin matter.

6.1 Overview of Polymeric Production Techniques

Polymeric production techniques are divided in main groups according to standard DIN 8580 (2003). Figure 6.1 lists the relevant main groups — primary shaping, moulding, machining and joining — suitable for making collector component geometries.

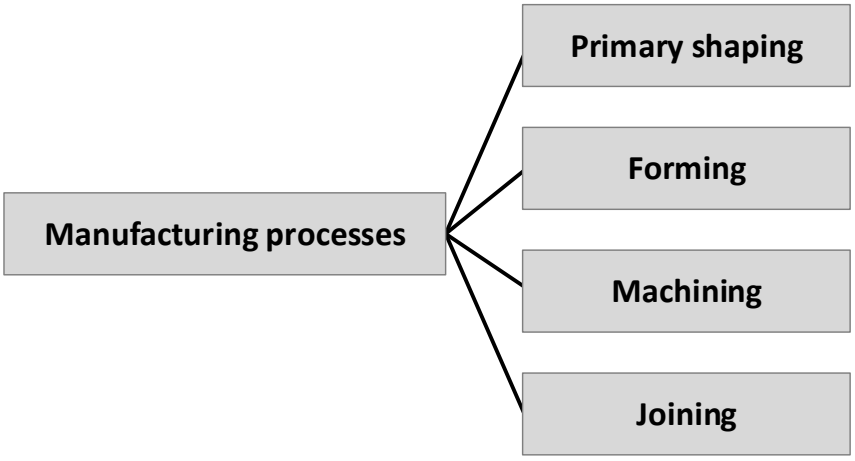

Figure 6.1: Overview on the main groups of relevant manufacturing processes for collector components

Primary shaping comprises the manufacturing techniques producing components from a liquid or pliable raw material. The most important processes for thermoplastics are injection moulding, extrusion and blow moulding. Thermoforming and twin sheet thermoforming are the relevant processing techniques of forming. These techniques and their use for collector components are described in the following.

Machining processes like milling are used for secondary processing of components manufactured by primary shaping or forming. The joining technique adhesive bonding is necessary for fixing components like absorber and glazing. Furthermore, welding is used for producing hollow components from two shapes.

6.1.1 Injection Moulding

Injection moulding is a technique for discontinuous processing of polymeric materials. By means of the following properties, injection moulding is perfectly suited for mass production:

- Direct path from raw material to finished component
- Total automation of the process
- Almost none finishing necessary
- High output rates

Injection moulding is suitable for small components like gear wheels as well as for large components like waste containers. The cycle times vary between a few seconds and 10^3 seconds. By means of the high mould and press costs is this process normally efficient for mass production (Biron 2013; Michaeli 2006).

The injection moulding cycle is described in Figure 6.2.

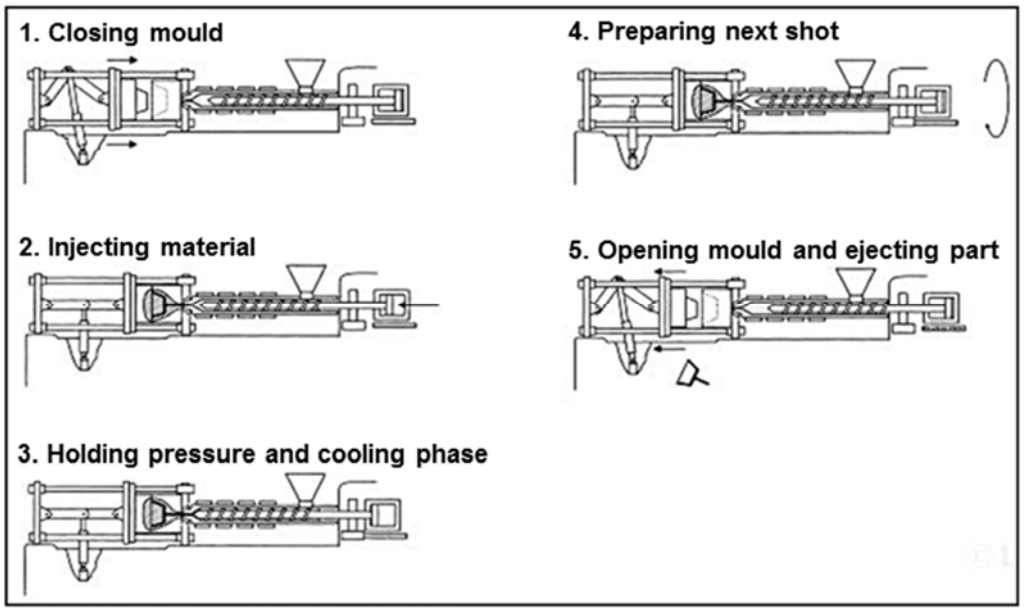

Figure 6.2: Injection moulding cycle (according to Michaeli 2006)

Injection moulding processes the most available polymeric materials and is applied in almost all industrial sectors. The automotive sector produces fenders and dash panels made of polyolefins. PC and PMMA is used for transparent components like headlights and taillights. Toys and home appliances are made from PS and ABS. PA and other engineering plastics appear in expensive components in the mechanical as well as electrical engineering sector (Michaeli 2006).

This polymer processing allows the realization of the most collector component geometries. Flat hollow components like the absorber are difficult to manufacture. However, two absorber components with fluid channels can be fixed together to reproduce the component with cavity. Glazing, casing and frame components are flat geometries and ideal for low cycle times. Also, insulation by mixing gas in the shot (thermoplastic foam injection moulding) is realisable. Thus, the component

is lightweight and has a low heat conductance. Figure 6.3 represents the capabilities for the collector component production.

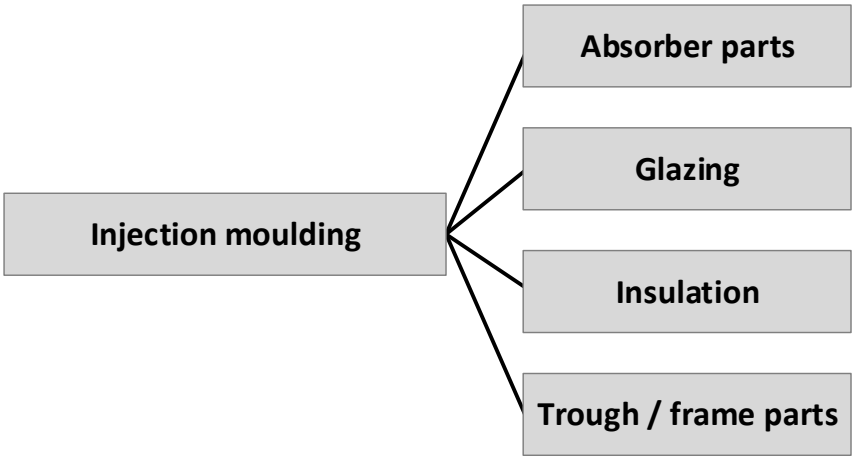

Figure 6.3: Capabilities of components manufactured by injection moulding

6.1.2 Extrusion

Extrusion is a continuous processing method for two-dimensional component geometries. Melted raw material is pressed by a screw through a die and is formed to a profile of unlimited length. The material as granulate or powder is melted within the barrel by a heating and frictional heat caused by the extrusion screw.

A polymer extrusion screw consists of three zones:

- Feed zone:
  Supplies the extruder with raw material
- Melting zone:
  Melting and compression of the material by the extrusion screw
- Metering zone:
  Homogenisation of the melted material and pressure build-up

Figure 6.4 shows these zones in a schematic build-up of an extruder.

Finally, the melted material is passing the feed pipe unit and the die. The extruded material has to be cooled down by a water bath and cooling rolls (Kaiser 2007; Michaeli 2006).

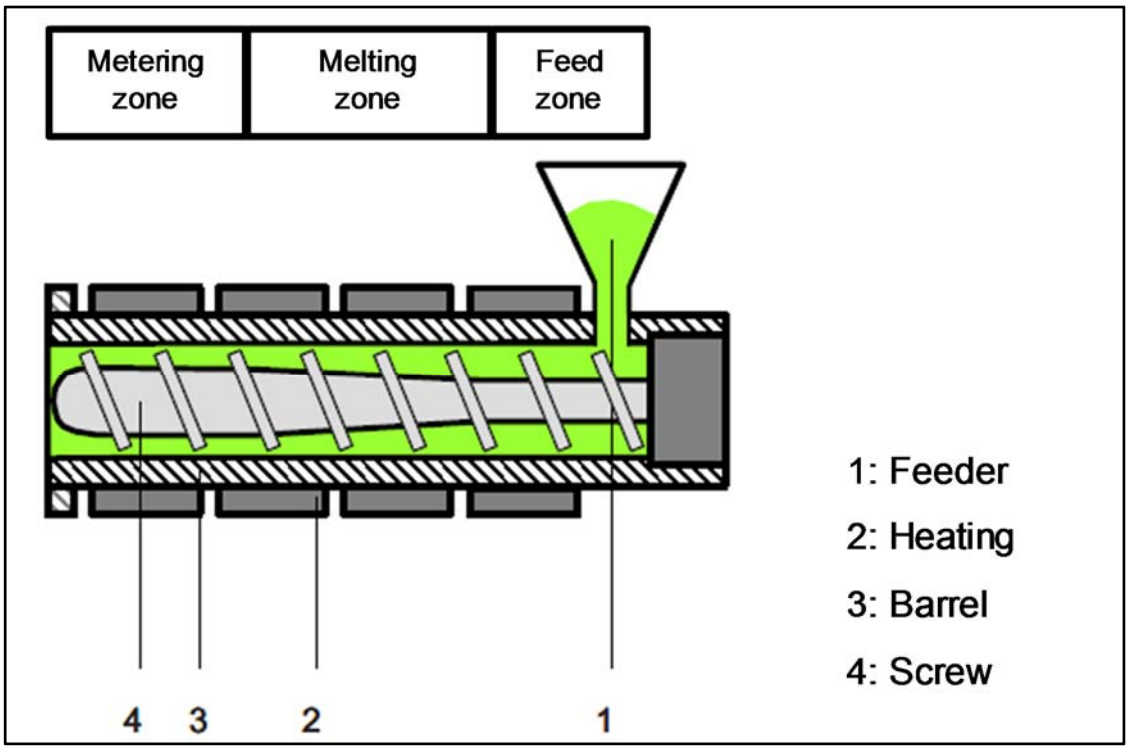

Figure 6.4: Schematic build-up of a plastic extruder (according to Kaiser 2007)

The output of the extrusion process varies between kgh^{-1} and $tonsh^{-1}$. Hence, extrusion is suitable for mass production depending on the die and the machinery size. The profile size of pipes, for example, reaches until 2,000 mm diameter and 40 mm wall thickness. The extrusion process is used for compounding, profile extrusion, sheet extrusion, jacketing, film extrusion and coating (Michaeli 2006). The materials for processing requires a sufficient melt viscosity to keep the shape between die and cooling unit. Typical materials are PVC, PP, PE, PC and PMMA (Johannaber 2004).

The possible extruded components for collectors are sheets for glazing and housing, profiles for frame components and multi-wall sheets for absorber, glazing and housing (Figure 6.5).

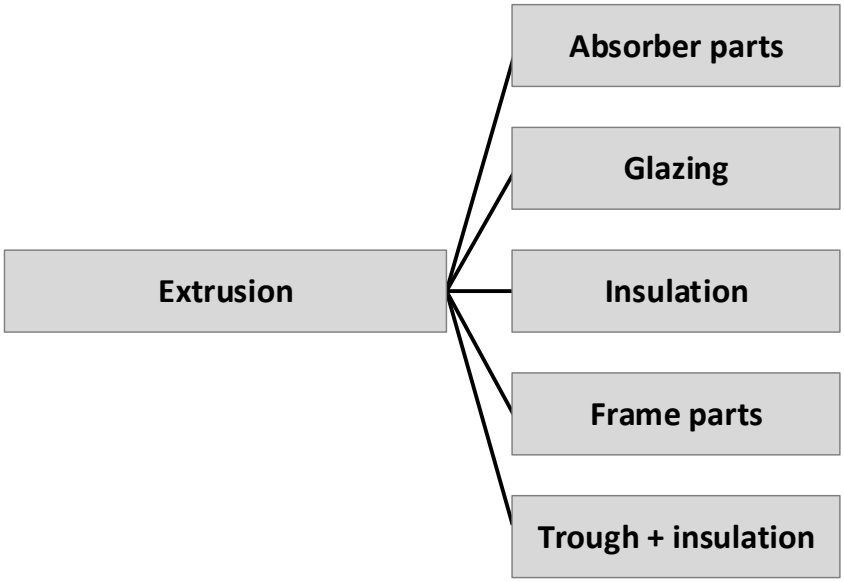

Figure 6.5: Capabilities of components manufactured by extrusion

The channels within the multi-wall sheets can be used for absorber channels as well as for insulation in glazing and housing by means of air enclosures. Such multi-wall sheets require additional components to close the profiles. By mixing a gas into the melted polymer the extruded material expands. The expanded polymer or rather the foam is ideal for insulation and also for a casing with integrated insulation.

6.1.3 Blow Moulding

Most hollow components are produced by blow moulding or rather extrusion blow moulding. The products embrace packaging items like bottles or canisters as well as technical components like hard shell cases. Blow moulding enables product sizes from packing for the pharmaceutical industry up to fuel oil tanks with 13,000 l volume (Michaeli 2006).

The blow moulding process begins with the vertical extrusion of a parison. In the second step close the moulds and through the blow pin enters compressed air. The parison is blown against the mould and hardens. Afterwards, the moulds open and eject the component. Figure 6.6 represents the blow moulding cycle. Commonly used materials are commodity plastics like PE, PP and PVC. Also technical polymers like PC, PA and polyphenylenether (PPE) are suitable.

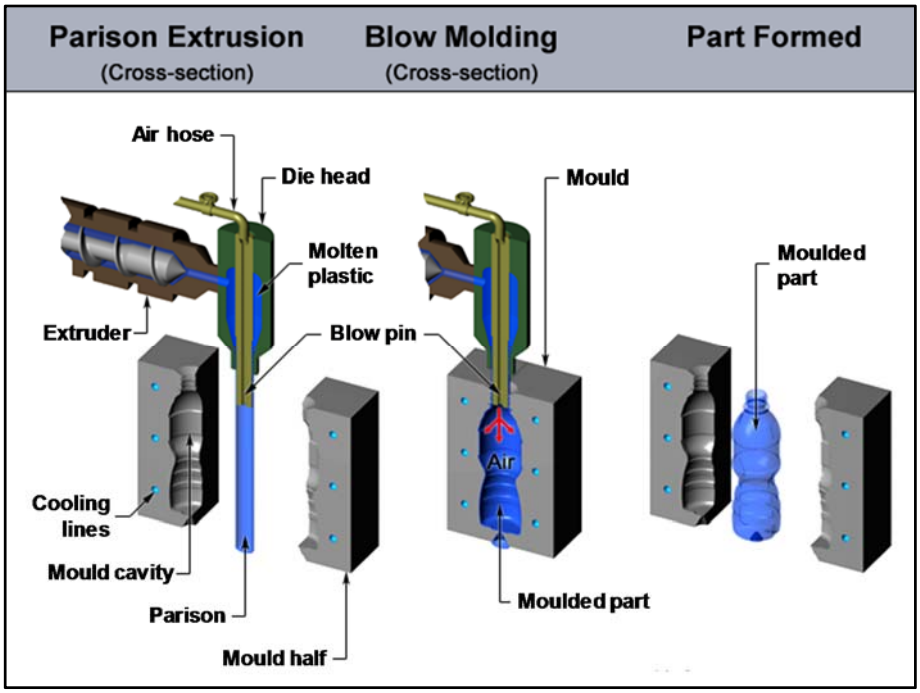

Figure 6.6: Blow moulding cycle (CustomPartNet 2008)

The high production rate and the low labour costs due to the high automation are advantageous. However, blow moulding has a poor control of wall thicknesses and geometrical details (Biron 2013).

Blow moulding is suitable for the production of the absorber with its fluid channels and connectors. Such components are already produced as pool absorbers. Using the enclosed air layer for the reduction of the convective losses, a double-walled glazing or casing can be realised. This air layer may replace the insulation in the housing. Also a second production step by filling the air gap with polyurethane foam for insulation is possible. Figure 6.7 represents the components which can be produced by blow moulding.

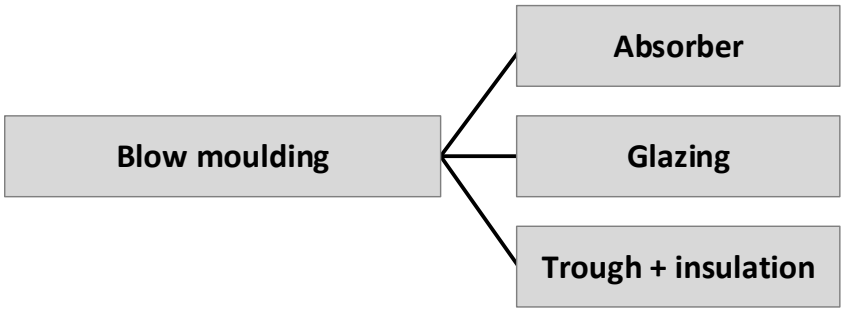

Figure 6.7: Capabilities of components manufactured by blow moulding

6.1.4 Thermoforming

Thermoforming is a production process of the main group of forming and requires a semi-finished component as input. Commonly, this component is an extruded plate or film. The thermoforming process is suitable for the production of moulded components without any cavities. The products range from yogurt cups in the packaging industry with an output until 100,000 units per hour to basins for pools or garden ponds with an output until 1.5 units per hour. The possible component size is quite large with 8,000 x 4,000 x 1,500 mm for pool basins for example (Michaeli 2006).

The thermoforming process begins with clamping the sheet or film into a holding device. A heating softens the material via convection or radiation. The softened sheet is stretched and pressed into a mould. After cooling down and hardening, the component is ejected from the mould. The thermoforming cycle is described in Figure 6.8 by means of the vacuum forming process.

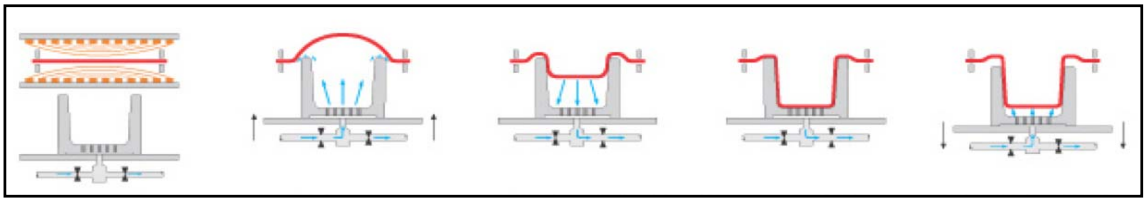

Figure 6.8: Vacuum forming cycle (DUROtherm Kunststoffverarbeitung GmbH (n.d.))

Three types of thermoforming – vacuum forming, pressure forming and mechanical forming – are differentiated by the method of moulding the material in the tool. Beside vacuum and air pressure, also a core plug can force the softened material into the mould. Most thermoplastics can be processed by thermoforming. Commonly used materials are PE, PP, PVC, PC, PMMA and PS (Kaiser 2007).

Thermoforming is distinguished by low mould costs, short cycle times, details with high quality and thin wall thicknesses for efficient material effort. However, the degree of automation is relatively low and trimming of the material being clamped in the holding device is required. Thus, there are an additional material effort and a post-processing by milling necessary. Also undercuts in the component geometry are difficult to realise.

Thermoforming is suitable for the production of absorber components by forming two shapes with the fluid channels. Afterwards the two components have to be fixed together to manufacture the complete absorber. Also the glazing can be adjusted to higher stability by curving. The most suitable component for thermoforming is the casing (Figure 6.9). Thermoformed covers and casings are still on the market (Chapter 1.2.3).

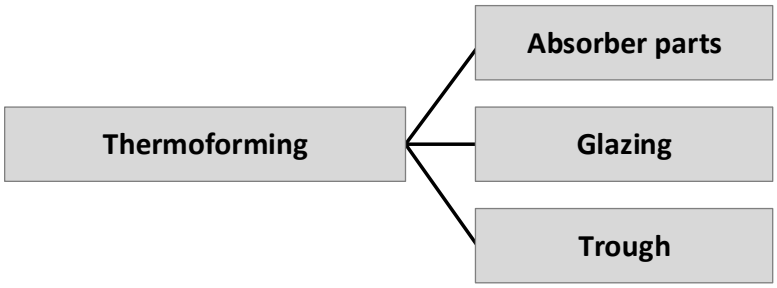

Figure 6.9: Capabilities of components manufactured by thermoforming

An improvement of thermoforming is twin sheet thermoforming. This processing consists of two thermoforming processes in parallel to manufacture hollow components. The thermoforming cycle is similar and has an additional step where the already moulded components are pressed together. The components being still at forming temperature are welded at the contact areas (Figure 6.10).

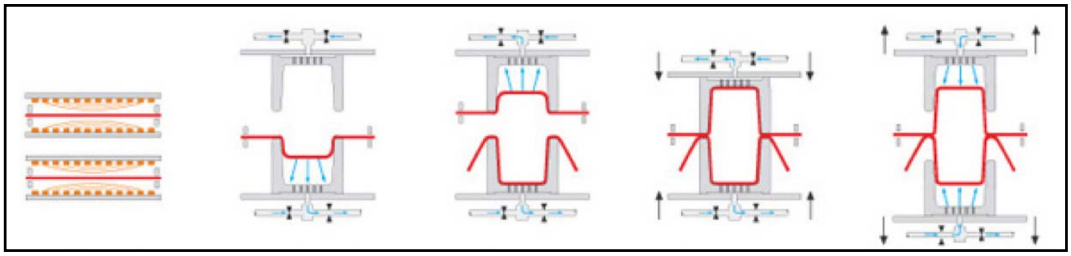

Figure 6.10: Twin sheet thermoforming cycle (DUROtherm Kunststoffverarbeitung GmbH n.d.)

The hollow components being suitable for twin sheet thermoforming are absorbers, double glazing and casings with enclosed air layer (Figure 6.11).

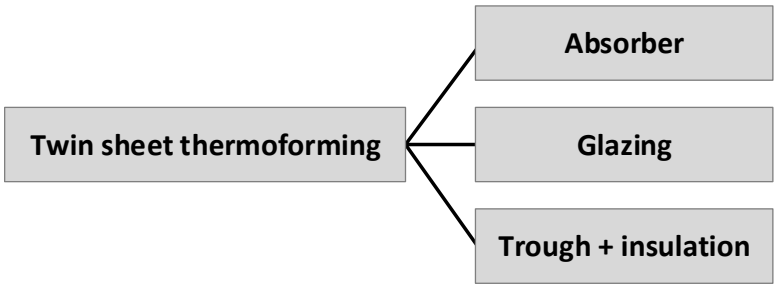

Figure 6.11: Capabilities of components manufactured by twin sheet thermoforming

6.2 Polymeric Collector Designs

On the basis of the described manufacturing processes new design concepts for collectors were derived and compared regarding their costs for a conventional collector size of about 2,000 x 1,000 mm. The chosen materials for the investigation are described in the following.

6.2.1 Non-transparent Materials

The polymeric materials for absorber, casing and insulation of the collector designs embrace the basic types of commodity plastics. Depending on the component, various requirements to the materials have to be fulfilled. The absorber and the areas with direct contact need the highest thermal resistance. Thus, the short-term as well as long-term services temperatures have to be increased. In cases of pressurised absorbers the mechanical properties have to be increased. Especially at high temperatures the stability of the component should be enabled. Therefore, the material should have also a high heat deflection temperature. The resistance of the absorber material against hot fluid mediums (water and glycol) has to be high. Also the absorption of water should be low for the size accuracy of the component. The insulation material has only requirements regarding the temperature loads. Depending on the distance to the absorber, the temperatures can reach the same level. The lowest thermal loads are at the casing. However, the main hurdle for that material is the degradation by means of the ambient conditions. Thus, the UV-resistance is the most important property. In further development stages the material properties (mechanical, thermal or optical) can be additionally improved by additives, fillers and fibres.

PE is a cheap, resistant and light polymer. PE is commonly used for containers like fuel oil tanks or for piping for tap as well as sewerage water. The material is suitable for all mentioned manufacturing techniques (Domininghaus et al. 2012). There is a high resistance against many chemicals and hydrolysis. The low weather resistance, especially against UV radiation, can be increased by UV-

stabilisers or protective agents. Usually 2–3 % carbon black improves this resistance (Biron 2013). The low thermal properties limit the field of application to the casing. The material data of PE is listed in Table 6.1.

Table 6.1: Properties of PE (Domininghaus et al. 2012; Kunststoffinformation n.d.)

PE		
Density	0.95	[gcm^{-3}]
Stress at yield	20–30	[MPa]
Short-term service temperature	90–120	[°C]
Long-term service temperature	70–80	[°C]
Material costs	1.23	[$GBPkg^{-1}$]

PP is the most promising material for collector components. The material properties are similar to PE (Table 6.2). The thermal properties are increased. PP can also be manufactured as foam. PP appears in bumpers, piping, insulations and garden furniture, for example.

Table 6.2: Properties of PP (Domininghaus et al. 2012; Kunststoffinformation n.d.)

PP		
Density	0.91	[gcm^{-3}]
Stress at yield	30	[MPa]
Short-term service temperature	140	[°C]
Long-term service temperature	100	[°C]
Material costs	1.19	[$GBPkg^{-1}$]

For increased mechanical and thermal properties glass fibres show a great potential as reinforcement agent in PP. The so called PP GF30 contains 30 % glass fibres and has especially an improved long-term service temperature (Table 6.3).

Table 6.3: Properties of PP GF30 (Domininghaus et al. 2012; Kunststoffinformation n.d.)

PP GF30		
Density	1.14	[gcm^{-3}]
Stress at yield	>33	[MPa]
Short-term service temperature	155	[°C]
Long-term service temperature	120	[°C]
Material costs	1.71	[$GBPkg^{-1}$]

6.2.2 Glazing

The most suitable transparent materials for polymeric covers are PMMA and PC. They are already used for windows in cars and planes, for green houses as well as for sunbeds.

PMMA has a high light transmittance as well as a high resistance against weathering (Table 6.4). Furthermore, the material can be processed by all mentioned techniques.

Table 6.4: Properties of PMMA (Domininghaus et al. 2012; Kunststoffinformation n.d.)

PMMA		
Density	1.18	[gcm^{-3}]
Stress at yield	70	[MPa]
Short-term service temperature	84–108	[°C]
Long-term service temperature	74–98	[°C]
Light transmittance	92	[%]
Material costs	2.54	[$GBPkg^{-1}$]

PC is also a very transparent material and has an increased thermal behaviour (Table 6.5). The sensitive behaviour against UV radiation is improved by suitable anti-UV agents or coatings. Also PC can be used for the relevant manufacturing techniques.

Table 6.5: Properties of PC (Domininghaus et al. 2012; Kunststoffinformation n.d.)

PC		
Density	1.20	[gcm^{-3}]
Stress at yield	>55	[MPa]
Short-term service temperature	150	[°C]
Long-term service temperature	130	[°C]
Light transmittance	91	[%]
Material costs	2.84	[$GBPkg^{-1}$]

Ruesch and Brunold (2008) and Ruesch et al. (2008) showed in a 20 year weathering test for glazing materials the best results for PMMA, PC and solar glass regarding resistance against degradation and dirt.

The collector glazing has to withstand distributed loads from wind and snow. But also the thickness should be minimal to enable low material costs, low weight and high transmittance. Three possible geometries for glazing were considered on the basis of available purchased components. The polymeric sheets are made from PMMA and bases on the data from EVONIK (2011).

The highest transmittance for polymeric covers represents a single glazing. However, this shape has the lowest stability against deflection. For an overview, plate thicknesses of 3 mm and 4 mm were chosen. A corrugated version of a single glazing provide more stability, but has increased costs and weight due to the higher material content. The stiffest and lightest glazing type is a double-walled cover. Because of the additional boundary surfaces, the transmittance is lower. However, the enclosed air layers reduce the thermal losses. The complex structure also increases the costs. Table 6.6 lists the costs and weights of the different PMMA glazing types for a cover with 2 m² area.

Table 6.6: Costs and weight of various PMMA glazing types (EVONIK 2011)

Type	Costs [GBP]	Weight [kg]
PMMA, planar, 3 mm	20.50	7.1
PMMA, planar, 4 mm	27.10	9.5
PMMA, corrugated, 3 mm	23.00	7.6
PMMA, double-walled	26.30	5.7

Apart from polymeric covers a state-of-the-art glazing made of solar glass also shows great properties for polymeric collectors. Transmittance, stability and aging behaviour are advantageous. Jäger and Terschüren (2007) identified unit costs of 158 GBP for a state-of-the-art collector. The share of the glazing is 13 % according to Figure 1.5 (Hochreiter and Trinkl 2008; Treikauskas and Zörner 2005b). Thus, the costs of 20.70 GBP are the lowest of all mentioned glazing types (Table 6.7). By using the stiffness of the cover sheet for the collector stability, the dimensions of the housing can be reduced.

Table 6.7: Costs and weight of a single glazing made of solar glass

Type	Costs [GBP]	Weight [kg]
Solar glass, planar, 3.2 mm	20.70	15.7

According to the better physical properties and the lower costs a state-of-the-art glazing is the most interesting option for the following investigation of polymeric collector concepts.

6.2.3 Cost Basis for Evaluation

The first economic comparison of the collector approaches is carried out according to the unit costs consisting of the costs for manufacturing and material. Table 6.8 lists the boundary conditions for the manufacturing costs of the collector designs in the concept stage. The production line is configured to an optimum annual capacity utilisation of the processing machine.

Table 6.8: Boundary conditions for the calculation of the manufacturing costs

Cost category	Parameter		
Production data			
	Days of production	250	[da^{-1}]
	Number of shifts	3	[-]
	Hours per shift	8	[h]
	Capacity utilisation	92	[%]
	→ Production hours per year	5,520	[ha^{-1}]
Financing data			
	Imputed interest per year	7	[%]
	Amortisation period	5	[a]
Staff data			
	Labour costs	20.00	[$GBPh^{-1}$]
	Non-wage labour costs	70	[%]

6.2.4 Absorber Concepts

The disadvantageous low heat conductivity of polymers has to be compensated by the absorber design to gain a collector efficiency factor F' being comparable metallic sheet-pipe absorbers. The main factor of F', which can be influenced, is the heat transfer via conduction $\dot{Q}_{cond}$ within the component shown in equation (6.1) and (6.2). The parameters being independent from the material are the distance s and the area A.

$$\dot{Q}_{cond} = h_{cond} A (T_1 - T_2) \tag{6.1}$$

$$h_{cond} = \frac{k}{s} \tag{6.2}$$

Figure 6.12 shows the geometries of a sheet-pipe and the volumetric absorber as well as the heat conduction within the component. The distance s for heat conduction of the sheet-pipe absorber represents the average value.

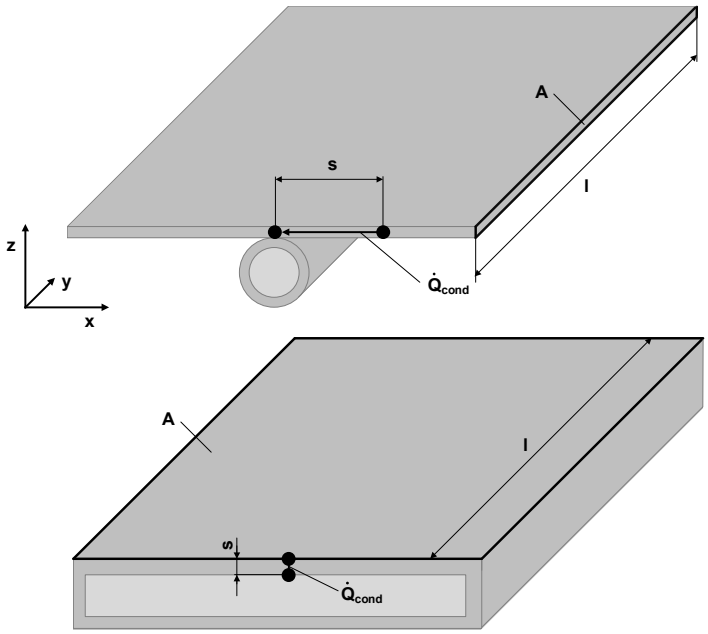

Figure 6.12: Heat conduction in a sheet-pipe (above) and a volumetric absorber (below)

The extreme low heat conductivity of the material is balanced by a short distance and a large area in the polymeric absorber design. Table 6.9 describes the differences in heat conduction between the two absorbers in an exemplary calculation depending on the pipe length l. As a result, the volumetric absorber shows a 3.8 times increased heat transfer from the light absorbing surface to the inner surface of the fluid channel.

Table 6.9: Comparison of the heat conduction in a metallic sheet-pipe and a polymeric volumetric absorber

Absorber type	k [Wm^{-1}K^{-1}]	$\frac{1}{s}$ [m^{-1}]	$\frac{A}{l}$ [m²m^{-1}]	$\frac{k}{s}\frac{A}{l}$ [WK^{-1}m^{-1}]
Sheet-pipe (Copper)	360	0.025^{-1}	0.0002	2.9
Volumetric (PP)	0.22	0.002^{-1}	0.1	11
Factor of difference [-] $\left(\frac{\text{volumetric}}{\text{sheet}-\text{pipe}}\right)$	0.0006	12.5	500	3.8

A second aspect of this design is the increased area for convective heat transfer between absorber and fluid. Thus, both design aspects leads to a comparable or improved collector efficiency factor F'.

The necessary channel design to gain a homogenous flow behind the absorber surface was investigated by Treikauskas (2009) especially for metal-based absorbers. Beside the harp and the serpentine design there are also complex channel structures. Reiter et al. (2013) identified a volumetric absorber design for polymeric collectors with parallel channels which shows a homogenous fluid flow and a low pressure drop. However, the structure and the channel dimensions have a secondary influence on the estimation of the unit costs.

The twin sheet thermoforming process enables the production of the absorber with all relevant details for fluid channels and pipe connections. The whole absorber requires only a production step as well as a post-processing by milling. Figure 6.13 shows an exemplary absorber design for twin sheet thermoforming. A plane surface or rather an asymmetric design enables improved results for the application of a selective paint.

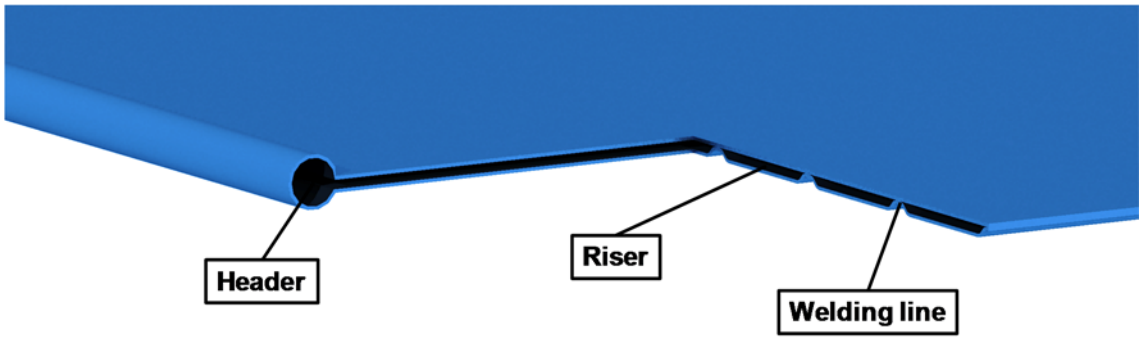

Figure 6.13: Sectional view of a twin sheet thermoformed absorber

The 2 mm thick PP sheets for the absorber are considered as purchased components for 7.00 GBP. The costs for the purchased components base on the costs for PMMA sheets being adjusted according to the specific material price. The output of the production line (thermoforming and milling) is 80,000 units per year and has a total investment of 560,000 GPB. This leads to manufacturing costs of 4.60 GBP according to the boundary conditions. The unit costs for such an absorber is estimated to 18.60 GPB (Table 6.10). Using sheets with 1 mm, the unit

costs would be lowered to 9.70 GBP. However, the inherent rigidity is quite low and there would be no resistance against fluid pressure.

Table 6.10: Unit costs of a twin sheet thermoformed absorber

Type of costs	**Costs [GBP]**	
	1 mm	**2 mm**
Material (purchased components)	7.00	14.00
Manufacturing	2.70	4.60
Sum	9.70	18.60

A cost-efficient alternative to this design is an absorber made of film material. Therefore, two films or a film hose are welded according to the design of the absorber structure. Such an absorber involves an extremely low material effort and low manufacturing costs. Thus, expensive resistant materials can be chosen without increasing the unit costs considerably. However, the component has to be fixed in the housing because of the missing inherent rigidity. Also the flexing material in a drain-back system or the pressure in a closed system represent a hurdle for the approach for a life time of more than 15 years.

Another design version is a twin-wall sheet with enhanced headers. Therefore, an extruded sheet has to be combined with injection moulded headers by adhesive bonding or welding. Figure 6.14 shows an example in serpentine design.

The unit costs for the components (twin-wall sheet and headers) made of PP with 1 mm wall thickness are estimated to 20.30 GBP in case for using the twin-wall sheet as purchased component. The following process for combining the single components causes a slight increase of the unit costs. The in-house production of the twin-wall sheet can reduce the unit costs considerably.

By means of the total investment, the number of production steps, the component properties and the unit costs poses the thermoformed absorber the best design concept for the following evaluation.

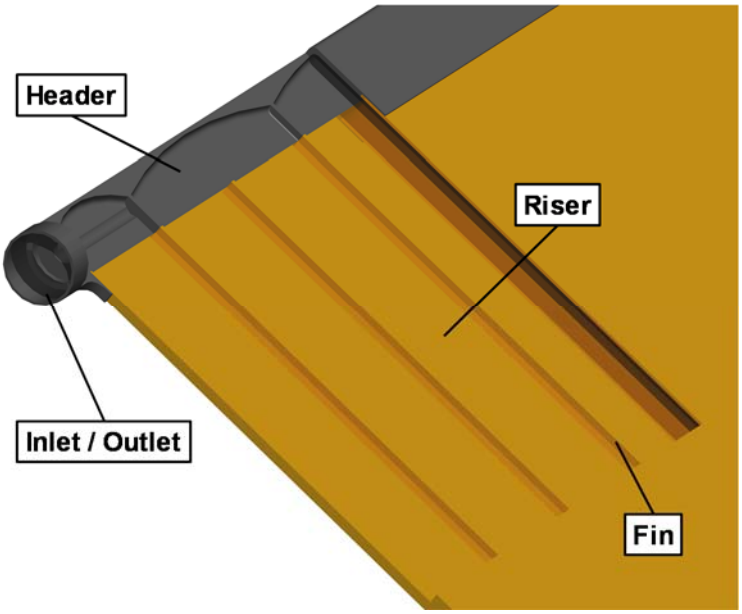

Figure 6.14: Sectional view of an extruded absorber with serpentine structure

6.2.5 Casing Concept

The simplest concept for a casing is the analogue of a state-of-the-art aluminium casing (Figure 6.15). Using the stiffness and stability of the solar glass, the casing can be thin dimensioned. Moulding a rib structure increases the stiffness of the casing. Recesses in the component enable easy handling for installation. The cover can be fixed at the housing by clipping or adhesive bonding.

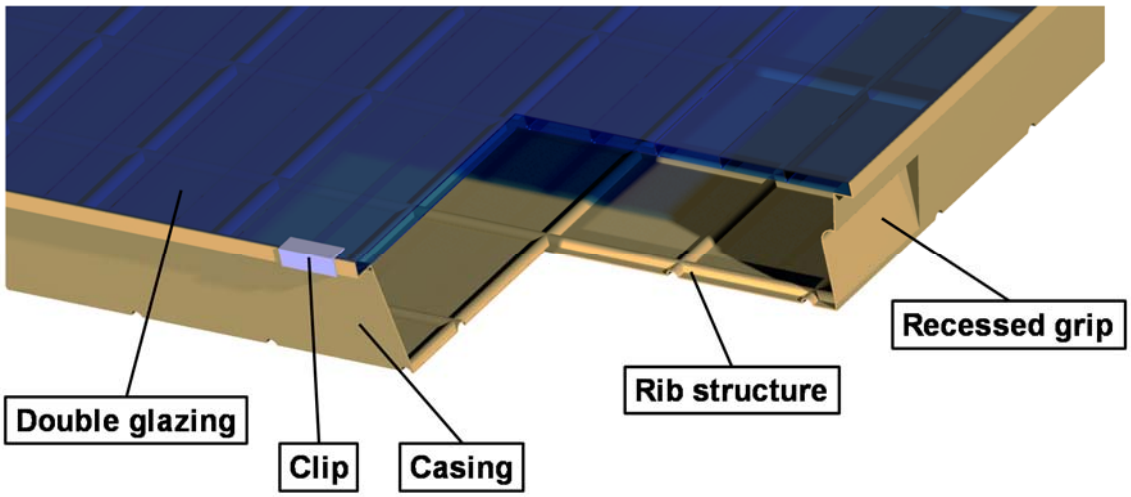

Figure 6.15: Sectional view of a polymeric collector casing with exemplary clipped double glazing

For production, thermoforming as well as injection moulding is suitable. Due to the low thermal loads at the housing, PE as well as PP can be chosen. The actual

market situation favours the cheaper PP. The casing dimensions for the determination of the costs are 2,000 x 1,000 x 80 mm. A low thickness of the plate may cause defective wall thicknesses at the shaped region. Therefore, plate thicknesses of 2 mm and 3 mm were chosen.

The thermoformed component reaches unit costs of 9.50 GBP or rather 13.80 GBP and an output of 160,000 / 107,000 units per year (Table 6.11). The low manufacturing costs are caused by short cycle times and moderate investment costs of 480,000 GBP.

Table 6.11: Unit costs of a thermoformed casing

Type of costs	**Costs [GBP]**	
	2 mm	**3 mm**
Material	7.00	10.50
Manufacturing	2.50	3.30
Sum	9.50	13.80

The injection moulded component has an output of 210,000 / 160,000 units per year and reaches unit costs between 6.50 GBP and 10.70 GBP (Table 6.12). The large dimensions of the casing requires a machine with high closing force. Thus, the investment costs of about 1.35 million GBP are quite higher than for a thermoforming machine and increase the manufacturing costs. The costs are not scalable to the casing thickness because of constant sprue and non-linear cycle times.

Table 6.12: Unit costs of an injection moulded casing

Type of costs	**Costs [GBP]**	
	1 mm	**2 mm**
Material	3.30	6.50
Manufacturing	3.20	4.20
Sum	6.50	10.70

Finally, the costs of the casing vary between 6.50 and 13.80 GBP depending on the requirements regarding investment costs and stability.

The housing is suitable for any kind of insulation like mineral wool or polymer foam. The substitution of a fraction of the insulation by an air layer reduces the material effort whereas the thermal performance remains on a similar level (Figure 6.16).

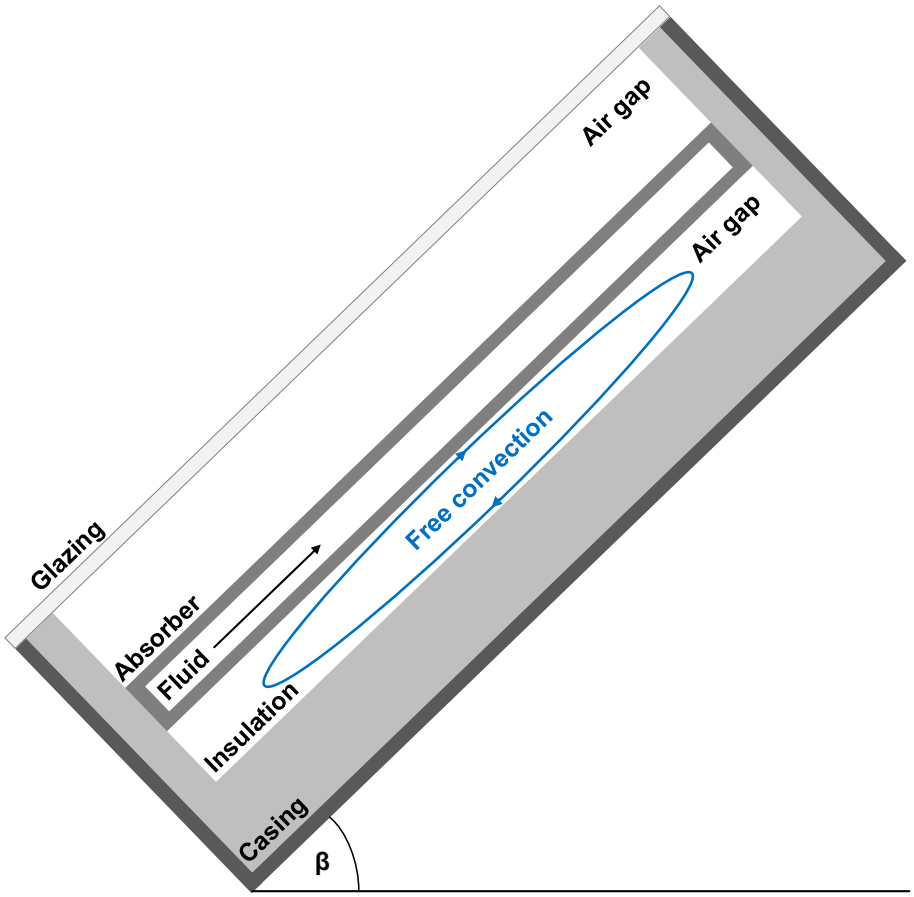

Figure 6.16: Cross section of the collector with casing and insulation

6.2.6 Double-Walled Casing Concept

The concept of a double-walled casing focuses on the advantage of combining casing and insulation in a single component (Figure 6.17). Therefore, the insulation is replaced by an air layer. This leads to low component and assembly costs. Furthermore, the collector is insensitive to moisture. Formed ribs increase the stiffness of the casing.

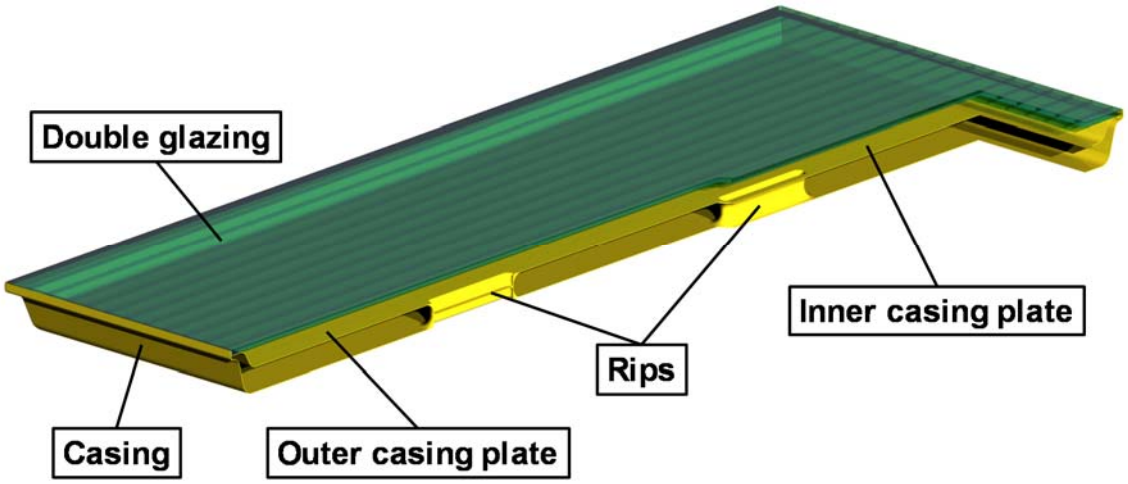

Figure 6.17: Sectional view of a double-walled casing with exemplary fixed double glazing

The position of the absorber has to be distanced to the inner sheet of the casing to create a second air layer. The inner sheet functions as a barrier to reduce the convection (Figure 6.18).

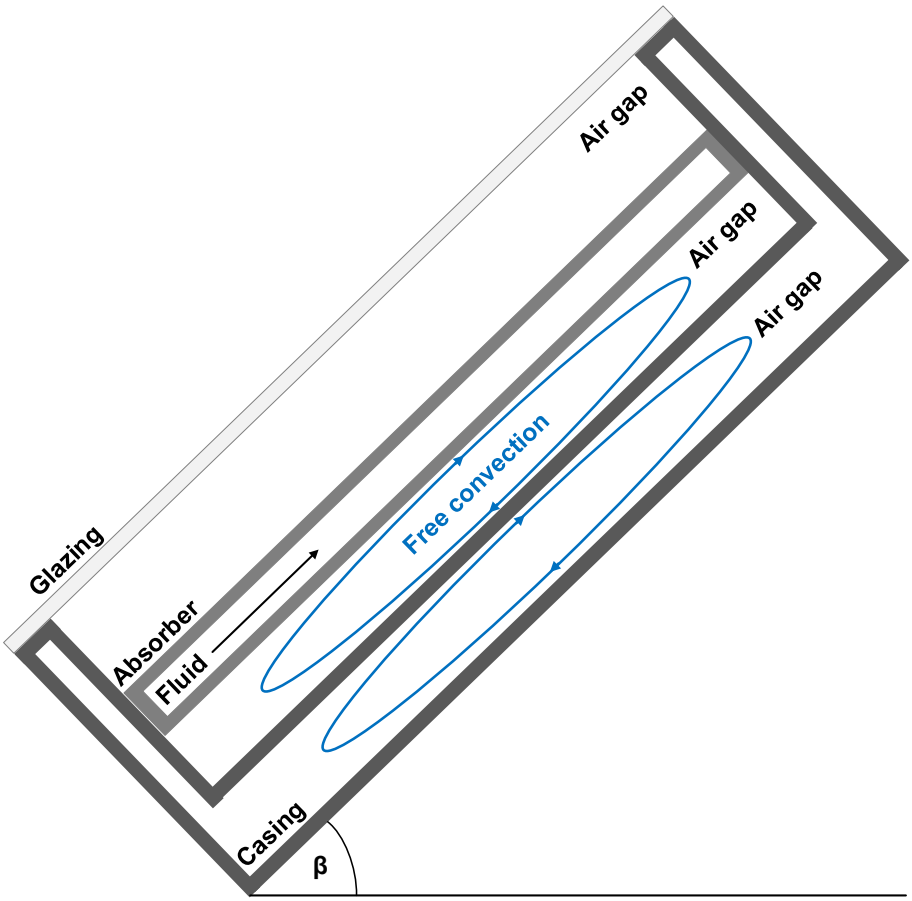

Figure 6.18: Cross section of the collector with double-walled casing

The design is suitable for twin sheet thermoforming as well as for blow moulding. The dimensions are similar to the simple casing concept.

Twin sheet thermoforming offers the option for combining two different sheets. Therefore, the casing can consist of a cost-effective shell material and heat resistant sheet near the absorber. Also the inner sheet can be configured with lower plate thickness due to the reduced requirements for stability. The calculation is similar to the absorber concept. Due to the different sheet thicknesses and cycle times result unit costs of 18.60 GBP and an output of 80,000 units per year for a component with 2 mm wall thickness (Table 6.13). The version with a 2 mm interlayer and a 3 mm shell causes unit costs of 23.20 GPB and has an output of 64,000 units per year.

Table 6.13: Unit costs of a thermoformed double-walled casing

Type of costs	**Costs [GBP]**	
	2 / 2 mm	**2 / 3 mm**
Material	14.10	17.60
Manufacturing	4.50	5.60
Sum	18.60	23.20

Depending on the wall thickness, the blow moulded casing has unit costs of 17.80 GBP or rather 24.60 GBP and an output of 105,000 / 90,000 units per year. Especially the high investment costs of 1.35 million GBP causes the increased manufacturing costs.

Table 6.14: Unit costs of a blow moulded double-walled casing

Type of costs	**Costs [GBP]**	
	2 mm	**3 mm**
Material	11.80	17.60
Manufacturing	6.00	7.00
Sum	17.80	24.60

The unit costs of the double-walled casing differ between 17.80 GBP and 24.60 GBP whereas the thermoformed casing (2 / 3 mm) the best balance between economic and technical advantages represents.

6.2.7 Evaluation of the Unit Costs for the Collector

The first economic evaluation of the polymeric collector concepts was conducted by comparing the unit costs against state-of-the-art collectors. The unit costs of 158 GBP for a state-of-the-art collector with aluminium casing from Jäger and Terschüren (2007) are the reference value for the evaluation. These costs were referenced to the single items according to the breakdown of the unit costs of flat-plate collectors from Figure 1.5 (Hochreiter and Trinkl 2008; Treikauskas and Zörner 2005b).

Table 6.15: Typical breakdown of the unit costs of the reference collector

Component	Share [%]	Costs [GBP]
Absorber	46	72.70
Housing	20	31.60
Glazing	13	20.50
Miscellaneous	12	19.00
Insulation	9	14.20
Sum	100	158

The costs for assembling, sealing and adhesive were summed up to 19.00 GBP (12 %) as miscellaneous. The mineral wool insulation (~50 mm) is estimated to 14.20 GBP (9 %). The purchased component appears also in the casing concept. Therefore, two chases were chosen for comparison. A 10 mm insulation in combination with a 20 mm air layer and a single 30 mm insulation were taken into account. The proportional costs are 2.80 GBP and 8.50 GPB.

Table 6.16 lists the compositions of the collector concepts for the evaluation of the unit costs. Therefore, the cost-effective and the expensive components were combined to illustrate the range of the concept costs.

Table 6.16: Composition of collector concepts for the evaluation

Concept	Absorber	Glazing	Housing
Casing concepts:			
	Twin sheet, 1 mm	Solar glass	Injection moulded, 1 mm + mineral wool
	Twin sheet, 2 mm	Solar glass	Thermoformed, 3 mm + mineral wool
Double-walled casing concepts:			
	Twin sheet, 1 mm	Solar glass	Blow moulded, 2 mm
	Twin sheet, 2 mm	Solar glass	Blow moulded, 3 mm

The comparison of the concepts in Figure 6.19 illustrates a possible cost benefit of more than 50 %.

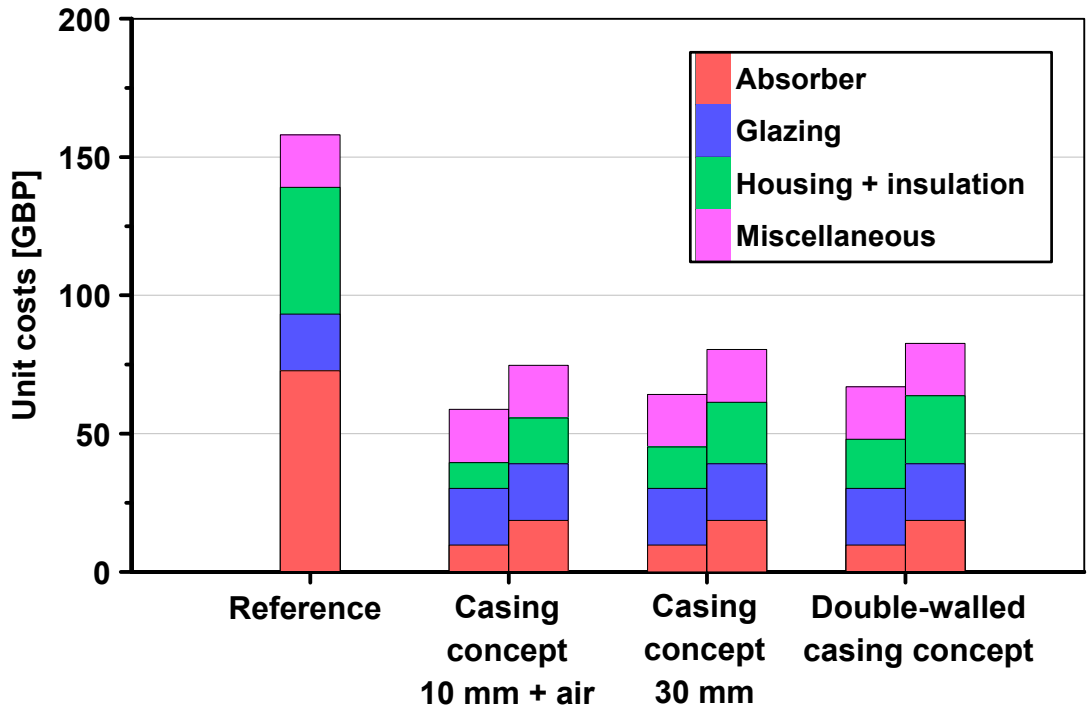

Figure 6.19: Comparison of the unit costs of the polymeric collector concepts

The concepts are designed to low weight and costs which leads to a low stability. Depending on the requirements, the concepts represent the lowest possible dimensioning. The missing selective coating reduces the costs as well as the efficiency. Thus, the influence of the concepts on the system yield has to be investigated. Furthermore, the limited thermal properties of the cost-effective material has to be analysed.

Table 6.17 lists the unit costs of the collector components and shows the decrease according to the reference collector.

Table 6.17: Composition and decrease of the unit costs of the collector concepts

Concept	Absorber [GBP]	Glazing [GBP]	Housing + insulation [GBP]	Miscellaneous [GBP]	Decrease of unit costs [%]
Reference	72.70	20.50	45.80	19.00	--
Casing concepts 10 mm + air:					
Low costs	9.70	20.50	9.30	19.00	-63.0
High costs	18.60	20.50	16.60	19.00	-52.5
Casing concepts 30 mm:					
Low costs	9.70	20.50	15.00	19.00	-59.5
High costs	18.60	20.50	22.30	19.00	-49.0
Double-walled casing concepts:					
Low costs	9.70	20.50	17.80	19.00	-57.5
High costs	18.60	20.50	24.60	19.00	-47.5

Annotation: The costs of the item “miscellaneous” is set to a constant value. However, the included assembly costs should be lower for the double-walled casing concept because of the missing production step of inlaying the insulation.

6.3 Thermal Analysis

The reduced thermal efficiency of the design concepts and the influence on the system level has to be analysed via simulation in order to evaluate the benefit from solar-thermal systems with cost-effective collectors. Therefore, the validated collector model was used for the prediction of the collector and system behaviour. Additionally, a test stand for stagnation according to DIN EN 12975-2 (2006) was built to identify the maximum temperatures under standardised conditions (Table 6.18). This simulation set-up provides a second reference of maximum thermal loads under defined conditions being comparable to collector measurements.

Table 6.18: Test conditions for stagnation according to DIN EN 12975-2 (2006)

Parameter		
G	1,000	[Wm^{-2}]
T_{amb}	30	[°C]
u_{wind}	1	[ms^{-1}]
β	45	[°]

The dataset of the weather is provided by source blocks of *Simulink* with constant values. Figure 6.20 shows the subsystem of the weather block in *Simulink* for the stagnation test.

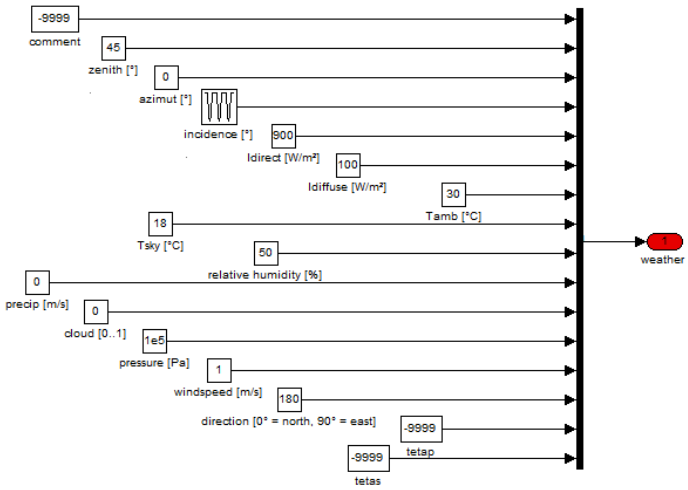

Figure 6.20: Build-up of the subsystem of the weather block for the stagnation test in *Simulink*

6.3.1 Adjustment of the Reference Results

The collector being used for measurement and simulation showed up an extraordinary collector efficiency curve. Thus, a moderate efficiency curve of a flat-plate collector was chosen in the annual system simulation for not overestimating the difference between state-of-the-art and polymeric collectors. Table 6.19 lists the differences between the two reference collectors. The collector area is equal in all cases.

Table 6.19: Reference results from simulation of two different state-of-the-art flat-plate collectors

Model type	Collector curve parameters			f_{sav}	Relative decrease
	[-]	[$Wm^{-2}K^{-1}$]	[$Wm^{-2}K^{-2}$]	[%]	[%]
Previous reference:					
Dynamic	$\eta_0 = \sim 0.798$	$a = \sim 3.34$	$b = \sim 0.0075$	20.0	--
Curve-based	$\eta_0 = 0.798$	$a = 3.34$	$b = 0.0075$	19.4	-3.0
New reference:					
Curve-based	$\eta_0 = 0.771$	$a = 3.68$	$b = 0.0127$	17.9	-10.5

The pressure loads were neglected in the system simulations for being able to compare two identical systems without any changes beside the collectors.

6.3.2 Adjustment of the Collector Model

The validated model of the state-of-the-art collector from Chapter 4.1 has to be adjusted to the design concepts of polymer collectors. The most parameters in the new model which have to be changed, are material data and component distances. However, due to the new absorber design, the collector model has to be changed. Figure 6.21 shows the basis of a polymeric collector model.

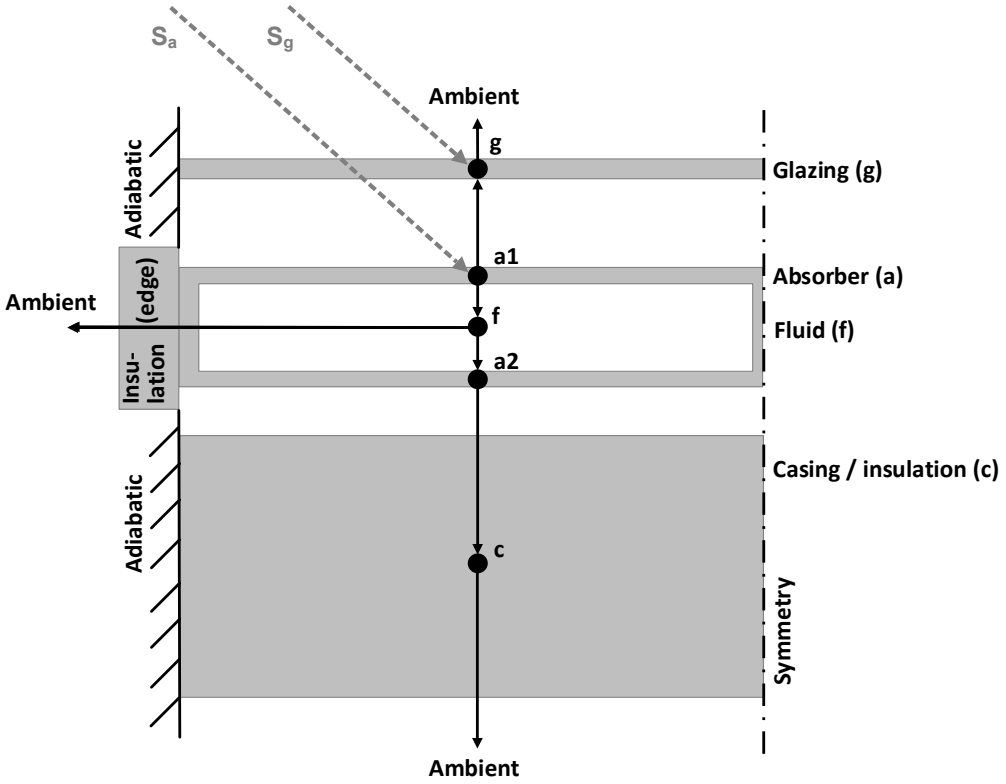

Figure 6.21: Cross section of the polymeric collector model with nodes and energy fluxes

The equations (6.3) to (6.7) give an overview on the energy balance drawn in the collector model describing the capacities of each node as well as the energy fluxes between the nodes.

Glazing (g):
$$m_g c_g \frac{dT_g}{dt} = S_g + \dot{Q}_{a1-g} - \dot{Q}_{g-amb} \tag{6.3}$$

Absorber 1 (a1):
$$m_{a1} c_{a1} \frac{dT_{a1}}{dt} = S_{a1} - \dot{Q}_{a1-f} - \dot{Q}_{a1-g} - \dot{Q}_{a1-edge} \tag{6.4}$$

Fluid (f):
$$m_f c_f \frac{dT_f}{dt} = \dot{m}_f c_f * \left(T_{in} - T_f\right) + \dot{Q}_{a1-f} - \dot{Q}_{f-a2} \tag{6.5}$$

Absorber 2 (a2):
$$m_{a2} c_{a2} \frac{dT_{a2}}{dt} = \dot{Q}_{f-a2} - \dot{Q}_{a2-c} \tag{6.6}$$

Casing (c):
$$m_c c_c \frac{dT_c}{dt} = \dot{Q}_{a2-c} - \dot{Q}_{c-amb} \tag{6.7}$$

The heat transfer of the forced convection in the absorber channels was calculated according to the approach from Chapter 0 for forced convection in ducts. The new geometry of the absorber channels consisting of two parallel plates requires an adjustment of the equation. Therefore, the doubled gap height instead of the commonly used pipe diameter represents the characteristic length L and the transition from laminar to turbulent flow begins at a Reynolds number of 2,800 instead of 2,300 (Mills 1999, Stephan 2010). The hydrodynamically developed laminar flow for Reynolds numbers below 2,800 is set to the constant Nusselt number 5.385 (Mills 1999). The approach for the Nusselt number was used for convective heat transfer coefficients between absorber front (a1) and fluid as well as between fluid and absorber back (a2). The fins between the absorber sheets were neglected because of their low influence.

6.3.3 Casing Concept

The casing concept with 10 mm mineral wool insulation and air enclosure has a decrease of the fractional energy savings of 24.5 % in comparison to the reference system. The concept with 30 mm insulation shows a relative decrease of only 18.5 % (Table 6.20).

Table 6.20: Fractional energy savings and efficiency decrease of the reference system as well as of the systems with polymeric collectors in annual simulations

System	f_{sav} [%]	Relative decrease [%]
Reference system	17.9	--
System with polymeric collectors (10 mm + air)	13.5	-24.5
System with polymeric collectors (30 mm)	14.6	-18.5

The collector concept with 10 mm insulation and air layer reaches a maximum absorber temperature of 117°C in the annual system simulation. The dry collector in stagnation has its climax at 126°C.

Figure 6.22 shows the occurrences of thermal loads on the absorber depending on duration and temperature level over one year. The data is prepared to display

the duration when a temperature level is exceeded and the number of occurrences of this effect. Due to the strong dependency on the sun, the increase of the absorber temperature is similar to the gradient of the solar irradiance (cf. Chapter 2.2.1). The gradient of the peaks in the diagram (yellow dashed line) from more than 360 minutes above 60°C to states with short durations at maximum temperatures illustrates the thermal behaviour of the collector on clear days. The thermal absorber loads within the pattern at moderate temperatures and shorter durations occur on cloudy days in the summer period as well as on clear days in winter.

Analysing the data with regard to the material properties of the absorber material, the collector behaviour can be classified as non-critical. The most loads do not exceed 100°C, the long-term service temperature of PP. Only a few situations appear in the short-term service temperature array (up to 2 h and 140°C).

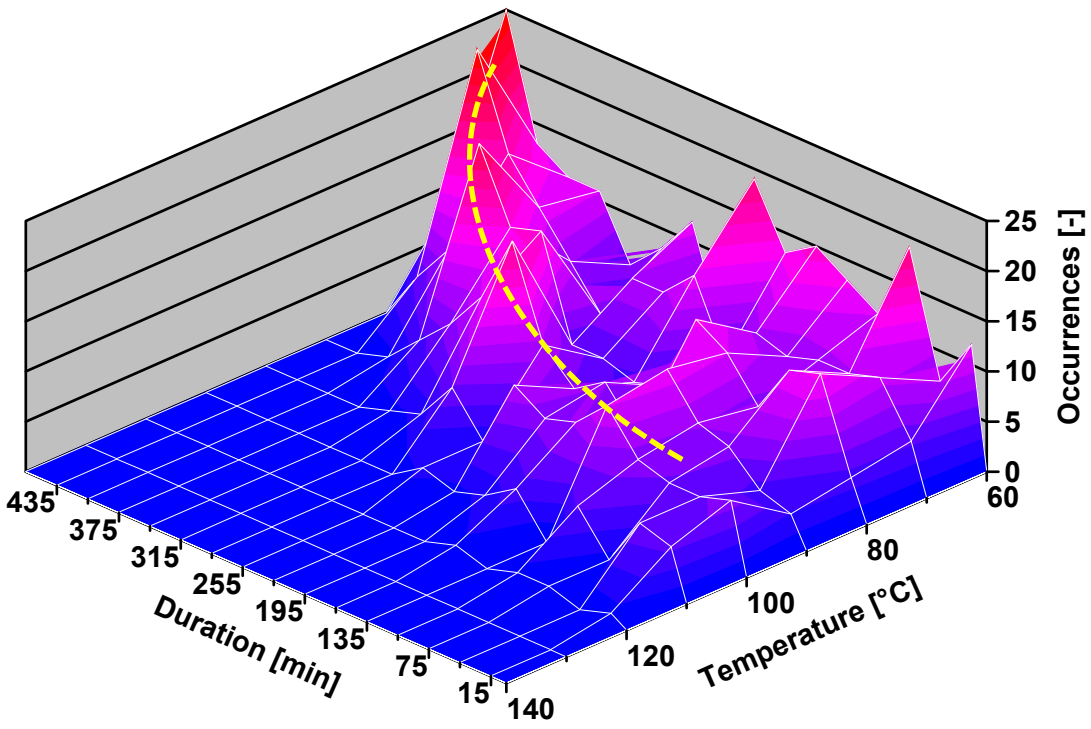

Figure 6.22: Occurrences of thermal loads depending on duration and temperature level on a polymeric absorber with 10 mm mineral wool insulation and air enclosure during stagnation over one year

The concept with 30 mm mineral wool reaches maximum values of 130°C in operation and 133°C in permanent stagnation. The thermal loads on the absorber are slightly increased in the second concept (Figure 6.23). Thus, there is a more distinctive pattern at higher temperature levels. However, the thermal loads do not considerably exceed the recommended boundaries of PP.

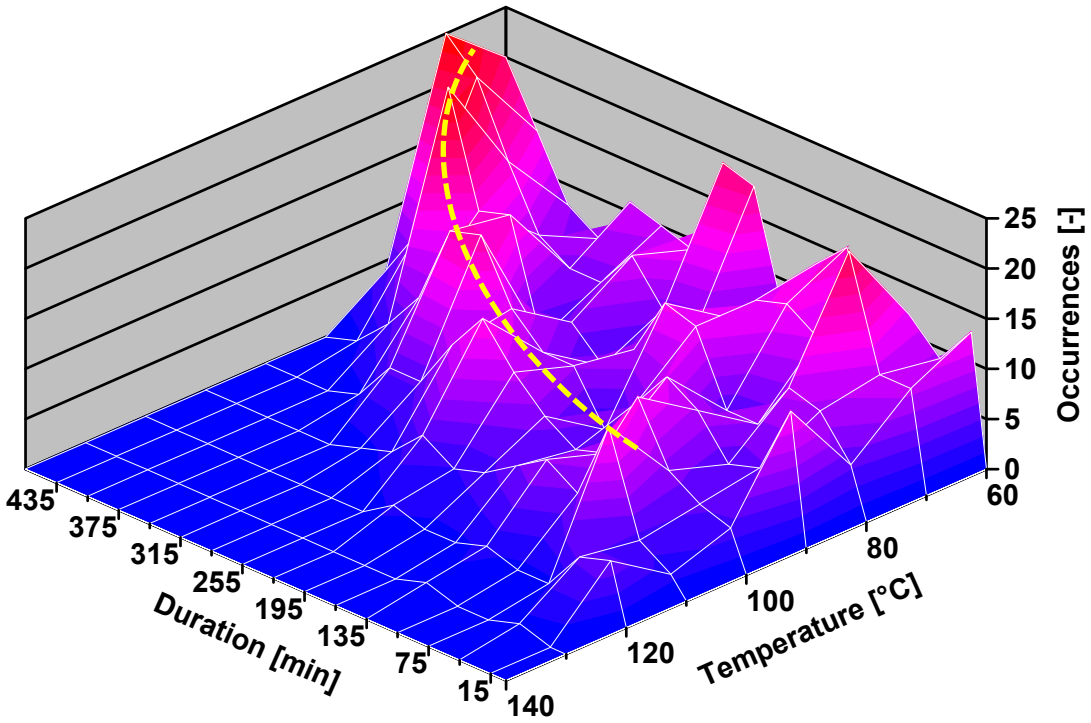

Figure 6.23: Occurrences of thermal loads depending on duration and temperature level on a polymeric absorber with 30 mm mineral wool insulation during stagnation over one year

In the additional stagnation test according to DIN EN 12975-2 (2006) remain the simulation results also within the boundaries of the proposed material (Table 6.21).

Table 6.21: Stagnation temperatures according to DIN EN 12975-2 (2006) of the polymeric collector concepts with mineral wool insulation

Stagnation temperatures [°C]	Absorber	Glazing	Insulation (inside)	Casing (outside)
Casing concept (10 mm + air)	123	74	91	49
Casing concept (30 mm)	131	78	120	43

6.3.4 Double-Walled Casing Concept

The air gap distances between absorber and inner casing wall as well as between inner and outer casing wall were set to a similar value. Simulations with various air gap parameters between 10 and 30 mm show almost no influence on the thermal performance. The maximum temperatures are identical and the discrepancy in the fractional energy savings is approximately 1 %.

The fractional energy savings in Table 6.22 are quite lower according to the reference system. The decrease of 27.5 % is mainly due to the poor collector efficiency at the necessary temperature levels being required from the system. However, the maximum absorber temperature of 110°C is optimal for the absorber material.

Table 6.22: Fractional energy savings and efficiency decrease of the reference system as well as of the system with polymeric collectors with double-walled casing in annual simulations

System	f_{sav} [%]	Relative decrease [%]
Reference system	17.9	--
System with polymeric collectors	13.0	-27.5

Also the absorber temperatures of the dry collector in stagnation reach a maximum of only 122°C. The thermal loads in Figure 6.24 are moderate and cover with the requirements from the short-term and long term services temperatures of PP. Furthermore, the diagram shows that the collector is also able to reach temperature levels between 60–80°C for quite long durations, however, the peak values of thermal loads are reduced due to the lower collector efficiency. On many clear days, the gradient of the absorber temperature reaches only maximum temperatures below 90°C. Thus, there are many peaks in the range between 60–90°C and 0–210 minutes.

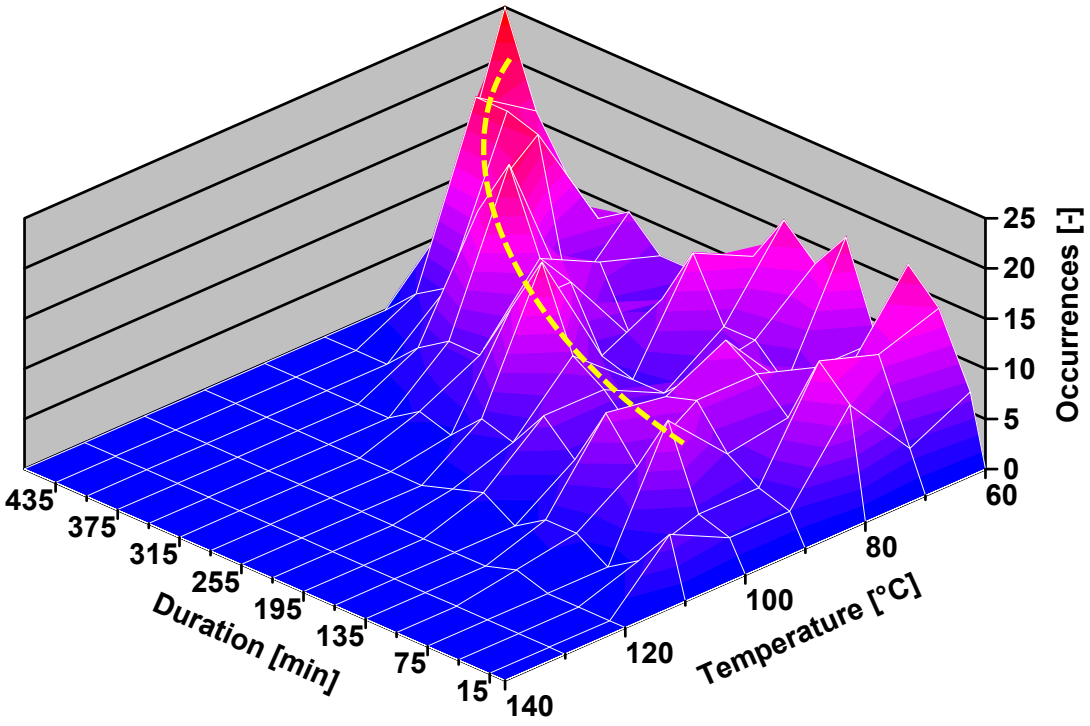

Figure 6.24: Occurrences of thermal loads depending on duration and temperature level on a polymeric absorber with double-walled housing during stagnation over one year

The results of the stagnation test in Table 6.23 also show component temperatures being suitable for PP. Especially the casing temperatures are quite low.

Table 6.23: Stagnation temperatures according to DIN EN 12975-2 (2006) of the polymeric collector concept with double-walled casing

Stagnation temperatures [°C]	Absorber	Glazing	Casing (inside)	Casing (outside)
Double-walled casing concept	119	72	80	52

6.3.5 Optional Efficiency Increase

The emission coefficients of the absorber backside and the casings ($\varepsilon = 0.95$) cause a relatively high heat transfer coefficient for radiation and increase the backside losses. Applying a mirror for infrared radiation can lower the heat transfer coefficient. The simplest way is the implementation of an aluminium film ($\varepsilon = 0.04$) at the surface. Equation (6.8) demonstrates that the reduction of the heat

transfer coefficient is independent from deposition of the film (at hot or cold surface).

$$h_{rad} = \frac{\sigma}{\left(\frac{1}{\varepsilon_1} + \frac{1}{\varepsilon_2} - 1\right)} (T_1^2 + T_2^2)(T_1 + T_2) \tag{6.8}$$

Table 6.24 shows the influence of aluminium films on the heat transfer coefficient for radiation. The decrease of h_{rad} for constant surface temperatures has its optimum with one aluminium sheet when the material effort is also considered.

Table 6.24: Influence of the emission coefficients on the heat transfer coefficient for radiation

Emission coefficients of the surfaces	$\frac{1}{\left(\frac{1}{\varepsilon_1} + \frac{1}{\varepsilon_2} - 1\right)}$	Relative decrease [%]
$\varepsilon_1 = \varepsilon_2 = 0.95$	0.90	--
$\varepsilon_1 = 0.95$ & $\varepsilon_2 = 0.04$	0.04	-95.5
$\varepsilon_1 = \varepsilon_2 = 0.04$	0.02	-97.7

Table 6.25 shows the relative increases of the fractional energy savings as well as the stagnation temperatures for collector concepts equipped with one aluminium film.

Table 6.25: Influence of the aluminium film on the fractional energy savings and the stagnation temperatures of the absorber according to DIN EN 12975-2 (2006)

Concept	Increase of f_{sav} [%]	T_{stag} [°C]
Casing concept	+2.0	135
Double-walled casing concept	+7.0	129

The good insulation properties of the backside insulation in the casing concept cause a small temperature difference between the surfaces and limit the heat transfer via radiation. Thus, the influence of the aluminium film is relatively low in this concept. The aluminium film in the double-walled casing concept shows with a relative increase of 7.0 % an efficient measure to improve the limited thermal

performance. The absorber temperatures during stagnation are in both cases slightly higher but stay below the short-term service temperatures of the material.

6.4 Economic Evaluation of the Systems with Polymeric Collector Approaches

The final economic evaluation of the polymeric collector approaches is based on the total costs for consumers for the investigated solar-thermal system in Germany. Therefore, the average total costs for customers of three systems with a similar configuration like the analysed reference system were considered. The average total costs for customers of the system amount to 13,100 GBP (incl. 19 % VAT). Furthermore, the relative values of the average total costs were separated. According to the breakdown of Figure 6.25, the collectors' share has a percentage of 36 %.

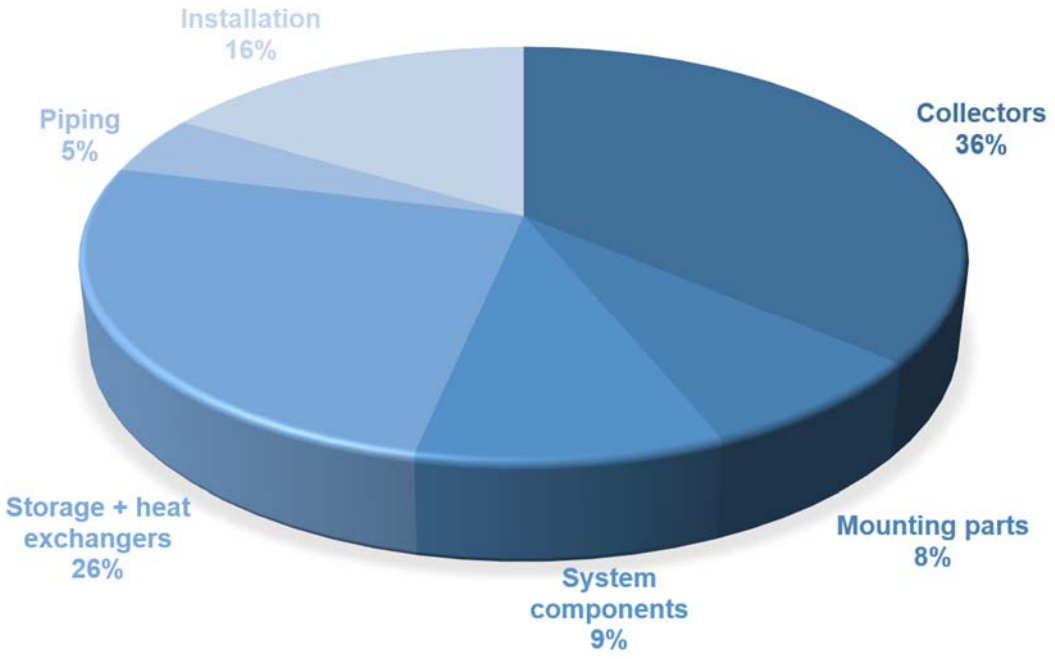

Figure 6.25: Typical breakdown of the total costs for end-users of the reference system

The proposed reduction originating from the polymeric collector approaches has to put in relation to the share of the total system costs. This percentage represents the cost benefit from polymeric collectors according to the total costs for

customers of the complete system. Table 6.26 shows the influence on the system costs.

Table 6.26: Influences of the polymeric collector concepts on the system costs for customers

Influences on the system costs for customers	Decrease of collector costs [%]	Decrease of system costs [%]	System costs [GBP]
Reference:	--	--	13,100
Casing concept 10 mm + air:			
Low costs	-63.0	-22.5	10,150
High costs	-52.5	-19.0	10,600
Casing concept 30 mm:			
Low costs	-59.5	-21.5	10,300
High costs	-49.0	-17.5	10,800
Double-walled casing concept:			
Low costs	-57.5	-20.5	10,400
High costs	-47.5	-17.0	10,850

The savings from the system costs have to balance the decrease of the solar yield to gain an economic advantage with the alternative collector approaches. Therefore, the additional costs for fuel oil over a defined life time of 20 years (Verein Deutscher Ingenieure e.V. 2012) have to be considered. Based on the German price development for fuel oil from 2000 to 2012 carried out by BMWI (n.d.), two scenarios for the price development were taken into account (Figure 6.26). The moderate scenario refers to a linear approximation of the fuel oil price. The extreme scenario refers to a quadratic approximation. The two scenarios lead to an average price increase of about 3.7 % or rather 6.8 % per year in the extrapolated period between 2013 and 2032, which is considered in the economic evaluation.

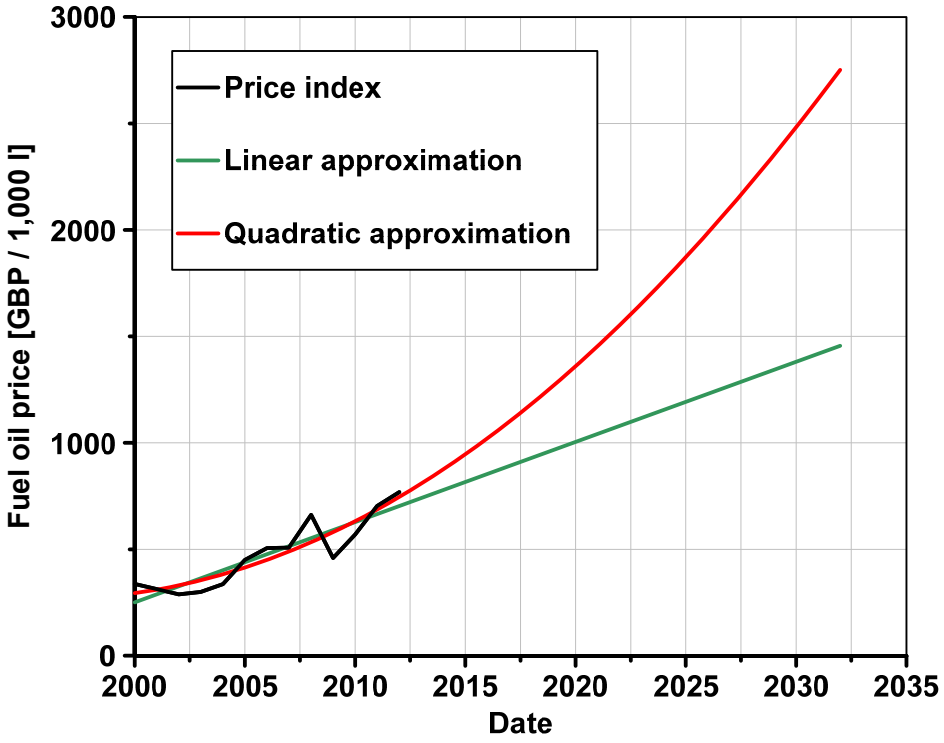

Figure 6.26: Development of the fuel oil price

The annual energy consumption of the heater from the simulations was used as a basis for determining the fuel oil consumption. Table 6.27 represents the fuel oil consumption by means of the heating value of 10.85 kWhl^{-1} (IWO n.d.) as well as the energy costs for 20 years based on the two price development scenarios.

Table 6.27: Energy costs of the reference system over 20 years

Energy costs of the reference system ($f_{sav} = 17.9\,\%$)	Energy consumption [kWh]	Fuel oil consumption [l]	Energy costs [GBP]
1 year	16,510	1,522	--
20 years – Linear price development	412,750	38,050	33,430
20 years – Quadratic price development	412,750	38,050	50,790

Table 6.28 represents the energy costs of the systems with polymeric collector concepts over the period of 20 years by using the annual fuel oil consumption from the simulations.

Table 6.28: Energy costs of the systems with polymeric collector concepts over 20 years

Energy costs over 20 years	Linear price development [GBP]	Quadratic price development [GBP]
Reference:	33,430	50,790
Casing concept 10 mm + air:	35,230	53,530
Casing concept 30 mm:	34,730	52,760
Double-walled casing concept:	35,480	53,900

The total costs for the customer for a solar-based heat supply comprise the sum of the system costs and energy costs. The results were compared to the reference solar-thermal system to show the influence on the total costs for customers by changing the collectors. Table 6.29 lists the cost savings from the systems with polymeric collector concepts in the period from 2013 to 2032 with a linear fuel oil price development. The economic benefit is slightly positive for most approaches in relation to the reference system.

Table 6.29: Influences of the polymeric collector concepts on the total costs for customers with linear fuel price development over 20 years

Influences on the costs for customers	Difference in system costs [GBP]	Difference in energy costs [GBP]	Difference in total costs [GBP]	Economic benefit [%]
Casing concept 10 mm + air:				
Low costs	-2,950	+1,800	-1,150	+2.5
High costs	-2,500	+1,800	-700	+1.5
Casing concept 30 mm:				
Low costs	-2,800	+1,300	-1,500	+3.0
High costs	-2,300	+1,300	-1,000	+2.0
Double-walled casing concept:				
Low costs	-2,700	+2,050	-650	+1.5
High costs	-2,250	+2,050	-200	+0.5

Contrary to that, Table 6.30 shows the results with a quadratic fuel oil price development. The increasing energy costs lead to slightly negative economic benefits.

Table 6.30: Influences of the polymeric collector concepts on the total costs for customers with quadratic fuel price development over 20 years

Influences on the costs for customers	Difference in system costs [GBP]	Difference in energy costs [GBP]	Difference in total costs [GBP]	Economic benefit [%]
Casing concept 10 mm + air:				
Low costs	-2,950	+2,740	-210	+0.5
High costs	-2,500	+2,740	+240	-0.5
Casing concept 30 mm:				
Low costs	-2,800	+1,970	-830	+1.5
High costs	-2,300	+1,970	-330	+0.5
Double-walled casing concept:				
Low costs	-2,700	+3,110	+410	-0.5
High costs	-2,250	+3,110	+860	-1.5

The economic impact from the polymeric collector concepts with reference to the total costs for customers is very limited or even disadvantageous. Hence, the substitution of state-of-the-art collectors can hardly reach an economic benefit in the investigated system set-up.

Annotation:
This evaluation is based on the assumption that costs for the system — except for the collectors — remain stable. However, there are slight differences in fluid content, glycol degradation and operational costs. The maintenance costs were also assumed to be similar. Furthermore, subsidies and financing were neglected for this comparison.

All costs of the calculations are referenced to German prices in € and were converted to GBP with the exchange rate of 0.82 GBP€$^{-1}$ (Bankenverband n.d.).

7 Conclusions and Outlook

This research covers the development and the analysis of collector concepts made of polymers with regard to a cost reduction of solar-thermal systems for domestic hot water preparation and space heating. The main focus was on the analysis and the reduction of the mostly unknown and high thermal loads on the collector components which represent the major hurdle for the implementation of polymers against the background of low material costs. Apart from that, the adaption of the collector component design to the boundaries of relevant plastics processing techniques for an efficient production and low unit costs was necessary research work. The subsequent simulation analysis was used to check the thermal loads on the components and, hence, on the chosen polymeric materials. Furthermore, the function of the collector concepts within the solar-thermal system was demonstrated via simulation. The final evaluation was based on the comparison between the possible decrease of the system costs caused by the polymeric collector concepts and the influence on the annual solar yield of the system. The outcomes are summarised below.

7.1 Thermal Collector Loads

The high thermal loads on the components in collectors were identified by field testing. State-of-the-art flat-plate collectors showed very high absorber temperatures in the period between spring and autumn. Furthermore, the occurrences or rather the durations at temperature levels which are critical for cost-effective commodity plastics are relatively high. In contrast to these loads, the temperatures at glazing, frame and backside are suitable for alternative material selections. Thus, conventional collectors only show critical temperatures for polymeric materials at the absorber and at sections with direct contact to the absorber. The increased thermal loads cause an accelerated degradation of the polymers as well as a decrease of the stability of the component.

The high thermal loads identified in state-of-the-art collectors have to be reduced by measures or approaches to enable the implementation of commodity plastics. Therefore, viable concepts are to control or reduce temperatures by changing the optical efficiency or by removing the thermal energy.

The relevant aspects from the technical point of view for the evaluation of the identified concepts are reachable temperature reduction, life time and intrinsic safety of the collector. Especially, the active measures with triggered protection — like devices for the reduction of the transmission, ventilation and heat dissipation — show a high temperature reduction. However, these approaches have a limited life time or no intrinsic safety. Furthermore, the economic point of view with regard to solar yield, additional unit costs and additional operational costs is a main problem of most measures that are able to cause a high temperature reduction. Finally, early development stages and problems with the application on polymeric substrates can be named as further drawbacks of the concepts identified.

The most promising concepts for temperature reduction are the active measures that change the optical efficiency or the radiation losses. The thermotropic and thermochromic layers are temperature controlled and independent from secondary influences. However, current thermotropic layers show a transparency too low in the clear state for being used efficiently in the collector. The thermochromic absorber layer with a switchable emission coefficient is the most appropriate measure to enable high collector efficiencies. The small switching range, however, is a major drawback for an overheating protection of proposed polymeric materials.

The micro-structured layer controlling the solar irradiance at the absorber by means of the incidence angle is the most suitable passive approach. The layer proves to have less influence on the solar yield and has a relative simple and cost-effective set-up. However, the dependency on the incidence angle is problematic for a flexible application. In spite of using the measure in a correct way, extreme temperatures may occur.

The combination of the thermochromic or the micro-structured layer with temperature controlled service water cooling reaches a similar solar yield and an optimal temperature reduction. However, due to its considerable water consumption, this measure is not viable from an economic as well as ecological point of view.

Finally, the reduction of the collector efficiency by means of an accompanied cost reduction represents the best balance between temperature reduction, solar yield and unit costs. Saving the extra costs of a selective absorber layer by using a black absorber material is the most relevant adjustment in collector design for overheating protected polymer collectors. An additional decrease of the backside insulation enables the best results for the alternative collector concepts.

7.2 Polymeric Collectors

The considered standard manufacturing techniques for polymeric materials prove interesting options for new absorber as well as casing designs. Therefore, the focus of the analysis was on a simple casing design similar to the state-of-the-art housing as well as on a double-walled casing design. The most promising material for absorber and casing is PP, a material which greatly fulfils the requirements of temperature resistance, ageing stability and costs. Furthermore, the material can be processed by all relevant manufacturing techniques. Apart from that, polymeric covers only benefit from lower component weight in comparison to state-of-the-art glazing. The material costs and the ageing resistance are the major drawbacks of transparent plastics. Furthermore, the stability of the solar glass can be used for the stiffness of the collector as well as for the mounting components.

The relative savings of the unit costs were between 47.5 % and 63.0 % in comparison to state-of-the-art collectors. The simulation results prove the suitability of the material selection regarding thermal loads and show decreases of the annual solar yield between 18.5 % and 27.5 % by substituting the collectors of the system. Especially, the double-walled casing showed a considerable decrease in

efficiency, although the design represents advantages in manufacturing and assembling. Since the collector costs only make up for a small percentage of the total system costs, savings on the system level are relatively moderate. For an assumed life time of 20 years, the lowered solar yield or rather the increased energy costs produce almost the same total costs for system and heat supply.

Finally, the research has proven the feasibility of polymeric collectors for hot water preparation and space heating in central European climates, especially for the German market. However, the economic benefit of alternative collectors in standard systems is negligible. As a result, further changes regarding performance and costs are necessary for a considerable advantage of polymeric materials in solar-thermal systems.

7.3 Recommendations for Further Investigations

Three further research fields are necessary for the development of cost-efficient polymeric applications in solar-thermal systems. The improvement of current overheating protection measures, the detailed investigation of the collector design and the adjustment of set-up of the solar-thermal system can be named as the main objectives.

The overheating protection measures have to be improved with respect to their limited performance as well as to their costs. Especially, the above-mentioned problems of the thermotropic and thermochromic layers have to be solved to enable the useful polymeric material application in collectors. Furthermore, the manufacturing costs have to be very low to gain an economic advantage. Otherwise, the limited cost potential of systems with polymeric collectors cannot be balanced under the current conditions.

The collector designs have to be investigated especially regarding mechanical loads. The components have to fulfil the standards for wind and snow loads. Therefore, a detailed analysis of the developed components has to be conducted. The main focus has to be on the loads during high collector temperatures

whereas the stiffness is reduced. The necessary structures and material thicknesses will influence the material effort and the manufacturing costs. The resulting unit costs will change the economic benefit of the design approaches.

Another design aspect should be the structure of the fluid channels to gain an optimal fluid distribution and, hence, an increased collector efficiency. The development of the volumetric design has to consider the geometrical boundaries from the manufacturing process as well as the fluid-mechanical design parameters.

The adjustment of the system set-up is the most important field for further investigations. The decreased stability of polymeric materials at high temperatures and the parallel increasing pressure in the solar circuit are not compatible with each other. These pressure loads cause extreme stresses and deformations in particular for the necessary volumetric absorber design. This problem has to be solved by a solar circuit with lower or no pressure at all. Thus, a drain-back system represents a viable option. According to such a system set-up, the implementation of polymeric materials should be extended to the solar circuit aiming for a cost-effective solar-thermal system with reduced costs for components, installation and maintenance. The open system requires no air bleed valves, pressure relief valves, diaphragm expansion vessels or a pressure resistant piping. Water as heat carrier also reduces the total costs further. Thus, the adjusted system decreases the total costs and influences the economic benefit by a compromised system solution. However, changing the set-up into a drain-back system causes increased pump energy. The filling of the collectors at the start of the system operation needs additional pump energy to lift the water column against the static pressure. Thus, the influence of the pump energy has to be considered in the economic evaluations as well. Therefore, the simulation model has to be extended regarding pressure drop in piping and electric power consumption of the pumps.

References

ARNOLD, J.N., CATTON, I. and EDWARDS, D.K. (1976) Experimental investigation of natural convection in inclined rectangular regions of differing aspect ratios. *Journal of Heat Transfer*, Volume 98 (Issue 1), pp. 67-71.

ASHRAE 93-2003 (2003) *Methods for testing to determine the thermal performance of solar collectors*.

AVENTASOLAR (n.d.) *A new generation of energy technology* [WWW] Aventa AS. Available from: http://www.aventa.no/index.php?/eng [Accessed: 26/04/11].

BABULANAM, S.M., ERIKSSON, T.S., NIKLASSON, G:A: and GRANQVIST, C.G. (1987) Thermochromic VO_2 films for energy-efficient windows. *Solar Energy Materials*, Volume 16 (Issue 5), pp. 347-363.

BANKENVERBAND (n.d.) *Währungsrechner* [WWW] Bankenverband. Available from: http://bankenverband.de/service/waehrungsrechner [Accessed: 31/01/14].

BARTELSEN, B., ROCKENDORF, G., VENNEMANN, N., TEPE, R., LORENZ, K. and PURKARTHOFER, G. (1999) Elastomer-metal-absorber: Development and application. *Solar Energy,* Volume 67 (Issues 4-6), pp. 215-226.

BASSIOUNY, M.K. and MARTIN, H. (1983a) Flow Distribution and Pressure Drop in Plate Heat Exchangers - I. *Chemical Engineering Science*, Vol. 39 (No. 2), pp. 693-700.

BASSIOUNY, M.K. and MARTIN, H. (1983b) Flow Distribution and Pressure Drop in Plate Heat Exchangers - II. *Chemical Engineering Science*, Vol. 39 (No. 4), pp. 701-704.

BECKER, R., ROMMEL, M. and WITTWER, C. (2006) Regelungstechnische Untersuchung zur Vermeidung von Stillstandssituationen bei großen solarthermischen Anlagen. In: *16. Symposium Thermische Solarenergie, Bad Staffelstein (DE), May 2006*. Regensburg (DE): Ostbayerisches Technologie-Transfer-Institut e. V. (OTTI), pp. 371-376.

BEIKIRCHER, T. and SCHMIDT, M. (2009) Prototyp eines Flachkollektors mit Folienisolation und Überhitzungsschutz für höhere Betriebstemperaturen. In: *19. Symposium Thermische Solarenergie, Bad Staffelstein (DE), May 2009*. Regensburg (DE): Ostbayerisches Technologie-Transfer-Institut e. V. (OTTI), pp. 176-189.

BINE INFORMATIONSDIENST (2002) *Schaltbare und regelbare Verglasungen* [WWW] BINE Informationsdienst. Available from: http://www.bine.info/fileadmin/content/Publikationen/Themen-Infos/I_2002/themen0102internetx.pdf [Accessed: 22/12/09].

BIRON, M. (2013) *Thermoplastics and Thermoplastic Composites*. 2nd Edition. Oxford (GB): Elsevier.

BLISS, R.W. (1961) Atmospheric radiation near the surface of the ground: A summary for engineers. *Solar Energy*, Volume 5 (Issue 3), pp. 103-120.

BMWI (n.d.) *Energiedaten - Gesamtausgabe* [WWW] German Federal Ministry for Economic Affairs and Energy. Available from: http://www.bmwi.de/DE/Themen/Energie/Energiedaten-und-analysen/Energiedaten/gesamtausgabe,did=476134.html [Accessed: 27/03/14].

BRANDEMUEHL, M.J. and BECKMAN, W.A. (1980) Transmission of Diffuse Radiation Trough CPS and Flat Plate Collector Glazing. *Solar Energy*, Volume 24 (Issue 5), pp. 511-513.

BRUNOLD, S. (2010) Entwicklung von Kunststoffkollektoren: Grundlegende Fragestellungen und Ergebnisse eines Forschungsprojektes. In: *20. Symposium Thermische Solarenergie, Bad Staffelstein (DE), May 2010*. Regensburg: Ostbayerisches Technologie-Transfer-Institut e. V. (OTTI), pp. 162-167.

BRUNT, D. (1932) Notes on radiation in the atmosphere. *Quarterly Journal of the Royal Meteorological Society*, Volume 58 (Issue 247), pp. 389-420.

BUCKLEY, B.S. (1979) Apparatus for preventing high temperatures in glazed solar collector. *United States Patent.* 4,150,659.

BUCKLEY, B.S. and GULDMAN, T.A.R. (1983) Method and apparatus for over-temperature control of solarwater heating system. *United States Patent*. 4,399,807.

CADAFALACH, J. (2009) A detailed numerical model for flat-plate solar thermal devices. *Solar Energy*, Volume 83 (Issue 12), pp. 2157-2164.

CHAABANE, M., MHIRI, H. and PHILIPPE, B. (2014) Thermal performance of an integrated collector storage solar water heater (ICSSWH) with phase change materials (PCM). *Energy Conversion and Management*, Volume 78, pp. 897-903.

CHURCHILL, W.S. (1977) A comprehensive correlating equation for laminar, assisting, forced and free convection. *AIChE Journal*, Volume 23 (Issue 1), pp. 10-16.

CHURCHILL, W.S. and CHU, H. (1975) Correlating equations for laminar and turbulent free convection from a vertical plate. *International Journal of Heat and Mass Transfer*, Volume 18 (Issue 11), pp. 1323-1329.

CHURCHILL, W.S. and USAGI, R. (1972) A general expression for the correlation of rates of transfer and other phenomena. *AIChE Journal,* Volume 18 (Issue 6), pp. 1121-1128.

COLOR (n.d.) *SUNCOLOR PUR 2-pack polyurethane spectrally selective paint - TECHNICAL DATA SHEET* [WWW] Color, d.d. Available from: http://www.color.si/ [Accessed: 07/12/09].

CRISTOFARI, C., NOTTON, G., POGGI, P. and LOUCHE, A. (2002) Modelling and performance of a copolymer solar water heating collector. *Solar Energy*, Volume 72 (Issue 2), pp. 99-112.

CUMMINGS, R.D. (1978) Temperature control in solar-to-thermal energy converters. *United States Patent*. 4,102,325.

CUSTOMPARTNET (2008) *Blow Moulding* [WWW] CustomPartNet. Available from: http://www.custompartnet.com/wu/blow-molding [Accessed: 27/01/14].

DIN 8580 (2003) *Manufacturing processes – Terms and definitions, division*; German version 8580:2003. DIN German Institute for Standardization. Berlin (DE): Beuth Verlag GmbH.

DIN EN 12975-2 (2006) *Thermal solar systems and components – Solar collectors – Part 2: Test metho*ds; German version EN 12975-2:2006. DIN German Institute for Standardization. Berlin (DE): Beuth Verlag GmbH, pp. 16.

DIN EN 12977-2 (2012) *Thermal solar systems and components – Custom built systems – Part 2: Test methods for solar water heaters and combisystems*; German version EN 12977-2:2012. DIN German Institute for Standardization. Berlin (DE): Beuth Verlag GmbH, pp. 21.

DIN EN ISO 75-1 (2013) *Plastics – Determination of temperature of deflection under load – Part 1: General test method*; German version EN ISO 75-1:2013. DIN German Institute for Standardization. Berlin (DE): Beuth Verlag GmbH.

DIN EN ISO 175 (2011) Plastics; Determination of the effects of liquid chemicals, including water; German version EN ISO 175:2010. ISO International Organization for Standardization. Berlin (DE): Beuth Verlag GmbH.

DITTRICH, J. (2003) *Elektrochrome Gläser – Neue Technologien für Elektriker* [WWW] Universität Bremen. Available from: http://www.ecosol.uni-bremen.de/zarm3/download/ echrom.pdf [Accessed: 22/12/09].

DOCKERY, W.E. (1972) Self-defrosting windshield with automatically variable transparency. *United States Patent*. 3,695,681.

DOMININGHAUS, H. et al. (2012) *Kunststoffe – Eigenschaften und Anwendungen*. 8th Edition. Heidelberg (DE): Springer-Verlag.

DUFFIE, J.A. and BECKMAN, W.A. (2006) *Solar engineering of thermal processes*. 3rd Edition. New York (US): John Wiley & Sons.

DUROTHERM KUNSTSTOFFVERARBEITUNG GMBH (n.d.) *Technologies* [WWW] DUROtherm Kunststoffverarbeitung GmbH. Available from: http://www.durotherm.de/english/technologies/technologies.html [Accessed: 27/01/14].

COOPER, P.I. and DUNKLE, R.V. (1981) A non-linear Flat-plate collector model. *Solar Energy*, Volume 26 (Issue 2), pp. 133-140.

EICKER, U. (2003) *Solar Technologies for Buildings*. 1st Edition. Chichester: John Wiley & Sons.

FARID, M., KHUDHAIR, A.M., RAZACK, S.A.K. and AL-HALLAJ, S. (2004) A review on phase change energy storage: materials and applications. *Energy Conversion and Management*, Volume 45, pp. 1597-1615.

FLACHGLAS MARKENKREIS (n.d.) *INFRASELECT* [WWW] Flachglas MarkenKreis GmbH. Available from: http://www.flachglas-markenkreis.de/catalog/infraselect_/a78b9056-69f7-4ab1-8b61-0fbda4f6ec1d.aspx [Accessed: 20/08/13].

FUJII, T. and IMURA, H. (1972) Natural-convection heat transfer from a plate with arbitrary inclination. *International Journal of Heat and Mass Transfer*, Volume 15, pp. 755-767.

GEM'INNOV (2008) *Live colors microcapsules* [WWW] Gem'innov. Available from: http://www.geminnov.com/geminnov/cms/114-83/live-colors-customized-microcapsules.dhtml [Accessed: 12/01/10].

GEORG, A., GRAF, W., SCHWEIGER, D., WITTWER, V., NITZ, P. and WILSON, H.R. (1998) Switchable glazing with a large dynamic range in total solar energy transmittance (TSET). *Solar Energy*, Volume 62 (Issue 3), pp. 215-228.

GERTZOS, K.P. and CAOURIS, Y.G. (2007) Experimental and computational study of the developed flow field in a flat plate integrated collector storage (ICS) solar device with recirculation. Experimental Thermal and Fluid Science, Volume 31, pp.1133-1145.

GESIMAT (n.d.) *Thermochrome Verbundgläser* [WWW] GESIMAT GmbH. Available from: http://www.gesimat.de/data/produktinformation-tc-kl.pdf [Accessed: 20/08/13].

GNIELINSKI, V. (1974) New equations for heat and mass transfer in turbulent pipe and channel flow. *International Journal of Chemical Engineering*, Volume 16, pp. 359-369.

GNIELINSKI, V. (1995) Ein neues Berechnungsverfahren für die Wärmeübertragung im Übergangsbereich zwischen laminarer und turbulenter Rohrströmung. *Forschung im Ingenieurswesen*, 61, pp. 240-248.

GRANQVIST, C.G. (1992) Electrochromism and smart window design. *Solid State Ionics*, Volume 53-56 (Part 1/July-August), pp. 479-489.

GRIESSEN, R. and VAN DER SLUIS, P. (2001) Schaltbare Spiegel: Elektronenkorrelationen in der Anwendung. *Physik in unserer Zeit*, 32 (March), pp. 76-83.

HADAMOVSKI, H.-F. and JONAS, D. (2000) *Solaranlagen*. 1st Edition. Würzburg (DE): Vogel Buchverlag.

HAFNER, B. et al. (1999) Carnot Blockset Version 1.0 - Conventional and renewable energy systems optimization blockset - User's guide. Solar-Institut Jülich, Fachhochschule Aachen.

HARRISON, D.C. (1975) Heat energy transmission control panel. *United States Patent*. 3,903,665.

HARRISON, H. and HARRISON, H.C. (1979) Protective cooling system for solar heat collector. *United States Patent*. 4,153,040.

HARRISON, S.J., LIN, Q. and MESQUITA, L.C.S. (2004) Integral stagnation temperature control for solar collectors. In: *SESCI 2004 Conference, August 2004*. Waterloo (BE): University of Waterloo.

HATICON GMBH (2006) Solarkollektor mit einem belüftbaren Gehäuse. *Gebrauchsmusterschrift.* DE 20 2006 013 263 U1.

HOCHREITER, E. and TRINKL, C. (2008) Werkstoffe und Verarbeitungstechnologien für solarthermische Kollektoren. In: *6. Werkstoffkongress „Optionen für Energieeinsparung und Energieerzeugung"*, Leoben (AT), November 2008.

HELIOCOL (n.d.) *Residential Pools* [WWW] Heliocol. Available from: http://www.heliocol.com/ residential/ easy1.html [Accessed: 26/04/11].

HOLLANDS, K.G.T., UNNY, T.E., RAITHBY, G.D. and KONICEK, L. (1976) Free convective heat transfer across inclined air layers. *Journal of Heat Transfer*, Volume 98 (Issue 2), pp. 189-193.

HOTTEL, H.C. and WHILIER, A. (1958) Evaluation of Flat-Plate Collector Performance. In: *Trans. of the Conf. on the Use of Solar Energy*, 2 (1), pp. 74-76.

HUIBERTS, J.N., GRIESSEN, R., RECTOR, J.H., WIJNGAARDEN, R.J., DEKKER, J.P., DE GROOT, D.G. and KOEMAN, N.J. (1996) Yttrium and lanthanum hydride films with switchable optical properties. *Nature*, Volume 380 (March), pp. 231-234.

HUOT, G., SCHÜLER, A. and ROECKER, C. (2008) *Evaluation of the Potential of Optical Switching Materials for Overheating Protection of Thermal Solar Collectors*. Final Report, Swiss Federal Office of Energy (BFE 280008), Bern (CH), 2008.

IMAGINATION SOLAR LTD. (n.d.) *Installation Guide* [WWW] Imagination Solar Ltd. Available from: http://www.imaginationsolar.com/PDFs/newPDFs/Installation%20and%20User%20Guides/A1%20Planning%20The%20Collector%20Installation%202.pdf [Accessed: 02/12/11].

INSTITUT FÜR SOLARTECHNIK SPF (2005) *Solar Collector Factsheet: SPF-Nr. C526* [WWW] Institut für Solartechnik SPF. Available from: http://www.solarenergy.ch/fileadmin/daten/reportInterface/kollektoren/factsheets/scf526de.pdf [Accessed: 04/11/14].

INTERPANE (n.d.) *ipaview CF* [WWW] Interpane Glas Indurtrie AG. Available from: http://www.iwo.de/fachwissen/brennstoff/ [Accessed: 25/03/14].

IWO (n.d.) *Brennstoff Heizöl* [WWW] IWO – Institut für Wärme und Oeltechnik. Available from: http://www.interpane.com/ipaview_cf_113.html?sprache=englisch [Accessed: 21/08/13].

JÄGER, H. and TERSCHÜREN, K.-H. (2007) Produktionsverfahren für Solarkollektoren – von der Manufaktur zur Automatisierung. In: *Produktionsthemen für die Solarenergie*, Hannover (GER), September 2007. Berlin (DE): Forschungs-Verbund Sonnenenergie.

JOHANNABER, F. (2004) *Kunststoff-Maschinenführer*. 4th Edition. Munich (DE): Carl Hanser Verlag.

KAHLEN, S. and WALLNER, G.M. (2008) Ageing behaviour of polymeric solar-thermal absorber materials. In: *2. Leobener Symposium 'POLYMERIC SOLAR MATERIALS', Leoben (AT), February 2008*. Leoben: G.M. Wallner / R.W. Lang, pp. XII 1-6.

KAISER, A., FINK, C., HAUSNER, R. and RAMSCHAK, T. (2012) Leistungsanforderungen an Polymermaterialien in solarthermischen Systemen. In: *Gleisdorf SOLAR 2012 – 10. Internationale Konferenz für thermische Solarenergienutzung, Gleisdorf (AT), September 2012*. Gleisdorf: AEE INTEC, pp. 296-306.

KAISER, W. (2007) *Kunststoffchemie für Ingenieure.* 2nd Edition. Munich (DE): Carl Hanser Verlag.

KEARNEY, M., DAVIDSON, J. and MANTELL, S. (2005) Polymeric absorbers for Flat Plate Collectors: Can Venting Provide Adequate Overheat Protection? *Journal of Solar Energy Engineering*, Volume 127 (August), pp. 421-424.

KLEIN, S., DUFFIE, J.A. and BECKMAN, W.A. (1974) Transient considerations of flat-plate solar collectors. *Trans. of ASME: Journal Engineering for Power*, 96A, pp. 109-113.

KOENIG, R.H. (1983) Venting means for solar collectors. *United States Patent.* 4,396,004.

KOO, J.-M. (1999) Development of a Flat-Plate Solar Collector Design Program. Published Thesis (Master of Science), University of Wisconsin-Madison.

KUNSTSTOFFINFORMATION (n.d.) *Polymerpreise Detailseite - Dezember 2013* [WWW] Kunststoff Information Verlagsgesellschaft mbH. Available from: http://www.kiweb.de/default.aspx?pageid=200 [Accessed: 31/01/14].

KURZBÖCK, M., WALLNER, G.M. and LANG, R.W. (2012) Black pigmented polypropylene materials for solar absorbers. *Energy Procedia - 1st International Conference on Solar Heating and Cooling for Buildings and Industry (SHC 2012)*, Volume 30, pp. 438-445.

MANGOLD, D. (1996) *Kostenanalyse der Herstellung von Solarkollektoren und mögliche Kostenreduktionen durch Massenfertigung*. In: *6. Symposium Thermische Solarenergie, Bad Staffelstein (DE), May 1996*. Regensburg (DE): Ostbayerisches Technologie-Transfer-Institut e.V. (OTTI).

MARTY, H., BRUNOLD, S. and VOGELSANGER, P. (2008) Überhitzungsschutzschutz mit thermochromen Solarabsorberschichten. In: *18. Symposium Thermische Solarenergie, Bad Staffelstein (DE), April 2008*. Regensburg (DE): Ostbayerisches Technologie-Transfer-Institut e.V. (OTTI), pp. 80-85.

MATHEW, J.G.H., SAPERS, S.P., CUMBO, M.J., O'BRIEN, N.A., SARGENT, R.B., RAKSHA, V.P., LAHADERNE, R.B. and HICHWA, B.P. (1997) Large area electrochromics for architectural applications. *Journal of Non-Crystalline Solids*, 218 (September), pp. 342-346.

MATHWORKS (n.d.) *Simulink* [WWW] The MathWorks, Inc. Available from: http://www.mathworks.com/help/toolbox/simulink/index.html [Accessed: 20/09/13].

MATUSKA, T. and ZMRHAL, V. (2009) *KOLEKTOR 2.2 – reference handbook*. 1st Edition. Prague (CZ): Czech Technical University.

MAZDA-SOLAR (n.d.) *MAZDA-EPDM-Absorber* [WWW] MAZDA-SOLAR. Available from: http://www.mazda-solar.de/shop/article_1f%253Cbr%253EMZ1070RM/roter-MAZDA-EPDM-AbsorberMZ1070RM.html?shop_param=cid%3D221%26aid%3 D1f%253Cbr%253EMZ1070RM%26 [Accessed: 02/12/11].

MEIR, M.G. (2008) *IEA-SHC Task 39: Polymeric solar thermal Collectors - State of the art*. In: *2. Leobener Symposium POLYMERIC SOLAR MATERIALS Tagungshandbuch: SOLARTECHNIK – Neue Möglichkeiten für die Kunststoffbranche, Leoben (AT), February 2008*. Leoben: Polymer Competence Center Leoben GmbH, pp. I-1 - I-5.

MEIR, M.G., REKSTAD, J.B., GJESSING, J. and RUMLER, N. (2008) Overheating protection of polymeric solar collectors by triggered ventilation. In: *EUROSUN 2008 – International Conference on Solar Heating, Cooling and Buildings - Book of Abstracts, Lisbon (PT), October 2008*. Lisbon: SPES – Sociedade Portuguesa de Energia Solar, pp. 264.

MICHAELI, W. (2006) *Einführung in die Kunststoffverarbeitung.* 5th Edition. Munich (DE): Carl Hanser Verlag.

MILLS, A.F. (1999) *Heat Transfer*. 2nd Edition. New Jersey (US): Prentice Hall.

MOORE, S.W. (1983) Solar collector apparatus having increased energy rejection during stagnation. *United States Patent.* 4,392,481.

MÜLLER, H. and ZÖRNER, W. (2008) Kurzstudie *Produktionsprozesse* für die Deutsche Solarthermie-Technologie Plattform [WWW]. Available from: http://www.solarthermietechnologie.de/fileadmin/img/Service/PDF/Studien/st_ag1_prodtech.pdf [Accessed: 27/07/10].

EVONIK (2011) 'Data of Plexiglas®' [Online] *Evonik Röhn GmbH: 29th March 2011*. Available from: stefan.muschinski@evonik.com.

NITZ, P. (2004) Sonnenschutz und Lichtlenkung durch mikrostrukturierte Oberflächen. In: *DGG-Glasforum der Deutschen Glastechnischen Gesellschaft e.V., Würzburg (DE), März 2004.* Würzburg: Fraunhofer ISC, pp. 1-5.

NITZ, P. (2006) Solarkollektor mit transluzenter Abdeckung. *Patent application*. DE 10 2004 043 556 A1.

NITZ, P., GIOWANNETTI, F., WEINLÄNDER, H. and WIENOLD, J. (2008) Neue Verglasungstechniken für Tageslicht und Wärmeschutz. In: *Themen 2008: Energieeffizientes und solares Bauen, Berlin (DE), September 2008*. Berlin: ForschungsVerbund Erneuerbare Energien (FVEE), pp. 45-48.

NITZ, P. and HARTWIG, H. (2005) Solar control with thermotropic layers. *Solar Energy*, Volume 79 (Issue 6), pp. 573-582.

NITZ, P., BLÄSI, B., MICK, J., WALZE, G. and GOMERT, A. (2007) Verglasungen mit mikrostrukturierten optisch-funktionalen Komponenten. In: *3. Symposium Licht + Architektur, Tageslicht - Kunstlicht – Energie, Bad Staffelstein (DE), February 2007*. Regensburg (DE): Ostbayerisches Technologie-Transfer-Institut e.V. (OTTI), pp. 20-25.

NITZ, P., GIOWANNETTI, F., WEINLÄNDER, H. and WIENOLD, J. (2008) Neue Verglasungstechniken für Tageslicht und Wärmeschutz. In: *Themen 2008: Energieeffizientes und solares Bauen, Berlin (DE), September 2008*. Berlin: ForschungsVerbund Erneuerbare Energien (FVEE), pp. 45-48.

NITZ, P. and WILSON, H.R. (2008) Modellierung thermotroper Materialien. In: *2. Leobener Symposium POLYMERIC SOLAR MATERIALS Tagungshandbuch: SOLARTECHNIK – Neue Möglichkeiten für die Kunststoffbranche, Leoben (AT), Februar 2008*. Leoben: Polymer Competence Center Leoben GmbH, pp. XIII-1 - XIII-6.

O'BRIEN-BERNINI, F.C. and MCGOWAN, J.G. (1984) Performance modelling of non-metallic flat-plate solar collectors. *Solar Energy*, Volume 33 (Issues 3-4), pp. 305-319.

OCHS, F., STUMPP, H., MANGOLD, D., HEIDEMANN, W. and MÜLLER-STEINHAGEN, H. (2004) Bestimmung der feuchte- und temperaturabhängigen Wärmeleitfähigkeit von Dämmstoffen. In: *14. Symposium Thermische Solarenergie, Bad Staffelstein (DE), May 2004*. Regensburg (DE): Ostbayerisches Technologie-Transfer-Institut e.V. (OTTI), pp. 118-122.

OKU OBERMAIER GMBH (n.d.) *Thermosiphon-Solaranlage zur Brauchwassererwärmung* [WWW] OKU Obermaier GmbH. Available from: http://www.okuonline.com/docs/de/solartechnik/sola/siph-comfort200.php [Accessed 26/04/11].

OREL, B., KUNIC, R., KOZELJ, M., VUK, A.S., VILCNIK, A., PERSE, L.S., MERLINI, D. and BRUNOLD, S. (2009) Adhesion and thermal stability of thickness insensitive spectrally selective (TISS) polyurethane-based paint coatings on copper substrates. *Solar Energy Materials & Solar Cells*, Volume 93 (Issue 5), pp. 630-640.

OREL, B., JERMAN, I. and KOZELJ, M. (2010) The effect of polyhedral oligomeric silsesquioxane dispersant and low surface energy additives on spectrally selective paint coatings with self-cleaning properties. *Solar Energy Materials and Solar Cells*, Volume 94 (Issue 2), pp. 232-245.

PAHL et al. (2007) *Engineering Design — A Systematic Approach*. 3rd Edition. London (GB): Springer-Verlag.

PALMER, D.W. (1980) Vented solar panel. *United States Patent*. 4,219,009.

PRINTCOLOR AG (2009) *UV-Thermochromfarben* [WWW] Printcolor AG. Available from: http://www.printcolor.ch/tds/download/German/Product-Group-500/590-T31-xx-05.pdf [Accessed: 12/01/10].

RADIANT FLOOR COMPANY (n.d.) *Overheating Protection for Solar Collectors* [WWW] Radiant Floor Company. Available from: http://www.radiantcompany.com/system/heatdump.shtml [Accessed: 25/09/2014].

REITER, C., MÜLLER, H., TREIKAUSKAS, F.-D., TRINKL, C. and ZÖRNER, W. (2009a) Kunststoffe in Solarkollektoren: Anforderungsdefinition, Konzeptentwicklung und Machbarkeitsbewertung. In: *19. Symposium Thermische Solarenergie, Bad Staffelstein (DE), May 2009*. Regensburg (DE): Ostbayerisches Technologie-Transfer-Institut e.V. (OTTI), pp. 80-85.

REITER, C., MÜLLER, H., TREIKAUSKAS, F.-D., TRINKL, C. and ZÖRNER, W. (2009b) Polymeric Solar Thermal Collectors: Definition of Requirements, Concept Development and Feasibility Evaluation. In: *estec2009 - Proceedings, Munich (GER), May 2009*. Brussels (NED): ESTIF - European Solar Thermal Industry Federation, pp. 275-279.

REITER, C., HANBY, V., TRINKL, C. and ZÖRNER, W. (2010a) Experimentelle Ermittlung der thermischen Bauteilbelastungen von Solarkollektoren im realen Betrieb. In: *20. Symposium Thermische Solarenergie, Bad Staffelstein (DE), May 2010*. Regensburg (DE): Ostbayerisches Technologie-Transfer-Institut e.V. (OTTI), pp. 56-61.

REITER, C., HANBY, V., TRINKL, C. and ZÖRNER, W. (2010b) Überhitzungsschutzmaßnahmen für solarthermische Kollektoren. In: *20. Symposium Thermische Solarenergie, Bad Staffelstein (DE), May 2010*. Regensburg (DE): Ostbayerisches Technologie-Transfer-Institut e.V. (OTTI), pp. 68-73.

REITER, C., HANBY, V., TRINKL, C. and ZÖRNER, W. (2010c) Thermal Load Analysis of a Solar-Thermal Flat-Plate Collector in a Domestic Heating System.

In: *EUROSUN 2010 – International Conference on Solar Heating, Cooling and Buildings – Book of Abstracts, Graz (AT), September 2010*. Graz: AEE INTEC, pp. 113.

REITER, C., TRINKL, C. and ZÖRNER, W. (2011) *Solarthermie2000plus: Kunststoffe in solarthermischen Kollektoren - Anforderungsdefinition, Konzeptentwicklung und Machbarkeitsbewertung*, Final Report BMU (0329285A), Berlin (DE), 2011.

REITER, C., TRINKL, C. and ZÖRNER, W. (2012) Thermal Loads on Solar Collectors and Options for their Reduction. In: M. KOEHL et al., eds. *Polymeric Materials for Solar Thermal Applications*. 1st Edition. Weinheim (DE): Wiley-VCH Verlag GmbH & Co. KGaA.

REITER, C., TRINKL, C. and ZÖRNER, W. (2013) Entwicklung eines Kunststoffabsorbers: Strömungsmechanische und fertigungstechnische Gestaltung. In: *23. Symposium Thermische Solarenergie, Bad Staffelstein (DE), April 2013*. Regensburg (DE): Ostbayerisches Technologie-Transfer-Institut e.V. (OTTI), pp. 40-41.

RESCH, K., HAUSNER, R. and WALLNER, G.M. (2007) All polymeric flat-plate collector – Potential of thermotropic layers to prevent overheating. In: *ISES Solar World Congress 2007: Solar energy and human settlement, Beijing 2007*. Berlin (DE): Springer, pp. 561-565.

RESCH, K. and WALLNER, G.M. (2009) Thermotropic layers for flat-plate collectors – A review of various concepts for overheating protection with polymeric materials. *Solar Energy Materials & Solar Cells*, Volume 93 (Issue 1), pp. 119-128.

RESCH, K., HAUSNER, R. and WALLNER, G.M. (2009) Phase separated thermotropic layers based on UV cured acrylate resins – Effect of material formulation on overheating protection properties and application in a solar collector. *Solar Energy*, Volume 83 (Issue 9), pp. 1689-1697.

RICH, A.C. (1995) Solar collector venting system. *United States Patent.* 5,404,867.

ROBERTS, J., BRANDEMUEHL, M.J., BURCH, J. and GAWLIK, K.M. (2000) Overheating Protection for Passive Solar Water Heating Systems Using Natural

Convection Loops. In: *Proceedings of the Solar 2000 Conference, Madison (USA), June 2000.* Boulder: American Solar Energy Society, pp. 273-278.

ROMMEL, M., KÖHL, M., GRAF, W., WELLENS, F., BRUCKER, F., LUSTIG, K. and BAHR, P. (1997) Corrosion-free collectors with selectively coated plastic absorbers. *Desalination*, Volume 109 (Issue 2), pp. 149-155.

ROTH WERKE GMBH (n.d.) *Referenzen* [WWW] Roth Werke GmbH. Available from: http://www.roth-werke.de/ [Accessed: 26/04/11].

RUESCH, F. and BRUNOLD, S. (2008) Ageing Performance of Collector Glazing Materials – Results from 20 Years of Outdoor Weathering. In: *EUROSUN 2008 – 1st International Conference on Solar Heating, Cooling and Buildings – Book of Abstracts, Lisbon (PT), October 2010*. Lisbon: SPES – Sociedade Portuguesa de Energia Solar, pp. 386-387.

RUESCH, F., BRUNOLD, S., FREI, U., HÄUSELMANN, T. and FRANK, E. (2008) Langzeit-Alterungsuntersuchung an Abdeckungsmaterialien für thermische Sonnenkollektoren, Final Report, Schweizer Bundesamt für Energie (BfE), Rapperswill (CH), 2008.

SAINT-GOBAIN GLASS (n.d.) *SGG PRIVA-LITE* [WWW] Saint-Gobain Glass. Available from: http://nordic.saint-gobain-glass.com/b2c/default.asp?nav1=pr&nav2=single%20pane&id=10975 [Accessed: 21/08/13].

SAINT-GOBAIN SEKURIT (n.d.) *ELECTROCHROMIC GLASS* [WWW] Saint-Gobain Sekurit. Available from: http://www.sekurit.com/EN/index.asp?nav1=PR&nav2=VPD&id=372 [Accessed: 20/08/13].

SCHARFMAN, H. (1977) Vented solar collector. *United States Patent.* 4,043,317.

SCHLICHTING, H. (1958) *Grenzschicht-Theorie*. 3rd Edition. Karlsruhe (DE): Verlag G. Braun.

SCHMIDT, P. (1992) Solarkollektor mit Verlustreduzierung. *Gebrauchsmuster.* G 92 09 439.2.

SCOTT, P.B. (1977) Solar heater with automatic venting. *United States Patent*. 4,046,134.

SERALE, G., BARONETTO, S., GOIA, F. and PERINO, M (2013) Characterization and energy performance of a slurry PCM-based solar thermal collector: a numerical analysis. *Energy Procedia*, Volume 48, pp. 223-232.

SHARPE, T.E. (1984) Solar heat collector system. *United States Patent*. 4,219,009.

SOLAR-INSTITUT JUELICH and EXPERTCONTROL GMBH (1999) *Carnot Blockset Version 1.0 - Conventional and renewable energy systems optimization blockset - User's guide.* Herrsching (DE): ExpertControl GmbH.

SOULIOTIS, M., CHEMISANA, D., CAOURIS, Y.G. and TRIPANAGNOSTOPOULOS, Y. (2013) Experimental study of integrated collector storage solar water heaters. *Renewable Energy*, Volume 50, pp. 1083-1094.

SOLAR TWIN LTD. (n.d.) Zero carbon solar power & water heating [WWW] Solar Twin Ltd. Available from: http://www.solartwin.com/ [Accessed: 26/04/11].

STEPHAN, P. (2010) *VDI Heat Atlas*. 2nd Edition. Düsseldorf (DE): VDI-Verlag GmbH.

STEPHENS, R.B. (1981) Fluid optical switch for a solar collector. *United States Patent*. 4,270,517.

STIBETHERM S.A. (n.d.) *Solar Energy Products* [WWW] Stibetherm S.A. Available from: http://stibetherm.com/stibetherm/en/default.html [Accessed: 04/12/11].

STREICHER, W. (2008) Überlegungen zu Hydrauliken und Regelungen für Kunststoffkollektoren. In: *2. Leobener Symposium POLYMERIC SOLAR MATERIALS Tagungshandbuch: SOLARTECHNIK – Neue Möglichkeiten für die Kunststoffbranche, Leoben (AT), Februar 2008*. Leoben: Polymer Competence Center Leoben GmbH, pp. V-1 - V-2.

SWINBANK, W.C. (1963) Long-wave radiation from clear skies. *Quarterly Journal of the Royal Meteorological Society*, Volume 89 (Issue 381), pp. 339-348.

TABOR, H. (1958) Radiation, convection and conduction in solar collectors. *Bulletin of the Research Council of Israel*, Volume 8C, pp. 155-176.

TEXSUN AB (n.d.) *El Nino* [WWW] Texsun AB. Available from: http://www.texsun.se/modules.php?_name=_Content&op=showcontent&id=34&cat=7 [Accessed: 26/04/11].

TREIKAUSKAS, F.-D. and ZÖRNER, W. (2005a) Alternative casings for solar-thermal collectors. In: *2nd European Solar Thermal Energy Conference - estec2005 Proceedings, Freiburg (DE), June 2005.* Freiburg: European Solar Thermal Industry Federation ESTIF, pp. 325-328.

TREIKAUSKAS, F.-D. and ZÖRNER, W. (2005b) *Optimierter Absorber für thermische Solaranlagen in Bezug auf Fertigungsprozess, Herstellkosten und Wirkungsgrad – Vorstudie zu Absorberkonzepten*, Final Report, DBU (AZ: 21543), Ingolstadt (DE), 2005.

TREIKAUSKAS, F.-D. (2009) *Development of a volumetric solar thermal absorber*. Dissertation, De Montfort University Leicester (GB).

UFE SOLAR GMBH (1999) Solarkollektor, bestehen aus einem belüftbaren Gehäuse. *Offenlegungsschrift.* DE 199 54 238 A1.

VAN DER SLUIS, P., OUWERKERK, M. and DUINE, P.A. (1997) Optical switches based on magnesium lanthanide alloy hydrides. *Applied Physics Letters*, Volume 70 (June), Nr. 3356.

VDI 2225 (1998) *Design engineering methodics — Engineering design at optimum cost — Valuation of costs*. VDI-Gesellschaft Entwicklung Konstruktion Vertrieb. Berlin (DE): Beuth Verlag GmbH.

VEREIN DEUTSCHER INGENIEURE E.V. (2012) *Economic efficiency of building calculation*; English version VDI 2067. VDI-Gesellschaft Bauen und Gebäudetechnik (GBG). Berlin (DE): Beuth Verlag GmbH.

WALLNER, G.M., HAUSNER, R. and RESCH, K. (2008) Property and performance requirements for thermotropic layers to prevent overheating in an all polymeric flat-plate collector. *Solar Energy Materials & Solar Cells*, Volume 92 (Issue 6), pp. 614-620.

WALZE, G. (2005) *Mikrostrukturierte Oberflächen in Kombination mit optischen Schaltungsmechanismen zum Tageslichtmanagement*. Dissertation, Albert-Ludwigs-Universität Freiburg im Breisgau (DE).

WESTMETALL (n.d.) *Market data* [WWW] Westmetall GmbH & Co. KG. Available from: http://www.westmetall.com/de/markdaten.php [Accessed: 12/12/13].

WIJEYSUNDERA, N.E. (1978) Comparison of transient heat transfer models for flat plate collectors. *Solar Energy*, Volume 21 (Issue 6), pp. 517-521.

ZAE BAYERN (2001) Solarenergienutzung mit schaltbarer Wärmedämmung (SWD) [WWW] ZAE Bayern. Available from: http://www.isoteg.de/KOMP-OPT/fr_schaltbar.html [Accessed: 08/06/09].

ZAUNER, C., LAGER, D. and HOHENAUER, W. (2011) Thermophysikalische und Spektroskopische Methoden zur Analyse von Isolationsmaterialien für Solarthermische Anwendungen. In: *19. Symposium Thermische Solarenergie, Bad Staffelstein (DE), May 2009*. Regensburg (DE): Ostbayerisches Technologie-Transfer-Institut e.V. (OTTI), pp. 288-293.

ZÖRNER, W. (2004) Use of plastics as structural material for solar-thermal flat-plate collectors. In: *EUROSUN 2004 Proceedings Volume 1, Freiburg (DE), June 2004*. Freiburg: ISES Europe, pp. 814-821.